

The nutritional immunological effects and mechanisms of chemical constituents from the homology of medicine and food

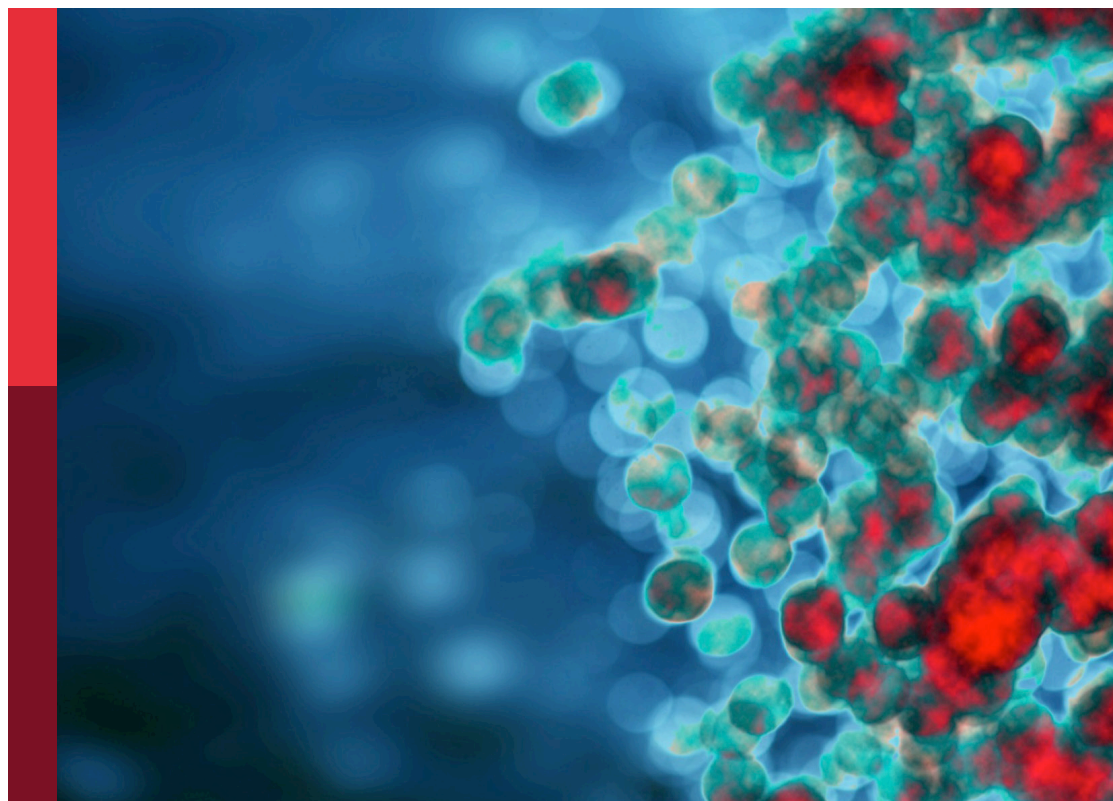
Edited by

Peng Ji, Yi Wu and Guiyan Yang

Published in

Frontiers in Immunology

Frontiers in Nutrition



FRONTIERS EBOOK COPYRIGHT STATEMENT

The copyright in the text of individual articles in this ebook is the property of their respective authors or their respective institutions or funders. The copyright in graphics and images within each article may be subject to copyright of other parties. In both cases this is subject to a license granted to Frontiers.

The compilation of articles constituting this ebook is the property of Frontiers.

Each article within this ebook, and the ebook itself, are published under the most recent version of the Creative Commons CC-BY licence. The version current at the date of publication of this ebook is CC-BY 4.0. If the CC-BY licence is updated, the licence granted by Frontiers is automatically updated to the new version.

When exercising any right under the CC-BY licence, Frontiers must be attributed as the original publisher of the article or ebook, as applicable.

Authors have the responsibility of ensuring that any graphics or other materials which are the property of others may be included in the CC-BY licence, but this should be checked before relying on the CC-BY licence to reproduce those materials. Any copyright notices relating to those materials must be complied with.

Copyright and source acknowledgement notices may not be removed and must be displayed in any copy, derivative work or partial copy which includes the elements in question.

All copyright, and all rights therein, are protected by national and international copyright laws. The above represents a summary only. For further information please read Frontiers' Conditions for Website Use and Copyright Statement, and the applicable CC-BY licence.

ISSN 1664-8714
ISBN 978-2-8325-2958-4
DOI 10.3389/978-2-8325-2958-4

About Frontiers

Frontiers is more than just an open access publisher of scholarly articles: it is a pioneering approach to the world of academia, radically improving the way scholarly research is managed. The grand vision of Frontiers is a world where all people have an equal opportunity to seek, share and generate knowledge. Frontiers provides immediate and permanent online open access to all its publications, but this alone is not enough to realize our grand goals.

Frontiers journal series

The Frontiers journal series is a multi-tier and interdisciplinary set of open-access, online journals, promising a paradigm shift from the current review, selection and dissemination processes in academic publishing. All Frontiers journals are driven by researchers for researchers; therefore, they constitute a service to the scholarly community. At the same time, the *Frontiers journal series* operates on a revolutionary invention, the tiered publishing system, initially addressing specific communities of scholars, and gradually climbing up to broader public understanding, thus serving the interests of the lay society, too.

Dedication to quality

Each Frontiers article is a landmark of the highest quality, thanks to genuinely collaborative interactions between authors and review editors, who include some of the world's best academicians. Research must be certified by peers before entering a stream of knowledge that may eventually reach the public - and shape society; therefore, Frontiers only applies the most rigorous and unbiased reviews. Frontiers revolutionizes research publishing by freely delivering the most outstanding research, evaluated with no bias from both the academic and social point of view. By applying the most advanced information technologies, Frontiers is catapulting scholarly publishing into a new generation.

What are Frontiers Research Topics?

Frontiers Research Topics are very popular trademarks of the *Frontiers journals series*: they are collections of at least ten articles, all centered on a particular subject. With their unique mix of varied contributions from Original Research to Review Articles, Frontiers Research Topics unify the most influential researchers, the latest key findings and historical advances in a hot research area.

Find out more on how to host your own Frontiers Research Topic or contribute to one as an author by contacting the Frontiers editorial office: frontiersin.org/about/contact

The nutritional immunological effects and mechanisms of chemical constituents from the homology of medicine and food

Topic editors

Peng Ji — Gansu Agricultural University, China

Yi Wu — Nanjing Agricultural University, China

Guiyan Yang — University of California, United States

Topic Coordinator

Fanlin Wu — Gansu Agricultural University, China

Citation

Ji, P., Wu, Y., Yang, G., eds. (2023). *The nutritional immunological effects and mechanisms of chemical constituents from the homology of medicine and food*. Lausanne: Frontiers Media SA. doi: 10.3389/978-2-8325-2958-4

Table of contents

- 05 ***Portulaca oleracea* L. extracts alleviate 2,4-dinitrochlorobenzene-induced atopic dermatitis in mice**
Wei-jie Lv, Jie-yi Huang, Shu-peng Li, Xiao-pei Gong, Jing-bo Sun, Wei Mao and Shi-ning Guo
- 17 **Regulation of dietary polyphenols on cancer cell pyroptosis and the tumor immune microenvironment**
Xiaoxia Huang, Yao Wang, Wenhui Yang, Jing Dong and Lin Li
- 32 **Polysaccharide from *Atractylodes macrocephala* Koidz binding with zinc oxide nanoparticles: Characterization, immunological effect and mechanism**
Ruonan Bo, Xiaopan Liu, Jing Wang, Simin Wei, Xinyue Wu, Ya Tao, Shuya Xu, Mingjiang Liu, Jingui Li and Huan Pang
- 49 **Triptolide increases resistance to bile duct ligation-induced liver injury and fibrosis in mice by inhibiting RELB**
Zihang Yuan, Jie Wang, Haoran Zhang, Yingying Miao, Qianhui Tang, Ziqiao Yuan, Cheng Nong, Zhicheng Duan, Luyong Zhang, Zhenzhou Jiang and Qinwei Yu
- 62 **Polysaccharide from *Atractylodes macrocephala* Koidz. ameliorates DSS-induced colitis in mice by regulating the Th17/Treg cell balance**
Mengjiao Yang, Qianwen Zhang, Reham Taha, Mohammed Ismail Abdelmotalab, Qing Wen, Yuzhu Yuan, Yongrui Zhao, Qingyu Li, Chunyu Liao, Xin Huang, Zhenzhou Jiang, Chenghan Chu, Chunhua Jiao and Lixin Sun
- 78 ***Moringa oleifera* leaf polysaccharide alleviates experimental colitis by inhibiting inflammation and maintaining intestinal barrier**
Hosameldeen Mohamed Husien, WeiLong Peng, Hongrui Su, RuiGang Zhou, Ya Tao, JunJie Huang, MingJiang Liu, RuoNan Bo and JinGui Li
- 00 **Berberine a traditional Chinese drug repurposing: Its actions in inflammation-associated ulcerative colitis and cancer therapy**
CuiPeng Zhu, Kaiqi Li, Xiao-Xu Peng, Tong-Jia Yao, Zi-Yu Wang, Ping Hu, Demin Cai and Hao-Yu Liu
- 99 **Desmosterol: A natural product derived from macroalgae modulates inflammatory response and oxidative stress pathways in intestinal epithelial cells**
Huan Qu, Qiufang Zong, Ping Hu, Zhaojian Li, Haifei Wang, Shenglong Wu, Hao-Yu Liu, Wenbin Bao and Demin Cai
- 109 **Three-phase extraction of polysaccharide from *Stropharia rugosoannulata*: Process optimization, structural characterization and bioactivities**
Xinxin Li, Zhiqiang Zhang, Li Wang, Haoqiang Zhao, Yahui Jia, Xia Ma, Jinzhan Li, Yi Wang and Bingji Ma

- 123 **Potential of *Spirulina platensis* as a feed supplement for poultry to enhance growth performance and immune modulation**
Nahed A. El-Shall, Shouqun Jiang, Mayada R. Farag, Mahmoud Azzam, Abdulaziz A. Al-Abdullatif, Rashed Alhotan, Kuldeep Dhama, Faiz-ul Hassan and Mahmoud Alagawany
- 135 **Transcriptomics and metabolomics analysis reveal the anti-oxidation and immune boosting effects of mulberry leaves in growing mutton sheep**
Xiaopeng Cui, Yuxin Yang, Minjuan Zhang, Shuang Liu, Hexin Wang, Feng Jiao, Lijun Bao, Ziwei Lin, Xinlan Wei, Wei Qian, Xiang Shi, Chao Su and Yonghua Qian



OPEN ACCESS

EDITED BY

Guiyan Yang,
University of California, Davis,
United States

REVIEWED BY

Yi Wu,
Nanjing Agricultural University, China
Zhenrui Shi,
Sun Yat-sen University, China

*CORRESPONDENCE

Jing-bo Sun
gdszyysjb@gzucm.edu.cn
Wei Mao
maowei@gzucm.edu.cn
Shi-ning Guo
shining@scau.edu.cn

†These authors have contributed
equally to this work and share first
authorship

SPECIALTY SECTION

This article was submitted to
Nutritional Immunology,
a section of the journal
Frontiers in Nutrition

RECEIVED 05 July 2022

ACCEPTED 28 July 2022

PUBLISHED 16 August 2022

CITATION

Lv W-j, Huang J-y, Li S-p, Gong X-p,
Sun J-b, Mao W and Guo S-n (2022)
Portulaca oleracea L. extracts alleviate
2,4-dinitrochlorobenzene-induced
atopic dermatitis in mice.
Front. Nutr. 9:986943.
doi: 10.3389/fnut.2022.986943

COPYRIGHT

© 2022 Lv, Huang, Li, Gong, Sun, Mao
and Guo. This is an open-access
article distributed under the terms of
the [Creative Commons Attribution
License \(CC BY\)](#). The use, distribution
or reproduction in other forums is
permitted, provided the original
author(s) and the copyright owner(s)
are credited and that the original
publication in this journal is cited, in
accordance with accepted academic
practice. No use, distribution or
reproduction is permitted which does
not comply with these terms.

Portulaca oleracea L. extracts alleviate 2,4- dinitrochlorobenzene-induced atopic dermatitis in mice

Wei-jie Lv[†], Jie-yi Huang[†], Shu-peng Li¹, Xiao-pei Gong¹,
Jing-bo Sun^{2*}, Wei Mao^{2*} and Shi-ning Guo^{1,3,4,5*}

¹College of Veterinary Medicine, South China Agricultural University, State Key Laboratory of
Dampness Syndrome of Chinese Medicine, Guangzhou, China, ²State Key Laboratory of Dampness
Syndrome of Chinese Medicine, The Second Affiliated Hospital of Guangzhou University of Chinese
Medicine, South China Agricultural University, Guangzhou, China, ³Guangdong Technology
Research Center for Traditional Chinese Veterinary Medicine and Natural Medicine, Guangzhou,
China, ⁴Guangdong Provincial Key Laboratory of Prevention and Control for Severe Clinical Animal
Diseases, Guangzhou, China, ⁵International Institute of Traditional Chinese Veterinary Medicine,
Guangzhou, China

Atopic dermatitis (AD) is a common chronic allergic skin disease characterized clinically by severe skin lesions and pruritus. *Portulaca oleracea* L. (PO) is a resourceful plant with homologous properties in medicine and food. In this study, we used two different methods to extract PO, and compared the therapeutic effects of PO aqueous extract (POAE) and PO ultrasound-assisted ethanol extract (POEE) on 2,4-dinitrochlorobenzene (DNCB)-induced AD mice. The results showed that in POAE and POEE, the extraction rates of polysaccharides were 16.95% and 9.85%, while the extraction rates of total flavonoids were 3.15% and 3.25%, respectively. Compared with AD mice, clinical symptoms such as erythema, edema, dryness and ulceration in the back and left ear were alleviated, and pruritus behavior was reduced after POAE and POEE treatments. The thickness of the skin epidermis was thinned, the density of skin nerve fibers labeled with protein gene product 9.5 (PGP9.5) was decreased, and mast cell infiltration was reduced. There was a decrease in blood lymphocytes, eosinophils and basophils, a significant decrease in spleen index and a noticeable decrease in serum immunoglobulin E (Ig E). POEE significantly reduced the concentration of the skin pruritic factor interleukin (IL)-31. POAE and POEE reduced the concentration of skin histamine (His), down-regulated mRNA expression levels of interferon- γ (Ifn γ), tumor necrosis factor- α (Tnf- α), thymic stromal lymphopoietin (Tslp) and IL-4, with an increase of Filaggrin (Flg) and Loricrin (Lor) in skin lesions. These results suggested that POAE and POEE may inhibit atopic response and alleviate the clinical symptoms of AD by inhibiting the expression of immune cells, inflammatory mediators and cytokines. PO may be a potential effective drug for AD-like diseases.

KEYWORDS

atopic dermatitis, *Portulaca oleracea* L., immunomodulation, anti-inflammatory, anti-pruritic, 2,4-dinitrochlorobenzene (DNCB)

Introduction

Atopic dermatitis (AD) is a common, chronic, inflammatory skin disease, which is often accompanied by severe pruritus and high recurrence rate. Children have the highest incidence and are prone to relapse in adulthood. According to an extensive epidemiological survey, the prevalence rate is about 15–30% for children and 2–10% for adults around the world (1). In recent years, the incidence of AD shows a rising trend (2).

The clinical symptoms of AD include severe pruritus, impaired skin barrier, edema, erythema, dryness, ulcers, etc. In addition, AD is a primary immune abnormality, with elevated serum immunoglobulin E (Ig E) and immune cell infiltration. Because of the obvious appearance of the lesions, the tendency of the disease to recur, and the high cost of long-term treatment, the quality of work and life of AD patients are seriously affected, and even their emotions are inevitably disturbed (3). Therefore, it is of great significance to find some potential therapeutic agents for AD with low economic burden and effective in relieving dermatitis symptoms.

The pathogenesis of AD is not completely clear. Studies have shown that AD is driven by defects in terminal keratin-forming cell differentiation and strong type 2 immune responses (4). Currently, clinical medications used to treat AD include basic moisturizing creams, external application therapies, vitamin D supplements, topical corticosteroids, oral anti-inflammatory and antihistamines (5, 6). Steroids and calcineurin inhibitors (cyclosporine, tacrolimus) are still the first choice of drugs in acute attacks of AD (7). However, there is still a large unmet need for novel therapeutic approaches as these drugs have serious side effects, including adrenal failure, skin atrophy, neurotoxicity, nephrotoxicity and skin canceration (8).

Herbs have been reported to improve the severity of symptoms such as skin lesions and pruritus in AD (9). Clinical studies have found that the use of herbal medicines, such as Xiao-Feng-San, *Glycyrrhiza uralensis* Fisch., and *Lonicera japonica* Thunb., reduces the frequency of corticosteroid use and decreases exposure to corticosteroids in children with AD (10). Given the heterogeneity of the disease and the limitations of studies, more research is needed to demonstrate the effectiveness of herbs for AD. *Portulaca oleracea* L. (PO), which is called longevity vegetable in folklore, a medicinal food homolog (11). External use of PO for treating skin injuries and dermatitis has also been reported extensively. In general, the role of PO is to stimulate the angiogenesis of injured skin, regulate the proliferation of skin fibroblasts, promote the production of collagen fibers in the skin, and accelerate wound healing in the skin (12, 13). Previous studies on the active ingredients have revealed that polysaccharides and flavonoids of PO play important roles in the treatment of various diseases (14). However, the underlying mechanisms are still unclear.

In this study, the aqueous and ultrasound-assisted ethanolic extracts of PO (POAE and POEE) were used to compare the

extraction rates of polysaccharides and total flavonoids. As well, we investigated the therapeutic effect of external application of PO on mice with AD-like lesions.

Materials and methods

Drug preparation

PO aqueous extract

PO (30 g), purchased from Guangzhou Nanbei Traditional Chinese Medicine Decoction Pieces Co., Ltd. (China), was first soaked in 300 mL of distilled water for 30 min. Then heated up to 180°C and maintained at 80°C for 30 min and filtered out the first extract. Repeat the above steps with another 300 mL of distilled water. Mix the extracts obtained. After concentrated to 30 mL by rotary evaporator, the aqueous extract of PO with the concentration of 1 g/mL was obtained and stored at 4°C. Our preliminary study found that 1 mg/mL POAE was more effective than 0.5 mg/mL POAE, so we chose this concentration as the PO extract concentration (Supplementary Figure 1).

PO ultrasound-assisted ethanol extract

PO (30 g) were broken to pieces and sieved through 60 pieces of mesh, dissolved in 600 mL of 70% ethanol, and extracted with ultrasound at 50°C for 40 min. The extract was filtered, and the upper layer of the solution was centrifuged and collected. After concentrated to 30 mL by rotary evaporator, the ethanol extract of PO with the concentration of 1 g/mL was obtained and stored at 4°C.

Hydrocortisone butyrate cream

0.1% hydrocortisone butyrate cream (HBC) was purchased from Shubang Pharmaceutical Co., Ltd. (China), as a positive control drug in this study.

Determination of polysaccharide and total flavonoid contents

The concentrations of polysaccharides in POAE and POEE were measured using a multimode reader (EnSight, United States) at a wavelength of 490 nm, compared with glucose. The absorbance was measured at 510 nm and compared with rutin to calculate the total flavonoid concentration in POAE and POEE. Polysaccharide and total flavonoid extraction rates were expressed as a percentage of polysaccharide and total flavonoid content and PO raw material mass. Anhydrous glucose standard (NO. MO309BS) purchased from Dalian Meilun Biotechnology Co., Ltd. (China), and rutin standard (NO. PRF21071301) was purchased from Chengdu Biopurify Phytochemicals Co., Ltd. (China).

Animals

Following AAALAC guidelines, all animal experimental procedures comply with the standards of the South China Agricultural University Experimental Animal Ethics Committee. The animal experimental procedures were approved by the Ethics Committee.

Six-week-old KM male mice, weighing 30 ± 2 g, purchased from the Experimental Animal Management Center of Southern Medical University. Animals were kept in the South China Agricultural University Laboratory Animal Center (SYXK 2019-0136) at a room temperature of $25 \pm 2^\circ\text{C}$ and relative humidity of $55 \pm 5\%$. Mice were free to feed and drink.

Sensitization and treatment of AD mice

After 7 days of adaptation, all mice were shaved on the back ($2.5\text{ cm} \times 2.5\text{ cm}$). The mice were randomly divided into 5 groups: Control, DNCB, HBC, POAE, POEE groups, 5 mice in each group.

Sensitization: 2% DNCB and 0.5% DNCB dissolved in a mixture of acetone and olive oil (3:1 v/v) (15, 16). 2% DNCB was challenged on the dorsal skin (200 μL) and left ear (100 μL) of the DNCB, HBC, POAE and POEE groups, followed by 0.5% DNCB every two days starting on day 3 for 4 weeks. Equal volumes of acetone and olive oil mixture were used as controls in Control group.

Intervention: Starting from the second week (day 8), each group of mice was given external drug intervention on the dorsal skin twice a day for 3 weeks (until day 28). POAE group was treated with 3 mL 1 g/mL POAE, POEE group was treated with 3 mL 1 g/mL POEE, HBC group was treated with 1 g 0.1% HBC, while Control and DNCB group was treated with 3 mL 0.9% normal saline (NS). At the end of the animal experiments, samples were collected as needed.

Clinical symptoms and SCORing of atopic dermatitis

Mental status, activity and mortality were observed and recorded for each group of mice. According to a previous study, dorsal skin severity scores were recorded weekly for AD mice based on four skin symptoms (erythema, edema, dryness and ulceration) (17). The scoring range indicators were 0 (none), 1 (mild), 2 (moderate) and 3 (severe). The specific symptom classification is shown in Table 1. The sum of the four symptom scores was calculated to assess SCORing of atopic dermatitis (SCORAD), with a maximum score of 12. In addition, the thickness of the skin lesion area and left ear of the mice were measured using electronic Vernier calipers (18). We got the skin images of the mice's dorsal surface with a camera after anesthesia.

TABLE 1 AD score reference (maximum score: 12).

Score 1	Erythema
0	No erythema
1	Faintly visible punctate erythema
2	Patchy red papules
3	Dark red irregularly raised
Score 2	Edema
0	No edema
1	Slight edema
2	Localized edema with pitting exudate
3	Massive edema, more oozing, crusting
Score 3	Dryness
0	No dryness
1	Slight dryness of epidermis
2	Moderately dry epidermis with peeling
3	Severe dryness of epidermis with flaking
Score 4	Ulceration
0	No ulceration
1	Mild epidermal ulceration
2	Moderate epidermal ulceration
3	Severe infected epidermal ulcers

Scoring of pruritic behavior

Pruritic behavior was observed. The pruritus score was defined by the duration of the pruritus behavior, that is, the time spent scratching and rubbing the skin of the ears and back with the limbs (16, 18, 19). On the last day of the experiment, the total duration of pruritic behavior of mice within 20 min was recorded with a high-definition camera. Scratching time less than 1.5 s was added 1 point each time; scratching time less than 3 s was added 2 points each time; scratching time more than 3 s was added 3 points each time; no scratching was scored 0 points. The total score was recorded as the pruritus score of mice.

Pathological histological analysis of skin lesions

The dorsal skin of mice was collected and fixed in 10% neutral formalin for more than 48 h. The tissues were made into paraffin-embedded sections and stained with hematoxylin and eosin (H&E) and toluidine blue (TB). The histological changes of skin pathology on the dorsal skin of mice were observed under a light microscope at $100 \times$ magnification. The thickness of the epidermis was measured, and the mast cell infiltration in the dermis was counted.

Immunofluorescence staining analysis

The growth of PGP9.5 nerve fibers in the dorsal lesions of mice were analyzed by immunofluorescence staining of skin paraffin sections and observed under a fluorescent microscope. PGP9.5 antibody was purchased from Wuhan Servicebio Technology Co., Ltd. (China). Under ultraviolet laser, cell nuclei showed blue light after DAPI treatment, and PGP9.5 showed red light under the labeling of fluorescent secondary antibody. The fluorescence area and intensity were analyzed using Image J software.

Calculation of spleen index

On the last day of the experiment, the spleens were weighed, and the splenic indices (spleen weight/body weight) were calculated.

Immune cell counting

Blood was collected into tubes with EDTA, and the numbers of lymphocytes, eosinophils and basophils were counted using a hematology analyzer (Mindray).

Enzyme-linked immunosorbent assay

The blood was collected and centrifuged at 3,000 r/min for 5 min, then the upper serum layer was separated and stored at -80°C . Serum levels of Ig E were determined using enzyme-linked immunosorbent assay (ELISA) kits (CUSABIO)¹ according to the manufacturer's instructions. Serum levels of Histamine (His) and IL-31 were measured by ELISA kit purchased from Shanghai Enzyme-linked Biotechnology Co., Ltd. (China).

¹ <https://www.cusabio.com/>

TABLE 2 Sequence of primers used for quantitative RT-PCR assay.

Gene	Forward primer (5'–3')	Reverse primer (5'–3')
β -Actin	TGCTGTCCCTGTATGCCTCTG	CTGTAGCCACGCTCGGTCA
Flg	CAATCCCACTCCAAACCATCTCCAG	GACTGTCTCTGCTCCTGATCC
Ifn- γ	CTCAAGTGGCATAGATGTGGAAG	TGACCTCAAACCTGGCAATACTC
IL-4	GGTCTCAACCCCAGCTAGT	GCCGATGATCTCTCTCAAGTGAT
Lor	TTACTCCTCTCAGCAGACCAGTCAG	CCTCCACAGCTACCACCTCCTC
Tnf- α	CTGATGAGAGGGAGGCCATT	GCCTCTTCTCATTCTGCTTG
Tslp	CTGCCATGATGAGGTGGTCTGAA	TCTGCTACGAATTGTACTGTCCT

Real-time quantitative PCR

Total tissue RNA was extracted using the RNA isolater Total RNA Extraction Reagent kit, and RNA was reverse transcribed to cDNA using the HiScript III RT SuperMix for qPCR (+ gDNA wiper) reverse transcription kit. The reaction system was configured and performed according to the ChamQ Universal SYBR qPCR Master Mix kit. These kits were purchased from Nanjing Vazyme Biotech Co., Ltd. (China). The primers were synthesized by Beijing Tsingke Biotechnology Co., Ltd. (China). The primer sequences are listed in Table 2. The relative expression of target genes was analyzed by the $2^{-\Delta\Delta\text{Ct}}$ method.

Statistical analysis

The experimental data were statistically analyzed using GraphPad Prism 7.0 software. Data comparison between two groups was analyzed by *t*-test. Multiple data groups were compared using one-way ANOVA and Tukey's multiple comparisons to analyze the variability between groups. $P < 0.05$ were considered statistically significant.

Results

Extraction rates of polysaccharides and total flavonoids from PO aqueous extract and PO ultrasound-assisted ethanol extract

Measurements of the phenol-sulfuric acid method showed that the polysaccharide extraction rates of POAE and POEE were 16.95% and 9.85%, respectively. The results of $\text{NaNO}_2\text{-Al}(\text{NO}_3)_3$ colorimetric method showed that the extraction rate of total flavonoids in POAE and POEE were 3.15% and 3.25%, respectively (Figures 1A,B). The above results indicated that the extraction rate of PO total flavonoids was similar, while the extraction rate of polysaccharides of POAE was better than that of POEE.

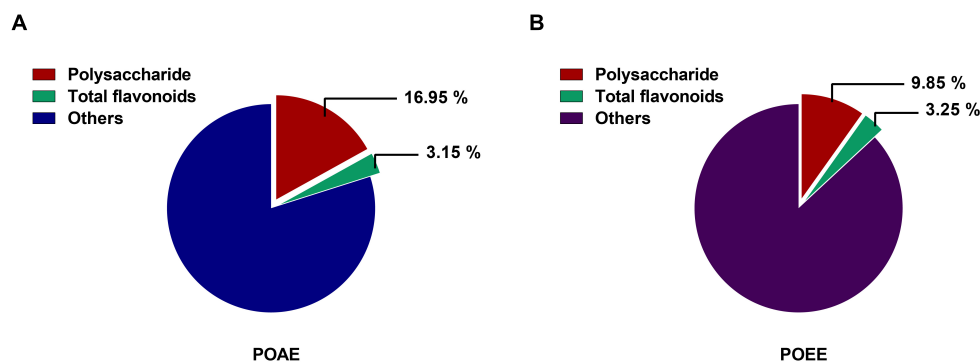


FIGURE 1

Polysaccharide and total flavonoid extraction rates of POAE and POEE in this study. (A) Polysaccharide and total flavonoid extraction rates of POAE. (B) Polysaccharide and total flavonoid extraction rates of POEE. Absorbance was measured at least 3 times and calculated based on the standard products (Glucose and Rutin). The data were expressed as mean.

PO aqueous extract and PO ultrasound-assisted ethanol extract significantly alleviate 2,4-dinitrochlorobenzene -induced AD clinical symptoms in mice

We established a model of AD-like lesions in KM mice induced by DNCB and used HBC as a positive drug to investigate the role of POAE and POEE in AD mice (Figure 2A). Photographs of the dorsal skin of mice (Figure 2B) and SCORAD scores (Figure 2C) showed that POAE and POEE interventions significantly alleviated the clinical symptoms of dorsal skin. Pruritus lasted longer in the DNCB group, while the scratching behavior was strongly reduced after POAE and POEE interventions, comparable to that of the Control group (Figure 2D). The thickness of the dorsal skin and the left ear were effectively reduced after POAE and POEE treatments (Supplementary Figure 2). Generally, POAE and POEE interventions alleviate the symptoms of skin lesion and pruritus in AD mice.

PO aqueous extract and PO ultrasound-assisted ethanol extract reduced the density of nerve fibers in the dorsal skin

Next, we took a more in-depth observation of the dorsal skin of the mice. H&E-stained sections showed significant epidermal thickening in DNCB mice, whereas there was no significant difference between POAE and POEE groups and Control group (Figures 3A,B). Immunofluorescence-labeled skin sections showed that the fluorescence area of protein gene product 9.5 (PGP9.5) in the dorsal skin tissue of the DNCB

group was obviously increased compared to Control group, indicating that repeated stimulation of the dorsal skin of mice by DNCB increased the density of nerve fibers. After treatment, the PGP9.5 fluorescence area was significantly reduced and nerve fiber density was decreased in the POAE and POEE groups compared with the DNCB group, which was remarkable (Figures 3C,D).

PO aqueous extract and PO ultrasound-assisted ethanol extract reduced the number of immune cells and abnormal increase in serum Ig E in AD mice

It is well-known that the spleen serves as the main organ of the body's immunity, and an enlarged spleen indicates the activation of an immune response in metaplastic diseases (20). We found a significant increase in spleen index in DNCB-induced AD mice, while there was a marked decrease in spleen index in AD mice after POAE and POEE treatments (Figure 4A). The number of lymphocytes, eosinophils and basophils was significantly increased in the AD mice of the DNCB group, while POAE and POEE interventions caused different decreases in the number of these immune cells (Figures 4B–F). TB-stained sections of the dorsal skin showed severe mast cell infiltration in the dermis in the DNCB group, while mast cells were greatly reduced in the POAE and POEE groups (Figures 4G,H). In addition, serum Ig E levels were increased in the DNCB group compared to the control group, which were an important clinical indicator of AD; while serum Ig E was significantly decreased in the POAE and POEE groups compared to DNCB-induced mice (Figure 4I). The results showed that POAE and POEE reduced the number of immune cells and serum Ig E levels in mice.

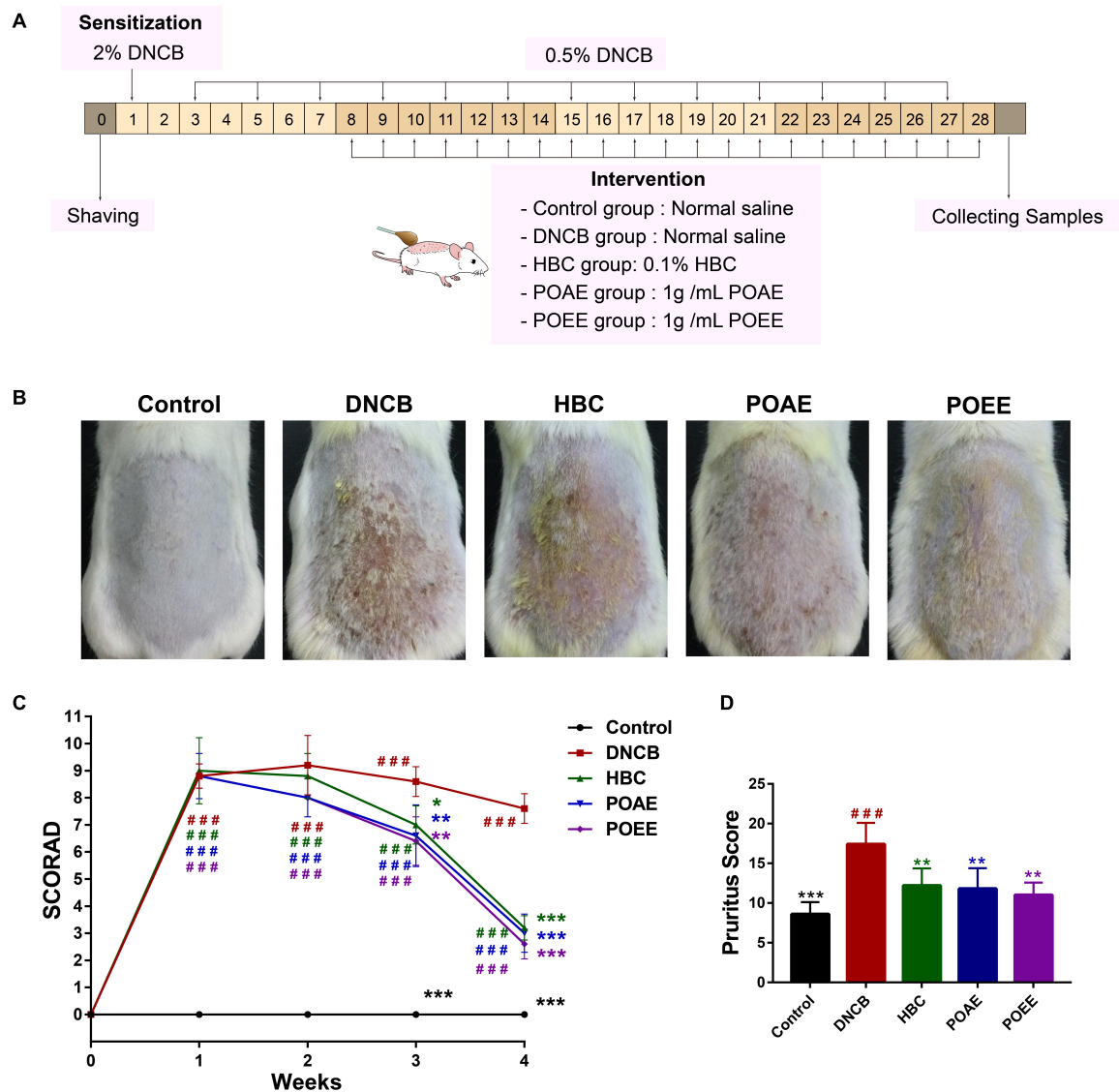


FIGURE 2

POAE and POEE significantly alleviate DNCB-induced AD clinical symptoms in mice. (A) Animal experiments. (B) Representative dorsal skin photographs of each group of mice. (C) SCORAD scores of each group of mice. (D) Pruritus scores of mice in each group. The data were expressed as mean \pm SD ($n = 5$ per group). ### $P < 0.001$, vs. control groups; * $P < 0.05$, ** $P < 0.01$, *** $P < 0.001$, vs. model (DNCB) groups.

PO aqueous extract and PO ultrasound-assisted ethanol extract inhibit skin lesions and pruritus-associated cytokines in AD mice

His is an important mediator of pruritus. Compared to the control group, DNCB induced an increase in skin His content in mice, while POAE and POEE were effective in reducing skin His concentration compared to the DNCB group (Figure 5A). In addition, the level of skin pruritic factor IL-31 was significantly

increased, and it was lower in the POEE group (Figure 5B). The relative mRNA expression of inflammatory factors in skin lesions showed that interferon- γ (Ifn- γ), tumor necrosis factor- α (Tnf- α), thymic stromal lymphopoietin (Tslp) and IL-4 were significantly increased in DNCB-induced AD mice, and the relative mRNA expressions of Ifn- γ , Tnf- α , Tslp and IL-4 were significantly decreased after POAE and POEE treatments (Figures 5C–F). In addition, the relative mRNA expression of Filaggrin (Flg) and Loricrin (Lor) was impaired in AD mice, whereas POAE and POEE increased the mRNA levels of skin barrier proteins Flg and Lor (Figures 5G,H). The above results showed that POAE and POEE reduced the levels of skin His and

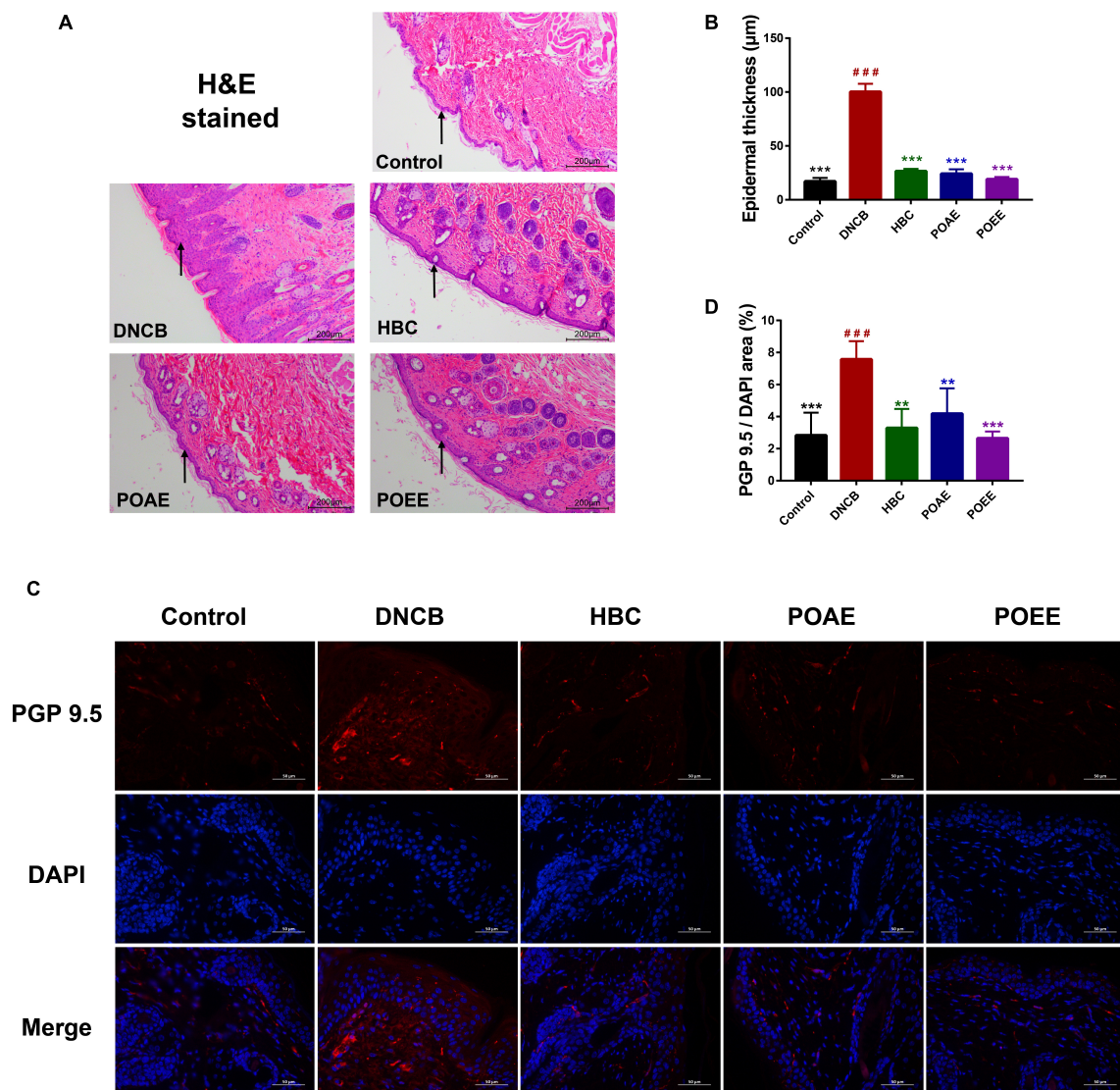


FIGURE 3

POAE and POEE reduced the density of nerve fibers in the dorsal skin. (A) Representative photographs of H&E staining of the dorsal skin of each group of mice (Scale bar: 200 μm). The black arrow indicates the epidermal layer of the skin. (B) Thickness of the epidermal layer of the dorsal skin of each group of mice ($n = 3$ per group). (C) Immunofluorescence staining of representative dorsal skin nerve fibers from each group of mice (Scale bar: 50 μm). The nuclei showed blue fluorescence after DAPI staining, and PGP9.5 showed red fluorescence under the labeling of fluorescent secondary antibody. (D) The ratio of PGP9.5/DAPI fluorescence area in each group of mice ($n = 4$ per group). The data were expressed as mean \pm SD. ### $P < 0.001$, vs. control groups; ** $P < 0.01$, *** $P < 0.001$, vs. DNCB (model) groups.

IL-31 and down-regulated the mRNA levels of skin lesion-related factors, thereby suppressing the excessive immune response to AD and increasing the expression of skin barrier proteins.

Discussion

PO has a high content of vitamins, minerals, omega-3 fatty acids, and is also rich in polysaccharides, flavonoids, alkaloids, terpenoids, and sterols. Thus, it is not only rich

in nutritional value, but also has excellent pharmacological properties, and has great potential for use under sustainable development strategies (21). Recent reports indicate that PO has neuroprotective, antibacterial, antidiabetic, antioxidant, anti-inflammatory, anti-ulcer and anticancer activities, and plays an important role in alleviating symptoms such as inflammation, fever, headache, and insomnia (22, 23). Moreover, PO can regulate the gut microbiota, promote probiotics and inhibit pathogenic bacteria (24). Several studies have shown that PO has strong immunomodulatory effects, improving T-helper (Th)

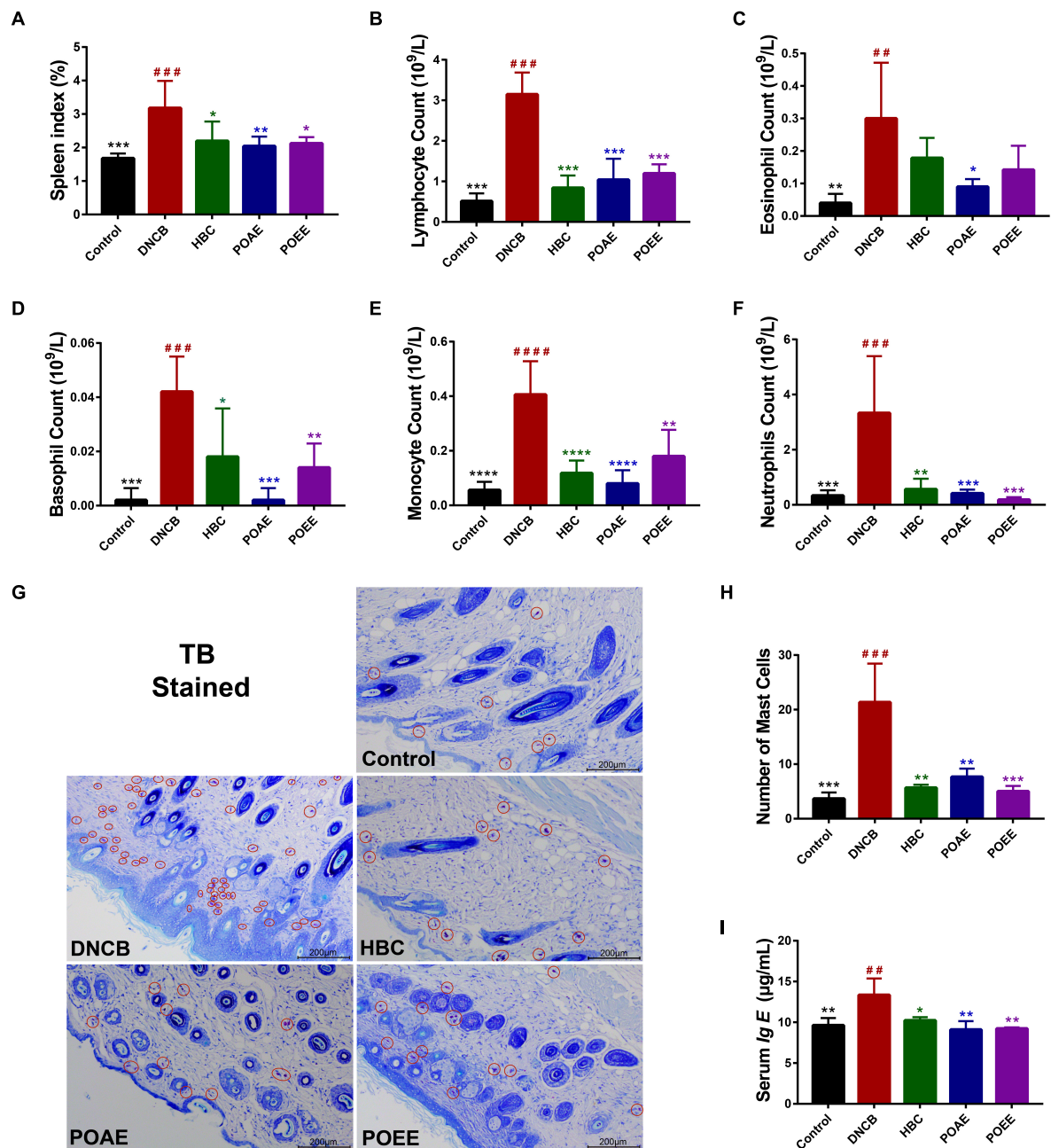


FIGURE 4
POAE and POEE reduced the number of immune cells and abnormal increase in serum Ig E in AD mice. **(A)** Spleen indices of mice in each group ($n = 5$ per group). **(B–F)** The number of lymphocytes, eosinophils, basophils, monocytes and neutrophils in each group of mice ($n = 5$ per group). **(G)** Pictures of representative dorsal skin TB staining of each group. Red circles mark some of the mast cells (Scale bar: 200 μm). **(H)** The number of mast cells in the dermis of each group ($n = 3$ per group). **(I)** Serum Ig E concentration of mice in each group ($n = 3$ per group). The data were expressed as mean \pm SD. ## $P < 0.01$, ### $P < 0.001$, #### $P < 0.0001$, vs. control groups; * $P < 0.05$, ** $P < 0.01$, *** $P < 0.001$, **** $P < 0.0001$, vs. model (DNCB) groups.

1/Th2 and Th2/regulatory T (Treg) balance and reducing Ig E levels, thus exerting anti-inflammatory effects (25–27).

It has been reported that external application of a mixture of herbal extracts can alleviate skin inflammation and restore skin barrier integrity in AD mice (28). Studies

show that Huanglian jiedu decoction can treat AD by modulating the antigen-presenting function of dendritic cells and attenuating T-lymphocyte activation, in turn exerting anti-inflammatory and anti-pruritic effects (29). Considering the abundant resources and numerous medicinal values of

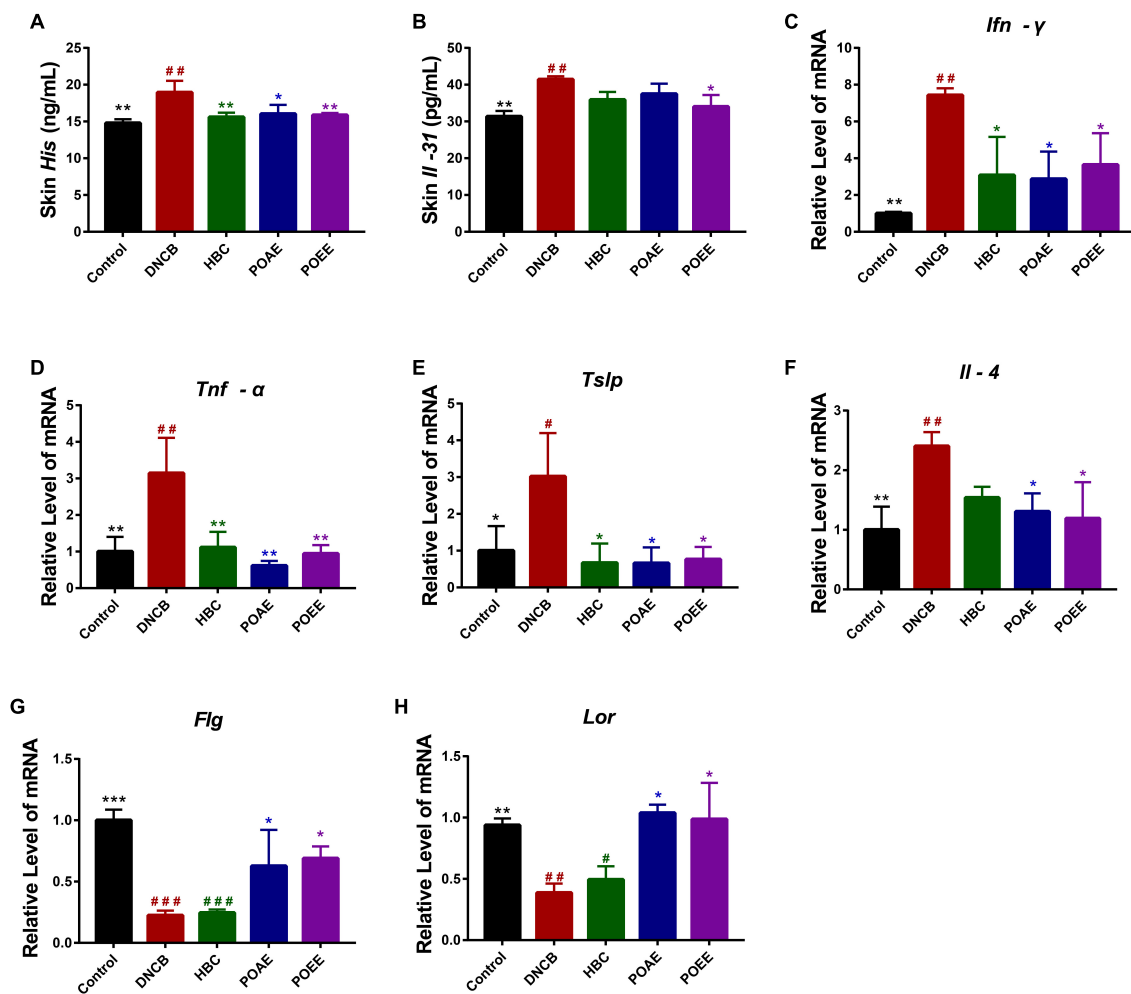


FIGURE 5

POAE and POEE inhibit skin lesions and pruritus-associated cytokines in AD mice. (A) Skin His concentrations in each group of mice. (B) Skin IL-31 concentrations in each group of mice. (C–H) Relative mRNA expression of *Ifn-γ*, *Tnf-α*, *Tslp*, *IL-4*, *Flg*, and *Lor* in each group of mice. The data were expressed as mean \pm SD ($n = 3$ per group). # $P < 0.05$, ## $P < 0.01$, ### $P < 0.001$, vs. control groups; * $P < 0.05$, ** $P < 0.01$, *** $P < 0.001$, vs. model (DNCB) groups.

PO, we wondered whether external application of PO could alleviate AD-like skin lesions. Evidently, our studies showed that PO significantly alleviated the clinical symptoms and pathological changes of AD.

AD is a chronic recurrent skin disease characterized by eczematous, inflammatory, and severe pruritus. Previous study found that children with a family history of allergic disease or a parental history of AD were more likely to develop AD (30). Since AD is a heterogeneous disease with unique clinical manifestations in different age and ethnic groups, its pathogenesis is not yet completely clarified (31). In general, the pathogenesis of AD includes both genetic and external environmental factors of the organism. Imbalance of the body's immune system, disruption of the skin barrier, induced infections and dysregulation of the skin microbiota, especially

Staphylococcus aureus, also contribute to the pathogenesis of AD (32).

It is reported that Ig E and reactive T cells contribute to the pathophysiological development of AD (33). The increased level of Ig E is a sign of AD occurrence, as Ig E binds to numerous immune cells *via* high-affinity Ig E receptors, mediating the development of allergic inflammation (34). In this study, external application of POAE and POEE significantly reduced the serum Ig E levels in DNCB-induced AD mice. Moreover, lymphocytes, eosinophils and basophils were also reduced to varying degrees in the intervened AD mice. Eosinophils and mast cells mediate a large number of inflammatory molecules, including histamine, leukotrienes and interleukins, causing pruritus and mossy lesions in patients with AD (35). We found that the thickened epidermal layer and mast cell infiltration in AD-like lesioned mice were alleviated after PO intervention.

As mentioned above, pruritus is one of the most prominent and difficult features of AD. On the one hand, acute scratching serves as an adaptive defense against pruritogenic substances; on the other hand, chronic pruritus exacerbates the pruritic-scratching circulation, continuously leading to hair loss and skin damage (36). The sensation of pruritus is triggered by excitation of the nerve endings of the sensory nerves in the skin; furthermore, inflammatory mediators released by immune cells or skin cells may also sensitize sensory nerves and further exacerbate pruritic sensations (37). There are two main signals of pruritus in AD, histamine-dependent and non-histamine-dependent pathways, which seem completely independent, although the two systems are closely related (38). Histamine is an important pruritic mediator that induces a histamine-dependent pruritic response by binding to H1 or H4 histamine receptors and activating transient receptor potential vanilloid-1 (TRAV1) channels (39). IL-4 can rapidly amplify neuronal sensitization, including histamine-induced scratching behavior in response to various pruritogens. Non-histamine-dependent pruritic mechanisms involve numerous cytokines, neuropeptides, endogenous secretory factors, and sensitized nervous system (40). Abnormal increase in cutaneous nerve fibers is thought to be an important factor in causing pruritus symptoms in AD. In our study, skin nerve fiber density in AD mice was explored by using immunofluorescence to visualize protein gene product 9.5 (PGP9.5)⁺ nerve fibers (41). The external application of PO reduced the skin nerve fiber density in AD mice, which was important in alleviating the exacerbation of skin lesions in AD mice caused by intense pruritus.

Abnormal immune responses in Th1/Th2 have been proposed to be critical in the development of AD. Most studies hold the view that Th2-type cells play a key role in acute AD and $\text{Tnf-}\alpha$ is required for antigen-specific Ig E production and induction of Th2-type cytokines and chemokines (42). Tslp is a key cytokine to promote the Th2 immune response that is essential for the regulation of downstream IL-4/IL-13 and Th2 differentiation (43). IL-4, secreted by Th2 cells, is a cytokine closely related to the biological function of AD and continuously activate mast cells to produce more Ig E (44). It has been shown that elevated Th2 cytokines IL-4/IL-13 in AD lesions inhibit keratinocyte differentiation markers (FLG, LOR, keratin 1, and keratin 10) to impair skin barrier function (45). Accordingly, down-regulation of IL-4 expression is an important strategy for the treatment of AD. Transient receptor potential A1 (TRPA1) is mainly involved in non-histamine such as IL-31, Tslp-related pruritus, which is associated with pruritic transmission in the central nervous system (46). IL-31 is produced by activated T cells and is capable of inducing nerve fiber elongation (47). IL-31 can not only promote the release of pruritus-related neuropeptides, but also regulate the pathogenesis of AD by activating TRPV1 + /TRPA1 + sensory neurons (48). In addition, overexpression of IL-31 induced AD-like lesions, and comparison of TH1/TH2 cytokines suggested

that IL-31 expression is associated with IL-4 and IL-13 but not $\text{Ifn-}\gamma$ (49). The chronic phase of AD exhibits a local Th1 response, mainly associated with $\text{Ifn-}\gamma$. The down-regulation of $\text{Ifn-}\gamma$ expression in patients after successful treatment of atopic dermatitis is remarkable (50). Mature Th1 cells secrete $\text{Ifn-}\gamma$ and promote more Th1 cell differentiation. Dominance of $\text{Ifn-}\gamma$ -producing T cells leads to chronicity of AD lesions and determines disease severity (51). Consistent with this, we observed that DNCB-induced AD-like lesion mice showed abnormal immune responses of Th1 and Th2, whereas external application of PO extract effectively reversed the significant elevation of serum Ig E, skin His, IL-31 levels and mRNA levels of IL-4, Tslp, $\text{Tnf-}\alpha$ and $\text{Ifn-}\gamma$, thereby alleviating AD-like atopic lesions and pruritus. These results suggest that PO is effective in ameliorating DNCB-induced AD in mice.

In conclusion, the main therapeutic targets in AD are IL-4/13, IL-5, IL-12/23, IL-17, IL-22, IL-31, IL-33, Tslp, and IgE (52). So far, what has been proven is that T cells are important drivers of AD and that the Th2 axis (especially IL-4/13, IL-31) contributes considerably to human AD. Therefore, most of the advanced AD drugs act on Th2 immunity, including the IL-4r antagonist Dupilumab, the biologic agent Dupixent targeting IL-4/13, the biologic agent Lebrikizumab targeting IL-13, and the humanized monoclonal anti-IL-31R α antibody Nemolizumab (53). In addition, oral JAK inhibitors are considered promising drugs because they block a range of cytokine, growth factor, and hormone receptor signaling pathways (54). The oral JAK inhibitors Baricitinib and Abrocitinib are highly anticipated (55). But predictably, these emerging drugs would be extremely expensive. So, it would be an utmost blessing for AD patients to find cheaper yet effective drugs. Evidently, our study strongly supports that PO is a promising herb for the management of AD.

According to the results of this study, we found that PO can repair the skin barrier function (Flg and Lor) and also broadly modulate cytokines. PO reduces the release of $\text{Tnf-}\alpha$ from macrophages, IL-4, IL-31, and Tslp from the Th2 axis, and $\text{Ifn-}\gamma$ from the Th1 axis, regulates the balance of immune cells, reduces the number of mast cells, lymphocytes, monocytes, neutrophils, eosinophils and basophils, reduces the secretion of His and Ig E, and thus alleviates allergic reactions, skin nerve fiber density and pruritus (38). We therefore speculate that the mechanism by which PO alleviates AD may be related to the inhibition of the release of Th1 and Th2 immune factors. PO plays an effective role in the management of AD lesion-like lesions by influencing the activity of immune cells through immunomodulatory effects. However, more detailed mechanisms need to be further investigated.

Conclusion

In summary, this study provides an insight into the beneficial effects of PO on AD, which can help develop effective

prevention or treatment strategies to combat AD and other inflammatory skin diseases. More detailed mechanistic, clinical and translational studies are needed to further substantiate the potential application of PO as a therapeutic agent for AD.

Data availability statement

The raw data supporting the conclusions of this article will be made available by the authors, without undue reservation.

Ethics statement

The animal study was reviewed and approved by the South China Agricultural University Experimental Animal Ethics Committee.

Author contributions

W-JL and S-NG designed the overall research experiments. W-JL, J-YH, S-PL, and X-PG performed the experiments. J-YH and X-PG analyzed the data. W-JL and J-YH wrote the manuscript. S-NG, J-BS, and WM revised the manuscript. All authors contributed to the article and approved the submitted version.

References

- Asher MI, Montefort S, Björkstén B, Lai CK, Strachan DP, Weiland SK, et al. Worldwide time trends in the prevalence of symptoms of asthma, allergic rhinoconjunctivitis, and eczema in childhood: ISAAC phases one and three repeat multicountry cross-sectional surveys. *Lancet*. (2006) 368:733–43. doi: 10.1016/S0140-6736(06)69283-0
- Klonowska J, Gleń J, Nowicki RJ, Trzeciak M. New cytokines in the pathogenesis of atopic dermatitis-new therapeutic targets. *Int J Mol Sci*. (2018) 19:3086. doi: 10.3390/ijms19103086
- Drucker AM, Wang AR, Li WQ, Sevetson E, Block JK, Qureshi AA. The burden of atopic dermatitis: summary of a report for the National Eczema Association. *J Invest Dermatol*. (2017) 137:26–30. doi: 10.1016/j.jid.2016.07.012
- Brunner PM, Guttman-Yassky E, Leung DY. The immunology of atopic dermatitis and its reversibility with broad-spectrum and targeted therapies. *J Allergy Clin Immunol*. (2017) 139:S65–76. doi: 10.1016/j.jaci.2017.01.011
- Chong M, Fonacier L. Treatment of eczema: corticosteroids and beyond. *Clin Rev Allergy Immunol*. (2016) 51:249–62. doi: 10.1007/s12016-015-8486-7
- Dattola A, Bennardo L, Silvestri M, Nisticò SP. What's new in the treatment of atopic dermatitis? *Dermatol Ther*. (2019) 32:e12787. doi: 10.1111/dth.12787
- Weidinger S, Novak N. Atopic dermatitis. *Lancet*. (2016) 387:1109–22. doi: 10.1016/S0140-6736(15)00149-X
- Yosipovitch G, Berger T, Fassett MS. Neuroimmune interactions in chronic itch of atopic dermatitis. *J Eur Acad Dermatol Venereol*. (2020) 34:239–50. doi: 10.1111/jdv.15973
- Tan HY, Zhang AL, Chen D, Xue CC, Lenon GB. Chinese herbal medicine for atopic dermatitis: a systematic review. *J Am Acad Dermatol*. (2013) 69:295–304. doi: 10.1016/j.jaad.2013.01.019
- Chen HY, Lin YH, Wu JC, Hu S, Yang SH, Chen JL, et al. Use of traditional Chinese medicine reduces exposure to corticosteroid among atopic dermatitis children: a 1-year follow-up cohort study. *J Ethnopharmacol*. (2015) 159:189–96. doi: 10.1016/j.jep.2014.11.018
- Nemzer B, Al-Taher F, Abshiru N. Phytochemical composition and nutritional value of different plant parts in two cultivated and wild purslane (*Portulaca oleracea* L.) genotypes. *Food Chem*. (2020) 320:126621. doi: 10.1016/j.foodchem.2020.126621
- Alves Barros AS, Oliveira Carvalho H, Dos Santos IVF, Taglialegna T, Dos Santos Sampaio TI, Duarte JL, et al. Study of the non-clinical healing activities of the extract and gel of *Portulaca pilosa* L. in skin wounds in wistar rats: a preliminary study. *Biomed Pharmacother*. (2017) 96:182–90. doi: 10.1016/j.biopha.2017.09.142
- Rashed AN, Afifi FU, Disi AM. Simple evaluation of the wound healing activity of a crude extract of *Portulaca oleracea* L. (growing in Jordan) in *Mus musculus* JVI-1. *J Ethnopharmacol*. (2003) 88:131–6. doi: 10.1016/S0378-8741(03)00194-6
- Berezutsky MA, Durnova NA, Sheremetyeva AS, Matvienko UA, Kurchatova MN. [Experimental studies of geroprotective and anti-aging effects of chemical compounds of *Portulaca oleracea* L. (review).]. *Adv Gerontol*. (2021) 34:715–20.
- Arakawa T, Sugiyama T, Matsuura H, Okuno T, Ogino H, Sakazaki F, et al. Effects of supplementary seleno-L-methionine on atopic dermatitis-like skin lesions in mice. *Biol Pharm Bull*. (2018) 41:1456–62. doi: 10.1248/bpb.b18-00349

Funding

This work was supported by the Specific Fund of State Key Laboratory of Dampness Syndrome of Chinese Medicine (SZ2021ZZ10 and SZ2021ZZ1005).

Conflict of interest

The authors declare that the research was conducted in the absence of any commercial or financial relationships that could be construed as a potential conflict of interest.

Publisher's note

All claims expressed in this article are solely those of the authors and do not necessarily represent those of their affiliated organizations, or those of the publisher, the editors and the reviewers. Any product that may be evaluated in this article, or claim that may be made by its manufacturer, is not guaranteed or endorsed by the publisher.

Supplementary material

The Supplementary Material for this article can be found online at: <https://www.frontiersin.org/articles/10.3389/fnut.2022.986943/full#supplementary-material>

16. Kim SH, Seong GS, Choung SY. Fermented *Morinda citrifolia* (Noni) alleviates DNCB-induced atopic dermatitis in NC/Nga mice through modulating immune balance and skin barrier function. *Nutrients*. (2020) 12:249. doi: 10.3390/nu12010249
17. Leung DY, Hirsch RL, Schneider L, Moody C, Takaoka R, Li SH, et al. Thymopentin therapy reduces the clinical severity of atopic dermatitis. *J Allergy Clin Immunol*. (1990) 85:927–33. doi: 10.1016/0091-6749(90)90079-J
18. Wang L, Xian YF, Hu Z, Loo SKF, Ip SP, Chan WY, et al. Efficacy and action mechanisms of a Chinese herbal formula on experimental models of atopic dermatitis. *J Ethnopharmacol*. (2021) 274:114021. doi: 10.1016/j.jep.2021.114021
19. Takano N, Arai I, Kurachi M. Analysis of the spontaneous scratching behavior by NC/Nga mice: a possible approach to evaluate antipruritics for subjects with atopic dermatitis. *Eur J Pharmacol*. (2003) 471:223–8. doi: 10.1016/S0014-2999(03)01828-4
20. Jabeen M, Boisgard AS, Danoy A, El Kholti N, Salvi JP, Bouliou R, et al. Advanced characterization of imiquimod-induced psoriasis-like mouse model. *Pharmaceutics*. (2020) 12:789. doi: 10.3390/pharmaceutics12090789
21. Srivastava R, Srivastava V, Singh A. Multipurpose benefits of an underexplored species purslane (*Portulaca oleracea* L.): a critical review. *Environ Manage*. (2021). doi: 10.1007/s00267-021-01456-z [Epub ahead of print].
22. Iranshahi M, Javadi B, Iranshahi M, Jahanbakhsh SP, Mahyari S, Hassani FV, et al. A review of traditional uses, phytochemistry and pharmacology of *Portulaca oleracea* L. *J Ethnopharmacol*. (2017) 205:158–72. doi: 10.1016/j.jep.2017.05.004
23. Farag MA, Shakour ZTA. Metabolomics driven analysis of 11 *Portulaca* leaf taxa as analysed via UPLC-ESI-MS/MS and chemometrics. *Phytochemistry*. (2019) 161:117–29. doi: 10.1016/j.phytochem.2019.02.009
24. Fu Q, Zhou S, Yu M, Lu Y, He G, Huang X, et al. *Portulaca oleracea* polysaccharides modulate intestinal microflora in aged rats in vitro. *Front Microbiol*. (2022) 13:841397. doi: 10.3389/fmicb.2022.841397
25. Askari VR, Rezaee SA, Abnous K, Iranshahi M, Boskabady MH. The influence of hydro-ethanolic extract of *Portulaca oleracea* L. on Th/Th balance in isolated human lymphocytes. *J Ethnopharmacol*. (2016) 194:1112–21. doi: 10.1016/j.jep.2016.10.082
26. Kaveh M, Eidi A, Nemati A, Boskabady MH. Modulation of lung inflammation and immune markers in asthmatic rats treated by *Portulaca oleracea*. *Avicenna J Phytomed*. (2017) 7:409–16.
27. Alfwaiares MA, Algefare AI, Afkar E, Salam SA, El-Moaty HIA, Badr GM. Immunomodulatory assessment of *Portulaca oleracea* L. extract in a mouse model of colitis. *Biomed Pharmacother*. (2021) 143:112148. doi: 10.1016/j.biopha.2021.112148
28. Ahn SH, Shin S, Do Y, Jo Y, Ryu D, Ha KT, et al. Topical application of galgeunhwanggeumhwangryeon-tang recovers skin-lipid barrier and ameliorates inflammation via flaggrin-thymic stromal lymphopoietin-interleukin 4 pathway. *Medicina (Kaunas)*. (2021) 57:1387. doi: 10.3390/medicina57121387
29. Xu Y, Chen S, Zhang L, Chen G, Chen J. The anti-inflammatory and anti-pruritus mechanisms of Huanglian jiedu decoction in the treatment of atopic dermatitis. *Front Pharmacol*. (2021) 12:735295. doi: 10.3389/fphar.2021.735295
30. Ravn NH, Halling AS, Berkowitz AG, Rinnov MR, Silverberg JJ, Egeberg A, et al. How does parental history of atopic disease predict the risk of atopic dermatitis in a child? A systematic review and meta-analysis. *J Allergy Clin Immunol*. (2020) 145:1182–93. doi: 10.1016/j.jaci.2019.12.899
31. Nomura T, Wu J, Kabashima K, Guttman-Yassky E. Endophenotypic variations of atopic dermatitis by age, race, and ethnicity. *J Allergy Clin Immunol Pract*. (2020) 8:1840–52. doi: 10.1016/j.jaip.2020.02.022
32. Geoghegan JA, Irvine AD, Foster TJ. *Staphylococcus aureus* and atopic dermatitis: a complex and evolving relationship. *Trends Microbiol*. (2018) 26:484–97. doi: 10.1016/j.tim.2017.11.008
33. Badloe FMS, De Vriese S, Coolens K, Schmidt-Weber CB, Ring J, Gutermuth J, et al. IgE autoantibodies and autoreactive T cells and their role in children and adults with atopic dermatitis. *Clin Transl Allergy*. (2020) 10:34. doi: 10.1186/s13601-020-00338-7
34. Nunomura S, Gon Y, Yoshimaru T, Suzuki Y, Nishimoto H, Kawakami T, et al. Role of the FcεRI beta-chain ITAM as a signal regulator for mast cell activation with monomeric IgE. *Int Immunol*. (2005) 17:685–94. doi: 10.1093/intimm/dxh248
35. Liu FT, Goodarzi H, Chen HY. IgE, mast cells, and eosinophils in atopic dermatitis. *Clin Rev Allergy Immunol*. (2011) 41:298–310. doi: 10.1007/s12016-011-8252-4
36. Wimalasena NK, Milner G, Silva R, Vuong C, Zhang Z, Bautista DM, et al. Dissecting the precise nature of itch-evoked scratching. *Neuron*. (2021) 109:3075–87.e2. doi: 10.1016/j.neuron.2021.07.020
37. Bautista DM, Wilson SR, Hoon MA. Why we scratch an itch: the molecules, cells and circuits of itch. *Nat Neurosci*. (2014) 17:175–82. doi: 10.1038/nn.3619
38. Mollanazar NK, Smith PK, Yosipovitch G. Mediators of chronic pruritus in atopic dermatitis: getting the itch out? *Clin Rev Allergy Immunol*. (2016) 51:263–92. doi: 10.1007/s12016-015-8488-5
39. Shim WS, Oh U. Histamine-induced itch and its relationship with pain. *Mol Pain*. (2008) 4:29. doi: 10.1186/1744-8069-4-29
40. Ohmura T, Hayashi T, Satoh Y, Konomi A, Jung B, Satoh H. Involvement of substance P in scratching behaviour in an atopic dermatitis model. *Eur J Pharmacol*. (2004) 491:191–4. doi: 10.1016/j.ejphar.2004.03.047
41. Feld M, Garcia R, Buddenkotte J, Katayama S, Lewis K, Muirhead G, et al. The pruritus- and TH2-associated cytokine IL-31 promotes growth of sensory nerves. *J Allergy Clin Immunol*. (2016) 138:500–8.e24. doi: 10.1016/j.jaci.2016.02.020
42. Iwasaki M, Saito K, Takemura M, Sekikawa K, Fujii H, Yamada Y, et al. TNF-α contributes to the development of allergic rhinitis in mice. *J Allergy Clin Immunol*. (2003) 112:134–40. doi: 10.1067/mai.2003.1554
43. Walker JA, McKenzie ANJ. T(H)2 cell development and function. *Nat Rev Immunol*. (2018) 18:121–33. doi: 10.1038/nri.2017.118
44. Matsunaga MC, Yamauchi PS. IL-4 and IL-13 inhibition in atopic dermatitis. *J Drugs Dermatol*. (2016) 15:925–9.
45. Dai X, Utsunomiya R, Shiraishi K, Mori H, Muto J, Murakami M, et al. Nuclear IL-33 plays an important role in the suppression of FLG, LOR, keratin 1, and keratin 10 by IL-4 and IL-13 in human keratinocytes. *J Invest Dermatol*. (2021) 141:2646–55.e6. doi: 10.1016/j.jid.2021.04.002
46. Wang F, Trier AM, Li F, Kim S, Chen Z, Chai JN, et al. A basophil-neuronal axis promotes itch. *Cell*. (2021) 184:422–40.e17. doi: 10.1016/j.cell.2020.12.033
47. Dillon SR, Sprecher C, Hammond A, Bilsborough J, Rosenfeld-Franklin M, Presnell SR, et al. Interleukin 31, a cytokine produced by activated T cells, induces dermatitis in mice. *Nat Immunol*. (2004) 5:752–60. doi: 10.1038/ni1084
48. Xu J, Zanvit P, Hu L, Tseng PY, Liu N, Wang F, et al. The cytokine TGF-β induces interleukin-31 expression from dermal dendritic cells to activate sensory neurons and stimulate wound itching. *Immunity*. (2020) 53:371–83.e5. doi: 10.1016/j.immuni.2020.06.023
49. Neis MM, Peters B, Dreuw A, Wenzel J, Bieber T, Mauch C, et al. Enhanced expression levels of IL-31 correlate with IL-4 and IL-13 in atopic and allergic contact dermatitis. *J Allergy Clin Immunol*. (2006) 118:930–7. doi: 10.1016/j.jaci.2006.07.015
50. Grewe M, Gyufko K, Schöpf E, Krutmann J. Lesional expression of interferon-gamma in atopic eczema. *Lancet*. (1994) 343:25–6. doi: 10.1016/S0140-6736(94)90879-6
51. Grewe M, Bruijnzeel-Koomen CA, Schöpf E, Thepen T, Langeveld-Wildschut AG, Ruzicka T, et al. A role for Th1 and Th2 cells in the immunopathogenesis of atopic dermatitis. *Immunol Today*. (1998) 19:359–61. doi: 10.1016/S0167-5699(98)01285-7
52. Langan SM, Irvine AD, Weidinger S. Atopic dermatitis. *Lancet*. (2020) 396:345–60. doi: 10.1016/S0140-6736(20)31286-1
53. Newsom M, Bashyam AM, Balogh EA, Feldman SR, Strowd LC. New and emerging systemic treatments for atopic dermatitis. *Drugs*. (2020) 80:1041–52. doi: 10.1007/s40265-020-01335-7
54. Schwartz DM, Kanno Y, Villarino A, Ward M, Gadina M, O'Shea JJ. JAK inhibition as a therapeutic strategy for immune and inflammatory diseases. *Nat Rev Drug Discov*. (2017) 16:843–62. doi: 10.1038/nrd.2017.201
55. Drucker AM, Morra DE, Prieto-Merino D, Ellis AG, Yiu ZZN, Rochwerger B, et al. Systemic immunomodulatory treatments for atopic dermatitis: update of a living systematic review and network meta-analysis. *JAMA Dermatol*. (2022) 158:523–32. doi: 10.1001/jamadermatol.2022.0455



OPEN ACCESS

EDITED BY

Guiyan Yang,
University of California, Davis,
United States

REVIEWED BY

Hongxiu Diao,
China Agricultural University, China
Tong-Fei Li,
Hubei University of Medicine, China

*CORRESPONDENCE

Jing Dong
dongjing9834@syau.edu.cn
Lin Li
lilin619619@syau.edu.cn

SPECIALTY SECTION

This article was submitted to
Nutritional Immunology,
a section of the journal
Frontiers in Nutrition

RECEIVED 21 June 2022

ACCEPTED 29 July 2022

PUBLISHED 25 August 2022

CITATION

Huang X, Wang Y, Yang W, Dong J and
Li L (2022) Regulation of dietary
polyphenols on cancer cell pyroptosis
and the tumor immune
microenvironment.
Front. Nutr. 9:974896.
doi: 10.3389/fnut.2022.974896

COPYRIGHT

© 2022 Huang, Wang, Yang, Dong and
Li. This is an open-access article
distributed under the terms of the
[Creative Commons Attribution License
\(CC BY\)](https://creativecommons.org/licenses/by/4.0/). The use, distribution or
reproduction in other forums is
permitted, provided the original
author(s) and the copyright owner(s)
are credited and that the original
publication in this journal is cited, in
accordance with accepted academic
practice. No use, distribution or
reproduction is permitted which does
not comply with these terms.

Regulation of dietary polyphenols on cancer cell pyroptosis and the tumor immune microenvironment

Xiaoxia Huang^{1,2}, Yao Wang^{1,2}, Wenhui Yang^{1,2}, Jing Dong^{1,2*}
and Lin Li^{1,2*}

¹College of Animal Science and Veterinary Medicine, Shenyang Agricultural University, Shenyang, China, ²Key Laboratory of Livestock Infectious Diseases, Ministry of Education, Shenyang Agricultural University, Shenyang, China

Cancer is a major public health problem that threatens human life worldwide. In recent years, immunotherapy has made great progress in both clinical and laboratory research. But the high heterogeneity and dynamics of tumors makes immunotherapy not suitable for all cancers. Dietary polyphenols have attracted researchers' attention due to their ability to induce cancer cell pyroptosis and to regulate the tumor immune microenvironment (TIME). This review expounds the regulation of dietary polyphenols and their new forms on cancer cell pyroptosis and the TIME. These dietary polyphenols include curcumin (CUR), resveratrol (RES), epigallocatechin gallate (EGCG), apigenin, triptolide (TPL), kaempferol, genistein and moscatilin. New forms of dietary polyphenols refer to their synthetic analogs and nano-delivery, liposomes. Studies in the past decade are included. The result shows that dietary polyphenols induce pyroptosis in breast cancer cells, liver cancer cells, oral squamous cells, carcinoma cells, and other cancer cells through different pathways. Moreover, dietary polyphenols exhibit great potential in the TIME regulation by modulating the programmed cell death protein 1(PD-1)/programmed death-ligand 1 (PD-L1) axis, enhancing antitumor immune cells, weakening the function and activity of immunosuppressive cells, and targeting tumor-associated macrophages (TAMs) to reduce their tumor infiltration and promote their polarization toward the M1 type. Dietary polyphenols are also used with radiotherapy and chemotherapy to improve antitumor immunity and shape a beneficial TIME. In conclusion, dietary polyphenols induce cancer cell pyroptosis and regulate the TIME, providing new ideas for safer cancer cures.

KEYWORDS

tumor immune microenvironment, dietary polyphenols, pyroptosis, curcumin, antitumor immunity

Introduction

The incidence of cancer has continually risen to 25% since the 20th century. The ever-increasing incidence of cancer is associated with increased production patterns, lifestyles, and life expectancy (1). According to the latest projections from the American Cancer Bureau, 1,918,030 people will be diagnosed with cancer every day in the United States in 2022. In the end, 609,630 people will die of cancer (2). Going back to the nature of cancer itself, cancer can originate in any organ and structure of the body. Unlike other cells, cancer cells can continue to proliferate, replicate indefinitely, and resist death. Even cancer cells can lure immune cells to escape immune evasion (3). Therefore, it is especially difficult to cure cancer. As the three most important treatments, surgery, radiotherapy and chemotherapy have long been and will continue to be the weapons in the fight against cancer. However, all three methods have their own shortcomings and limitations. There is an urgent need to develop more effective anticancer approaches.

Cancer treatment has made landmark achievements in the past decade. In fact, cancer is not a direct cause of death. The weakened immunity and complications of cancer are. Immunotherapy aims to promote the “rebuilding” of the immune system. Some cancer-fighting immune cells are engineered to fight cancer. This involves a new concept of the TIME. In short, the TIME refers to the microenvironment formed by the interaction of tumor cells and immune cells. Some immune checkpoints and cytokines are also included. The TIME is the foundation of immunotherapy. In recent years, research related to immunotherapy has grown exponentially. Clinically, dendritic cells (DC) vaccines, CAR-T cell therapy, adoptive cell transfer, and immune checkpoint inhibitors have achieved surprising results (4).

Immunotherapy is not perfect due to tumor heterogeneity and dynamics. Therefore, it is particularly important to deepen the understanding of the TIME and to find drugs to enhance anti-tumor immunity. In view of this situation, dietary polyphenols have attracted the attention of some researchers due to their superior anti-inflammatory, anticancer, and immunomodulatory functions. Moreover, dietary polyphenols are widely present in everyday foods. They are safe and easily available.

Pyroptosis is a type of programmed cell death. Pro-inflammatory is the most significant feature of pyroptosis that distinguishes it from other programmed cell death such as apoptosis and autophagy (5). Is it possible to artificially induce cancer cell pyroptosis to make cancer regress? This issue is widely discussed. In the study, it is surprisingly found that dietary polyphenols not only induce cancer cell pyroptosis, but also drive a favorable anticancer immunity in the TIME.

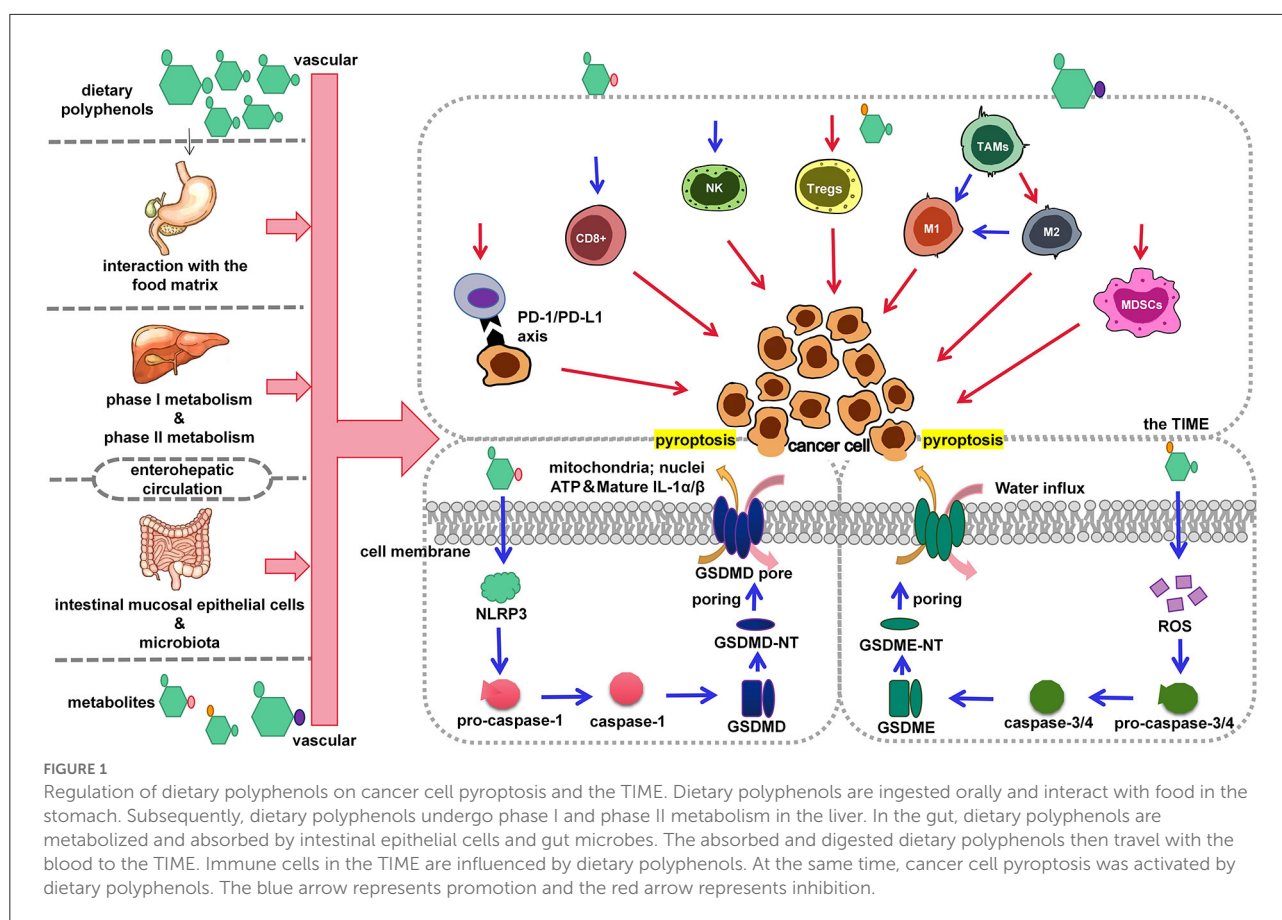
Pyroptosis

Pyroptosis is an inflammatory programmed cell death performed by a gasdermin (GSDM) protein family. When pyroptosis is activated, GSDM is cleaved into an auto-inhibitory C-terminal and an active N-terminal (NT). GSDM-NT then punches holes in the cell membrane, causing the cell to swell until it bursts. And a large amount of cellular contents, such as pro-inflammatory factors and lysosomes, are released, resulting in an inflammatory cascade (see Figure 1).

GSDM protein family includes GSDMA, GSDMB, GSDMC, GSDMD, and GSDME. In cancer, GSDMD and GSDME are the most studied. GSDMD induces pyroptosis mainly through two pathways (6). In the classical pyroptosis pathway, inflammasomes recognize pathogen-associated molecular patterns (PAMPs) or damage associated molecular pattern molecules (DAMPs). Then caspase-1 is activated and upregulated, and cleaves GSDMD into GSDMD-NT. This is the first pyroptosis pathway to be studied. In the non-canonical pyroptotic pathway, GSDMD cleavage is performed by caspase-4, 5 (human) and caspase-11 (mouse). Like GSDMD, GSDME also has two pathways. Typically, chemotherapeutic drugs induce caspase-3 to cleave GSDME to perform pyroptosis (7). Recently granzyme B (GZMB) was found to cleave GSDME at D270 to induce pyroptosis instead of caspase-3 (8).

Each GSDM protein has a high degree of expression variability and tissue specificity (8). This is rare in mammals. In different cancers, GSDMD and GSDME have different expression levels and functions. In gastric cancer cells, GSDMD is underexpressed and promotes proliferation (9). In non-small cell carcinoma, GSDMD is highly expressed and indicates higher invasiveness (10). In human colorectal cancer, GSDMD is underexpressed, which is detrimental to patient survival (11). In addition, high expression of GSDMD is associated with poor prognosis of lung adenocarcinoma and osteosarcoma (12). It can be seen that the expression and role of GSDMD in cancer are complex and variable. Even the subcellular localization of GSDMD affects cancer progression and immune response (13). Therefore, the idea of targeting GSDMD to induce cancer cell pyroptosis requires more careful selection and more in-depth exploration.

Different from GSDMD, GSDME acts more as a tumor suppressor. GSDME is normally expressed in the heart, kidney and brain. In most cancers, epigenetics and mutations lead to silencing of the GSDME gene (14). Different expression levels of GSDME determine whether cancer cells tend to apoptosis or pyroptosis during chemotherapy. In cancer cells with high expression of GSDME, caspase-3 specifically cleaves GSDME to convert apoptosis into pyroptosis (7, 15). However, caspase-3 tends to induce apoptosis in cancer cells with low GSDME expression. This phenomenon provides a new idea for anti-apoptotic cancer therapy. In addition to inhibiting cancer



cell proliferation, GSDME promotes immune cell infiltration (16, 17). Its expression in tumors converts immunologically “cold” tumors into “hot” tumors, thereby activating antitumor immunity (18).

GSDMA, GSDMB, GSDMC are less studied in cancer. But that doesn’t mean they are not important (see Table 1). Using drugs to induce pyroptosis of cancer cells is an important research direction at present. Various studies have shown that pyroptosis has broad prospects in cancer therapy.

TIME

The TIME is a complex ecosystem that acts as a double-edged sword in the progression of cancer. On the one hand, antitumor cells such as NK cells and cytotoxic T lymphocytes (CTLs, mainly CD8+ T cells) can identify and eliminate cancer cells. They play a role in cancer immune monitoring (21–23). On the other hand, immunosuppressive cells such as regulatory T cells (Tregs), TAMs, and myeloid-derived suppressor cells (MDSCs) protect cancer cells by evading immune surveillance. Subsequently, cancer cells can continue to invade, metastasize and induce angiogenesis (21–23). At the same time, cancer cells can induce, expand and recruit a

large number of tumor-promoting myeloid cells to establish a tumor immunosuppressive microenvironment by driving immunosuppression, regulating the generation of immune cell subtypes (21, 22). With the joint efforts of anti-tumor immune cells and cancer cells, cancer develops to malignant. However, the role of immune cells in the TIME is not immutable. For example, TAMs, signals in the TIME can directly affect the differentiation of TAMs and polarization between M1 and M2. The interaction between antitumor cells, immunosuppressive cells, and tumor cells is mainly achieved through exosomes, chemokines, and cytokines (see Figure 2) (24–31). This interaction plays a key role in the development of cancer.

All kinds of evidence show that pyroptosis is closely related to the TIME. For example, GSDMB/E can induce pyroptosis after specific cleavage by GZM secreted by CTLs. It was also recently found that macrophage-derived TNF- α activates caspase-8 to cleave GSDMC, resulting in cancer cell pyroptosis (20). However, the role of pyroptosis in the TIME is ambiguous. On the one hand, inflammatory factors released accompanying cancer cell pyroptosis form a chronic inflammatory microenvironment, including NLRP3, IL-18 and IL-1 β . This chronic inflammatory microenvironment has been

TABLE 1 GSDMs and their pathway of pyroptosis.

GSDMs	Pathway	References
GSDMB	CTLs/GZMA/GSDMB	(19)
GSDMC	Caspase-8/GSDMC	(20)
GSDMD	PAMPs or DAMPs/caspase-1/GSDMD LPS/caspase-4, 5, 11/GSDMD	(6)
GSDME	Chemotherapy drugs/caspase-3/GSDME CTLs/GZMB/GSDME	(7, 8)

shown to help cancer cells evade innate immune responses and promote cancer progression (10, 32–36). On the other hand, pyroptosis triggers strong antitumor immunity. Pyroptosis significantly increases the accumulation of immune cells and immune factors in solid tumors (37–39). Targeting pyroptosis and stimulating the TIME is a new idea for cancer treatment (40, 41).

The PD-1/PD-L1 axis is a core immunosuppression pathway in the TIME. For a long time, the PD-1/PD-L1 axis has been widely studied due to its immune checkpoint function. However, non-immune checkpoint functions of the PD-1/PD-L1 axis have been identified in studies of pyroptosis. Antibiotic chemotherapeutics induce GSDMC-mediated pyroptosis in hypoxic tumor environments by upregulating the nPD-L1/pro-signal transducer and activator of transcription 3 (p-STAT3) complex (20). In addition, the inflammatory environment created by pyroptosis may enhance the efficacy of anti-PD-L1 therapy. Whether pyroptosis have adverse effects on the immunity of cancer patients? No clear conclusions have been drawn. Is there a substance that can induce cancer cell pyroptosis, and promote anti-tumor immunity at the same time? Dietary polyphenols caught our eye.

Dietary polyphenols

Polyphenols, which literally means “having multiple phenolic groups,” are mostly found in plant foods. They are widely found in the daily human diet, including nuts, vegetables, fruits, dark chocolate, tea, red wine, and some natural Chinese herbal medicines. They are called “the seventh type of nutrient.” Most natural dietary polyphenols exist in the form of glycoside esters or free aglycones and are biotransformed mainly in the gastrointestinal tract, liver, and gut microbiota (see Table 2) (42–54). Due to factors such as chemical structure and biometabolic properties of dietary polyphenols, their low bioavailability has become a major factor that limits their efficacy *in vivo* and in clinical trials. Chinese herbal medicines rich in polyphenols have been widely used clinically. For example, turmeric, *Polygonum cuspidatum*, and *Tripterygium wilfordii* are used to treat cardiovascular disease, rheumatoid arthritis, and systemic lupus

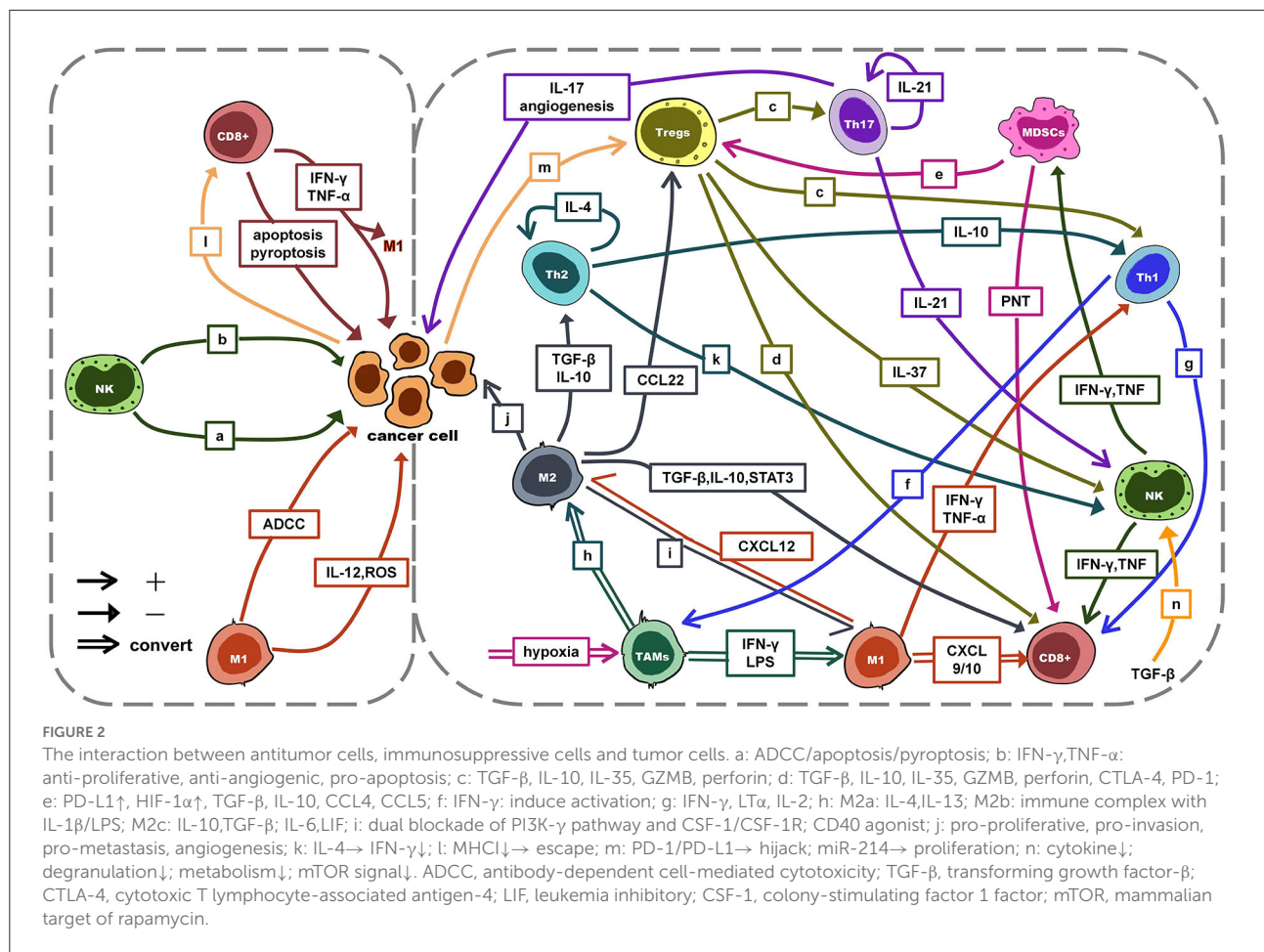
erythematosus (55, 56). In recent years, dietary polyphenols have been proven to have a wide range of biological activities. And their effective anti-inflammatory, antioxidant, anticancer, immunomodulatory, and cardiovascular protective properties have made them widely studied and used in food additives, skin care, medicine, health care (57). The anticancer properties of dietary polyphenols are mainly manifested in inhibiting tumor development (proliferation, growth, invasion, metastasis, and angiogenesis), regulating programmed cell death (apoptosis and pyroptosis), inhibiting chemoresistance, enhancing anticancer immune response, and regulating the TIME. In this review, we focus on the properties of dietary polyphenols that induce pyroptosis and regulate the TIME in cancer.

Regulation of various dietary polyphenols on cancer cell pyroptosis

Clinically, insufficient intake of dietary polyphenols does not cause a certain disease. However, dietary polyphenol intake is positively correlated with body health (58). As the study of pyroptosis becomes more and more extensive, the inner link between pyroptosis and disease is being revealed. It was found that dietary polyphenols have different effects on pyroptosis in different diseases. Microglia are phagocytic cells that reside in the brain. They play an important role in the immune response after central nervous system injury. Studies have shown that dietary polyphenols protect microglia by inhibiting pyroptosis. This is beneficial for Parkinson’s patients and those with spinal cord injuries (59–61). In addition, dietary polyphenols can reduce cardiomyocyte pyroptosis caused by chemotherapeutic drugs (doxorubicin) and adverse environment (ischemia/hypoxia) (62, 63). Studies have also reported that dietary polyphenols inhibit the pathological pyroptosis of liver and kidney cell (64, 65). Dietary polyphenols reduce cell pyroptosis induced by toxic heavy metals. It is of great significance for heavy metal exposure-related diseases. Therefore, we can conclude that dietary polyphenols protect the body by resisting pyroptosis. However, in cancer, dietary polyphenols tend to induce cancer cell pyroptosis to promote the body’s victory over cancer. In this section, we discuss how dietary polyphenols induce cancer cell pyroptosis (see Figure 1).

Dietary polyphenols induce GSDMD-mediated pyroptosis of cancer cells

CUR induces pyroptosis in MCF-7 breast cancer cells through the autophagy/cathepsin B (CTSB)/NLRP3/caspase-1/GSDMD signaling pathway (66). Anthocyanin activates



pyroptosis of Tca8113 and SCC15 oral squamous cell carcinoma cells through the NLRP3/caspase-1/GSDMD pathway. Besides, anthocyanin inhibits cancer cell viability, invasion, and metastasis (67). Similar to anthocyanin, chrysophanol up-regulated the expression of NLRP3 in gastric cancer cells. Subsequently, the caspase-1/GSDMD pathway is activated to induce cancer cell pyroptosis (68).

Dietary polyphenols induce GSDME-mediated pyroptosis of cancer cells

By treating different head and neck cancer cells with TPL, it has been found that TPL selectively induced pyroptosis in an HK1 squamous cell carcinoma cell line and a FaDu hypopharyngeal carcinoma cell line. This pyroptosis was achieved by inhibiting the expression of c-myc and mitochondrial hexokinase II (HK-II) in cancer cells, leading to the activation of the BAD/BAX-caspase-3 cascade, and then cleaves GSDME (69). CUR up-regulates

ROS levels, down-regulates pro-caspase-3 expression, and up-regulates GSDME-NT expression in a time- and dose-dependent manner to promote pyroptosis in HepG2 hepatoma cells (70). Kaempferol has been shown to trigger GSDME-mediated U87 MG and U251 glioblastoma cell line pyroptosis by inducing high levels of ROS autophagy and activating inflammasome/caspase-1/IL-1 β signaling *in vitro* and *in vivo* experiments (71). In another study on glioblastoma, researchers used genomic data to find that human gliomas express higher levels of GSDME than normal brains. Subsequently, *in vivo* and *in vitro* tests were carried out. They found that galangin induces GSDME-mediated pyroptosis in glioblastoma cells (72). Neobractatin is a kind of dietary polyphenol extracted from *Garcinia bracteata*. In esophageal cancer cells with high GSDME expression, neobractatin induces pyroptosis through the caspase-3/GSDME pathway. After GSDME was knocked out, pyroptosis transformed into apoptosis. Neobractatin treatment of esophageal cancer showed significant tumor regression (73). *Spatholobus suberectus* Dunn is called “Ji Xue Teng” in Chinese. Its percolation extract contains various dietary polyphenols such as catechin, procyanidin

B2, epicatechin, genistein, and formononetin. *Spatholobus suberectus* Dunn percolation extract induced pyroptosis of triple-negative breast cancer cells is also mediated by GSDME. However, GSDME is activated by caspase-4 rather than caspase-1 (74).

Related research on dietary polyphenol-induced pyroptosis of cancer cells

In some studies, dietary polyphenols have been shown to induce cancer cell pyroptosis. But the pyroptosis pathway was not revealed. These findings are also included in this review.

CUR delivers a double whammy against malignant mesothelioma cells. It induces pyroptosis through activation of caspase-1 by ROS. Moreover, CUR significantly down-regulated the expression levels of inflammasome-related genes such as NF- κ B, toll-like receptor (TLR), and IL-1 β (75). Researchers linked CUR to sound photodynamic therapy (SPDT). *In vitro* experiments showed that HepG2 cells underwent pyroptosis and apoptosis with CUR-PLGA-MB-SPDT (CUR-loaded poly (L-lactide-co-glycolide)-microbubble (MB)-mediated SPDT) treatment. The underlying mechanism is related to the loss of mitochondrial membrane potential (MMP) and the increase of ROS (76).

Moscaticin and RES can act as radiosensitizers in combination with 1 Gy X-ray or 200 J/m² UV-C radiation. Overlapping cell death pathways were activated by this combination in HepG2, SH-SY5Y and HaCaT cell lines, including necroptosis and pyroptosis (77). Moscatiline induces immunogenic death of cancer cells. The combination of Moscatiline and radiation induces pyroptosis of cancer cells, eventually leading to necroptosis (77). These findings validate the fact that dietary polyphenols induce cancer cell pyroptosis (see Table 3).

In fact, dietary polyphenols induce not only cancer cell pyroptosis but also various regulated cell deaths such as apoptosis, ferroptosis and autophagy (78–80). While one of cell death is inhibited, dietary polyphenols enhance other cell death (72). This is due to the crosstalk between different cell deaths. Therefore, targeting pyroptosis may be a potential therapy for some apoptosis-resistant cancer. And as mentioned in the section 3, pyroptosis may have a positive effect on the TIME. Taken together, targeting cancer cell pyroptosis is undoubtedly important and meaningful. So, we focused on the role of dietary polyphenols on cancer cell pyroptosis in this review. However, it is extremely important that dietary polyphenol-induced cancer cell death is not single.

Regulation of various dietary polyphenols on the TIME

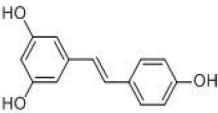
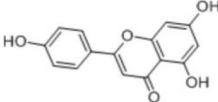
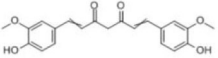
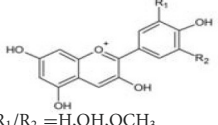
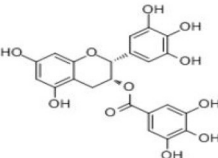
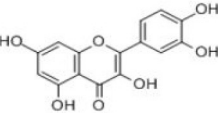
Dietary polyphenols shape an advantageous TIME by modulating the PD-1/PD-L1 axis

Among all immune checkpoint inhibition points, the PD-L1/PD-1 axis was the most well-studied. Because of its value as a therapeutic target for patients with multiple malignancies and advanced cancers, the PD-L1/PD-1 axis has received extensive attention. PD-L1 binds to PD-1 on the surface of antigen-specific T cells, and suppress antitumor immunity and maintain self-tolerance by regulating the number and activity of antigen-specific T cells in the TIME (81). Some studies have shown that dietary polyphenols can regulate the PD-1/PD-L1 axis between tumor cells and immune cells, driving the TIME to develop in an antitumor direction.

Studies have found that RES directly destroys the N-linked glycan modification and dimerization of PD-L1 in JIMT-1 breast cancer cells, inhibits the correct localization of glycosylated PD-L1 to the cell membrane, blocks the PD-1/PD-L1 axis between CTLs and cancer cells. The destruction of PD-1/PD-L1 axis by RES reduces the immune escape of cancer cells and enhances the immune activity of CTLs (82). RES upregulated PD-L1 expression in lung cancer cells *in vitro* and significantly induced apoptosis in Jurkat T cells with high PD-1 expression. The mechanism is related to the activation of the canonical Wnt signaling pathway and the reduction of IFN- γ in Jurkat T cells (83). Both luteolin and apigenin can inhibit STAT3 phosphorylation in non-small cell lung cancer (NSCLC) cells, down-regulate IFN- γ -induced PD-L1 expression, increase the activity and function of CD8⁺ T cells, and enhance the infiltration of CD8⁺ T cells in tumors (84). Like luteolin and apigenin, CUR can reduce STAT1 phosphorylation and inhibit IFN- γ -induced PD-L1 up-regulation in A375 human melanoma cells *in vitro* (85). For tongue squamous cell carcinoma, CUR down-regulates PD-L1 expression *in vitro* and *in vivo* and inhibits immunosuppressive signaling. CUR also increases CD8⁺ T cells in immune infiltration, promotes anti-tumor immunity (86).

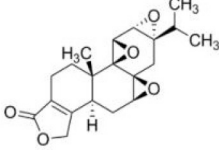
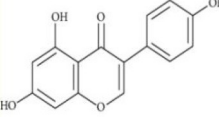
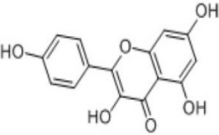
It is not difficult to see the synergistic effect of dietary polyphenols and anti-PD-1. And this inference has been confirmed in multiple studies. For luteolin and apigenin, anti-PD-1 can amplify the TIME-regulating effect of luteolin and apigenin and significantly enhance the anticancer effect, providing a prospective treatment strategy for KRAS-mutated NSCLC (84). CUR can reduce the expression of TGF- β 1 and PD-L1 on the surface of hepatoma cells and inhibit the PD-1/PD-L1 axis both *in vitro* and *in vivo*. At the same time, the proportion of CD8⁺ T cells increased and the expression of Foxp3⁺ Tregs decreased, which promoted anti-tumor immunity. Besides, the

TABLE 2 Dietary polyphenols involved in this review and their names, chemical formulas, structural formulas and metabolic absorption.

Name	Molecular formula	Structural formula	Primary source	Absorption site	Metabolic site	Metabolites (Enzymes)	References
RES	C ₁₄ H ₁₂ O ₃		Nuts, grapes, apples, hops, red Fruits, black olives, capers, red rice, red wine, peanuts, berries	Small intestine	Gut	Trans-resveratrol-3-O-sulfate (SULT1A1) Trans-resveratrol-4'-O-sulfate (SULT1A2) Trans-resveratrol-3,4'-O-disulfate (SULT1A2; SULT1A3) Trans-resveratrol-3-O-glucuronide (UGT1A1; UGT1A9) Trans-resveratrol-4'-O-glucuronide (UGT1A1; UGT1A9) Dihydroresveratrol/DHR 3,4'-O-dihydroxy-trans-stilbene Lunularin	(42)
Apigenin	C ₁₅ H ₁₀ O ₅		Celery, parsley, peas, chamomile, belimbi fruit, goji leaves	From stomach to colon	Liver; intestine	Glucuronidated apigenin (Phase II Enzymes) Sulphated apigenin (Phase II Enzymes) Luteolin	(43, 44)
CUR	C ₂₁ H ₂₀ O ₆		Turmeric, curcuma, calamus	Intestinal lumen, liver		Curcumin glucuronides (UGT1A1;UGT1A8;UGT1A10) Curcumin sulfates (SULT1A1;SULT1A3) Hexahydrocurcumin; Tetrahydrocurcumin (CYP450)	(45, 46)
Anthocyanin		 R ₁ /R ₂ =H,OH,OCH ₃	Blue, purple, and red fruits, flowers, leaves	From stomach to jejunum	Small intestine; big intestine; liver	Anthocyanin glucuronides Anthocyanin methylates Phenolic acid Phenolic acid conjugates	(47)
EGCG	C ₂₂ H ₁₈ O ₁₁		Green tea	Intestine	Gut microbiota; liver	EGC Gallic acid 5-(3,5-dihydroxyphenyl)-4-hydroxyvaleric acid (3,5-dihydroxyphenyl)-γ-valerolactone (-)-5-(5'-hydroxyphenyl)-(4R)-γ-valerolactone 3'-O-β-glucuronide (UGT1A1, 1A8 and 1A9) 4'-O-methyl-EGCG (COMT) 4''-O-methyl-EGCG (COMT) 4-4''-di-O-methyl-EGCG (COMT)	(48, 49)
Quercetin	C ₁₅ H ₁₀ O ₇		Onions, apples, tea, red wine, edible portion	Small intestine	Liver enteric bacteria; intestinal mucosal epithelial cells; colon bacteria	Thmethylated quercetin Quercetin sulfate Quercetin glucuronide Phenolic acid Smaller phenolics	(50)

(Continued)

TABLE 2 Continued

Name	Molecular formula	Structural formula	Primary source	Absorption site	Metabolic site	Metabolites (Enzymes)	References
TPL	C ₂₀ H ₂₄ O ₆		Tripterygium wilfordii Hook. f.		Liver microsomes	M1:17-Hydroxytriptolide M2:16-Hydroxytriptolide M3:triptolide M4:15-Hydroxytriptolide (CYP3A)	(51, 52)
Genistein	C ₁₅ H ₁₀ O ₅		Alfalfa, clover sprouts, broccoli, cauliflower, sunflower, barley meal, caraway, and clover seeds	Small intestine	Liver; small intestine; colon bacteria	Glucuronides (UGT1A8, 1A9, 1A10, 1A1) Sulfates (SULT1A1, 1A2, 1E, 2A1) 3'-OH-Gen, 6-OH-Gen, 8-OH-Gen (CYP1A2, CYP2E1, CYP2D6,CYP3A4) Dihydrogenistein	(53)
Kaempferol	C ₁₅ H ₁₀ O ₆		Spinach, kale, dill, chives, tarragon	Small intestine	Liver	Kaempferol-3-glucuronide Kaempferol mono- and di-sulfates	(54)

combination of anti-PD-1 and CUR significantly enhanced the TIME regulation function of CUR (87).

Bidirectional regulation of the TIME by dietary polyphenols by enhancing antitumor cell effects and attenuating immunosuppressive cell effects

As mentioned in section 2, antitumor cell immunity and immunosuppression in the TIME are in a state of mutual confrontation that is like two sides of a scale. Regardless of the form of action, dietary polyphenols always tip the balance in favor of the antitumor side (see Figure 1). CUR inhibits the maturation and immunosuppressive function of MDSCs by inhibiting the levels of arginase-1 (Arg-1), ROS, and IL-6 in the Lewis lung cancer model, reducing the inhibitory effect of MDSCs on T cell proliferation (88). The proportion of IFN-γ and CD8+ T cells increased and the proportion of CD4+ T cells decreased when huh-7 human hepatoma cells were treated with CUR. The addition of taurine significantly enhanced the effect of CUR (89, 90). In another study, it was found that curcuminoids promoted pancreatic cancer cell apoptosis by

enhancing the cytotoxicity of NK cells (90, 91). Subsequent experiments showed that the combination of CUR, omega-3 fatty acids and Smartfish (antioxidant-rich lipid emulsion) further enhanced the toxic effects of NK cells on pancreatic cancer cells. And CUR prevents NK cells from producing IFN-γ (90, 91). The researchers attempted to compare and combine CUR with Poly I: C (Toll-like receptor 3 agonist, PIC). It was demonstrated that CUR effectively inhibited PIC-dependent NF-κB activation and Tregs recruitment in head and neck squamous cell carcinoma, demonstrating a beneficial TIME regulation (92). In the co-culture system of MDA-MB-231 and NK-92, CUR bidirectionally enhanced the anticancer activity of NK-9 cells. CUR increases the expression and proportion of Stat4 and STAT5 in CD16+ and CD56dim NK-9 cells. In addition, the expression of pErk and PI3K in MDA-MB-231 was significantly downregulated by CUR (93). In the A375 mouse xenograft model, apigenin was observed to inhibit melanoma growth by significantly enhancing immune cell infiltration and T-cell-mediated tumor-cell killing (85). By comparison, CUR also has the same TIME-regulating effect as apigenin but is not as significant as that of apigenin (85).

CUR is the most dietary polyphenol in regulating the TIME, but other dietary polyphenols such as RES, EGCG, anthocyanins, and genistein are not inferior. RES enhances the overall cytotoxicity of NK cells, resulting in strong activation of NK cells in the TIME. The addition of IL-2 enhanced the

activation of NK cells in tumors (94). When non-cytotoxic concentrations of RES were used to treat hepatocellular carcinoma mice, RES was found to enhance anti-tumor immunity by reducing levels of Tregs and M2 macrophages and up-regulating levels of CD8+ T cells (95). Meanwhile, RES also modulated the TIME by regulating related cytokines, for example, up-regulating the anti-tumor cytokines TNF- α and IFN- γ , and down-regulating the immunosuppressive cytokines TGF- β 1 and IL-10 (95). Anthocyanin treatment of N-nitrosomethylbenzylamine-induced esophageal papilloma in rats showed good antitumor properties (96). Anthocyanins significantly reduced the recruitment and infiltration of CD68+/CD163- macrophages and CD163+ macrophages in tumors and reduced the accumulation of neutrophils (96). EGCG increased the proportion of CD4+ Tregs and CD8+ T cells in the breast cancer TIME and enhanced the antitumor immune response (83). In addition, EGCG targeted MDSCs in tumors through the Arg-1/iNOS/Nox2/NF- κ B/STAT3 classical pathway and non-classical pathways, such as the PI3K-Akt signaling pathway, focal adhesions, and ECM-receptor interactions, reducing their proportion (97). Genistein significantly reduced immune avoidance marker Foxp3 in tumors and upregulated cytotoxic T cell marker Cd8a at mRNA level. And lifetime intake of genistein improves anti-tumor immune response (98).

Dietary polyphenols targeting TAMs promote antitumor immunity in the TIME

TAMs affect tumor progression in different ways. They can be roughly divided into two distinct polarization states: antitumor M1 type and pro-tumor immunosuppressive M2 type. In recent years, TAMs targeting strategies have become a hot spot in antitumor therapy. Some dietary polyphenols inhibit the infiltration and polarization of TAMs to M2 type or promote TAMs polarization from M2 type to M1 type in the TIME. Studies found that apigenin restored SHIP-1 expression in pancreatic cancer mice, promoted MDSCs homeostasis, increased M1 expression and M2 polarized to M1, resulting in tumor regression (99). EGCG up-regulates Mir-16 in breast cancer cell exosomes both *in vitro* and *in vivo*. Subsequently, TAMs received mir-16 transferred from exosomes. Finally, TAMs infiltration and M2-type polarization were inhibited to inhibit NF- κ B activity through the IKK α /I κ B/NF- κ B pathway (100). Hs-1793, a synthetic RES analog, induces upregulation of IFN- γ in tumor tissue in breast cancer mice, leading to a significant reduction in M2 invasion and reprogramming. Favorable TIME changes were associated, such as decreased infiltration of Tregs and decreased immunosuppressive mediators (101).

Novel forms of dietary polyphenols enhance their bioavailability and enhance their TIME-regulating activity

Due to low solubility and bioavailability of dietary polyphenols, it is difficult to reach serum concentrations in clinical experimental models. Therefore, dietary polyphenols have certain shortcomings in clinical applications. In recent years, researchers have used liposome coating, nano-delivery systems, and synthetic analogs to improve this problem. The anticancer and the TIME-regulating effects of dietary polyphenols were significantly enhanced.

Cur-loaded nanomicelles (CUR@PPC) showed good TIME-regulating activity against melanoma *in vitro* in two aspects. First, it affects the expression of cytokines, including down-regulation of CCL-22, PD-L1, TGF- β and IL-10, and up-regulation of IFN- γ and TNF- α . Second, it affects immune cell infiltration, including reducing Tregs and enhancing CD8+ T cell immune infiltration (102). This study also found that anti-PD-1 and T cell-delivered NF- κ B inhibitors synergized and promoted each other with CUR@PPC, showing good TIME regulation and antitumor effects. This founding provides a new idea for the combined treatment of cancer with dietary polyphenols and immunotherapy (102). In a study of glioblastoma (GBM), researchers found that both liposomal TriCurin (CUR: EGCG: RES = 4:1:12.5) and phytosomal CUR (CCP) therapy induced GBM cells, GBM stem cells apoptosis, and M2-to-M1 polarization (103, 104). In studies using CCP, a large number of activated NK cells were found in the TIME, accompanied by M2-to-M1 polarization. It is speculated that monocyte chemoattractant protein-1 (MCP-1/CCL2) produced by M1 microglia in CCP-induced GBM first acts to induce M1 activation and release IL-12. Subsequently, IL-12 stimulates NK cells to express Cc chemokine receptor 2 and recruit NK cells to the TIME (104). In another experiment using tricurin, the researchers found similar results. Tricurin induces M2 to M1 polarization in human papillomavirus tumors, and IL-12-dependent NK cells and CTLs were recruited to the TIME (105). Nano-curcumin and RES work together to arrest the cell cycle reduce cell viability in rectal cancer cells. *In vivo* experiments, nanocurcumin and RES promoted macrophage recruitment and enhanced T lymphocyte infiltration (106). *In vitro* experiments, nano-curcumin was reported to support antitumor cells against pancreatic cancer through various pathways, including enhancing the expression of CD86 and driving DC maturation; significantly reducing the levels of various pro-inflammatory cytokines, such as TNF- α , IL-8, IL-6, IL-10, and IL-1 in activated T cells; and down-regulating IL-8 and up-regulating IFN- γ expression in CTLs (107, 108). CUR analog GO-Y030 exerts potent anticancer effects by reducing the generation, stability, and secretion (TGF- β , IL-10) of Tregs in

TABLE 3 Related studies on dietary polyphenols-induced pyroptosis of cancer cells.

Dietary polyphenols	Experimental model	Dose; treatment time	Mechanism	Pyroptosis pathway	References
CUR	<i>In vitro</i> : MCF-7 breast cancer cell line	8 μ M; 24 h	\uparrow LC3, CTSB, ASC, pro-caspase-1, GSDMD, NLRP3, caspase-1, GSDMD-N, IL-1 β , IL-18 \downarrow P62	Autophagy/CTSB/NLRP3/ caspase-1/GSDMD	(66)
	<i>In vivo</i> : Six-week-old SPF female BALB/c nude mice vaccinated with MCF-7; 5pcs/group, 2 groups	200 μ g/kg/d; 4 weeks			
Anthocyanin	<i>In vitro</i> : Tca8113 and SCC15 oral squamous cell carcinoma cell lines	250 μ g/ml; 48 h	\uparrow NLRP3, caspase-1, GSDMD, IL-1 β	NLRP3/ caspase-1/GSDMD	(67)
TPL	<i>In vitro</i> : HK1 squamous cell carcinoma cell line	0, 5, 25, 50, 150 nM; 24 h, 48 h	\downarrow HK-II \uparrow BAD/BAX-caspase-3, GSDME	HK-II/(BAD/ BAX-caspase-3)/GSDME	(69)
	<i>In vitro</i> : FaDu hypopharyngeal carcinoma cell line				
	<i>In vivo</i> : 5-week-old male BALB/c nude mice	1 mg/kg/d; 10 d			
CUR	<i>In vitro</i> : HepG2 human liver cancer cell line	0, 20, 30 μ M; 12 h	\downarrow full length GSDME, pro-caspase-3; Bcl-2 \uparrow GSDME-N, Bax, ROS, LDH	ROS/caspase-3 /GSDME	(70)
Kaempferol	<i>In vitro</i> : U87 MG and U251 Glioblastoma cell line	0, 20, 40, 80, 120 μ M; 24 h	\uparrow ROS, IL-1 β , ASC, P62, caspase-3, GSDME	ROS/caspase-3 /GSDME	(71)
	<i>In vivo</i> : 6-week-old male immune-deficient BALB/c nude mice vaccinated with U87 MG	40 mg/kg/2d; 3 weeks			
CUR	<i>In vitro</i> : HMESO malignant mesothelioma cells	40 μ M; 48h	\downarrow NF- κ B, TLR, IL-1 β , ASC \uparrow caspase-1, HMGB1, ROS	—	(75)
	<i>In vivo</i> : allograft model: 8 week-old male C57/BL6 mice vaccinated with mouse MM cells, 4-8 pcs/group	—; 3 weeks			
	<i>In vivo</i> : xenograft model: 6-8 week-old male Fox Chase SCID mice vaccinated with HMESO cells, 4-8pcs/group				
CUR-PLGA-MB-SPDT	<i>In vitro</i> : HepG2 human liver cancer cell line	0, 1.25, 2.5, 5, 10, 20, 40, 80 μ M, 2/3 h	\uparrow ROS, mitochondrial depolarization	—	(76)
Moscatilin RES	<i>In vitro</i> : HepG2, SH-SY5Y, HaCaT cell line	1, 10, 12.5 μ g/ml 5 μ g/ml moscatilin/resveratrol + X-ray (1 Gy)/UV-C (200 J/m ²)	\uparrow cell-cycle arrest, radiosensitivity	—	(77)

the melanoma TIME (109). Trans-Scirpusin A (TSA), a natural oligomer of RES. It reduces the number and ratio of Tregs and MDSCs in mouse colorectal cancer tumor tissue and induces antitumor immunity (108).

Dietary polyphenols play a role as adjuvants in regulating the TIME to improve the efficacy of chemotherapy and radiotherapy

Although immunotherapy and precision medicine have risen rapidly with the deepening of research in recent years. Surgery, chemotherapy, and radiotherapy are still the most utilized cancer treatments in clinical practice. Some scholars have tried to use dietary polyphenols to alleviate the interference of chemotherapy resistance and radiotherapy on the TIME, and have made some progress.

TPL reduces cisplatin (DDP) resistance in epithelial ovarian cancer mice and synergizes with DDP (110). Both TPL and TPL combined with DDP significantly increased the levels of NK cell-related proteins CD16 and CD56 in the TIME, and promoted cancer cell apoptosis. It provides a new possibility for improving the survival rate of patients with chemotherapy-resistant advanced ovarian cancer (110). Mammary chimeric mice that received sparse ionizing radiation (SIR) and dense ionizing radiation (DIR) had higher tumor incidence and tumor growth rates, accompanied by a distinct tumor immunosuppressive microenvironment (111). It manifested as a lack of lymphocyte infiltration, increased immunosuppressive myeloid cells, a lack of CD8⁺ T cells in some aged and fast-growing tumor mice, and a high expression of COX-2, PD-L1, and TGF- β (111). However, Phenyl caffeate was reported to effectively reverse this adverse effect of irradiation on the TIME (111). Joong Sun Kim et al. combined HS-1793 with radiotherapy. They found that HS-1793 could effectively alleviate the adverse effects of radiotherapy on the TIME in FM3A tumor-bearing mice by reducing the number and the infiltration of Tregs in tumor tissue. Meanwhile, HS-1793 upregulated the number of CD8⁺ T cells and upregulated IFN- γ secretion to attenuate TAM-induced immunosuppression (112). In another study, it was also found that modulated electrothermal therapy could create a more favorable TIME and significantly enhance the immunomodulatory and antitumor effects of nanocurcumin and RES (106) (see [Supplementary Table 1](#)).

Conclusions

In this review, we systematically reviewed the effects of dietary polyphenols on cancer cell pyroptosis and the

TIME. The results showed that dietary polyphenols induced pyroptosis in cancer cells mainly through the GSDMD and GSDME pathways. Furthermore, dietary polyphenols regulate the TIME by enhancing antitumor immune cells and weakening immunosuppressive cells. At the same time, TAMs are targeted by dietary polyphenols and reduce their tumor infiltration and promote their polarization from M2 to M1 type. Of course, there are also some issues that deserve to be considered.

Elevated IL-18, IL-1 β , NLRP3 are one of the main features of pyroptosis. These three inflammatory factors are often used as indicators of pyroptosis. However, overproduction of IL-18/1 β and NLRP3 leads to neonatal-onset multisystem inflammatory disease (NOMID) which damages the spleen, skin, liver, and bone a lot. Studies have shown that the pathogenesis of NOMID is GSDMD-dependent (113). The concomitant effects of IL-18, IL-1 β and NLRP3 elevation were ignored in studies claiming that GSDMD mediates pyroptosis in cancer cells. The same problem exists in all studies targeting pyroptosis to treat cancer. Some studies of dietary polyphenols inducing pyroptosis in cancer cells were performed only in cells. Unfortunately, in the *in vitro* studies, the effects of pyroptosis on the TIME and inflammation were ignored too. This may affect the prognosis and complications of cancer patients. There is no doubt that dietary polyphenols are beneficial for anti-tumor immunity in patients. But does this conclusion hold when using drugs to induce pyroptosis in cancer? It is a pity that this question has not been explored in depth.

Dietary polyphenols can reduce levels of pro-inflammatory mediators. This conclusion has been verified in many experiments. Taking CUR as an example, CUR alleviates inflammatory diseases by reducing major markers of inflammation, such as IL-6 and TNF- α , malondialdehyde, sensitive C-reactive protein, MCP-1 (114–116). The anti-inflammatory effect of dietary polyphenols is the basis of their biological activity. Are dietary polyphenols beneficial to the release of inflammatory factors induced by pyroptosis in cancer cells? This requires further research and discussion. Perhaps, we should consider the inflammatory nature of pyroptosis, the TIME, and pyroptosis as a whole. The global effects of dietary polyphenols targeting pyroptosis need to be discussed systematically. Accelerate the pace of dietary polyphenols from laboratory to clinical.

There is no doubt that the TIME is a huge, complex system. How to adjust the TIME to make it a tool to fight cancer will be a research hotspot into the future. Deeper research and exploration are required on other pathways and mechanisms of pyroptosis in cancer, the role of pyroptosis in tumor development, the impact of cancer cell pyroptosis on the TIME, and the appropriate degree of cancer cell pyroptosis. Among the above issues, dietary polyphenols deserve further attention. Of course, when it comes

to dietary polyphenols, their limited bioavailability cannot be ignored. Related researchers have greatly improved the bioavailability of dietary polyphenols by using nano-delivery systems, liposome coating. Dietary polyphenols are one step closer to clinic.

Pyroptosis is a new field. Targeting pyroptosis to treat cancer holds a aboard future. Dietary polyphenols offer a safer option. Based on the current research, it is also a good idea to combine dietary polyphenols with other drugs. Dietary polyphenols are also excellent as adjuvants for chemotherapy and radiotherapy.

Author contributions

JD and LL conceived and designed the study. XH and YW collected the literature and drafted the manuscript. JD, LL, and WY helped to review and revise the manuscript. All authors read and approved the final paper.

Funding

This work was supported by the National Natural Science Foundation of China (No. 32102736), Ruipeng Foundation and New Ruipeng Pet Medical Group Co., LTD (No. RPJJ2020033), Liaoning Province Xing Liao Talents Program Project (No. XLYC1807120), Shenyang Young and Middle-aged Scientific and Technological Innovation Talent Support Program (No. RC200431), Liaoning Province High-level Innovation Team Overseas Training Project (No. 2018LNGXJWPY-YB017), and

Liaoning Province General Undergraduate Intercollegiate Joint Training Project (No. 2021-24).

Conflict of interest

The authors declare that the research was conducted in the absence of any commercial or financial relationships that could be construed as a potential conflict of interest.

Publisher's note

All claims expressed in this article are solely those of the authors and do not necessarily represent those of their affiliated organizations, or those of the publisher, the editors and the reviewers. Any product that may be evaluated in this article, or claim that may be made by its manufacturer, is not guaranteed or endorsed by the publisher.

Supplementary material

The Supplementary Material for this article can be found online at: <https://www.frontiersin.org/articles/10.3389/fnut.2022.974896/full#supplementary-material>

References

- Roy PS, Saikia BJ. Cancer and cure: a critical analysis. *Indian J Cancer*. (2016) 53:441–2. doi: 10.4103/0019-509X.200658
- Siegel RL, Miller KD, Fuchs HE, Jemal A. Cancer statistics, 2022. *CA Cancer J Clin*. (2022) 72:7–33. doi: 10.3322/caac.21708
- Hanahan D, Weinberg RA. Hallmarks of cancer: the next generation. *Cell*. (2011) 144:646–74. doi: 10.1016/j.cell.2011.02.013
- Zhang Y, Zhang Z. The history and advances in cancer immunotherapy: understanding the characteristics of tumor-infiltrating immune cells and their therapeutic implications. *Cell Mol Immunol*. (2020) 17:807–21. doi: 10.1038/s41423-020-0488-6
- Green DR. The coming decade of cell death research: five Riddles. *Cell*. (2019) 177:1094–107. doi: 10.1016/j.cell.2019.04.024
- Shi J, Zhao Y, Wang K, Shi X, Wang Y, Huang H, et al. Cleavage of GSDMD by inflammatory caspases determines pyroptotic cell death. *Nature*. (2015) 526:660–5. doi: 10.1038/nature15514
- Wang Y, Gao W, Shi X, Ding J, Liu W, He H, et al. Chemotherapy drugs induce pyroptosis through caspase-3 cleavage of a gasdermin. *Nature*. (2017) 547:99–103. doi: 10.1038/nature22393
- Zhang Z, Zhang Y, Xia S, Kong Q, Li S, Liu X, et al. Gasdermin E suppresses tumour growth by activating anti-tumour immunity. *Nature*. (2020) 579:415–20. doi: 10.1038/s41586-020-2071-9
- Wang WJ, Chen D, Jiang MZ, Xu B, Li XW, Chu Y, et al. Downregulation of gasdermin D promotes gastric cancer proliferation by regulating cell cycle-related proteins. *J Dig Dis*. (2018) 19:74–83. doi: 10.1111/1751-2980.12576
- Gao J, Qiu X, Xi G, Liu H, Zhang F, Lv T, et al. Downregulation of GSDMD attenuates tumor proliferation via the intrinsic mitochondrial apoptotic pathway and inhibition of EGFR/Akt signaling and predicts a good prognosis in nonsmall cell lung cancer. *Oncol Rep*. (2018) 40:1971–84. doi: 10.3892/or.2018.6634
- Wu LS, Liu Y, Wang XW, Xu B, Lin YL, Song Y, et al. LPS enhances the chemosensitivity of oxaliplatin in HT29 cells via GSDMD-mediated pyroptosis. *Cancer Manag Res*. (2020) 12:10397–409. doi: 10.2147/CMAR.S244374
- Lin R, Wei H, Wang S, Huang Z, Chen H, Zhang S, et al. Gasdermin D expression and clinicopathologic outcome in primary osteosarcoma patients. *Int J Clin Exp Pathol*. (2020) 13:3149–57.
- Wang J, Kang Y, Li Y, Sun L, Zhang J, Qian S, et al. Gasdermin D in different subcellular locations predicts diverse progression, immune microenvironment and prognosis in colorectal cancer. *J Inflamm Res*. (2021) 14:6223–35. doi: 10.2147/JIR.S338584
- Wang Y, Peng J, Xie X, Zhang Z, Li M, Yang M. Gasdermin E-mediated programmed cell death: an unpaved path to tumor suppression. *J Cancer*. (2021) 12:5241–8. doi: 10.7150/jca.48989
- Rogers C, Fernandes-Alnemri T, Mayes L, Alnemri D, Cingolani G, Alnemri ES. Cleavage of DFNA5 by caspase-3 during apoptosis mediates progression to secondary necrotic/pyroptotic cell death. *Nat Commun*. (2017) 8:14128. doi: 10.1038/ncomms14128
- Hu K, Xu Z, Yao L, Yan Y, Zhou L, Li J. Integrated analysis of expression, prognostic value and immune infiltration of GSDMs in hepatocellular carcinoma. *Aging*. (2021) 13:24117–35. doi: 10.18632/aging.203669

17. Zhang Z, Zhao S, Yang H, Chen Y, Feng H, An M, et al. Prognostic and immunological role of gasdermin E in pan-cancer analysis. *Front Oncol.* (2021) 11:706266. doi: 10.3389/fonc.2021.706266
18. Zhang Z, Zhang Y, Lieberman J. Lighting a fire: can we harness pyroptosis to ignite antitumor immunity? *Cancer Immunol Res.* (2021) 9:2–7. doi: 10.1158/2326-6066.CIR-20-0525
19. Zhou Z, He H, Wang K, Shi X, Wang Y, Su Y, et al. Granzyme A from cytotoxic lymphocytes cleaves GSDMB to trigger pyroptosis in target cells. *Science.* (2020) 368:eaz7548. doi: 10.1126/science.aaz7548
20. Hou J, Zhao R, Xia W, Chang CW, You Y, Hsu JM, et al. PD-L1-mediated gasdermin C expression switches apoptosis to pyroptosis in cancer cells and facilitates tumour necrosis. *Nat Cell Biol.* (2020) 22:1264–75. doi: 10.1038/s41556-020-0575-z
21. Li MO, Wolf N, Raulet DH, Akkari L, Pittet MJ, Rodriguez PC, et al. Innate immune cells in the tumor microenvironment. *Cancer Cell.* (2021) 39:725–9. doi: 10.1016/j.ccell.2021.05.016
22. Liu Y, Cao X. Immunosuppressive cells in tumor immune escape and metastasis. *J Mol Med.* (2016) 94:509–22. doi: 10.1007/s00109-015-1376-x
23. Fu X, He Y, Li M, Huang Z, Najafi M. Targeting of the tumor microenvironment by curcumin. *Biofactors.* (2021) 47:914–32. doi: 10.1002/biof.1776
24. Ohue Y, Nishikawa H. Regulatory T (Treg) cells in cancer: can treg cells be a new therapeutic target? *Cancer Sci.* (2019) 110:2080–9. doi: 10.1111/cas.14069
25. Melaiu O, Lucarini V, Cifaldi L, Fruci D. Influence of the tumor microenvironment on NK cell function in solid tumors. *Front Immunol.* (2019) 10:3038. doi: 10.3389/fimmu.2019.03038
26. Myers JA, Miller JS. Exploring the NK cell platform for cancer immunotherapy. *Nat Rev Clin Oncol.* (2021) 18:85–100. doi: 10.1038/s41571-020-0426-7
27. Kumar V, Patel S, Tcyganov E, Gabrilovich DI. The nature of myeloid-derived suppressor cells in the tumor microenvironment. *Trends Immunol.* (2016) 37:208–20. doi: 10.1016/j.it.2016.01.004
28. Farhood B, Najafi M, Mortezaee K. CD8(+) cytotoxic T lymphocytes in cancer immunotherapy: a review. *J Cell Physiol.* (2019) 234:8509–21. doi: 10.1002/jcp.27782
29. Wu K, Lin K, Li X, Yuan X, Xu P, Ni P, et al. Redefining tumor-associated macrophage subpopulations and functions in the tumor microenvironment. *Front Immunol.* (2020) 11:1731. doi: 10.3389/fimmu.2020.01731
30. Pan Y, Yu Y, Wang X, Zhang T. Tumor-associated macrophages in tumor immunity. *Front Immunol.* (2020) 11:583084. doi: 10.3389/fimmu.2020.583084
31. Zhu J. T helper cell differentiation, heterogeneity, and plasticity. *Cold Spring Harb Perspect Biol.* (2018) 10:a030338. doi: 10.1101/cshperspect.a030338
32. Chen L, Huang CF, Li YC, Deng WW, Mao L, Wu L, et al. Blockage of the NLRP3 inflammasome by MCC950 improves anti-tumor immune responses in head and neck squamous cell carcinoma. *Cell Mol Life Sci.* (2018) 75:2045–58. doi: 10.1007/s00018-017-2720-9
33. Daley D, Mani VR, Mohan N, Akkad N, Pandian G, Savadkar S, et al. NLRP3 signaling drives macrophage-induced adaptive immune suppression in pancreatic carcinoma. *J Exp Med.* (2017) 214:1711–24. doi: 10.1084/jem.20161707
34. Wang F, Li G, Ning J, Chen L, Xu H, Kong X, et al. Alcohol accumulation promotes esophagitis via pyroptosis activation. *Int J Biol Sci.* (2018) 14:1245–55. doi: 10.7150/ijbs.24347
35. Barber G, Anand A, Katarzyna O, Phelan JJ, Heeran AB, Flis E, et al. Characterizing caspase-1 involvement during esophageal disease progression. *Cancer Immunol Immunother.* (2020) 69:2635–49. doi: 10.1007/s00262-020-02650-4
36. Pachathundikandi SK, Blaser N, Bruns H, Backert S. *Helicobacter pylori* avoids the critical activation of NLRP3 inflammasome-mediated production of oncogenic mature IL-1 β in human immune cells. *Cancers.* (2020) 12:803. doi: 10.3390/cancers12040803
37. Zhao P, Wang M, Chen M, Chen Z, Peng X, Zhou F, et al. Programming cell pyroptosis with biomimetic nanoparticles for solid tumor immunotherapy. *Biomaterials.* (2020) 254:120142. doi: 10.1016/j.biomaterials.2020.120142
38. Bollino D, Colunga A, Li B, Aurelian L. DeltaPK oncolytic activity includes modulation of the tumour cell milieu. *J Gen Virol.* (2016) 97:496–508. doi: 10.1099/jgv.0.000353
39. Wang Q, Wang Y, Ding J, Wang C, Zhou X, Gao W, et al. A bioorthogonal system reveals antitumor immune function of pyroptosis. *Nature.* (2020) 579:421–6. doi: 10.1038/s41586-020-2079-1
40. Gao Y, Zhang H, Zhou N, Xu P, Wang J, Gao Y, et al. Methotrexate-loaded tumour-cell-derived microvesicles can relieve biliary obstruction in patients with extrahepatic cholangiocarcinoma. *Nat Biomed Eng.* (2020) 4:743–53. doi: 10.1038/s41551-020-0583-0
41. Peng Z, Wang P, Song W, Yao Q, Li Y, Liu L, et al. GSDME enhances Cisplatin sensitivity to regress non-small cell lung carcinoma by mediating pyroptosis to trigger antitumor immunocyte infiltration. *Signal Transduct Target Ther.* (2020) 5:159. doi: 10.1038/s41392-020-00274-9
42. Springer M, Moco S. Resveratrol and its human metabolites-effects on metabolic health and obesity. *Nutrients.* (2019) 11:143. doi: 10.3390/nu11010143
43. Tang D, Chen K, Huang L, Li J. Pharmacokinetic properties and drug interactions of apigenin, a natural flavone. *Expert Opin Drug Metab Toxicol.* (2017) 13:323–30. doi: 10.1080/17425255.2017.1251903
44. Wang M, Firman J, Liu L, Yam K. A review on flavonoid apigenin: dietary intake, ADME, antimicrobial effects, and interactions with human gut microbiota. *Biomed Res Int.* (2019) 2019:7010467. doi: 10.1155/2019/7010467
45. Adiwidjaja J, McLachlan AJ, Boddy AV. Curcumin as a clinically-promising anti-cancer agent: pharmacokinetics and drug interactions. *Expert Opin Drug Metab Toxicol.* (2017) 13:953–72. doi: 10.1080/17425255.2017.1360279
46. Tsuda T. Curcumin as a functional food-derived factor: degradation products, metabolites, bioactivity, and future perspectives. *Food Funct.* (2018) 9:705–14. doi: 10.1039/C7FO01242J
47. Fang J. Bioavailability of anthocyanins. *Drug Metab Rev.* (2014) 46:508–20. doi: 10.3109/03602532.2014.978080
48. Scholl C, Lepper A, Lehr T, Hanke N, Schneider KL, Brockmoller J, et al. Population nutrigenetics of green tea extract. *PLoS ONE.* (2018) 13:e0193074. doi: 10.1371/journal.pone.0193074
49. Gan RY, Li HB, Sui ZQ, Corke H. Absorption, metabolism, anti-cancer effect and molecular targets of epigallocatechin gallate (EGCG): an updated review. *Crit Rev Food Sci Nutr.* (2018) 58:924–41. doi: 10.1080/10408398.2016.1231168
50. Li Y, Yao J, Han C, Yang J, Chaudhry MT, Wang S, et al. Quercetin, inflammation and immunity. *Nutrients.* (2016) 8:167. doi: 10.3390/nu8030167
51. Liu J, Zhou X, Chen XY, Zhong DF. Excretion of [³H]triptolide and its metabolites in rats after oral administration. *Acta Pharmacol Sin.* (2014) 35:549–54. doi: 10.1038/aps.2013.192
52. Li XJ, Jiang ZZ, Zhang LY. Triptolide: progress on research in pharmacodynamics and toxicology. *J Ethnopharmacol.* (2014) 155:67–79. doi: 10.1016/j.jep.2014.06.006
53. Yang Z, Kulkarni K, Zhu W, Hu M. Bioavailability and pharmacokinetics of genistein: mechanistic studies on its ADME. *Anticancer Agents Med Chem.* (2012) 12:1264–80. doi: 10.2174/187152012803833107
54. Dabeek WM, Marra MV. Dietary quercetin and kaempferol: bioavailability and potential cardiovascular-related bioactivity in humans. *Nutrients.* (2019) 11:2288. doi: 10.3390/nu11102288
55. Bar-Sela G, Epelbaum R, Schaffer M. Curcumin as an anti-cancer agent: review of the gap between basic and clinical applications. *Curr Med Chem.* (2010) 17:190–7. doi: 10.2174/092986710790149738
56. Law SK, Simmons MP, Tehen N, Khan IA, He MF, Shaw PC, et al. Molecular analyses of the Chinese herb leigongteng (*Tripterygium wilfordii* Hook.f.). *Phytochemistry.* (2011) 72:21–6. doi: 10.1016/j.phytochem.2010.10.015
57. Yahfoufi N, Alsadi N, Jambi M, Matar C. The immunomodulatory and anti-inflammatory role of polyphenols. *Nutrients.* (2018) 10:1618. doi: 10.3390/nu10111618
58. Fraga CG, Croft KD, Kennedy DO, Tomas-Barberan FA. The effects of polyphenols and other bioactives on human health. *Food Funct.* (2019) 10:514–28. doi: 10.1039/C8FO01997E
59. Cai M, Zhuang W, Lv E, Liu Z, Wang Y, Zhang W, et al. Kaempferol alleviates pyroptosis and microglia-mediated neuroinflammation in Parkinson's disease via inhibiting p38MAPK/NF- κ B signaling pathway. *Neurochem Int.* (2022) 152:105221. doi: 10.1016/j.neuint.2021.105221
60. Liu Z, Yao X, Sun B, Jiang W, Liao C, Dai X, et al. Pretreatment with kaempferol attenuates microglia-mediated neuroinflammation by inhibiting MAPKs-NF- κ B signaling pathway and pyroptosis after secondary spinal cord injury. *Free Radic Biol Med.* (2021) 168:142–54. doi: 10.1016/j.freeradbiomed.2021.03.037
61. Tufekci KU, Eltutan BI, Isci KB, Genc S. Resveratrol Inhibits NLRP3 inflammasome-induced pyroptosis and miR-155 expression in microglia through sirt1/AMPK pathway. *Neurotox Res.* (2021) 39:1812–29. doi: 10.1007/s12640-021-00435-w

62. Yu W, Qin X, Zhang Y, Qiu P, Wang L, Zha W, et al. Curcumin suppresses doxorubicin-induced cardiomyocyte pyroptosis via a PI3K/Akt/mTOR-dependent manner. *Cardiovasc Diagn Ther.* (2020) 10:752–69. doi: 10.21037/cdt-19-707
63. Li W, Chen L, Xiao Y. Apigenin protects against ischemia/hypoxia-induced myocardial injury by mediating pyroptosis and apoptosis. *In Vitro Cell Dev Biol Anim.* (2020) 56:307–12. doi: 10.1007/s11626-020-00434-9
64. Ding T, Zhao T, Li Y, Liu Z, Ding J, Ji B, et al. Vitexin exerts protective effects against calcium oxalate crystal-induced kidney pyroptosis *in vivo* and *in vitro*. *Phytomedicine.* (2021) 86:153562. doi: 10.1016/j.phymed.2021.153562
65. He C, Yang J, Jiang X, Liang X, Yin L, Yin Z, et al. Kaempferol alleviates LPS-ATP mediated inflammatory injury in splenic lymphocytes via regulation of the pyroptosis pathway in mice. *Immunopharmacol Immunotoxicol.* (2019) 41:538–48. doi: 10.1080/08923973.2019.1666405
66. Duan HN. Curcumin induces pyroptosis of human breast cancer cells (MCF-7) through autophagy-CTSB-inflammasome signaling pathway. *Dalian Med Univ.* (2021).
67. Yue E, Tuguzbaeva G, Chen X, Qin Y, Li A, Sun X, et al. Anthocyanin is involved in the activation of pyroptosis in oral squamous cell carcinoma. *Phytomedicine.* (2019) 56:286–94. doi: 10.1016/j.phymed.2018.09.223
68. Binfen H, Zhao L, Deng M. Chrysophanol inhibits the progression of gastric cancer by activating NLRP3. *Res Square.* (2021). doi: 10.21203/rs.3.rs-1073406/v1
69. Cai J, Yi M, Tan Y, Li X, Li G, Zeng Z, et al. Natural product triptolide induces GSDME-mediated pyroptosis in head and neck cancer through suppressing mitochondrial hexokinase-Iotaota. *J Exp Clin Cancer Res.* (2021) 40:190. doi: 10.1186/s13046-021-01995-7
70. Liang WF, Gong YX, Li HF, Sun FL, Li WL, Chen DQ, et al. Curcumin activates ROS signaling to promote pyroptosis in hepatocellular carcinoma HepG2 cells. *In Vivo.* (2021) 35:249–57. doi: 10.21873/in vivo.12253
71. Chen S, Ma J, Yang L, Teng M, Lai ZQ, Chen X, et al. Anti-glioblastoma activity of kaempferol via programmed cell death induction: involvement of autophagy and pyroptosis. *Front Bioeng Biotechnol.* (2020) 8:614419. doi: 10.3389/fbioe.2020.614419
72. Kong Y, Feng Z, Chen A, Qi Q, Han M, Wang S, et al. The natural flavonoid galangin elicits apoptosis, pyroptosis, and autophagy in glioblastoma. *Front Oncol.* (2019) 9:942. doi: 10.3389/fonc.2019.00942
73. Tan JQ, Li Z, Chen G, Wu M, Feng JL, Kong SY, et al. The natural compound from garcinia bracteata mainly induces GSDME-mediated pyroptosis in esophageal cancer cells. *Phytomedicine.* (2022) 102:154142. doi: 10.1016/j.phymed.2022.154142
74. Zhang F, Liu Q, Ganesan K, Kewu Z, Shen J, Gang F, et al. The antitriple negative breast cancer efficacy of spatholobus suberectus dunn on ROS-Induced noncanonical inflammasome pyroptotic pathway. *Oxid Med Cell Longev.* (2021) 2021:5187569. doi: 10.1155/2021/5187569
75. Miller JM, Thompson JK, MacPherson MB, Beuschel SL, Westbom CM, Sayan M, et al. Curcumin: a double hit on malignant mesothelioma. *Cancer Prev Res.* (2014) 7:330–40. doi: 10.1158/1940-6207.CAPR-13-0259
76. Zhu JX, Zhu WT, Liu JH, Yang W, Liu P, Liu QH, et al. Curcumin-Loaded Poly(L-lactide-co-glycolide) microbubble-mediated sonodynamic therapy in liver cancer cells. *Ultrasound Med Biol.* (2020) 46:2030–43. doi: 10.1016/j.ultrasmedbio.2020.03.030
77. Pujari I, Thomas A, Thomas J, Jhawar N, Guruprasad KP, Rai PS, et al. Cytotoxicity and radiosensitizing potency of Moscatilin in cancer cells at low radiation doses of X-ray and UV-C. *Biotech.* (2021) 11:281. doi: 10.1007/s13205-021-02827-3
78. Sharma A, Kaur M, Katnoria JK, Nagpal AK. Polyphenols in food: cancer prevention and apoptosis induction. *Curr Med Chem.* (2018) 25:4740–57. doi: 10.2174/0929867324666171006144208
79. Lesjak M, Simin N, Srail SKS. Can polyphenols inhibit ferroptosis? *Antioxidants.* (2022) 11:150. doi: 10.3390/antiox11010150
80. Musial C, Siedlecka-Kroplewska K, Kmiec Z, Gorska-Ponikowska M. Modulation of autophagy in cancer cells by dietary polyphenols. *Antioxidants.* (2021) 10:123. doi: 10.3390/antiox10010123
81. Sun C, Mezzadra R, Schumacher TN. Regulation and function of the PD-L1 checkpoint. *Immunity.* (2018) 48:434–52. doi: 10.1016/j.immuni.2018.03.014
82. Verdura S, Cuyas E, Cortada E, Brunet J, Lopez-Bonet E, Martin-Castillo B, et al. Resveratrol targets PD-L1 glycosylation and dimerization to enhance antitumor T-cell immunity. *Aging.* (2020) 12:8–34. doi: 10.18632/aging.102646
83. Yang M, Li Z, Tao J, Hu H, Li Z, Zhang Z, et al. Resveratrol induces PD-L1 expression through snail-driven activation of Wnt pathway in lung cancer cells. *J Cancer Res Clin Oncol.* (2021) 147:1101–13. doi: 10.1007/s00432-021-03510-z
84. Jiang ZB, Wang WJ, Xu C, Xie YJ, Wang XR, Zhang YZ, et al. Luteolin and its derivative apigenin suppress the inducible PD-L1 expression to improve anti-tumor immunity in KRAS-mutant lung cancer. *Cancer Lett.* (2021) 515:36–48. doi: 10.1016/j.canlet.2021.05.019
85. Xu L, Zhang Y, Tian K, Chen X, Zhang R, Mu X, et al. Apigenin suppresses PD-L1 expression in melanoma and host dendritic cells to elicit synergistic therapeutic effects. *J Exp Clin Cancer Res.* (2018) 37:261. doi: 10.1186/s13046-018-0929-6
86. Liao F, Liu L, Luo E, Hu J. Curcumin enhances anti-tumor immune response in tongue squamous cell carcinoma. *Arch Oral Biol.* (2018) 92:32–7. doi: 10.1016/j.archoralbio.2018.04.015
87. Guo L, Li H, Fan T, Ma Y, Wang L. Synergistic efficacy of curcumin and anti-programmed cell death-1 in hepatocellular carcinoma. *Life Sci.* (2021) 279:119359. doi: 10.1016/j.lfs.2021.119359
88. Liu D, You M, Xu Y, Li F, Zhang D, Li X, et al. Inhibition of curcumin on myeloid-derived suppressor cells is requisite for controlling lung cancer. *Int Immunopharmacol.* (2016) 39:265–72. doi: 10.1016/j.intimp.2016.07.035
89. Abd-Rabou AA, Zoheir KM, Ahmed HH. Potential impact of curcumin and taurine on human hepatoma cells using Huh-7 cell line. *Clin Biochem.* (2012) 45:1519–21. doi: 10.1016/j.clinbiochem.2012.06.032
90. Halder RC, Almasi A, Sagong B, Leung J, Jewett A, Fiala M. Curcuminoids and omega-3 fatty acids with anti-oxidants potentiate cytotoxicity of natural killer cells against pancreatic ductal adenocarcinoma cells and inhibit interferon gamma production. *Front Physiol.* (2015) 6:129. doi: 10.3389/fphys.2015.00129
91. Fiala M. Curcumin and omega-3 fatty acids enhance NK cell-induced apoptosis of pancreatic cancer cells but curcumin inhibits interferon-gamma production: benefits of omega-3 with curcumin against cancer. *Molecules.* (2015) 20:3020–6. doi: 10.3390/molecules20023020
92. Kottling C, Hofmann L, Lotfi R, Engelhardt D, Laban S, Schuler PJ, et al. Immune-stimulatory effects of curcumin on the tumor microenvironment in head and neck squamous cell carcinoma. *Cancers.* (2021) 13:1335. doi: 10.3390/cancers13061335
93. Lee HH, Cho H. Improved anti-cancer effect of curcumin on breast cancer cells by increasing the activity of natural killer cells. *J Microbiol Biotechnol.* (2018) 28:874–82. doi: 10.4014/jmb.1801.01074
94. Lee Y, Shin H, Kim J. *In vivo* anti-cancer effects of resveratrol mediated by NK cell activation. *J Innate Immun.* (2021) 13:94–106. doi: 10.1159/000510315
95. Zhang Q, Huang H, Zheng F, Liu H, Qiu F, Chen Y, et al. Resveratrol exerts antitumor effects by downregulating CD8(+)CD122(+) Tregs in murine hepatocellular carcinoma. *Oncotarget.* (2020) 9:1829346. doi: 10.1080/2162402X.2020.1829346
96. Peiffer DS, Wang LS, Zimmerman NP, Ransom BW, Carmella SG, Kuo CT, et al. Dietary consumption of black raspberries or their anthocyanin constituents alters innate immune cell trafficking in esophageal cancer. *Cancer Immunol Res.* (2016) 4:72–82. doi: 10.1158/2326-6066.CIR-15-0091
97. Xu P, Yan F, Zhao Y, Chen X, Sun S, Wang Y, et al. Green tea polyphenol EGCG attenuates MDSCs-mediated immunosuppression through canonical and non-canonical pathways in a 4T1 murine breast cancer model. *Nutrients.* (2020) 12:1042. doi: 10.3390/nu12041042
98. Zhang X, Cook KL, Warri A, Cruz IM, Rosim M, Riskin J, et al. Lifetime genistein intake increases the response of mammary tumors to tamoxifen in rats. *Clin Cancer Res.* (2017) 23:814–24. doi: 10.1158/1078-0432.CCR-16-1735
99. Villalobos-Ayala K, Ortiz Rivera I, Alvarez C, Husain K, DeLoach D, Krystal G, et al. Apigenin increases SHIP-1 expression, promotes tumoricidal macrophages and anti-tumor immune responses in murine pancreatic cancer. *Cancers.* (2020) 12:3631. doi: 10.3390/cancers12123631
100. Jang JY, Lee JK, Jeon YK, Kim CW. Exosome derived from epigallocatechin gallate treated breast cancer cells suppress tumor growth by inhibiting tumor-associated macrophage infiltration and M2 polarization. *BMC Cancer.* (2013) 13:421. doi: 10.1186/1471-2407-13-421
101. Jeong SK, Yang K, Park YS, Choi YJ, Oh SJ, Lee CW, et al. Interferon gamma induced by resveratrol analog, HS-1793, reverses the properties of tumor associated macrophages. *Int Immunopharmacol.* (2014) 22:303–10. doi: 10.1016/j.intimp.2014.07.004
102. Xiao Z, Su Z, Han S, Huang J, Lin L, Shuai X. Dual pH-sensitive nanodrug blocks PD-1 immune checkpoint and uses T cells to deliver NF-kappaB inhibitor for antitumor immunotherapy. *Sci Adv.* (2020) 6:eay7785. doi: 10.1126/sciadv.aay7785
103. Mukherjee S, Fried A, Hussaini R, White R, Baidoo J, Yalamanchi S, et al. Phytosomal curcumin causes natural killer cell-dependent repolarization of glioblastoma (GBM) tumor-associated microglia/macrophages and

elimination of GBM and GBM stem cells. *J Exp Clin Cancer Res.* (2018) 37:168. doi: 10.1186/s13046-018-0792-5

104. Mukherjee S, Baidoo JNE, Sampat S, Mancuso A, David L, Cohen LS, et al. Liposomal TriCurin, a synergistic combination of curcumin, epicatechin gallate and resveratrol, repolarizes tumor-associated microglia/macrophages, and eliminates glioblastoma (GBM) and GBM stem cells. *Molecules.* (2018) 23:201. doi: 10.3390/molecules23010201

105. Mukherjee S, Hussaini R, White R, Atwi D, Fried A, Sampat S, et al. TriCurin, a synergistic formulation of curcumin, resveratrol, and epicatechin gallate, repolarizes tumor-associated macrophages and triggers an immune response to cause suppression of HPV+ tumors. *Cancer Immunol Immunother.* (2018) 67:761–74. doi: 10.1007/s00262-018-2130-3

106. Kuo IM, Lee JJ, Wang YS, Chiang HC, Huang CC, Hsieh PJ, et al. Potential enhancement of host immunity and anti-tumor efficacy of nanoscale curcumin and resveratrol in colorectal cancers by modulated electro- hyperthermia. *BMC Cancer.* (2020) 20:603. doi: 10.1186/s12885-020-07072-0

107. Milano F, Mari L, van de Luijngaarden W, Parikh K, Calpe S, Krishnadath KK. Nano-curcumin inhibits proliferation of esophageal adenocarcinoma cells and enhances the T cell mediated immune response. *Front Oncol.* (2013) 3:137. doi: 10.3389/fonc.2013.00137

108. Hong EH, Heo EY, Song JH, Kwon BE, Lee JY, Park Y, et al. Trans-scirpusin A showed antitumor effects via autophagy activation and apoptosis induction of colorectal cancer cells. *Oncotarget.* (2017) 8:41401–11. doi: 10.18632/oncotarget.17388

109. MaruYama T, Kobayashi S, Nakatsukasa H, Moritoki Y, Taguchi D, Sunagawa Y, et al. The curcumin analog GO-Y030 controls the generation and stability of regulatory T cells. *Front Immunol.* (2021) 12:687669. doi: 10.3389/fimmu.2021.687669

110. Hu H, Huang G, Wang H, Li X, Wang X, Feng Y, et al. Inhibition effect of triptolide on human epithelial ovarian cancer via adjusting cellular immunity and angiogenesis. *Oncol Rep.* (2018) 39:1191–6. doi: 10.3892/or.2017.6158

111. Omene C, Ma L, Moore J, Ouyang H, Illa-Bochaca I, Chou W, et al. Aggressive mammary cancers lacking lymphocytic infiltration arise in irradiated mice and can be prevented by dietary intervention. *Cancer Immunol Res.* (2020) 8:217–29. doi: 10.1158/2326-6066.CIR-19-0253

112. Kim JS, Jeong SK, Oh SJ, Lee CG, Kang YR, Jo WS, et al. The resveratrol analogue, HS1793, enhances the effects of radiation therapy through the induction of antitumor immunity in mammary tumor growth. *Int J Oncol.* (2020) 56:1405–16. doi: 10.3892/ijo.2020.5017

113. Xiao J, Wang C, Yao JC, Alippe Y, Xu C, Kress D, et al. Gasdermin D mediates the pathogenesis of neonatal-onset multisystem inflammatory disease in mice. *PLoS Biol.* (2018) 16:e3000047. doi: 10.1371/journal.pbio.3000047

114. Liu Y, Wang Z, Gan Y, Chen X, Zhang B, Chen Z, et al. Curcumin attenuates prostatic hyperplasia caused by inflammation via up-regulation of bone morphogenetic protein and activin membrane-bound inhibitor. *Pharm Biol.* (2021) 59:1026–35. doi: 10.1080/13880209.2021.1953539

115. Mokgalaboni K, Ntamo Y, Ziqubu K, Nyambuya TM, Nkambule BB, Mazibuko-Mbeje SE, et al. Curcumin supplementation improves biomarkers of oxidative stress and inflammation in conditions of obesity, type 2 diabetes and NAFLD: updating the status of clinical evidence. *Food Funct.* (2021) 12:12235–49. doi: 10.1039/D1FO02696H

116. Brochard S, Pontin J, Bernay B, Boumediene K, Conrozier T, Bauge C. The benefit of combining curcumin, bromelain and harpagophytum to reduce inflammation in osteoarthritic synovial cells. *BMC Complement Med Ther.* (2021) 21:261. doi: 10.1186/s12906-021-03435-7



OPEN ACCESS

EDITED BY

Peng Ji,
Gansu Agricultural University, China

REVIEWED BY

Xiaofei Shang,
Lanzhou Institute of Husbandry
and Pharmaceutical Sciences (CAAS),
China
Guangliang Shi,
Northeast Agricultural University,
China

*CORRESPONDENCE

Jingui Li
jgli@yzu.edu.cn
Huan Pang
panghuan@yzu.edu.cn

†These authors have contributed
equally to this work

SPECIALTY SECTION

This article was submitted to
Nutritional Immunology,
a section of the journal
Frontiers in Nutrition

RECEIVED 12 July 2022

ACCEPTED 29 August 2022

PUBLISHED 15 September 2022

CITATION

Bo R, Liu X, Wang J, Wei S, Wu X, Tao Y,
Xu S, Liu M, Li J and Pang H (2022)
Polysaccharide from *Atractylodes*
macrocephala Koidz binding with zinc
oxide nanoparticles: Characterization,
immunological effect and mechanism.
Front. Nutr. 9:992502.
doi: 10.3389/fnut.2022.992502

COPYRIGHT

© 2022 Bo, Liu, Wang, Wei, Wu, Tao,
Xu, Liu, Li and Pang. This is an
open-access article distributed under
the terms of the [Creative Commons
Attribution License \(CC BY\)](https://creativecommons.org/licenses/by/4.0/). The use,
distribution or reproduction in other
forums is permitted, provided the
original author(s) and the copyright
owner(s) are credited and that the
original publication in this journal is
cited, in accordance with accepted
academic practice. No use, distribution
or reproduction is permitted which
does not comply with these terms.

Polysaccharide from *Atractylodes macrocephala* Koidz binding with zinc oxide nanoparticles: Characterization, immunological effect and mechanism

Ruonan Bo^{1,2,3†}, Xiaopan Liu^{1†}, Jing Wang¹, Simin Wei¹,
Xinyue Wu⁴, Ya Tao¹, Shuya Xu¹, Mingjiang Liu^{1,2,3},
Jingui Li^{1,2,3*} and Huan Pang^{4*}

¹College of Veterinary Medicine, Yangzhou University, Yangzhou, China, ²Jiangsu Co-innovation
Center for Prevention and Control of Important Animal Infectious Diseases and Zoonoses,
Yangzhou, China, ³Joint International Research Laboratory of Agriculture and Agri-Product Safety,
The Ministry of Education of China, Yangzhou University, Yangzhou, China, ⁴School of Chemistry
and Chemical Engineering, Yangzhou University, Yangzhou, China

Atractylodes macrocephala Koidz (*A. macrocephala*) has been used both as a traditional medicine and functional food for hundreds of years in Asia. And it has a variety of biological activities, such as enhancing the ability of immunity and modulating effect on gastrointestinal motility. In this study, a water-soluble polysaccharide with molecular weight of 2.743×10^3 Da was isolated from the root of *A. macrocephala*. Polysaccharide from *A. macrocephala* (AMP) consisted of arabinose, galactose, glucose, xylose, mannose, ribose, galactose uronic acid, glucose uronic acid, with a percentage ratio of 21.86, 12.28, 34.19, 0.43, 0.92, 0.85, 28.79, and 0.67%, respectively. Zinc plays an important role in immune system. Therefore, we supposed that AMP binding with zinc oxide (ZnO) nanoparticles (AMP-ZnONPs) might be an effective immunostimulator. AMP-ZnONPs was prepared by Borch reduction, and its structural features were characterized by Scanning Electron Microscope (SEM), Transmission electron microscope (TEM), TEM-energy dispersive spectroscopy mapping (TEM-EDS mapping), Fourier transform infrared spectroscopy (FT-IR), X-ray photoelectron spectrometer (XPS), X-ray diffraction (XRD), particle size and zeta-potential distribution analysis. Then, its immunostimulatory activity and the underlying mechanism were evaluated using RAW264.7 cells. The results showed that AMP-ZnONPs remarkably promoted cell proliferation, enhanced phagocytosis, the release of nitric oxide (NO), cytokines (IL-6 and IL-1 β) and the expression of co-stimulatory molecules (CD80, CD86 and MHCII). Moreover, AMP-ZnONPs could promote

the expression of Toll-like receptor 4 (TLR4), Myeloid differentiation factor 88 (MyD88), TNF receptor associated factor 6 (TRAF6), phospho-I κ B α (P-I κ B α) and phospho-p65 (P-p65), and TLR4 inhibitor (TAK242) inhibited the expression of these proteins induced by AMP-ZnONPs. Therefore, AMP-ZnONPs activated macrophages by TLR4/MyD88/NF- κ B signaling pathway, indicating that AMP-ZnONPs could act as a potential immunostimulator in medicine and functional food.

KEYWORDS

polysaccharide from *Atractylodes macrocephala* Koidz, zinc oxide nanoparticles, immunostimulatory activity, TLR4 signaling pathways, potential immunostimulator

Introduction

In recent years, immunoregulatory polysaccharides are considered important macromolecules for stimulation of immune response, then gradually become a major research hot spot (1, 2). *Atractylodes macrocephala* Koidz (*A. macrocephala*) has been used both as traditional medicine and functional food for hundreds of years in Asia, and it was approved as a functional food by the National Health Commission of the People's Republic Health of China (3–5). Polysaccharide from *A. macrocephala* (AMP) has a variety of biological activities, such as enhancing the ability of immunity, modulating effect on gastrointestinal motility and decreasing the blood glucose level (6–8). However, a lot of natural polysaccharides exhibit only weak bioactivities due to the limitation of structural and conformational properties (9). Thus, further research about enhancing bioavailability of AMP is necessary.

Zinc (Zn) deficiencies in the body is a serious problem, which severely harms the health of the organism and causes the etiology of myocardial apoptosis, deregulated homeostasis (10–12). In addition, zinc is important for cellular homeostasis and also serves as a regulatory signaling molecule for immune cells (13, 14). Zinc oxide (ZnO) is listed as “commonly considered as safe” by the US Food and Drug Administration (FDA) (15). Some studies have shown that Zn has a significant role in the development and activation of effector cells of the innate and adaptive immune systems (16–18). ZnO nanoparticles (ZnONPs) have been exploited in biomedical and preclinical research for their advantages such as non-toxicity and low cost (19, 20). However, ZnONPs are limited their application in drug delivery due to their poor water solubility, strong agglomeration and less dispersion. Hence, it is imperative to develop an effective, safe and high-content Zn-supplement. To improve the dispersion of particles in water, a silane coupling agent (KH550) was used to modify the ZnONPs (21). In addition, KH550 was easily grafted at the ZnONPs interface, and the other side of KH550 carries an amino group that was easily grafted with polysaccharides.

Macrophages are one of the most important effector cells of the immune system, and play pivotal roles in the immune response (22). Phagocytosis is a marker of their activation. Upon activation, macrophages release NO, diverse cytokines and co-stimulatory molecules (23, 24). Many natural polysaccharides modulate the immune system through the activation of TLR4 in macrophages (25–29). Toll-like receptor 4 (TLR4), a key pattern recognition receptor involved in the activation of macrophages, is reported the major component of the signaling including nuclear factor- κ B (NF- κ B) signaling pathway.

We supposed that AMP binding with ZnONPs (AMP-ZnONPs) might provide a novel way to explore an effective immunostimulator. To enhance the dispersive capacity of ZnONPs in the water, γ -aminopropyltriethoxy silane (KH550) was applied to modify its surface. Then, AMP-ZnONPs was successfully prepared by the binding of KH550-ZnONPs and AMP *via* the Borch reduction between -NH₂ group and -CHO group (Figure 1). Its structural properties were characterized and then its immunostimulatory activities including cell viability, phagocytosis, surface molecules, cytokines release were evaluated using RAW264.7 cells. To further reveal the mechanism of immune stimulation, the effects of AMP-ZnONPs on the TLR4/MyD88/NF- κ B signaling pathways were analyzed. This study is expected to provide new ideas for the development and utilization of polysaccharides and microelements in the food and pharmaceutical industry.

Materials and methods

Reagents and materials

A. macrocephala was purchased from the Tongrentang Company in Beijing. The plant material was identified by Prof. Jingui Li. The purified AMP was prepared in our laboratory and the polysaccharide content was 96% (UV). RAW264.7 cells were obtained from American Type Culture Collection (ATCC,

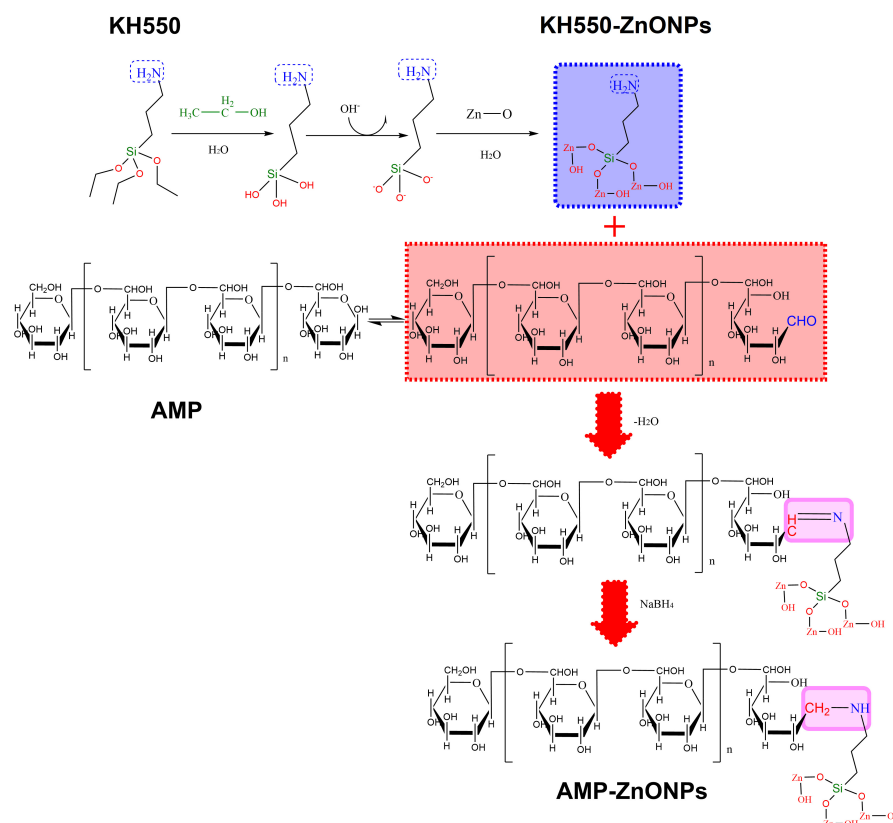


FIGURE 1

Schematic illustration of AMP-ZnONPs synthesis. The surface of ZnONPs was modified with KH550 through Borch reduction and then AMP was bond to the KH550-ZnONPs.

Rockville, MD, United States). Fucose (Cat No. B25632), arabinose (Cat No. B65342), rhamnose (Cat No. B50770), galactose (Cat No. B21893), glucose (Cat No. B21882), xylose (Cat No. B21880), mannose (Cat No. B21895), fructose (Cat No. B21896), ribose (Cat No. B21897), galacturonic acid (Cat No. B21894) and glucuronic acid (Cat No. B25302) were purchased from Shanghai Ye Yuan Biotechnology Co., Ltd. FITC-dextran (Cat No. 60842-46-8) and fetal bovine serum (Cat No. F8318) were purchased from Sigma Corporation of America. DMEM culture solution (Cat No. SH30022.01) was purchased from HyClone. NO test kit (Cat No. S0021) was obtained from Beyotime Biotechnology. Silane coupling agent (KH550, Cat No. A7440) and ZnONPs (purity 99.9%, Cas No. 1314-13-2) were the products of Sinopharm Chemical Reagent Ltd. RNA-easy Isolation Reagent (Cat No. R701) was purchased from Vazyme Biotech Co., Ltd. The CCK8 (Cat No. 40203ES80), Hifair® III 1st Strand cDNA Synthesis SuperMix for qPCR (gDNA digester plus) (Cat No. 11141ES60) and Hieff® qPCR SYBR Green Master Mix (High Rox Plus) (Cat No. 11184ES08) were the products of Yeasen Biotech Co., Ltd. Rabbit Anti-CD80 Polyclonal Antibody (Cat No. bs-1479R), Rabbit Anti-CD86 Polyclonal Antibody (Cat No. bs-1035R) and Rabbit

Anti-MHC Class II/HLA DMB Polyclonal Antibody (Cat No. bs-4107R) were purchased from Biosynthesis Biotechnology Inc. (Beijing, China). Antibodies of TLR4 (Cat No. 14358s), TRAF6 (Cat No. 67591s), MyD88 (Cat No. 4283s), phospho-IκBα (P-IκBα) (Cat No. 4812s), phospho-p65 (P-p65) (Cat No. 8242s) and β-actin (Cat No. 4970s) were the products of Cell Signaling Technology Pathways. TLR4 inhibitor (TAK242, Cat No. M4838) was purchased from Abmole (Houston, TX, United States).

Extraction and purification of polysaccharide from *Atractylodes macrocephala*

AMP was extracted by water extraction and alcohol precipitation methods. Briefly, *A. macrocephala* was first extracted with alcohol for 2 times to remove the impurity. Second, *A. macrocephala* was decocted in water. The aqueous extract was concentrated under a vacuum. After that, a threefold volume of alcohol was added, the precipitated was washed three times with anhydrous ethanol, acetone and diethyl

(30). Then, the protein was removed using sewage methods (31). The polysaccharide was dialyzed for 24 h. We further purified the crude polysaccharide through Sephadex G-100 column. Finally, the purified extraction was lyophilized and the polysaccharide content of AMP was determined by UV-VIS absorption spectrometry.

Molecular weight measurement of polysaccharide from *Atractylodes macrocephala*

The molecular weight of purified samples was determined by high-performance gel permeation chromatography (HPGPC; Agilent 1,260 Infinity). Three gel permeation columns (KS-805, KS-804 and KS-802) were linked in serials. The column temperature was kept at 70°C. Double distilled water was used as mobile phase and the flow rate was kept at 1 mL·min⁻¹. The calibration curve was constructed using different molecular weights of Dextran standards, and the molecular weight of AMP was calculated by Dextran standards.

Monosaccharide composition analysis of polysaccharide from *Atractylodes macrocephala*

5 mg of AMP and 1 mL of trifluoroacetic acid (TFA, 2 M) were hydrolyzed at 121°C for 2 h. The mixture was dried with nitrogen, and then washed with methanol 2–3 times followed. The monosaccharide standards included fucose, arabinose, rhamnose, galactose, glucose, xylose, mannose, fructose, ribose, galacturonic acid and glucuronic acid. Finally, samples were analyzed *via* high-performance anion-exchange chromatography (HPAEC) (ICS5000, Thermo Fisher Scientific, United States) with Dionex™ CarboPac™ PA-20 column (150 mm × 3.0 mm, 10 μm). Mobile phase A was 0.1 M NaOH, mobile phase B was 0.1 M NaOH, 0.2 M NaAc. The composition of eluent A was adjusted to 95% at 0 min, 80% at 30 min, 60% at 30.1 min, 60% at 45 min, 95% at 45.1 min, 95% at 60 min. The column temperature was 30°C. The flow rate was 0.5 mL·min⁻¹ and the injection volume was 5 μL. The determination of monosaccharide composition was made with an electrochemical detector and the peaks were processed using Chromeleon 7.2 CDS (Thermo Scientific).

Preparation of AMP-ZnONPs

In order to fully hydrolyze KH550, 4 mL KH550 was added to 400 mL of equal volumes of alcohol and water, the mixture was reacted for 10 min under ultrasonication, and then agitated for 20 min on a magnetic stirrer. The pH of the solution was

adjusted to between 6.5 and 7.0 with 0.2 M HCl to generate silicon-oxygen bonds for grafting the ZnONPs. Then, 4.5 g of ZnONPs was added to this solution, sonicated for 30 min, agitated for 30 min at 200 rpm on a magnetic stirrer (80°C), and then the mixture was collected and lyophilized. The surface of ZnONPs was modified with KH550 by these processes. KH550-ZnONPs (10 mg) was added to water (20 mL). After sonicating for 1 h, AMP was added to the KH550-ZnONPs ($m_{AMP}: m_{KH550-ZnONPs} = 4:1$) and stirred for 24 h. The -CHO of AMP and the -NH₂ of ZnONPs were linked to assemble AMP-ZnONPs by Borch reduction.

Characterization of AMP-ZnONPs

Scanning Electron Microscope (SEM, Zeiss Supra55, Germany) was used to detect the samples of ZnONPs, KH550-ZnONPs, AMP and AMP-ZnONPs, the image magnification was 5,000 x. The morphology of samples was also observed *via* a Transmission electron microscope (TEM, HT7800, Hitachi, Japan). The element distribution was observed by Transmission electron microscope-energy dispersive spectroscopy mapping (TEM-EDS mapping, Tecnai G2 F30 S-TWIN, FEI, US) to verify the connection of the ZnONPs and AMP. The Fourier transform infrared spectroscopy (FT-IR, Thermo Electron Corporation, United States) spectra were recorded in the mid-infrared region. The samples were determined at room temperature on an X-ray diffraction (XRD, D8 Advance, Germany), and operated at 40 kV and 40 mA. The samples were determined with X-ray photoelectron spectrometer (XPS, ESCALAB 250Xi, United States). Data were analyzed using the Advantage software. The laser particle size analyzer (NanoPlus 3, Micromeritics Instrument Corp., United States) was applied to measure average particle size, polydispersity index (PDI) and zeta-potential.

Cell culture

RAW264.7 cells were cultured in the Dulbecco's modified Eagle's medium (DMEM) with 10% fetal bovine serum. Cells were maintained under a humidified atmosphere at 37°C with 5% CO₂.

Cell activity assay

The cell activity of AMP and AMP-ZnONPs on RAW264.7 cells was determined according to the CCK-8 method. Cell viability of RAW264.7 cells was evaluated after treatment with AMP and AMP-ZnONPs (0.06–250 μg·mL⁻¹) for 24 h. Following this, the supernatants were discarded, then added fresh DMEM medium (100 μL·well⁻¹) containing CCK8 (10

$\mu\text{L}\cdot\text{well}^{-1}$) and cultivated for 1.5–4 h at 37°C. Finally, the absorbance at 450 nm was measured by microplate reader. The cell survival rate was calculated as follows:

$$\text{Cell activity (\%)} = A_2/A_1 \times 100\%$$

(Where A_1 and A_2 are the absorbances of the control and test samples, respectively).

Measurement of nitric oxide

In brief, RAW264.7 cells (1×10^5 cells·mL⁻¹) were separately exposed to ZnONPs, AMP-ZnONPs and AMP ($1.95 \mu\text{g}\cdot\text{mL}^{-1}$) for 24 h at 37°C in a constant temperature incubator ventilating with 5% CO₂. At the end of incubation, the NO amount in the supernatant was measured by a Griess reagent system kit K.

Quantitative real-time polymerase chain reaction

Real-time polymerase chain reaction (PCR) was employed for the determination of cytokines (IL-6 and IL-1 β) and TLR4, MyD88, TRAF6 mRNA expression. The total RNA of RAW264.7 cells was obtained with Trizol reagent, and then synthesized the corresponding cDNA. The Hieff qPCR SYBR Green Master Mix was employed to perform Quantitative real-time PCR assay. The primer sequences of genes were displayed in [Table 1](#). The following PCR protocol was referenced by our previous report (32). The expression of each gene was analyzed by the $2^{-\Delta\Delta\text{ct}}$ comparative method.

Determination of phagocytic function using CytExpert flow cytometer

RAW264.7 cells (1×10^6 ·mL⁻¹) were cultured in 6 well plates at 37°C for 12 h, and then exposed to ZnONPs, AMP, AMP-ZnONPs ($1.95 \mu\text{g}\cdot\text{mL}^{-1}$) or LPS ($0.5 \mu\text{g}\cdot\text{mL}^{-1}$) for 24 h, respectively. The cells were incubated with 1 mg·mL⁻¹ FITC-dextran for 1 h, then the reaction was stopped by cold PBS. The FITC-dextran intensity of cell samples was analyzed by CytExpert flow cytometer (Beckman Coulter, CA, United States).

High-resolution laser confocal microscopy

Cells were seeded at 1×10^5 cells·mL⁻¹ on coverslips in a 24 well plate, then stimulated with ZnONPs, AMP,

AMP-ZnONPs ($1.95 \mu\text{g}\cdot\text{mL}^{-1}$) or LPS ($0.5 \mu\text{g}\cdot\text{mL}^{-1}$), and incubated with 1 mg·mL⁻¹ FITC-dextran ($1 \text{ mg}\cdot\text{mL}^{-1}$) at 37°C for 1 h. After incubation, RAW264.7 cells were fixed with 4% paraformaldehyde for 10 min. Cell samples were stained with phalloidin for 1 h under dim light, followed by DAPI staining. The green fluorescence was measured by laser confocal microscopy (LSCM) (TCS SP8 STED, Germany).

Expression of cell surface molecule CD80, CD86, and MHCII

The cells (1×10^6 cells·mL⁻¹) were treated with AMP-ZnONPs for 24 h in a 6-well plate. Then, the cells were suspended and incubated with anti-CD80, anti-CD86 and anti-MHCII at 4°C for 30 min, and analyzed by the CytExpert flow cytometer.

Cell morphological observation

The cells (1×10^5 cells·mL⁻¹) were plated on coverslips in 24-well plates, and then treated with ZnONPs, AMP, AMP-ZnONPs ($1.95 \mu\text{g}\cdot\text{mL}^{-1}$), LPS ($0.5 \mu\text{g}\cdot\text{mL}^{-1}$) or DMEM. The RAW264.7 cells with glutaraldehyde-treated were prepared for 24 h. Next, the cells were evaporated using a 30, 50, 70, 80, 90, 95, and 100% ethanol gradient (10–15 min each time); then displaced in Na₂SO₄, dried at a tipping point, and finally scanned by SEM (HT7800, Hitachi, Japan) at 1,000 and 8,000 \times .

Western blotting analysis

The BCA protein assay kit was employed to detect the protein concentrations. Equal amounts (30 μg) of total protein were separated and transferred to the NC membrane (33). The membrane was incubated with 5% skim milk for 2 h and then incubated with gentle shaking with primary antibodies at 4°C overnight. Later incubated NC at 4°C with antibodies of TLR4 (rabbit, 1: 1,000), TRAF6 (rabbit, 1: 1,000), MyD88 (rabbit, 1: 1,000), P-p65 (rabbit, 1: 1,000), P-I κ B α (rabbit, 1: 1,000) and β -actin (rabbit, 1: 1,000). After incubation with the primary antibody, the membrane was exposed to goat anti-rabbit secondary antibody (1: 5,000) at room temperature for 1 h. The membrane was washed with TBST for 3 times, membrane-bound antibodies were visualized using the ECL Enhanced Chemiluminescence system, the protein band intensity was analyzed with Image J Analysis Software.

Statistical analysis

GraphPad Prism 5.0 Software was utilized for statistical analysis. Data were analyzed by one-way analysis of variance

(ANOVA) followed by Dunnett's multiple comparisons test. All the data were expressed using mean \pm standard deviation (SD). The criterion of significance was $P < 0.05$.

Results and discussion

Molecular weight and monosaccharide composition of polysaccharide from *Atractylodes macrocephala*

As shown in **Figure 2A**, the results of HPGPC implied a good homogeneity of AMP. The retention time was 24.98 min. The chromatographic result of HPGPC showed that AMP had one peak, which indicated that AMP was homogeneous polysaccharides. Based on the regression equation of the dextran standard curve, $y = 11.864079 - 0.338831 \times -0.005080 \times^2 + 0.000195 \times^3$, the molecule weight of AMP was calculated as 2.743×10^3 Da (**Figure 2B**). The result of monosaccharide composition obtained from AMP was described by HPAEC (**Figures 2C,D**). AMP was composed of arabinose, galactose, glucose, xylose, mannose, ribose, galactose uronic acid, glucose uronic acid, with a percentage ratio of 21.86, 12.28, 34.19, 0.43, 0.92, 0.85, 28.79, and 0.67%, respectively.

Characteristics of AMP-ZnONPs

Morphological characteristics of AMP-ZnONPs

Ultrastructure of ZnONPs, KH550-ZnONPs, AMP and AMP-ZnONPs was obtained with the SEM (**Figure 3A**). The AMP exhibited an irregular surface with many folds. ZnONPs showed rod morphology and a nano-lamellar structure. The KH550-ZnONPs after the surface modification displayed particles with uniform size, good monodispersity, and no obvious agglomeration. The surface of AMP appeared to be covered by rod-shaped ZnONPs, which was attributed to the strong interaction between amino in ZnONPs and hemiacetal in AMP because of hydroamination. Ultrastructure of ZnONPs, KH550-ZnONPs, AMP and AMP-ZnONPs as shown in **Figure 3B**. The ZnONPs showed strong clustering and

exhibited aggregation. The KH550-ZnONPs had smaller clusters and showed a homogenous dispersion, all aggregation was disrupted. As shown in the AMP-ZnONPs, KH550-ZnONPs were connected to the surface of AMP. The TEM-EDS mapping and EDS spectra showed that C, O and Zn elements were present in AMP-ZnONPs (**Figure 3C**). Therefore, the results strongly supported the formation of AMP-ZnONPs.

Fourier transform infrared spectroscopy analysis

As shown in **Figure 4A**, FT-IR spectra of AMP revealed that the characteristic peaks of polysaccharide at 3366.9 cm^{-1} , 2931.4 cm^{-1} , and 1427 cm^{-1} were attributed to O-H stretch vibration of hydroxyl group, C-H stretch vibration and O-H bending vibration, respectively (34). Moreover, the weak bands around 935.6 cm^{-1} and 818.9 cm^{-1} indicated that there were α -configuration and β -configuration (35, 36). FT-IR spectra of ZnONPs showed an intense peak at 571.1 cm^{-1} and a broad peak at 3442.1 cm^{-1} . The weak absorption peak at 3442.1 cm^{-1} could be attributed to stretching vibration of associating hydroxyls formed by weak hydrogen bonding as well as van der Waals interaction (37). The stretching vibration band at 571.1 cm^{-1} corresponding to the Zn-O bond (38). Compared with ZnONPs, KH550-ZnONPs displayed a new typical characteristic absorption peak of $-\text{NH}_2$ at 1582.6 cm^{-1} , which was attributed to the characteristic absorption peak of KH550. The AMP-ZnONPs spectra showed the characteristic absorption peaks of ZnONPs, KH550 and AMP. In addition, the signal in 1058.9 cm^{-1} was mainly assigned to the stretching vibration of the C-O-C group, the absorption peak at $1,629 \text{ cm}^{-1}$ corresponded to N-H stretching vibrations (39, 40). FT-IR spectra of AMP showed that the band at 1636.2 cm^{-1} corresponding to the C = O bond (41). There was no N-H bond in AMP, after connecting to ZnONPs, the presence of an N-H bond in AMP-ZnONPs indicated a possible connection. The result provided evidence for the successful grafting of the KH550-ZnONPs by the NH_2 groupings in KH550 agents onto AMP.

X-ray diffraction analysis

XRD, as a valuable instrument (42), could be used to further confirm the composition of AMP-ZnONPs (**Figure 4B**). The

TABLE 1 The primer sequences of target genes.

Gene	Sense (5'-3')	Antisense (5'-3')
IL-6	TTCATCCAGTTGCCTTCTTG	AATTAAGCCTCCGACTTGTGAA
IL-1 β	ATCTCGCAGCAGCACATCA	CCAGCAGGTTATCATCATCATCC
TLR4	TGGTCAGTGTGATTGTGGTATC	GCTTTCCTCTGCTGTACTT
MyD88	TCGATGCCTTTATCTGCTACTG	GGTCGGACACACAACCTTA
TRAF6	GCTGAGCCACAATACTCACTAA	TTCTAGCGGATGGACATTACAC
GADPH	ATGGTGAAGGTCGGTGTGAA	CCTTGACTGTGCCGTTGAAT

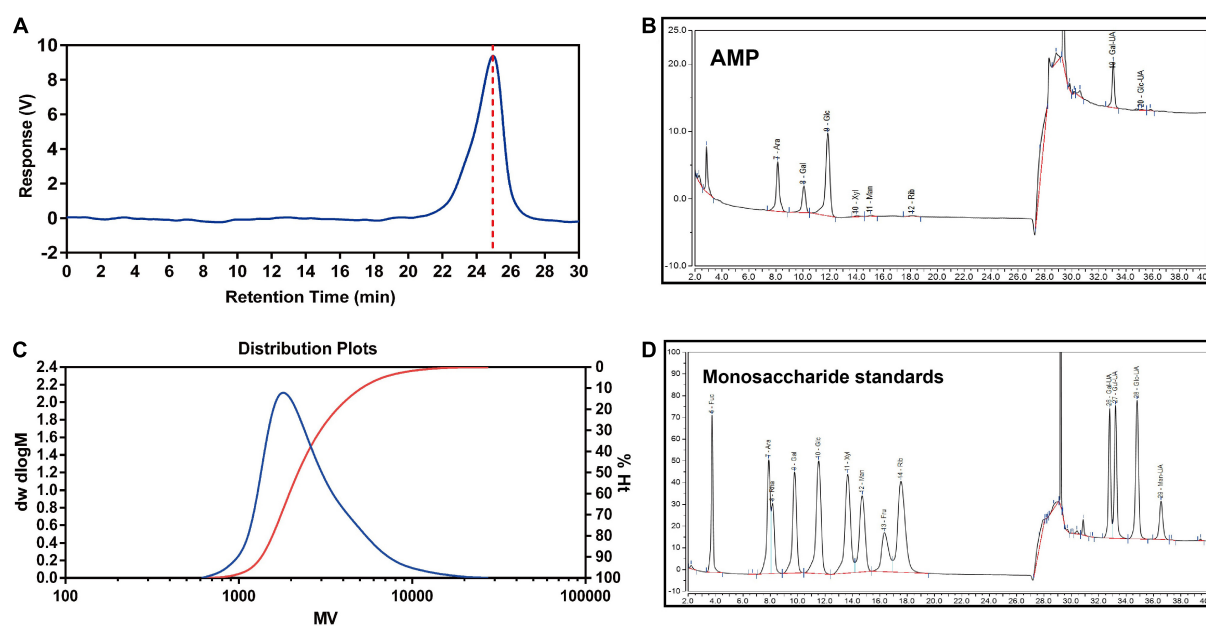


FIGURE 2

Molecular weight and monosaccharide composition of AMP. The peak at retention time of AMP (A) and molecular weight distribution (B) of AMP. HPAEC chromatograms of AMP (C) and monosaccharide standards (D). Fuc, fucose; Ara, arabinose; Rha, rhamnose; Gal, galactose; Glc, glucose; Xyl, xylose; Man, mannose; Fru, fructose; Rib, ribose; Gal-UA, galacturonic acid; Glu-UA, glucuronic acid.

characteristic peaks located at $2\theta = 31.7, 34.4, 36.2, 47.5, 56.6, 62.8, 66.3, 67.9, 69.1, 72.5, 76.9$, corresponding to the (100), (002), (101), (102), (110), (103), (200), (112), (201), (004), (202) planes, respectively, match well with characteristic reflections of ZnONPs (P63mc, JCPDS no. 89-0511). A similar curve of ZnONPs modified by KH550 proved that modification of KH550 did no effect on the phase formation of ZnONPs. The XRD results of AMP recorded between 10° and 30° suggested the presence of crystalline components, with major reflections at $12.0^\circ, 17.7^\circ$ and 21.8° . This profile was also observed in other different polysaccharides (43, 44). The XRD profile of AMP-ZnONPs showed that the main characteristic peaks of ZnONPs, confirming that the hexagonal structure of the ZnONPs was not affected after binding with AMP. Moreover, as sereov-shapederot affected aft $\theta = 10\text{--}20$, the modified AMP molecule maybe undergo a chemical structure change and convert to amorphous materials under this circumstance.

X-ray photoelectron spectrometer analysis

XPS was depicted in Figure 4C to investigate the surface compositions of the ZnONPs (45, 46). Compared with ZnONPs, the XPS spectra of the KH550-ZnONPs exhibited the characteristic peak components of Zn2p3, O1s, N1s, C1s and Si2p, suggesting that silane had successfully modified on the surface of ZnONPs. The AMP showed a Zn-free surface, the two peaks at 285, and 532 eV correspond to C1s and O1s, respectively. The C1s core-level spectrum of the KH550-ZnONPs was divided into three peak components: C-C, C-N

and C-Si (Figure 4D). The C1s core-level spectrum of the AMP was divided into two peak components: C-C and C-O (Figure 4E). The peaks of C-O (286.6 eV), C-C (284.8 eV), C-N (286.3 eV) and C-Si (283.5 eV) were also observed in the C1s spectrum of the AMP-ZnONPs (Figure 4F), the C-N single bond peak was introduced by KH550, and the C-O peak was introduced by AMP. The presence of a C-N bond confirmed that there was a cross-linking reaction between the AMP and the KH550-ZnONPs. Although the Zn2p3 peak was reduced due to the AMP shielding, some active sites of ZnONPs remain even. These results were in good agreement with previous results of XRD and FT-IR, indicating that the successful grafting of AMP and KH550-ZnONPs.

Particle size, polydispersity index and zeta potential

The particle size (Table 2 and Figure 5A) of the ZnONPs was larger than that of the KH550-ZnONPs, this result revealed that after KH550 being modified on the surface of ZnONPs promoted the particle size to be smaller. The particle size of AMP-ZnONPs was slightly larger than KH550-ZnONPs, which may be caused by the AMP binding on KH550-ZnONPs. The PDI values of AMP-ZnONPs was lower than 0.3, which was considered optimal for the dispersion and homogeneity (47). The zeta potential of AMP-ZnONPs was more negatively charged than KH550-ZnONPs (Figure 5B), with AMP-ZnONPs gaining additional negative charge of -4.43 mV. Negatively

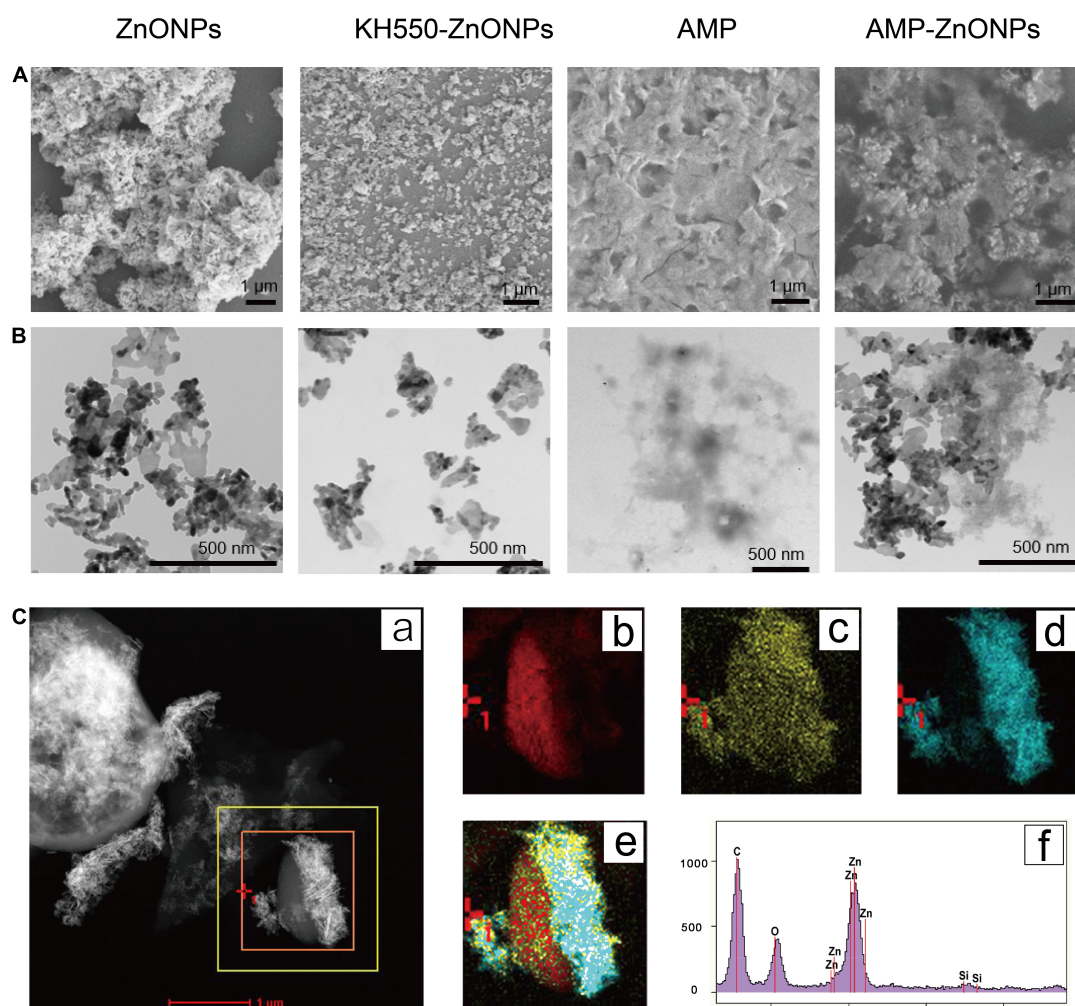


FIGURE 3

The SEM analyzes of ZnONPs, KH550-ZnONPs, AMP and AMP-ZnONPs (A). The TEM analyzes of ZnONPs, KH550-ZnONPs, AMP and AMP-ZnONPs (B). TEM-EDS mapping image of AMP-ZnONPs (C), TEM image (a), corresponding elements distribution of C (b), O (c) and Zn (d), merge (e), EDS spectrum (f).

charged nanoparticles are more likely to be internalized by cells than positively charged nanoparticles, this property underlies the fact that AMP-ZnONPs stimulates phagocytosis of RAW264.7 cells more significantly than either ZnONPs or AMP alone.

Cell viability

The cell viability of ZnONPs, AMP and AMP-ZnONPs on RAW264.7 cells were shown in **Figure 6A**. Compared with the control group, ZnONPs, AMP and AMP-ZnONPs exerted no damaging effect and promoted cell proliferation to a certain extent at a concentration of 0.24–1.95 $\mu\text{g}\cdot\text{mL}^{-1}$. When the concentration of AMP-ZnONPs was 0.49–3.91 $\mu\text{g}\cdot\text{mL}^{-1}$, the proliferation effect was proportional to the concentration. To compare the immune effects of ZnONPs, AMP and AMP-ZnONPs at the same concentration level, the concentration

of ZnONPs, AMP and AMP-ZnONPs at 1.95 $\mu\text{g}\cdot\text{mL}^{-1}$ were chosen in the following experiments.

AMP-ZnONPs induced cells nitric oxide production

NO is an important active substance associated with the immunomodulatory effect (48), which participates in apoptosis regulation and host defense function (49). The NO production was calculated from the standard curve formula. The results of NO release in AMP-ZnONPs were shown in **Figure 6B**. As a positive control, the NO content of LPS group (0.5 μgPS^{-1}) showed significantly higher than the control group ($P < 0.001$). And the release of NO in AMP-ZnONPs group was higher than that of the control, ZnONPs group ($P < 0.001$) and AMP group ($P < 0.05$). Therefore, AMP-ZnONPs could stimulate NO

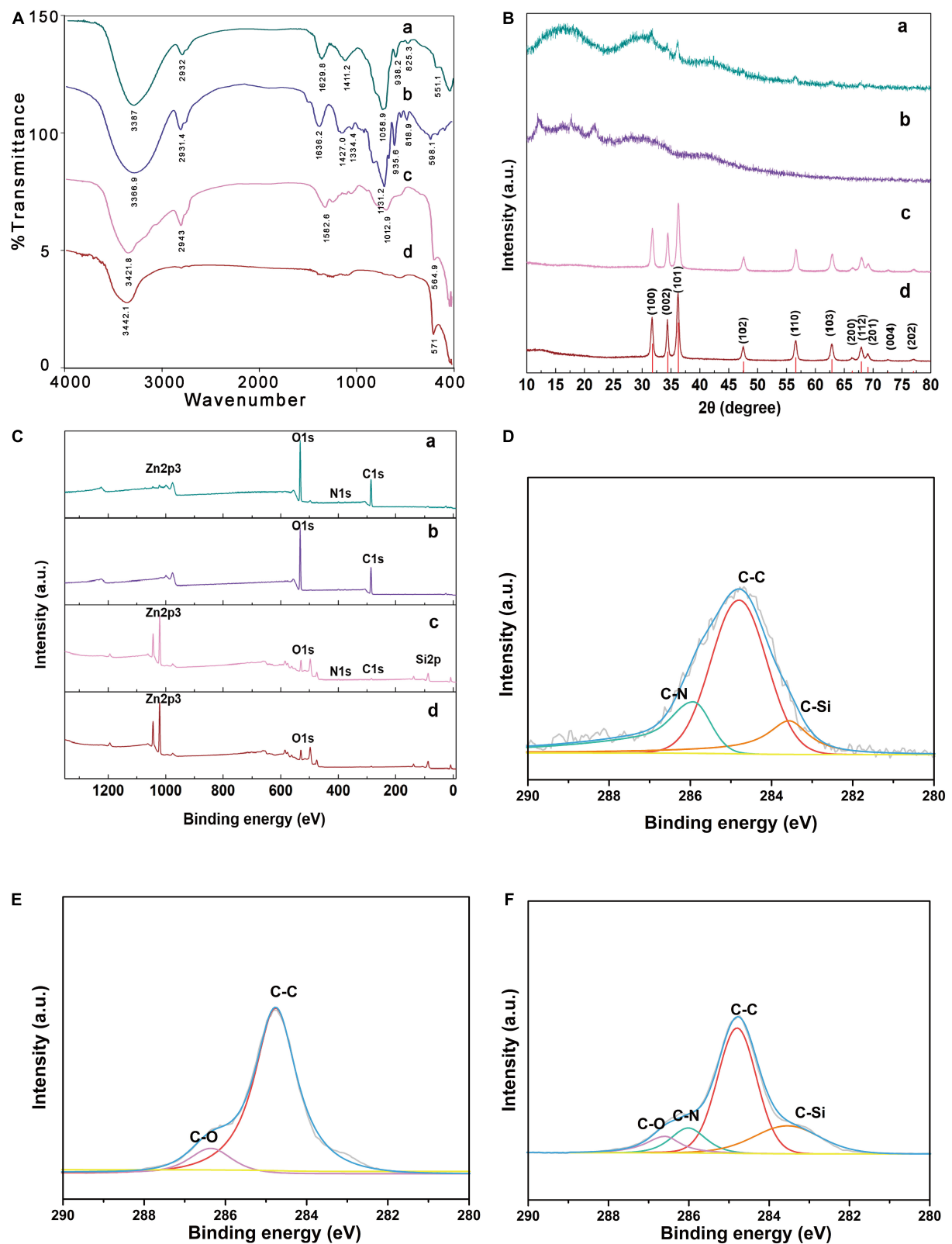
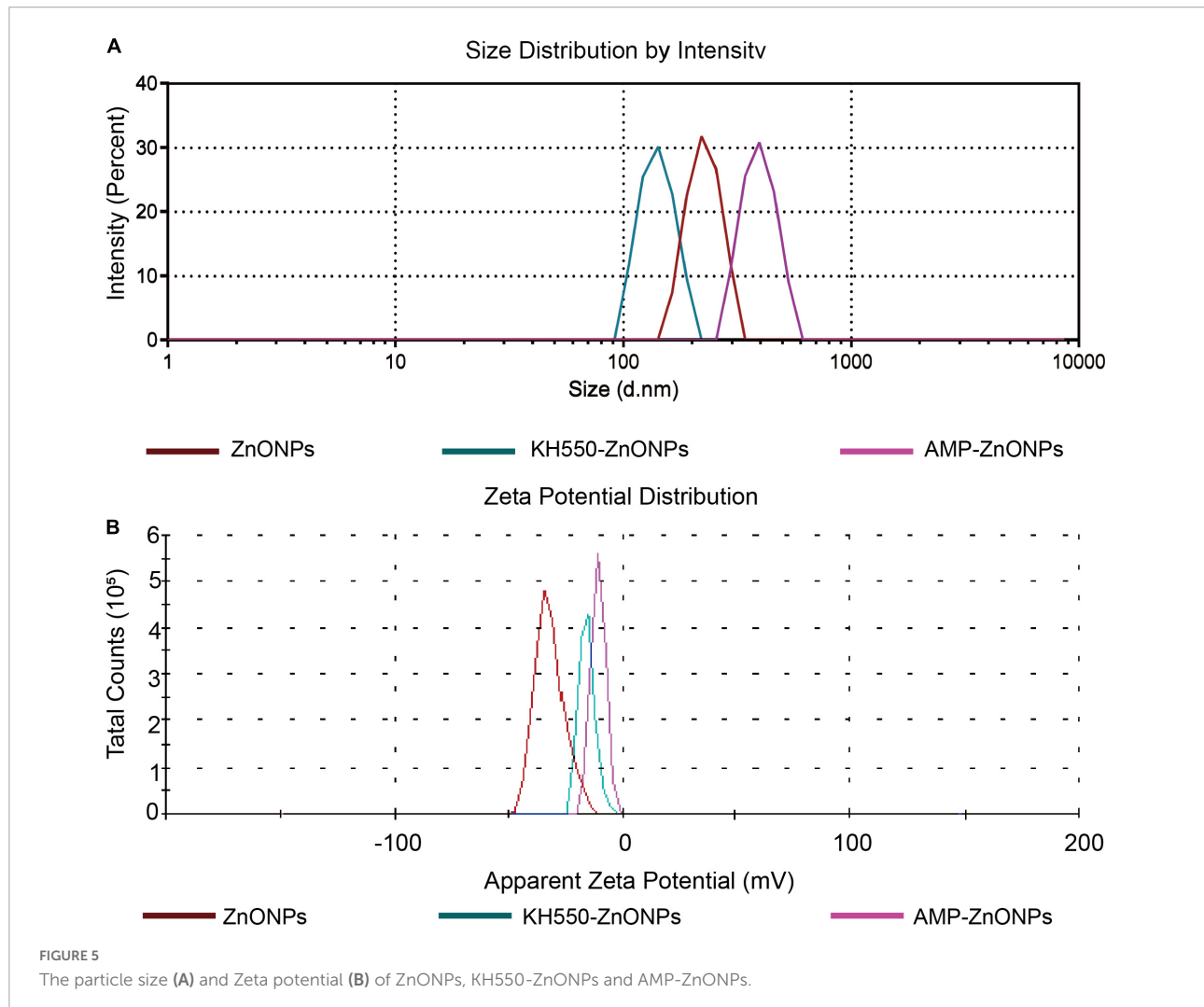


FIGURE 4

Spectroscopic characterization and curve-fitting spectra of AMP-ZnONPs. The FT-IR pattern (A), XRD pattern (B), XPS spectra (C) of AMP-ZnONPs (a), AMP (b), KH550-ZnONPs (c) and ZnONPs (d). The curve-fitting of C1s (D) spectra of AMP-ZnONPs. The curve-fitting of C1s (E) spectra of AMP. The curve-fitting of C1s (F) spectra of AMP-ZnONPs.

TABLE 2 The particle size, PDI, and zeta potential of ZnONPs, KH550-ZnONPs and AMP-ZnONPs ($n = 3$).

Samples	ZnONPs	KH550-ZnONPs	AMP-ZnONPs
Size (nm)	211.89 \pm 8.98	136.73 \pm 3.12	391.37 \pm 3.27
PDI	0.095 \pm 0.053	0.391 \pm 0.137	0.206 \pm 0.086
Zeta potential (mV)	-33.20 \pm 1.11	-10.97 \pm 0.32	-15.40 \pm 0.35



release more than AMP and ZnONPs in RAW264.7 cells, this suggested that ZnONPs displayed synergy with AMP.

AMP-ZnONPs induced cells cytokines secretion

Cytokines are the central logical targets for immune modulation as they influence the formation of a phenotype. They act as immunoregulators by either inducing or suppressing the production and maturation of immune cells (50). IL-1 β is a major mediator of inflammation secreted by various activated innate immune cells, such as macrophages, monocytes and dendritic cells (51). IL-6 is also one of the important mediators that can stimulate antibody production and participate in

immune response. Both IL-1 β and IL-6 are of great importance for immune homeostasis and barrier immunity. To further investigate the immunological activity of AMP-ZnONPs on RAW264.7 cells, the cytokine (IL-1 β and IL-6) contents in cells were evaluated by RT-qPCR in this study (Figures 6C,D). LPS stimulated the production of IL-1 β and IL-6 by more than 2,000 times compared to the control group ($P < 0.001$), which indicated that LPS could promote inflammation and lead to excessive cytokine release (52). Notably, AMP-ZnONPs treatment exerted a significant action on IL-1 β and IL-6 secretion than both AMP and ZnONPs ($P < 0.001$), which showed ZnONPs exerted a synergistic effect with

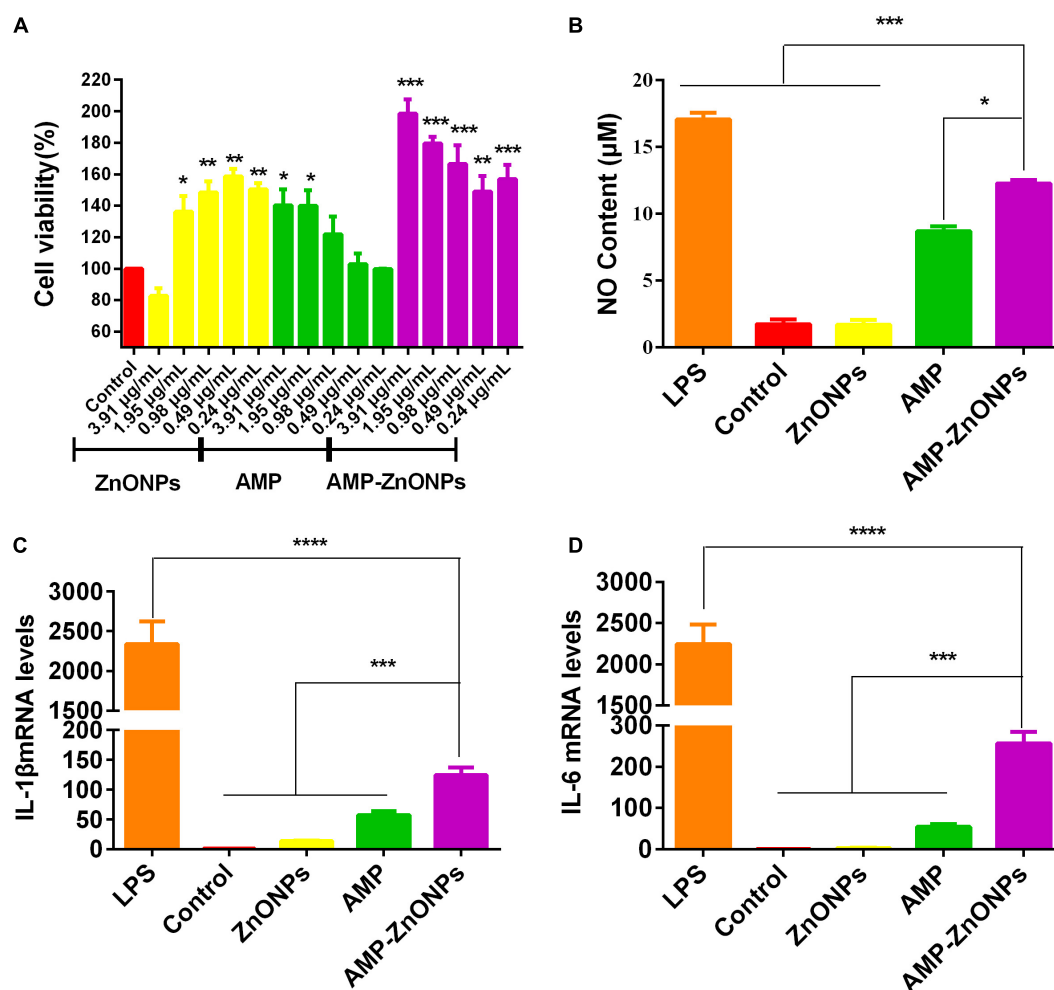


FIGURE 6

The proliferative activity of RAW264.7 cells stimulated by ZnONPs, AMP and AMP-ZnONPs (A). NO content of cell culture supernatant (B) and the mRNA expression of IL-1 β (C), IL-6 (D) in RAW264.7 cells of different groups. (* $P < 0.05$, ** $P < 0.01$, *** $P < 0.001$, **** $P < 0.0001$ vs. AMP-ZnONPs).

AMP. The results indicated that the AMP-ZnONPs had immunostimulatory effect, but it did not cause cell inflammation like LPS.

AMP-ZnONPs enhanced cells phagocytosis

Macrophages exist in virtually all tissues, phagocytosis, which is a classic index to evaluate macrophage activation, plays a critical role in the uptake and degradation (53–55). In addition, it is a signal-inducing process in which phagosomes bind to the antibody on the cell surface, consequently, cell morphology and signaling pathways are affected (56). The enhanced phagocytosis is one of the remarkable characteristics of activated macrophages, meanwhile indicating the activation of innate immunity. The results showed that compared with the control and ZnONPs, AMP-ZnONPs and AMP could significantly promote cell phagocytosis of macrophages (Figures 7A,B). Meanwhile, it should be highlighted that the stimulating effect

of AMP-ZnONPs on phagocytosis was remarkably higher than AMP ($P < 0.05$). Furthermore, FITC-dextran accumulation in RAW264.7 was measured by LSCM. As shown in Figure 7C, AMP-ZnONPs treatment markedly enhanced the fluorescence intensity of tested cells relative to AMP and ZnONPs, and the FITC-dextran were mainly distributed in the cytoplasm. These results demonstrated that the AMP binding with ZnONPs significantly improved the immune activity of RAW264.7, which indicated ZnONPs and AMP acted in synergy of immune system.

AMP-ZnONPs promoted cells costimulatory molecules expression

The activation and further differentiation of T cells and cellular immune function are closely related to the function of antigen-presenting cells (APC), especially macrophages, considered as professional antigen-presenting cells (57). CD80

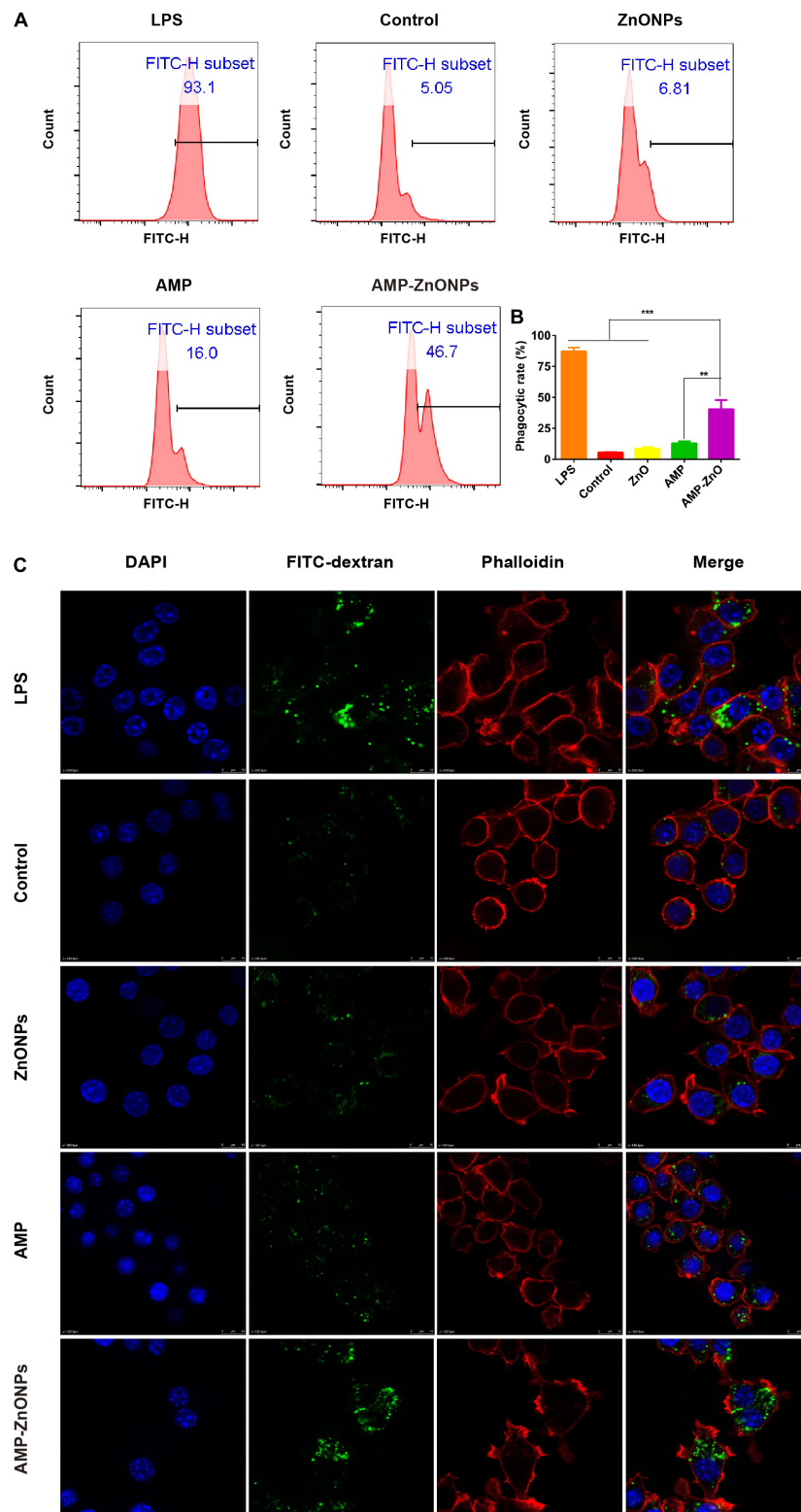


FIGURE 7

The phagocytosis was evaluated by flow cytometry (A). The histogram showed the positive rate of cells for FITC-dextran (B). (** $P < 0.01$, *** $P < 0.001$ vs. AMP-ZnONPs). Enhanced FITC-dextran uptake into RAW264.7 cells following incubation with AMP-ZnONPs. FITC-dextran (green) was mixed with ZnONPs, AMP, AMP-ZnONPs, LPS and DMEM medium (control) overnight avoiding light. Cytoskeleton and cell nuclei were stained with phalloidin (red) and DAPI (blue) respectively, (C).

and CD86 may differentially control the T-cell activation because of the distinct properties of each molecule. Once presented to T cells by MHCII, peptide antigens generally stimulate a typical T cell-dependent immune response and the induction of immune memory (58). In this study, the expression of phenotypic markers of CD80, CD86 and MHCII up-regulated after the RAW264.7 cells were exposed to LPS for 24 h (Figure 8A). Figures 8B–D documented

a significant increase in the percent of RAW264.7 cells positive for the expression of CD80, CD86, and MHCII following incubation with AMP-ZnONPs as compared to the control, ZnONPs and AMP. The results proved that AMP-ZnONPs significantly increased the expression of CD80, CD86 and MHCII compared with ZnONPs or AMP alone, which indicated ZnONPs and AMP showed synergetic effect with each other.

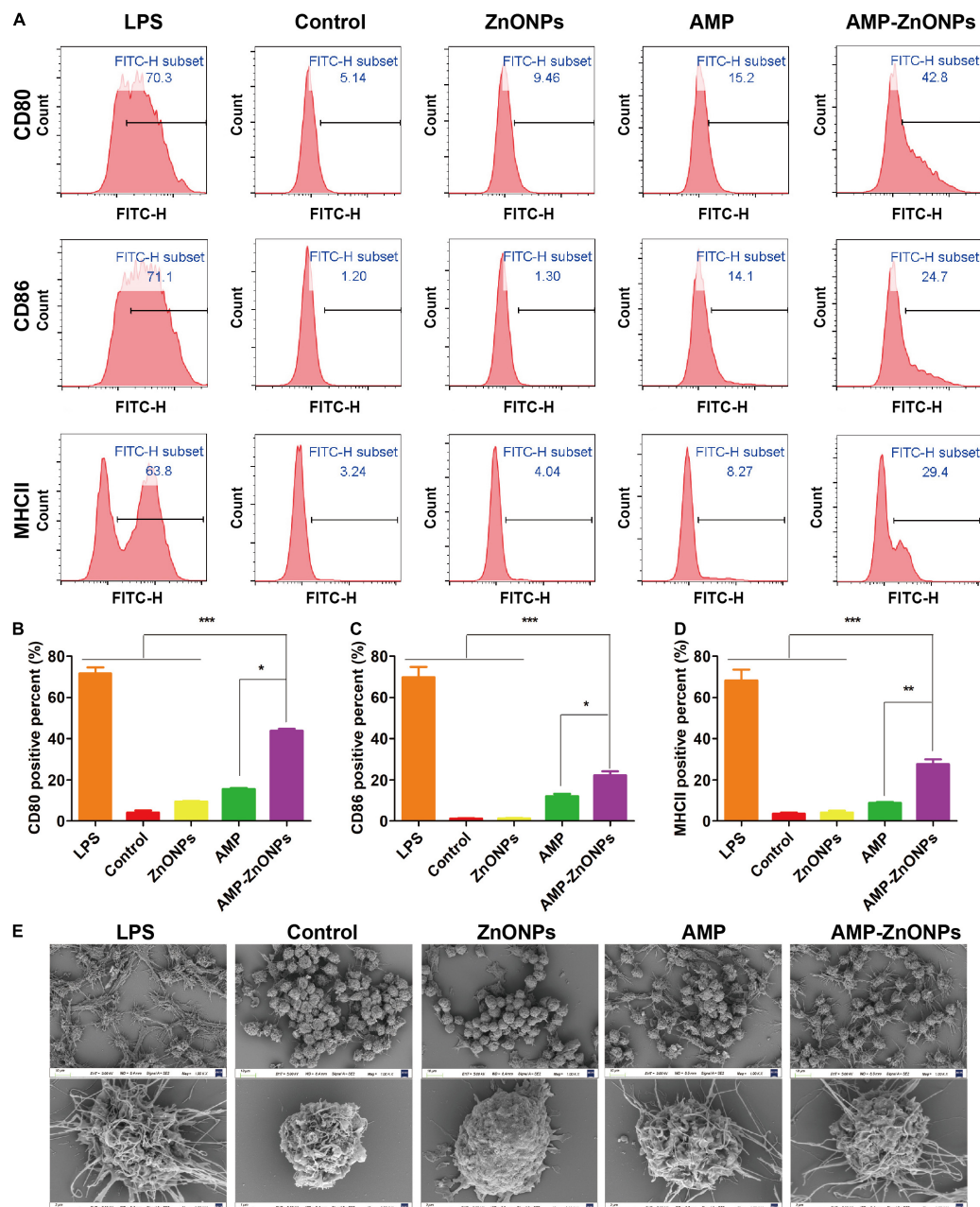


FIGURE 8

The production of CD80, CD86, MHCII in RAW264.7 cells were analyzed by flow cytometry (A). The histogram showed the positive rate of CD80 (B), CD86 (C), MHCII (D) in cells. (* $P < 0.05$, ** $P < 0.01$, *** $P < 0.001$ vs. AMP-ZnONPs). SEM analysis for morphological changes of RAW264.7 cells in different groups (E).

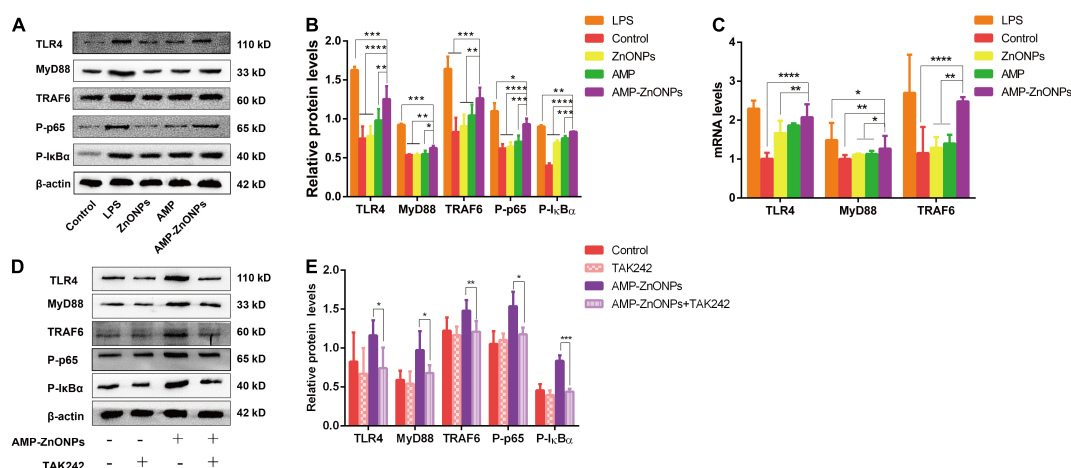


FIGURE 9

The relative expressions of proteins (A,B) and mRNAs (C) of the critical nodes in the TLR4/MyD88/NF-κB signaling pathways. Effects of TAK242 on TLR4, MyD88, TRAF6, P-IkBα and P-p65 expression stimulated by AMP-ZnONPs or not (D,E). The results were expressed as the mean ± SD ($n = 3$) (* $P < 0.05$, ** $P < 0.01$, *** $P < 0.001$, **** $P < 0.0001$ vs. AMP-ZnONPs).

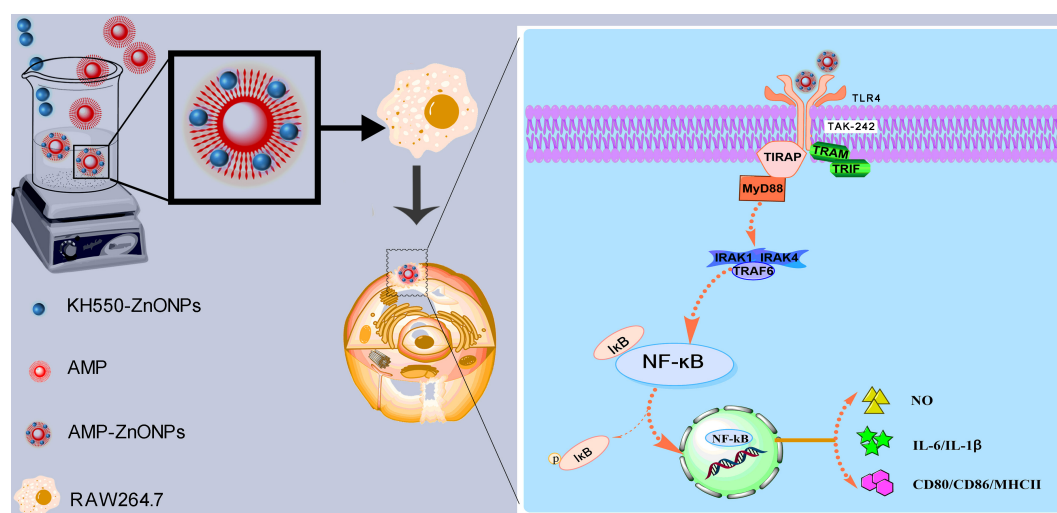


FIGURE 10

Schematic illustration depicts that a new approach was carried out to bind AMP with ZnONPs as an immunostimulator. AMP-ZnONPs could significantly activate RAW264.7 cells by TLR4/MyD88/NF-κB signaling pathway to improve its immune function. Therefore, AMP-ZnONPs remarkably enhanced phagocytosis, the release of NO, cytokines and the costimulatory molecules of RAW264.7 cells.

AMP-ZnONPs induced cells morphological changes

Macrophages engulf nutrients and pathogens by stretching their arms (59). The morphology was observed by SEM as shown in Figure 8E. Cells in the control group had a round shape and microvilli-like structures on the cell surface. RAW264.7 cells showed elongated and polygonal with many filopodia in the LPS group than in the other groups. In the AMP-ZnONPs group, even in the case of round-shaped RAW264.7 cells, their arms were stretching in various directions. The size, microvilli-like structures and surface folds of the AMP-ZnONPs treated group

were more than ZnONPs and AMP. These results indicated that AMP-ZnONPs could induce RAW264.7 cells activation visibly, which was inconsistent with the results of phagocytosis and cytokine secretion.

AMP-ZnONPs regulated the expression of TLR4/MyD88/NF-κB associated proteins

As an important member of the TLR family, TLR4 has been widely reported to recognize and bind to different pathogen-related molecular patterns, initiate intracellular signal transduction pathways, cause the release of cytokines or

chemokines, and play an effective innate immune response (60). Whether AMP-ZnONPs could mediate the immunomodulatory effect on RAW264.7 cells by the TLR4 signaling pathway was explored. The RT-qPCR and Western blot were used to detect the mRNA and proteins of key nodes in the TLR4/MyD88/NF- κ B signaling pathways. As shown in **Figures 9A,B**, compared with AMP group, the protein expression levels of TLR4, MyD88, TRAF6, P-I κ B α and P-p65 were upregulated in AMP-ZnONPs group. As shown in **Figure 9C**, AMP-ZnONPs significantly up-regulated the mRNA expression of TLR4, MyD88, TRAF6 in the RAW264.7 cells, compared with those in control, ZnONPs and AMP group. Therefore, the results indicated that AMP-ZnONPs was more effective than ZnONPs and AMP in activating the TLR4/MyD88/NF- κ B signaling pathway.

AMP-ZnONPs downregulated expression of TLR4/MyD88/NF- κ B associated proteins after treating with the TLR4 blocker TAK242

TAK242 is a specific inhibitor of TLR4 that affects the downstream signal transduction of TLR4 by interfering with the intracellular segment of TLR4 (61). In order to further verify that AMP-ZnONPs could activate the TLR4/MyD88/NF- κ B signaling pathway, RAW264.7 cells were treated with the TLR4 antagonist TAK242, and the expression of key proteins in the pathway were detected. After adding TAK242, the expression of each protein in the TLR4 pathway was shown in **Figure 9D**. Compared with the control group, the expression of TLR4, MyD88, TRAF6, P-I κ B α and P-p65 were increased after treatment with AMP-ZnONPs (**Figure 9B**), while the expression of the above proteins was significantly reduced after TAK242 was added (**Figure 9E**).

TLR4 generally signals *via* a MyD88-dependent pathway, then IKK phosphorylates I κ B and p65 resulting in degradation of I κ B and activation of NF- κ B, a nuclear factor that is responsible for the production of many cytokines (IL-6, IL-1 β) and the costimulatory molecules (CD80, CD86, MHCII). In this study, AMP-ZnONPs could significantly activate RAW264.7 cells by TLR4/MyD88/NF- κ B signaling pathway to improve its immune function. TAK242, a specific TLR4 inhibitor, reversely demonstrated that AMP-ZnONPs could promote the expression of TLR4 pathway-related proteins. In conclusion, this study can provide a new research idea for the development and utilization of polysaccharides and microelements in the food and pharmaceutical industry and presents a theoretical basis for research and development into new immunomodulatory nutraceutical or immune adjuvant (**Figure 10**).

Conclusion

In summary, by Borch reaction between AMP and ZnONPs modified by KH550, the AMP-ZnONPs was successfully prepared and its characterization was evaluated. AMP-ZnONPs

showed excellent immunostimulatory activity on macrophages and the activities were much better than those of ZnONPs or AMP applied alone. Furthermore, this study clarified that AMP-ZnONPs could significantly activate RAW264.7 cells by TLR4/MyD88/NF- κ B signaling pathway to improve its immune function. These data demonstrated that AMP binding with ZnONPs could potentially be used as an easily available source for immunomodulatory nutraceutical or immune adjuvant, which can be widely used in the food or medicine industry in the future.

Data availability statement

The datasets presented in this study can be found in online repositories. The names of the repository/repositories and accession number(s) can be found in the article/supplementary material.

Author contributions

RB: conceptualization, methodology, software, data curation, writing—original draft, review and editing, visualization, supervision, project administration, and funding acquisition. XL: conceptualization, methodology, investigation, software, data curation, writing—original draft, and visualization. JW: methodology, investigation, and software. SW: investigation and writing—review and editing. XW: investigation and software. YT and SX: visualization and investigation. ML: supervision. JL: conceptualization, methodology, project administration, and funding acquisition. HP: conceptualization and methodology. All authors contributed to the article and approved the submitted version.

Funding

This work was supported by the Natural Science Foundation of Jiangsu Province (Grant no. BK2020945), the National Natural Science Foundation of China (Grant nos. 32002324, 32072911, and U1904215), the China Postdoctoral Science Foundation (Grant no. 2021M692716), Postgraduate Research and Practice Innovation Program of Jiangsu Province (No. SJCX22-1806), and the Priority Academic Program Development of Jiangsu Higher Education Institutions (PAPD).

Conflict of interest

The authors declare that the research was conducted in the absence of any commercial or financial relationships that could be construed as a potential conflict of interest.

Publisher's note

All claims expressed in this article are solely those of the authors and do not necessarily represent those of their affiliated

organizations, or those of the publisher, the editors and the reviewers. Any product that may be evaluated in this article, or claim that may be made by its manufacturer, is not guaranteed or endorsed by the publisher.

References

- Yun C, Yao F, Ke M, Wang D, Hu Y, Liu J. Polysaccharides from traditional chinese medicines: Extraction, purification, modification, and biological activity. *Molecules*. (2016) 21:1705. doi: 10.3390/molecules21121705
- Qin J, Wang HY, Zhuang D, Meng FC, Lv GP. Structural characterization and immunoregulatory activity of two polysaccharides from the rhizomes of *Atractylodes lancea* (thunb.) dc. *Int J Biol Macromol*. (2019) 136:341–51. doi: 10.1016/j.ijbiomac.2019.06.088
- Wang P, Zhao YN, Xu RZ, Zhang XW, Sun YR, Feng QM, et al. Sesquiterpene Lactams and Lactones With Antioxidant Potentials From *Atractylodes macrocephala* Discovered by Molecular Networking Strategy. *Front Nutr*. (2022) 9:865257. doi: 10.3389/fnut.2022.865257
- Li J, Hu D, Zong W, Lv G, Zhao J, Li S. Determination of inulin-type fructooligosaccharides in edible plants by high-performance liquid chromatography with charged aerosol detector. *J Agr Food Chem*. (2014) 62:7707–13. doi: 10.1021/jf502329n
- Chau CF, Wu SH. The development of regulations of Chinese herbal medicines for both medicinal and food uses. *Trends Food Sci Tech*. (2006) 17:313–23. doi: 10.1016/j.tifs.2005.12.005
- Sun W, Meng K, Qi C, Yang X, Wang Y, Fan W, et al. Immune-enhancing activity of polysaccharides isolated from *Atractylodes macrocephala* Koidz. *Carbohydr Polym*. (2015) 126:91–6. doi: 10.1016/j.carbpol.2015.03.034
- Xu W, Fang S, Wang Y, Chi X, Ma X, Zhang T, et al. Receptor and signaling pathway involved in bovine lymphocyte activation by *Atractylodes macrocephala* polysaccharides. *Carbohydr Polym*. (2020) 234:115906. doi: 10.1016/j.carbpol.2020.115906
- Xue W, Gao Y, Li Q, Lu Q, Bian ZY, Tang L, et al. Immunomodulatory activity-guided isolation and characterization of a novel polysaccharide from *Atractylodes macrocephala* Koidz. *Int J Biol Macromol*. (2020) 161:514–24. doi: 10.1016/j.ijbiomac.2020.06.003
- Zhu S, Sun Y, Jia Y, Zhang W, Wang Y, Li L, et al. Acid site-regulated solid acids for polysaccharide se-functionalization: Structural explanations for high reactivity. *Carbohydr Polym*. (2020) 251:117028. doi: 10.1016/j.carbpol.2020.117028
- Satyavathi CT, Tomar RS, Ambawat S, Kheni J, Padhiyar SM, Desai H, et al. Stage specific comparative transcriptomic analysis to reveal gene networks regulating iron and zinc content in pearl millet [*Pennisetum glaucum* (L.) R. Br.]. *Sci Rep*. (2022) 12:276. doi: 10.1038/s41598-021-04388-0
- Sandek A, Doeberner W, Anker SD, Haehling S. Nutrition in heart failure: an update. *Curr Opin Clin Nutr Metab Care*. (2009) 12:384–91. doi: 10.1097/MCO.0b013e32832cd8b0f
- Alam S, Kelleher SL. Cellular mechanisms of zinc dysregulation: a perspective on zinc homeostasis as an etiological factor in the development and progression of breast cancer. *Nutrients*. (2012) 4:875–903. doi: 10.3390/nu4080875
- Vaikundamoorthy R, Hwang I. Zinc oxide nanoparticles promoting the formation of myogenic differentiation into myotubes in mouse myoblast C2C12 cells. *J Ind and Eng Chem*. (2020) 83:315–22. doi: 10.1016/j.jiec.2019.12.004
- Cunnane SC. Foetal mortality in moderately zinc-deficient rats is strictly related to the process of parturition: effect of maternal essential fatty acid supplementation. *Br J Nutr*. (1982) 47:495–504. doi: 10.1079/BJN19820062
- Li J, Chen H, Bing W, Cai C, Xu Y, Chai Z, et al. ZnO nanoparticles act as supportive therapy in DSS-induced ulcerative colitis in mice by maintaining gut homeostasis and activating Nrf2 signaling. *Sci Rep*. (2017) 7:43126. doi: 10.1038/srep43126
- Name JJ, Souza ACR, Vasconcelos AR, Prado PS, Pereira CPM. Zinc, Vitamin D and Vitamin C: Perspectives for COVID-19 With a Focus on Physical Tissue Barrier Integrity. *Front Nutr*. (2020) 7:606398. doi: 10.3389/fnut.2020.606398
- Maeres M, Haase H. Zinc and immunity: An essential interrelation. *Arch Biochem Biophys*. (2016) 611:58–65. doi: 10.1016/j.abb.2016.03.022
- Maywald M, Wessels I, Rink L. Zinc Signals and Immunity. *Int J Mol Sci*. (2017) 18:2222. doi: 10.3390/ijms18102222
- Meng S, Hong Y, Dai Z, Huang W, Dong X. Simultaneous detection of dihydroxybenzene isomers with ZnO nanorod/carbon cloth electrodes. *ACS Appl Mater Interfaces*. (2017) 9:12453–60. doi: 10.1021/acsami.7b00546
- Tanino R, Amano Y, Tong X, Sun R, Isobe T. Anticancer activity of ZnO nanoparticles against human small-cell lung cancer in an orthotopic mouse model. *Mol Cancer Ther*. (2019) 19:502–12. doi: 10.1158/1535-7163.MCT-19-0018
- Webster T, Maschhoff P, Geilich B. Greater fibroblast proliferation on an ultrasonicated ZnO/PVC nanocomposite material. *Int J Nanomed*. (2013) 9:257–63. doi: 10.2147/IJN.S54897
- Becker L, Gharib SA, Irwin AD, Wijsman E, Vaisar T, Oram JF, et al. A macrophage sterol-responsive network linked to atherogenesis. *Cell Metab*. (2010) 11:125–35. doi: 10.1016/j.cmet.2010.01.003
- Yang X, Zhou S, Li H, An J, Li C, Zhou R, et al. Structural characterization of alpiniae oxyphyllae fructus polysaccharide 2 and its activation effects on RAW264.7 macrophages. *Int Immunopharmacol*. (2021) 97:107708. doi: 10.1016/j.intimp.2021.107708
- Zhou R, Teng L, Zhu Y, Zhang C, Yang Y, Chen Y. Preparation of Amomum longiligulare polysaccharides 1- PLGA nanoparticle and its immune enhancement ability on RAW264.7 cells. *Int Immunopharmacol*. (2021) 99:108053. doi: 10.1016/j.intimp.2021.108053
- Zhu L, Wei L, Fan Z, Ye X, Lin R, Ban M, et al. Immunomodulatory activity of polysaccharide from *Arca granosa* Linnaeus via TLR4/MyD88/NFκB and TLR4/TRIF signaling pathways. *J Funct Foods*. (2021) 84:104579. doi: 10.1016/j.jff.2021.104579
- Chen Y, Zhou R, He L, Wang F, Chen H. Okra polysaccharide-2 plays a vital role on the activation of RAW264.7 cells by TLR2/4-mediated signal transduction pathways. *Int Immunopharmacol*. (2020) 86:106708. doi: 10.1016/j.intimp.2020.106708
- Xu Z, Lin R, Hou X, Wu J, Zhao W, Ma H, et al. Immunomodulatory mechanism of a purified polysaccharide isolated from isaria cicadae miquel on RAW264.7 cells via activating TLR4-MAPK-NF-κB signaling pathway. *Int J Biol Macromol*. (2020) 164:4329–38. doi: 10.1016/j.ijbiomac.2020.09.035
- Zhang M, Yan M, Yang J, Li F, Wang Y, Feng K, et al. Structural characterization of a polysaccharide from *Trametes sanguinea* Lloyd with immune-enhancing activity via activation of TLR4. *Int J Biol Macromol*. (2022) 206:1026–38. doi: 10.1016/j.ijbiomac.2022.03.072
- Xie Y, Wang L, Sun H, Wang Y, Yang Z, Zhang G, et al. Polysaccharide from alfalfa activates RAW264.7 macrophages through MAPK and NF-κB signaling pathways. *Int J Biol Macromol*. (2019) 126:960–8. doi: 10.1016/j.ijbiomac
- Xiong L, Ouyang KH, Jiang Y, Yang ZW, Hu WB, Chen H, et al. Chemical composition of *Cyclocarya paliurus* polysaccharide and inflammatory effects in lipopolysaccharide-stimulated RAW264.7 macrophage. *Int J Biol Macromol*. (2018) 107:1898–907. doi: 10.1016/j.ijbiomac.2017.10.055
- Qin T, Liu X, Luo Y, Yu R, Chen S, Zhang J, et al. Characterization of polysaccharides isolated from *Hericium erinaceus* and their protective effects on the don-induced oxidative stress. *Int J Biol Macromol*. (2020) 152:1265–73. doi: 10.1016/j.ijbiomac.2019.10.223
- Liu M, Zhang C, Xu X, Zhao X, Han Z, Liu D, et al. Ferulic acid inhibits LPS-induced apoptosis in bovine mammary epithelial cells by regulating the NF-κB and Nrf2 signalling pathways to restore mitochondrial dynamics and ROS generation. *Vet Res*. (2021) 52:104. doi: 10.1186/s13567-021-00973-3
- Zhu Y, Huang Y, Yang J, Tu R, Zhang X, He WW, et al. Intranasal insulin ameliorates neurological impairment after intracerebral hemorrhage in mice. *Neural Regen Res*. (2021) 17:210–6. doi: 10.4103/1673-5374.314320
- Liu X, Ren Z, Yu R, Chen S, Zhang J, Xu Y, et al. Structural characterization of enzymatic modification of *Hericium erinaceus* polysaccharide and its immune-enhancement activity. *Int J Biol Macromol*. (2021) 166:1396–408. doi: 10.1016/j.ijbiomac.2020.11.019

35. Feng YY, Ji HY, Dong XD, Liu AJ. An alcohol-soluble polysaccharide from *Atractylodes macrocephala* koidz induces apoptosis of Eca-109 cells. *Carbohydr Polym.* (2019) 226:115136. doi: 10.1016/j.carbpol.2019.115136
36. Yu-Hao D, Chun C, Xiong F, Rui L. Study on the pharmacokinetics of mulberry fruit polysaccharides through fluorescence labeling. *Int J Biol Macromol.* (2021) 186:462–71. doi: 10.1016/j.ijbiomac.2021.07.075
37. Hong RY, Li JH, Chen LL, Liu DQ, Li HZ, Zheng Y, et al. Synthesis, surface modification and photocatalytic property of ZnO nanoparticles. *Powder Technol.* (2009) 189:426–32. doi: 10.1016/j.powtec.2008.07.004
38. Du GX, Xue Q, Ding H, Li Z. Mechanochemical effects of ZnO powder in a wet super-fine grinding system as indicated by instrumental characterization. *Int J Miner Proc.* (2015) 141:15–9. doi: 10.1016/j.minpro.2015.06.008
39. Qiao Y, Li W, Bao J, Zheng Y, Feng L, Ma Y, et al. Controlled synthesis and luminescence properties of core-shell structured SiO₂@AIPA-S-Si-Eu@SiO₂ and SiO₂@AIPA-S-Si-Eu-phen@SiO₂ nanocomposites. *Sci Rep.* (2020) 10:3522. doi: 10.1038/s41598-020-60538-w
40. Pawar S, Shende P. 22 factorial design-based biocompatible microneedle arrays containing artemether co-loaded with lumefantrine nanoparticles for transepidermal delivery. *Biomed Microdevices.* (2020) 22:19. doi: 10.1007/s10544-020-0476-8
41. Hawash MM, Kahraman DC, Eren F, Cetin Atalay R, Baytas SN. Synthesis and biological evaluation of novel pyrazolic chalcone derivatives as novel hepatocellular carcinoma therapeutics. *Eur J Med Chem.* (2017) 129:12–26. doi: 10.1016/j.ejmech.2017.02.002
42. Ding Y, Sun H, Ren C, Zhang M, Sun K. A nonenzymatic glucose sensor platform based on specific recognition and conductive polymer-decorated CuCo₂O₄ carbon nanofibers. *Materials.* (2020) 13:2874. doi: 10.3390/ma13122874
43. Ji X, Hou C, Yan Y, Shi M, Liu Y. Comparison of structural characterization and antioxidant activity of polysaccharides from jujube (*ziziphus jujuba* mill.) fruit. *Int J Biol Macromol.* (2020) 149:1008–18. doi: 10.1016/j.ijbiomac.2020.02.018
44. Suvakanta D, Narsimha MP, Pulak D, Joshabir C, Biswajir D. Optimization and characterization of purified polysaccharide from *musa sapientum* l. as a pharmaceutical excipient. *Food Chem.* (2014) 149:76–83. doi: 10.1016/j.foodchem.2013.10.068
45. Copperthwaite RG, Kunze OA, Lloyd J, Neely JA, Tuma W. Surface analysis of insb by x-ray photoelectron spectroscopy (XPS). *Z Naturforsch A.* (1978) 33:523–7. doi: 10.1515/zna-1978-0503
46. Ding Z, Wang L, Xing Y, Zhao Y, Han J. Enhanced oral bioavailability of celecoxib nanocrystalline solid dispersion based on wet media milling technique: formulation, optimization and in vitro/in vivo evaluation. *Pharmaceutics.* (2019) 11:328. doi: 10.3390/pharmaceutics11070328
47. Liu X, Xie J, Jia S, Huang L, Wang Z, Li C, et al. Immunomodulatory effects of an acetylated *Cyclocarya paliurus* polysaccharide on murine macrophages RAW264.7. *Int J Biol Macromol.* (2017) 98:576–81. doi: 10.1016/j.ijbiomac.2017.02.028
48. Zhang M, Tian X, Wang Y, Wang D, Li W, Chen L, et al. Immunomodulating activity of the polysaccharide TLH-3 from *tricholomalobayense* in RAW264.7 macrophages. *Int J Biol Macromol.* (2017) 107:2678–85. doi: 10.1016/j.ijbiomac.2017.10.165
49. Guo G, Gong T, Shen H, Wang Q, Jiang F, Tang J, et al. Self-amplification immunomodulatory strategy for tissue regeneration in diabetes based on cytokine-zifs system. *Adv Funct Mater.* (2021) 31:2100795. doi: 10.1002/adfm.202100795
50. Srinivasan A, Ekambaram S, Selvan PS. Plant polysaccharides-An insight into its immunostimulatory properties. *Bioact Carbohydr Diet.* (2021) 25:100244. doi: 10.1016/j.bcdf.2020.100244
51. Yoo HG, Shin BA, Park JS, Lee KH, Jung YD. IL-1 β induces MMP-9 via reactive oxygen species and NF- κ B in murine macrophage RAW264.7 cells. *Biochem Biophys Res Commun.* (2002) 298:251–6. doi: 10.1016/S0006-291X(02)02431-2
52. Wufuer R, Bai J, Liu Z, Zhou K, Taoerdahong H. Biological activity of *Brassica rapa* L. polysaccharides on RAW264.7 macrophages and on tumor cells-ScienceDirect. *Bioorg Med Chem.* (2020) 28:115330. doi: 10.1016/j.bmc.2020.115330
53. Qian JY, Chen W, Zhang WM, Hao Z. Adulteration identification of some fungal polysaccharides with sem, xrd, ir and optical rotation: A primary approach. *Carbohydr Polym.* (2009) 78:620–5. doi: 10.1016/j.carbpol.2009.05.025
54. Cui F, Jiang L, Qian L, Sun W, Tao T, Zan X, et al. A macromolecular α -glucan from fruiting bodies of *Volvariella volvacea* activating RAW264.7 macrophages through MAPKs pathway. *Carbohydr Polym.* (2020) 230:115674. doi: 10.1016/j.carbpol.2019.115674
55. Zhang H, Li C, Lai PFH, Chen J, Ai L. Fractionation, chemical characterization and immunostimulatory activity of β -glucan and galactoglucan from *Russula vinosa* Lindblad. *Carbohydr Polym.* (2021) 256:117559. doi: 10.1016/j.carbpol.2020.117559
56. Zhang M, Zhao M, Qing Y, Luo Y, Xia G, Li Y. Study on immunostimulatory activity and extraction process optimization of polysaccharides from *Caulerpa lentillifera*. *Int J Biol Macromol.* (2020) 143:677–84. doi: 10.1016/j.ijbiomac.2019.10.042
57. Li X, Xing R, Xu C, Liu S, Qin Y, Li K, et al. Immunostimulatory effect of chitosan and quaternary chitosan: A review of potential vaccine adjuvants. *Carbohydr Polym.* (2021) 264:118050. doi: 10.1016/j.carbpol.2021.118050
58. Cobb BA, Wang Q, Tzianabos AO, Kasper DL. Polysaccharide processing and presentation by the MHCII pathway. *Cell.* (2004) 117:677–87. doi: 10.1016/j.cell.2004.05.001
59. Zong L, Zhang J, Dai L, Liu J, Yang Y, Xie J, et al. The Anti-Inflammatory Properties of *Rhododendron molle* Leaf Extract in LPS-Induced RAW264.7. *Chem Biodivers.* (2020) 17:e2000477. doi: 10.1002/cbdv.202000477
60. Liu Y, Yin H, Zhao M, Lu Q. TLR2 and TLR4 in autoimmune diseases: a comprehensive review. *Clin Rev Allergy Immunol.* (2014) 47:136–47. doi: 10.1007/s12016-013-8402-y
61. Engelmann C, Sheikh M, Sharma S, Kondo T, Loeffler-Wirth H, Zheng YB, et al. Toll-like receptor 4 is a therapeutic target for prevention and treatment of liver failure. *J Hepatol.* (2020) 73:102–12. doi: 10.1016/j.jhep.2020.01.011



OPEN ACCESS

EDITED BY

Yi Wu,
Nanjing Agricultural University, China

REVIEWED BY

Guiyan Yang,
University of California, Davis,
United States
Ruonan Bo,
Yangzhou University, China
Gianfranco Danilo Alpini,
Indiana University, United States
Chaohui Yu,
Zhejiang University, China

*CORRESPONDENCE

Zhenzhou Jiang
beaglejiang@cpu.edu.cn
Qinwei Yu
yuqinwei7213@cpu.edu.cn

SPECIALTY SECTION

This article was submitted to
Nutritional Immunology,
a section of the journal
Frontiers in Nutrition

RECEIVED 31 August 2022

ACCEPTED 28 September 2022

PUBLISHED 13 October 2022

CITATION

Yuan Z, Wang J, Zhang H, Miao Y,
Tang Q, Yuan Z, Nong C, Duan Z,
Zhang L, Jiang Z and Yu Q (2022)
Triptolide increases resistance to bile
duct ligation-induced liver injury
and fibrosis in mice by inhibiting RELB.
Front. Nutr. 9:1032722.
doi: 10.3389/fnut.2022.1032722

COPYRIGHT

© 2022 Yuan, Wang, Zhang, Miao,
Tang, Yuan, Nong, Duan, Zhang, Jiang
and Yu. This is an open-access article
distributed under the terms of the
[Creative Commons Attribution License](#)
(CC BY). The use, distribution or
reproduction in other forums is
permitted, provided the original
author(s) and the copyright owner(s)
are credited and that the original
publication in this journal is cited, in
accordance with accepted academic
practice. No use, distribution or
reproduction is permitted which does
not comply with these terms.

Triptolide increases resistance to bile duct ligation-induced liver injury and fibrosis in mice by inhibiting RELB

Zihang Yuan¹, Jie Wang¹, Haoran Zhang¹, Yingying Miao¹,
Qianhui Tang¹, Ziqiao Yuan¹, Cheng Nong¹, Zhicheng Duan¹,
Luyong Zhang^{1,2}, Zhenzhou Jiang^{1,3*} and Qinwei Yu^{1*}

¹New Drug Screening Center, Jiangsu Center for Pharmacodynamics Research and Evaluation, State Key Laboratory of Natural Medicines, China Pharmaceutical University, Nanjing, China,

²Center for Drug Research and Development, Guangdong Pharmaceutical University, Guangzhou, China, ³Key Laboratory of Drug Quality Control and Pharmacovigilance, Ministry of Education, China Pharmaceutical University, Nanjing, China

Cholestasis is a common, chronic liver disease that may cause fibrosis and cirrhosis. *Tripterygium wilfordii* Hook.f (TWHF) is a species in the Euonymus family that is commonly used as a source of medicine and food in Eastern and Southern China. Triptolide (TP) is an epoxy diterpene lactone of TWHF, as well as the main active ingredient in TWHF. Here, we used a mouse model of common bile duct ligation (BDL) cholestasis, along with cultured human intrahepatic biliary epithelial cells, to explore whether TP can relieve cholestasis. Compared with the control treatment, TP at a dose of 70 or 140 μ g/kg reduced the serum levels of the liver enzymes alanine transaminase, aspartate aminotransferase, and alkaline phosphatase in mice; hematoxylin and eosin staining also showed that TP reduced necrosis in tissues. Both *in vitro* and *in vivo* analyses revealed that TP inhibited cholangiocyte proliferation by reducing the expression of RelB. Immunohistochemical staining of CK19 and Ki67, as well as measurement of Ck19 mRNA levels in hepatic tissue, revealed that TP inhibited the BDL-induced ductular reaction. Masson 3 and Sirius Red staining for hepatic hydroxyproline showed that TP alleviated BDL-induced hepatic fibrosis. Additionally, TP substantially inhibited BDL-induced hepatic inflammation. In summary, TP inhibited the BDL-induced ductular reaction by reducing the expression of RelB in cholangiocytes, thereby alleviating liver injury, fibrosis, and inflammation.

KEYWORDS

RelB, bile duct ligation (BDL), triptolide, TNFSF14, cholangiocyte

Introduction

Cholestasis can reflect either a functional defect in bile formation at the hepatocyte level or impairment in bile secretion/flow at the bile duct level (1). Cholestasis manifests as the excessive accumulation of biliary components (e.g., bile acid, cholesterol, and bilirubin) in the liver and systemic circulation. The clinical symptoms include liver injury, severe pruritus, jaundice, and fatigue; severe cases can cause acute liver failure (2). Chronic cholestasis may eventually lead to liver fibrosis and cirrhosis (3).

Ursodeoxycholic acid and chenodeoxycholic acid are the preferred drugs for treatment of cholestasis (4). However, tolerance may develop (5). Recently, obeticholic acid (a 6-ethyl derivative of chenodeoxycholic acid) was approved for the treatment of primary biliary cirrhosis—in conjunction with ursodeoxycholic acid—in patients with inadequate responses to ursodeoxycholic acid; it was approved as monotherapy for patients who are unable to tolerate ursodeoxycholic acid (6–8). However, hepatic decompensation, liver failure, and death have been reported in patients with Child-Pugh B or C cirrhosis who receive doses of obeticholic acid above the recommended level. Thus, the Food and Drug Administration placed a black box warning on the obeticholic acid label for patients with decompensated liver disease. New, inexpensive therapeutic agents are needed for effective relief of cholestasis symptoms.

Traditional Chinese medicine dietary supplements alleviate various forms of liver injury including cholestasis (9–12). *Tripterygium wilfordii* Hook.f (TWHF) is a species of *Tripterygium* in the *Euonymus* family (13); the dried root (“thunder god vine”) serves as a “bitter and cold” traditional Chinese medicine (14) in Eastern and Southern China. The root is also cooked in southern China. Triptolide (TP) is an epoxy diterpene lactone of TWHF (15), as well as the principal active ingredient in TWHF (13). TP exhibits potent immunosuppressive and antiproliferative activities (16); it effectively treats rheumatoid arthritis (17), diabetic kidney disease (18), and prostate cancer (19, 20). A TP dietary supplement reportedly alleviates senile osteoporosis (21), reduces stress, and increases longevity (22). We previously showed that TP was active against colon cancer (23, 24). The NF- κ B protein complex regulates cell survival (25), aging (26), cytokine production (27), and obesity (28); NF- κ B is the principal target of TP. NF- κ B transcriptional inhibition by TP can suppress inflammation (29) and tumor growth (30). Thus far, the effects of TP on cholestasis remain unknown. In this study, we used a mouse model of common bile duct ligation (BDL) to explore whether TP can effectively treat cholestasis. Our findings provide a rationale for TP as complementary medicine of the preferred drugs or alternative medicine for cholestasis.

Materials and methods

Materials

Triptolide (CAS number 38748-32-2, purity > 98%) was purchased from Sanling Biotech (Guilin, China). TNFSF14 Elisa Kit (CSB-EL023991MO) was purchased from Cusabo (China).

Primary antibodies against RelB (10544), α -SMA (19245) and F4/80 (70076) was purchased from Cell Signaling Technology (USA). Primary antibody against CK19 (TROMA-III) was purchased from DSHB (USA). Primary antibody against GAPDH (60004-1-Ig) was purchased from Proteintech (China). Primary antibody against Ki67 (ab16667) was purchased from Abcam (USA). Primary antibody against Ly6g (4-5931-82) was purchased from Thermofisher (USA). Rabbit and Mouse secondary antibody (31460, 31430) were purchased from Thermofisher (USA). Rat secondary antibody (GB23302) were purchased from Serviciobio (China).

Animal surgery procedure

Male C57BL/6J mice (6–8 weeks) were supplied by Shanghai SLAC Laboratory Animal Co., Ltd (Shanghai, China). The animal study was reviewed and approved by the China Pharmaceutical University Experimental Animal Ethics Committee. Mice were housed in conditions with controlled light (12 h light/dark cycle), temperature ($24 \pm 2^\circ\text{C}$), and humidity (50–60%) and had adequate food and tap water. Cholestasis was induced by common bile duct ligation (BDL). Mice were anesthetized using 3% isoflurane and kept under anesthesia using 2–3% isoflurane during the entire infection procedure, where the abdominal cavity was opened from the abdominal midline. All experiments on mice were performed under the guidelines of Ethical Committee of China Pharmaceutical University. Triptolide in powder was suspended in 0.5% CMC-Na and administered to mice by gavage. The doses selected for TP in animal experiments were 70 $\mu\text{g/kg}$ and 140 $\mu\text{g/kg}$ (31). The common bile duct was ligated twice with a 7-0 nylon suture. The sham operation group involved the same operation, but the common bile duct was not ligated. After one-week acclimatization, the mice were then randomly separated into four groups ($n = 6$ per group): (1) Control mice (sham operated); (2) BDL mice; (3) BDL with TP at 70 $\mu\text{g/kg}$ administration; (4) BDL with TP at 140 $\mu\text{g/kg}$ administration. BDL performed at three days after TP treatment. Mice in sham and BDL group were given corresponding vehicle. After BDL the mice still were treated with TP once a day. Seven days after BDL surgery, mice were sacrificed (Figure 1A).

Serum alanine aminotransferase (ALT) and aspartate aminotransferase (AST) levels were measured using kits from Whitman Biotech (Nanjing, China). Hepatic hydroxyproline was measured using kits from Nanjing

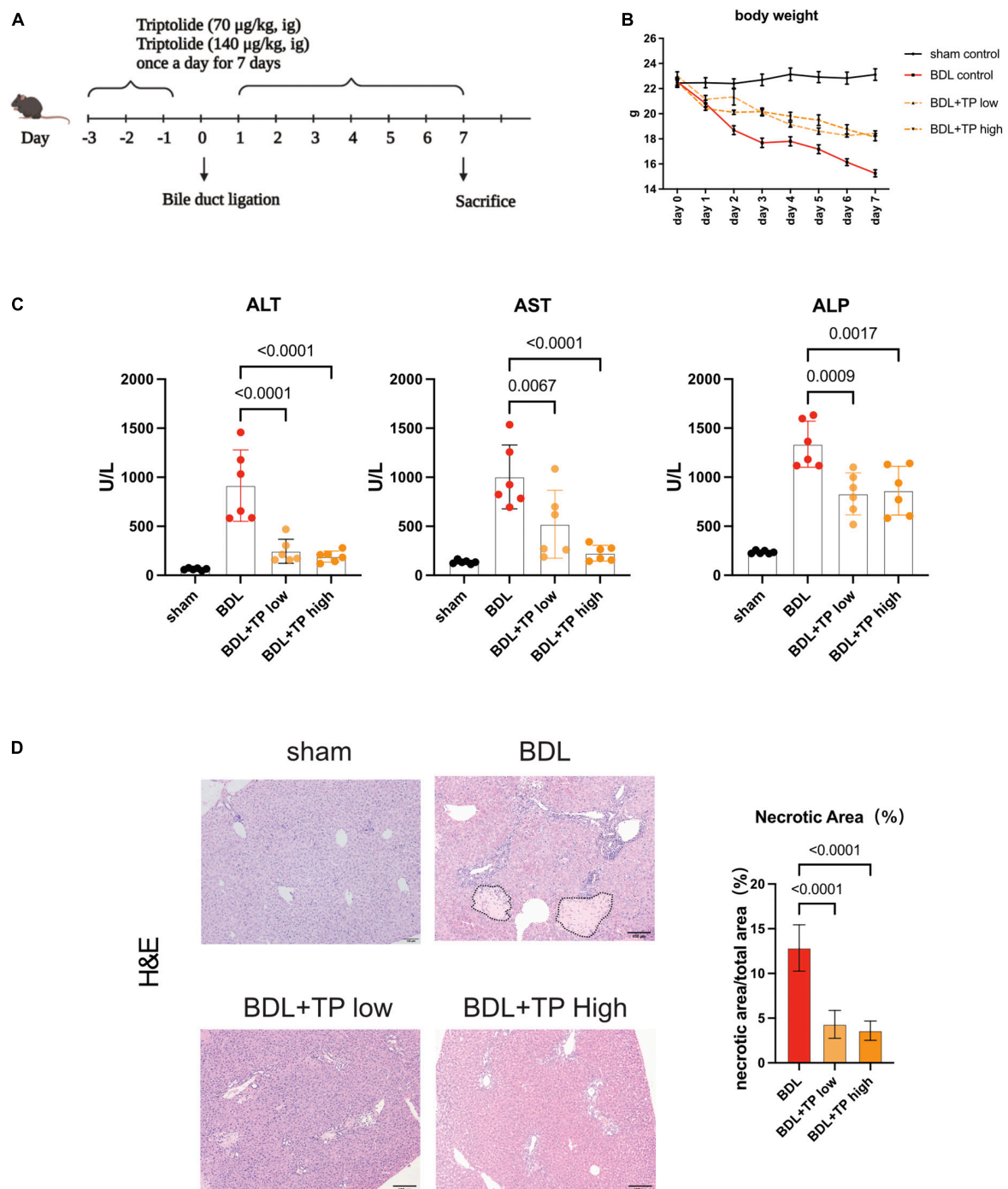


FIGURE 1

Triptolide alleviates liver injury induced by bile duct ligation. Male C57BL/6 mice were sacrificed at seven days after BDL or sham surgery. (A) The diagrammatic experimental procedures. (B) Body weight of mice (each group $n = 6$). (C) Serum levels of ALT, AST and ALP in mice sacrificed at 7 days after BDL or sham surgery. (D) Representative images of H&E (The black dotted line indicates the necrotic area) from liver tissues. Necrosis area statistics of H&E. Scale Bar: 100 μm . Data are shown as the mean \pm SD. Data represent at least 6 independent experiments with triplicate measurements. Analysis of variance (one-way ANOVA) was used. p values represents significance different from BDL group.

Jiancheng Bioengineering Institute (Nanjing, China). All kits were used according to the manufacturer's protocols. Fragments of mouse livers were fixed overnight in buffered formaldehyde

(10%) and embedded in paraffin for immunohistochemistry (IHC), hematoxylin and eosin (H&E), Masson's trichrome and Sirius Red. H&E staining of liver tissue was carried out to

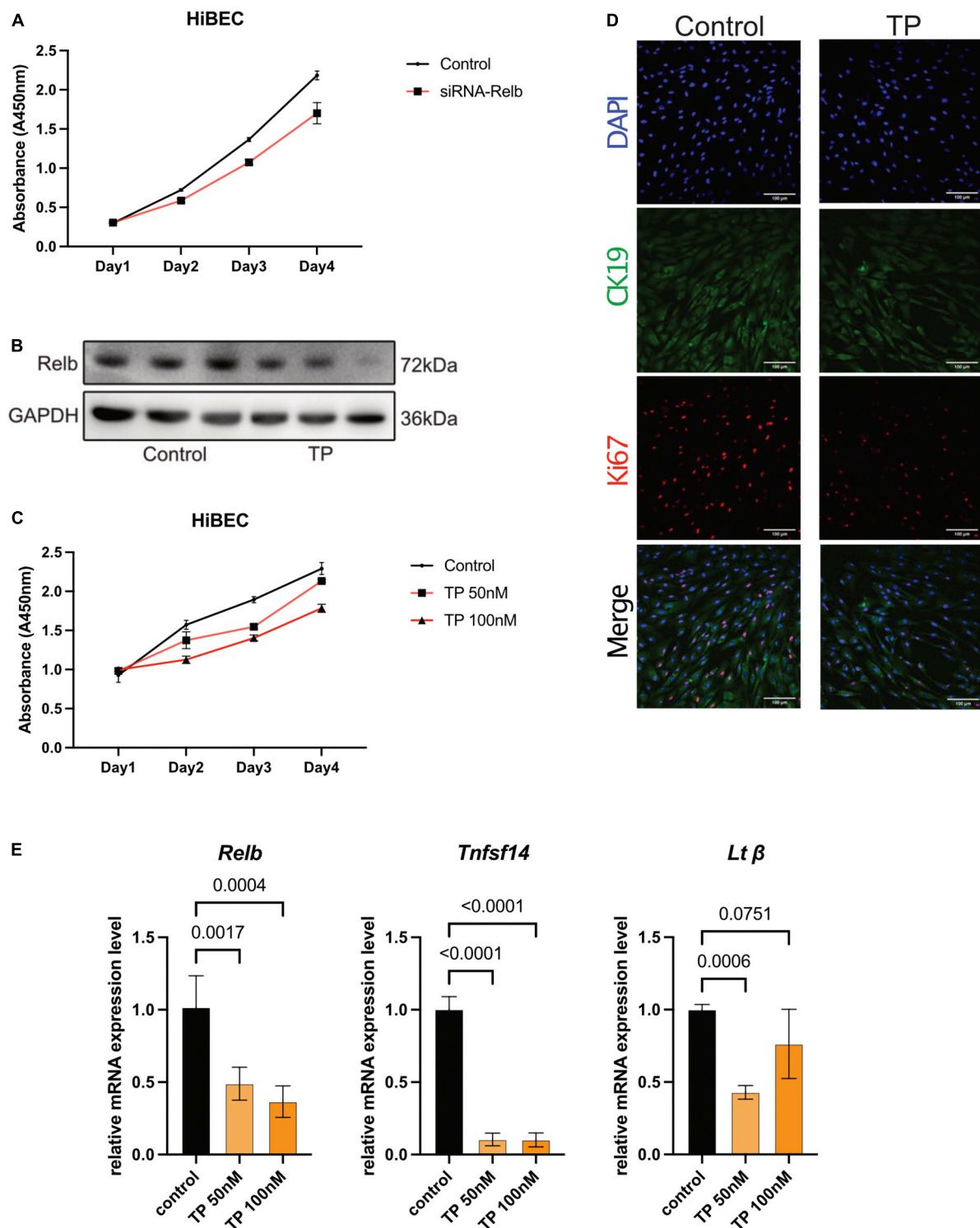


FIGURE 2

Triptolide inhibits proliferation and RelB expression in HiBEC. (A) The growth curve of HiBEC after transfection of siRNA-Relb. (B) The protein level of RelB in HiBEC after TP treatment. (C) The growth curve of HiBEC after TP treatment. (D) Double immunofluorescence staining for CK19 (green) and Ki67 (red) from HiBEC after TP treatment. Nuclei were counter-stained with DAPI (blue). (E) *Relb*, *Tnfsf14* and *Ltβ* mRNA was measured in HiBEC after TP treatment. Data are shown as the mean \pm SD. Data represent at least 3 independent experiments with triplicate measurements. Analysis of variance (one-way ANOVA) was used. *p* values represents significance different from control group.

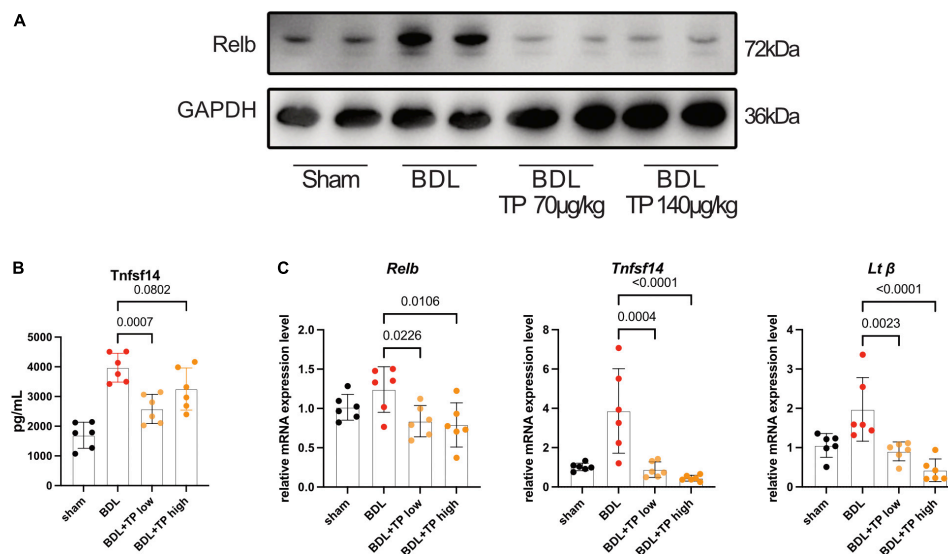


FIGURE 3

Triptolide inhibits BDL induced RelB and its downstream gene expression. (A) Western blot analysis of RelB in liver. (B) The serum TNFSF14 levels (ELISA data) of mice. (C) The mRNA level of *Relb*, *Tnfsf14* and *Ltβ* in liver tissues. Data are shown as the mean \pm SD. Data represent at least 6 independent experiments with triplicate measurements. Analysis of variance (one-way ANOVA) was used. *p* values represents significance different from BDL group.

observe pathological changes. All slides were scanned with a NanoZoomer S60 (Hamamatsu, Japan).

Cell culture

Human intrahepatic biliary epithelial cells (HiBEC) were purchased from ScienCell and cultured in a EpiCAM (ScienCell) (Zhongqiaoxinzhou) containing 2% fetal bovine serum (FBS), EpiCGs (ScienCell), 5 μ g/mL insulin and 0.5 μ M hydrocortisone.

Small interference RNAs (siRNA) were purchased from GenePharma (Shanghai). The siRNA sequences used in this study are as follows: RelB-1 siRNA sense: 5'-GCCCGUCUAUGACAAGAAATT-3'; antisense: 5'-UUUCUUGUCAUAGACGGGCTT-3'. RelB-2 siRNA sense: 5'-GCACAGAUGAAUUGGAGAU-3', antisense: 5'-AUCUCCAAUUCACUGUGCTT-3', Negative control siRNA: 5'-UUCUCCGAACGUGUCACGUTT-3'. HiBECs were seeded in six-well plate one day before transfection. HiBECs were transfected using Lipofectamine 3000 transfection kit (thermofisher, USA) according to the manufacturer's instructions. Transfected cells were used for the subsequent experiments 48 h after transfection.

The growth curve of HiBECs was measured with the cck-8 kit (vazyme, China) assay. HiBEC were seeded in 96-well plate (5000 cells per well). The plates were incubated in full EpiCAM. Cck-8 working fluid were added in the plate 100 μ L per well at 24h, 48h, 72h, 96h. After 1 h incubation with cck8,

OD450 was detected using a spectrophotometer (Multiskan MK3, Thermofisher, USA).

Quantitative real-time polymerase chain reaction

RNA from tissues and cells was extracted with TRIzol (vazyme, China). The RNA concentration was determined using Nanodrop2000 Spectrophotometers (Thermo Scientific, USA). cDNA was generated using BIO-RAD MyCyclerThermal Cycler (BIO-RAD, USA) and the HighCapacity cDNA Reverse Kit. qPCR was performed using StepOnePlus (Applied Biosystems, USA) with specific primers (Table 1). Primers were purchased from Genescript (China). Results were normalized using GAPDH as an internal control.

Immunoblot analysis

Protein content was analyzed by lysing tissues and cells with RIPA buffer containing protease inhibitors and the Bradford Protein Assay Kit. Western blot analysis was performed following a previously described method (32). Protein bands were detected with a Tanon 5200Muti (Tanon, China) using ECL reagents. The gray density of the protein bands was determined using ImageJ. All quantitative comparisons between samples were on the same gels/blots.

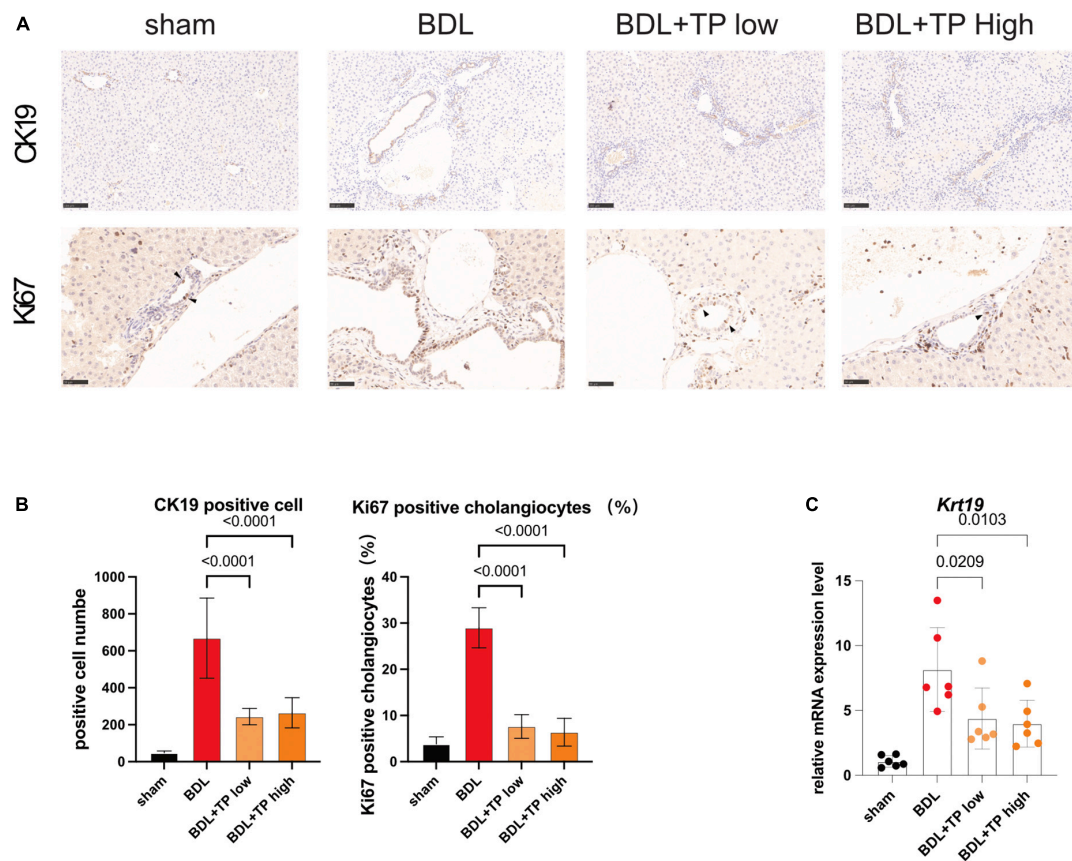


FIGURE 4

Triptolide relieves BDL-induced bile duct hyperplasia. (A) Representative images of IHC for CK19 and Ki67 (The black arrows indicate the regenerated cholangiocytes) from liver tissues. Scale Bar: 100 μ m. (B) Statistical analysis of immunohistochemically positive regions of (A). (C) The mRNA level of *Ck19* in liver tissues. Data are shown as the mean \pm SD. Data represent at least 6 independent experiments with triplicate measurements. Analysis of variance (one-way ANOVA) was used. *p* values represents significance different from BDL group.

TABLE 1 Primer sequences used for RT-PCR analysis.

Gene	Forward primer (5'-3')	Reverse primer (5'-3')
mouse <i>Ccn2</i>	GGGCCTCTTCTGCGATTTC	ATCCAGGCAAGTGCATTGGTA
mouse <i>Gapdh</i>	CTTTGGCATTGTGGAAGGGC	CAGGGATGATGTTCTGGGCA
mouse <i>Acta2</i>	TGCTGACAGAGGCACCACTGAA	CAGTTGTACGTCCAGAGGCATAG
mouse <i>Col1a1</i>	CCTCAGGGTATTGCTGGACAAC	CAGAAGGACCTTGTTTGCCAGG
mouse <i>Tgf-β1</i>	GCCACTGCCCATCGTCTACT	CACTTGACAGGAGCGACAAT
mouse <i>F4/80</i>	CGTGTGTGTGGTGGCACTGTGA	CCACATCAGTGTCCAGGAGAC
mouse <i>Il-1β</i>	TGGACCTTCCAGGATGAGGACA	GTTCTATCTCGGAGCCTGTAGTG
mouse <i>Krt19</i>	AATGGCGAGCTGGAGGTGAAGA	CTTGGAGTTGTCAATGGTGGCAC
mouse <i>Tnf-α</i>	GGTGCCTATGTCTCAGCCTCTT	GCCATAGAACTGATGAGAGGGAG
mouse <i>Relb</i>	GTTCTTGGACCACTTCCTGCCT	TAGGCAAAGCCATCGTCCAGGA
mouse <i>Tnfsf14</i>	GGAGACATAGTAGCTCATCTGCC	CCACCAATACCTATCAAGCTGGC
mouse <i>Ltβ</i>	CCTGTTGTGTGGCAGTGCTATC	GACGGTTTGCTGTATCCAGTC
Human <i>Relb</i>	TGTGGTGAGGATCTGCTTCCAG	TCGGCAAATCCGAGCTCTGAT
Human <i>Tnfsf14</i>	GGTCTCTTGCTGTGTGCTGATGG	TTGACCTCGTGAGACCTTCGCT
Human <i>Ltβ</i>	GGTTTCAGAAGCTGCCAGAGGA	CGTCAGAAACGCCTGTTCTCTC
Human <i>Gapdh</i>	GTCTCCTCTGACTTCAACAGCG	ACCACCCTGTGTGCTGTAGCCAA

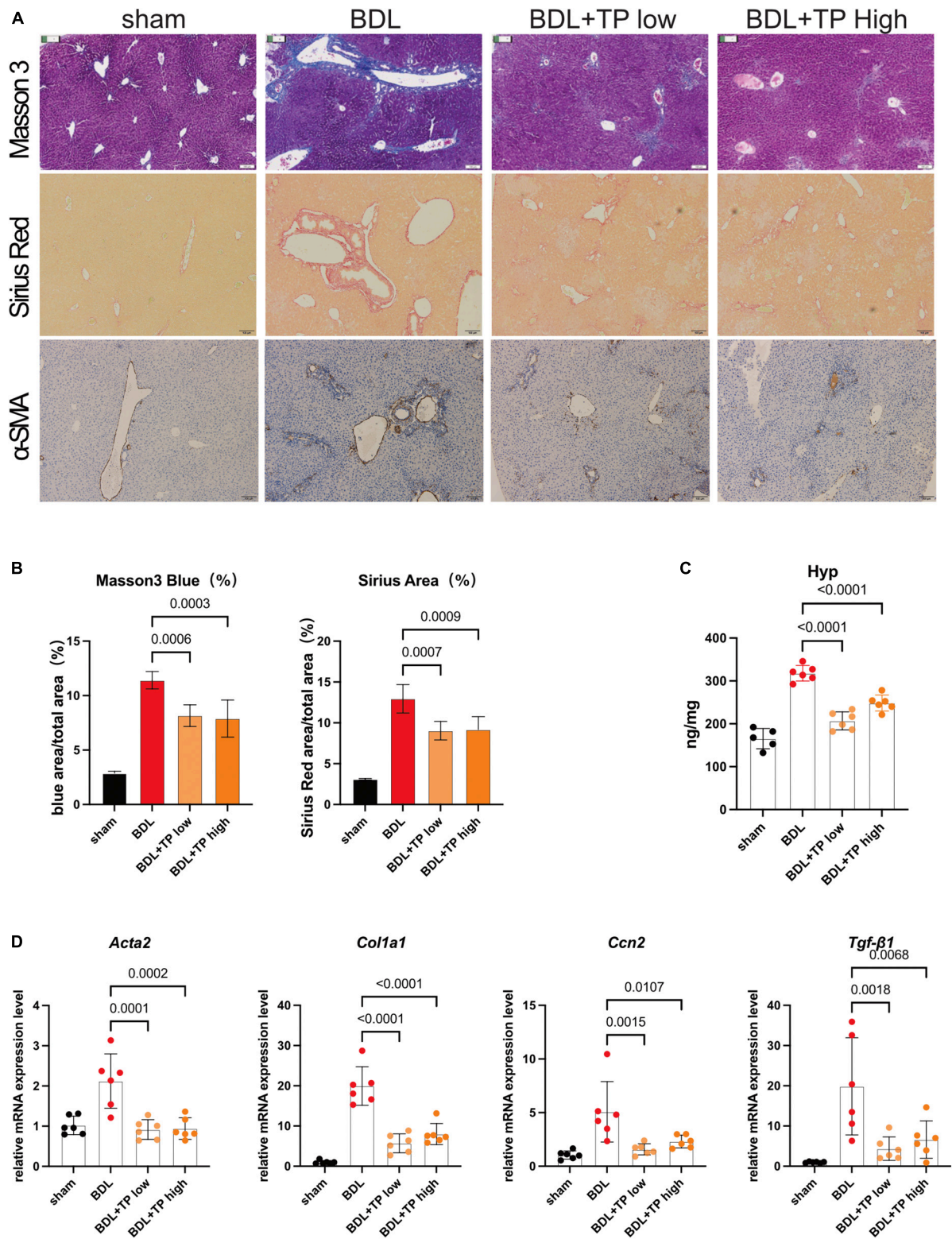


FIGURE 5
Triptolide relieves BDL-induced liver fibrosis. **(A)** Representative images of Masson 3, Sirius Red, and IHC for α -SMA from liver tissues. Scale Bar: 100 μ m. **(B)** Collagen positive area statistics of Masson3 and Sirius Red. **(C)** Hydroxyproline assay of liver tissues. **(D)** The mRNA levels of *Acta2*, *Col1a1*, *Ccn2*, and *Tgf- β 1* from liver tissues. Data represent at least 6 independent experiments with triplicate measurements. Analysis of variance (one-way ANOVA) was used. *p* values represents significance different from BDL group.

Immunofluorescence

Cells on coverslips were fixed in 4% paraformaldehyde for 15 min, washed with PBS, and permeabilized in PBS with 1% Triton for 10 min. Cells were then incubated with 5% goat serum in PBS for 1 h at room temperature before being incubated with antibodies overnight at 4°C. The next day, cells on a round coverslip were washed three times with PBS and incubated for 1 h at room temperature with secondary Alexa antibodies and DAPI. Fluorescence images were scanned using a FV3000 (Olympus, Japan).

Statistical analysis

All data were shown as mean \pm SD and at least three replicate experiments were performed *in vitro* and *in vivo*. The necrotic, Masson3 positive and Sirius Red positive area were analyzed using Image J software. Statistical significance was determined using one-way analysis of variance as appropriate (GraphPad Prism 9, GraphPad Software Inc., CA).

Results

Triptolide alleviates bile duct ligation-induced liver injury

To explore the effects of TP on cholestasis-induced liver injury, we established a mouse model of BDL and administered two TP doses by oral gavage; such doses were previously reported to attenuate chronic kidney disease (31). A schematic of the mouse model is depicted in **Figure 1A**. **Figure 1B** shows that TP at a dose of 70 or 140 μ g/kg attenuated the BDL-induced weight loss. BDL increased the serum levels of the liver enzymes alanine transaminase, aspartate aminotransferase, and alkaline phosphatase. Either dose of TP substantially reduced the levels of these enzymes (**Figure 1C**). Histopathological staining revealed less necrosis around the portal tract when BDL mice were treated with TP (**Figure 1D**). Thus, TP effectively treated BDL-induced liver injury.

Triptolide inhibits proliferation and RelB expression in human intrahepatic biliary epithelial cells

Bile duct hyperplasia is common in patients with cholestasis; cholangiocyte proliferation and a ductular reaction contribute to the onset and progression of liver disease (32–34). Members of the NF- κ B family of transcription factors act through

a canonical pathway and a non-canonical pathway. Non-canonical NF- κ B signaling activates predominantly p100-sequestered NF- κ B proteins, the most important of which is RelB (35). This protein is involved in the ductular reaction; the bile ducts of patients with primary sclerosing cholangitis and primary biliary cirrhosis exhibit increased levels of RelB. RelB and its downstream target lymphotoxin β (LT β) affect the proliferation of bile duct epithelial cells (36). TP inhibits the expression of NF- κ B proteins (37). Here, we analyzed HiBECs *in vitro*. We hypothesized that TP would reduce cholangiocyte proliferation by inhibiting the expression of RelB.

Growth curve analyses showed that siRNA-mediated RelB knockdown inhibited the growth of HiBECs (**Figure 2A**). Western blotting revealed that TP (100 nM) significantly inhibited the expression of RelB in HiBECs (**Figure 2B**). TP at 50 and 100 nM inhibited the growth of HiBECs (**Figure 2C**); this was confirmed (for TP at 100 nM) by immunofluorescence staining of CK19 and Ki67 (proliferation markers) (**Figure 2D**). Quantitative polymerase chain reaction (qPCR) analysis demonstrated that TP significantly reduced the mRNA expression levels of *Relb* and the downstream genes *Tnfsf14* and *Lt β* (**Figure 2E**).

Triptolide inhibits bile duct ligation-induced expression of RelB and downstream genes

Western blotting revealed that the protein level of RelB increased after BDL. Both TP doses substantially reduced the level of RelB (**Figure 3A**). Enzyme-linked immunosorbent assay analysis showed that BDL increased the expression of serum tumor necrosis factor superfamily member 14 (TNFSF14), whereas TP inhibited this increase (**Figure 3B**). qPCR analysis of hepatic tissue showed that BDL upregulated the mRNA expression levels of *Relb*, *Tnfsf14*, and *Lt β* , but these increases were inhibited by TP at a dose of 70 or 140 μ g/kg (**Figure 3C**).

Triptolide relieves bile duct ligation-induced bile duct hyperplasia

The above results indicated that TP inhibited the BDL-induced upregulation of *Relb* and downstream genes (*Tnfsf14* and *Lt β*) in hepatic tissue. Increased levels of RelB lead to a ductular reaction. Cytokeratin-19 (CK19) is solely expressed by cholangiocytes. Immunohistochemical analysis of CK19 revealed that BDL induced prominent bile duct hyperplasia; TP inhibited this process (**Figures 4A,B**). Immunohistochemical analysis of Ki67 revealed many positive cells (black arrows) in bile ducts after BDL; TP significantly reduced the numbers of these cells (**Figures 4A,B**), indicating that TP alleviated bile duct

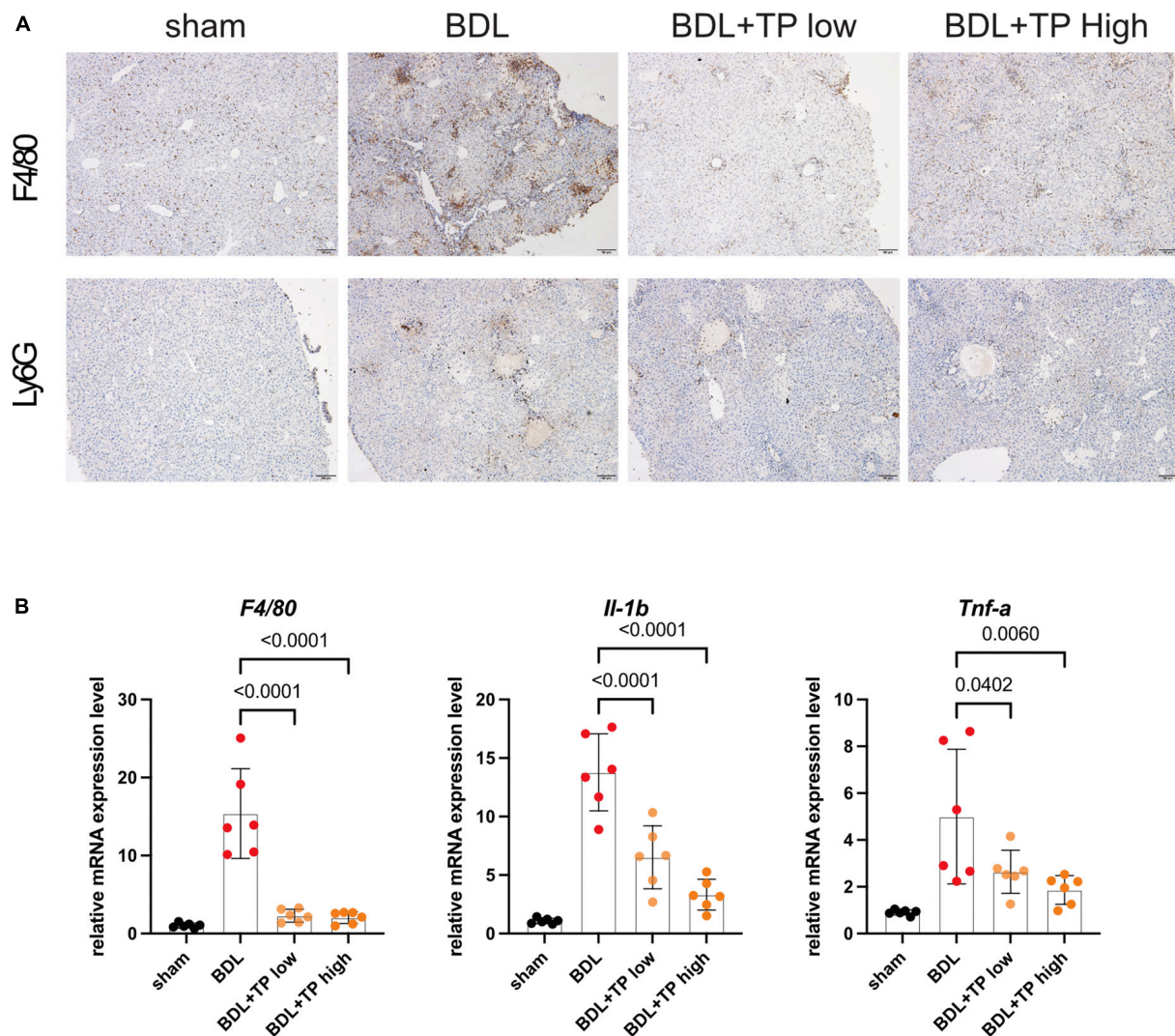


FIGURE 6

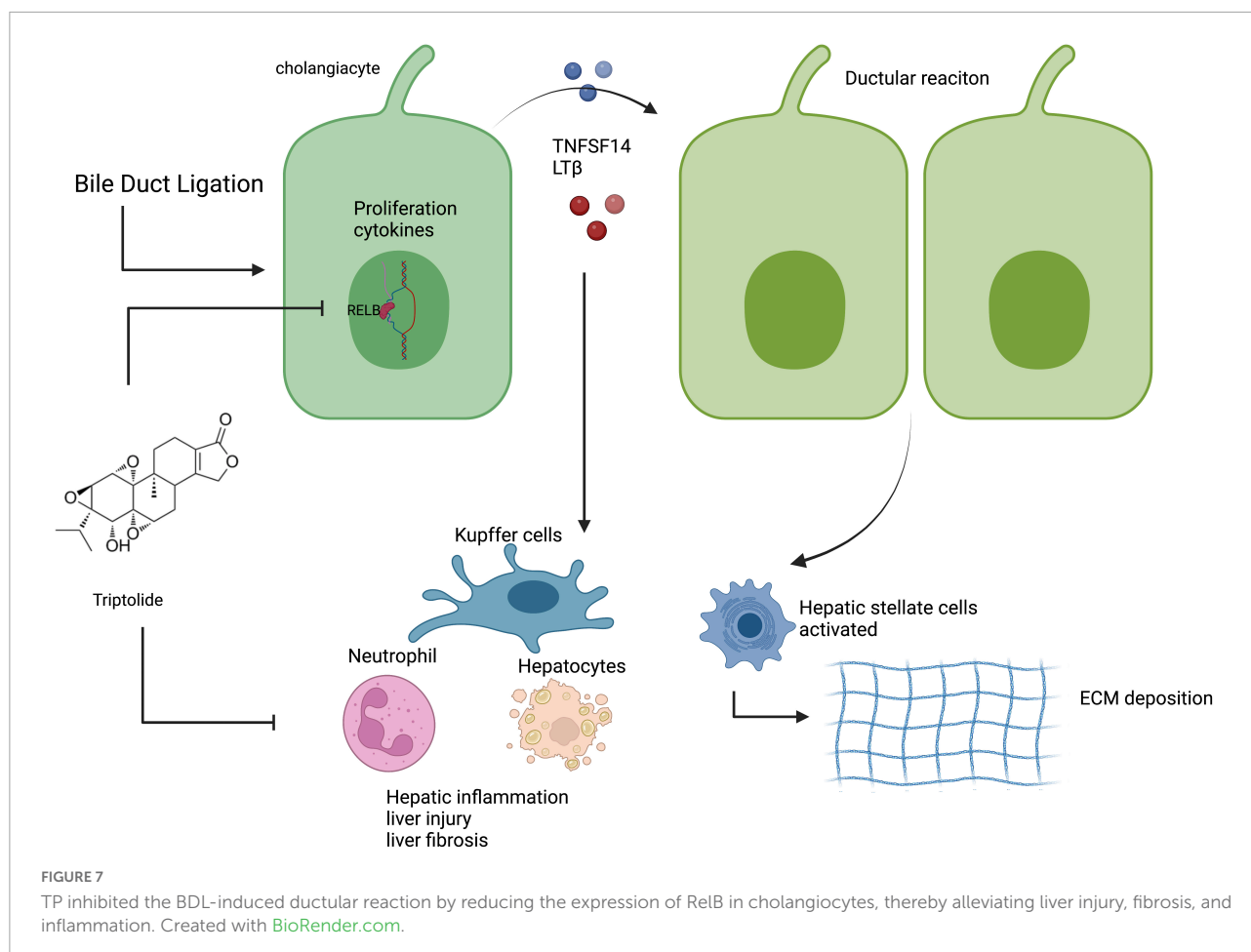
Triptolide relieves BDL-induced liver inflammation. (A) Representative images of IHC of F4/80 and LY6G from liver tissues. Scale Bar: 100 μ m. (B) The liver mRNA levels of *F4/80*, *IL-1 β* and *Tnf- α* from liver tissues. Data represent at least 6 independent experiments with triplicate measurements. Analysis of variance (one-way ANOVA) was used. *p* values represents significance different from BDL group.

hyperplasia. qPCR analysis showed that TP significantly reduced the BDL-induced upregulation of *Ck19* (Figure 4C).

Triptolide relieves bile duct ligation-induced liver fibrosis

TNFSF14, which acts downstream of RelB, promotes hepatic stellate cell activation and exacerbates liver fibrosis (38). Staining with Masson 3 and Sirius Red confirmed that TP decreased collagen deposition around the portal fields in BDL mice (Figures 5A,B). α -Smooth muscle actin [also known as actin alpha 2 (ACTA2)] is a marker of hepatic stellate cell activation; immunohistochemical staining of α -smooth muscle actin

decreased around the portal area (Figure 5A). Hydroxyproline is a characteristic component of collagen; in BDL mice, the hepatic levels of hydroxyproline were substantially lower after treatment with TP at a dose of 70 or 140 μ g/kg, compared with those levels in the control group (Figure 5C). Next, we examined the expression of liver fibrosis-related genes. *Col1a1* is an important collagen component, and its expression significantly increases in fibrotic tissues. Connective tissue growth factor [also known as cellular communication network factor 2 (CTGF/CCN2)] and transforming growth factor beta-1 (TGF- β 1) are markers of liver fibrosis, and they both directly activate hepatic stellate cells and promote collagen deposition; BDL elevates the levels of both proteins (39, 40). The mRNA expression levels of *Acta2*, *Col1a1*, *Ccn2*, and *Tgf- β 1* were



downregulated when BDL mice were treated with TP at a dose of 70 or 140 $\mu\text{g/kg}$ (Figure 5D).

Triptolide relieves bile duct ligation-induced hepatic inflammation

Ductular reactions are often accompanied by inflammatory infiltrates (33, 41). Therefore, we examined the effect of TP on hepatic inflammation. For this purpose, we conducted immunohistochemical staining of F4/80 (also known as mouse EGF-like module-containing mucin-like hormone receptor-like 1), which is expressed by various mature macrophages including Kupffer cells; we also performed immunohistochemical staining of the lymphocyte antigen 6 complex locus G6D (LY6G), a neutrophil-specific marker. BDL-induced enhancement of F4/80 and LY6G staining was decreased by TP at a dose of 70 or 140 $\mu\text{g/kg}$; thus, TP reduced hepatic inflammatory infiltration (Figure 6A). The mRNA expression levels of genes encoding the inflammatory factors F4/80, interleukin-1 β , and tumor necrosis factor- α were significantly reduced when BDL mice received TP at a dose of 70 or 140 $\mu\text{g/kg}$ (Figure 6B). These findings

indicated that TP attenuated hepatic inflammatory infiltration in BDL mice.

Discussion

We explored whether TP protected against liver injury progression in a mouse model of common BDL. TP at a dose of 70 or 140 $\mu\text{g/kg}$ effectively treated BDL-induced liver injury. Liver enzyme measurement and H&E staining revealed that TP at a dose of 70 or 140 $\mu\text{g/kg}$ significantly alleviated liver damage. Analysis of the liver hydroxyproline content, along with Masson 3 and Sirius Red staining, revealed that TP inhibited BDL-induced liver fibrosis. qPCR analysis of *Ck19* transcripts, as well as immunohistochemical staining of CK19 and Ki67, showed that TP significantly inhibited the BDL-induced ductular reaction. TP substantially reduced hepatic inflammatory infiltration after BDL, as revealed by immunohistochemical staining of F4/80 and Ly6G, as well as the mRNA expression levels of *F4/80*, *Il-1 β* , and *Tnf- α* in hepatic tissue. *In vitro* analysis demonstrated that TP dramatically downregulated the protein and mRNA

expression levels of RelB, as well as the downstream genes *Tnfrsf14* and *Ltβ*, thereby slowing the growth of HiBECs. Assessment of protein and mRNA expression levels in hepatic tissue revealed that TP attenuated the BDL-induced upregulation of RelB and downstream genes. The serum TNFSF14 assay confirmed that TP alleviated the BDL-induced upregulation of RelB. Graphic abstract was shown in **Figure 7**.

Tripterygium wilfordii Hook.f (TWHF) exhibits anti-inflammatory (41), anti-fertility (42), anti-colitis (43), and anti-cancer activities (44). At present, the clinical medication of TWHF is mainly used for rheumatoid arthritis, lupus and purpuric nephritis, psoriasis, erythroderma and allergic diseases. There are no clinical trials linking TWHF with cholestatic disease. However, the therapeutic window for TP is narrow; clinical applications are compromised by severe toxicities, including hepatotoxicity (37). The doses in this study were chosen because TP at a dose of 70 μg/kg substantially alleviated chronic kidney disease (31); we also used a higher dose for comparison. In our previous study, it was found that there was no obvious liver toxicity and cholestasis symptoms when TP 250 μg/kg was administered for 7 days (45). Therefore, we believe that the TP dose used in this study is a safe dose. TP-induced hepatotoxicity cannot be ignored. We previously found that TP was hepatotoxic at a dose of 500 or 600 μg/kg (46, 47). Evidently, TP at a dose of 70 or 140 μg/kg significantly alleviated BDL-induced liver injury, liver fibrosis, the ductular reaction, and hepatic inflammatory infiltration. Therefore, the role of TP in cholestasis is dose-dependent. The specific mechanism may be related to the complex immune homeostasis in the liver, and the specific mechanism will be carried out in future studies. The above content shows that TP needs more research before clinical treatment of cholestasis and may require structural modification and more accurate individualized diagnosis and treatment strategies.

Cholestasis can be caused by certain drugs, abnormal hormone levels, hepatitis, and dietary habits, but the underlying mechanism remains unknown (48). Recent studies have shown that the ductular reaction plays an important role in cholestasis-induced liver fibrosis and injury. The ductular reaction, characterized by cholangiocyte hyperproliferation, is commonly observed in patients with biliary disorders such as primary biliary cirrhosis, primary sclerosing cholangitis, or biliary atresia; this reaction is usually associated with liver fibrosis, and the extent of fibrosis is often correlated with mortality (32, 34). We presume that the reaction reflects the intense local inflammatory microenvironment present in cholangiocellular cholestasis; damaged cholangiocytes proliferate to compensate for reduced biliary cell function. The ductular reaction exacerbates hepatic inflammation, inhibits liver regeneration, and promotes fibrosis (41, 49–52). Previous studies showed that

inhibition of the ductular reaction alleviated cholestasis-induced liver damage, inflammation, and fibrosis (53, 54).

Some authors reported that the level of RelB was directly related to the extent of ductular reaction. RelB and LTβ were highly expressed in cholangiocytes from patients with chronic liver diseases (hepatitis C and hepatitis B virus infections, alcoholic liver disease, non-alcoholic fatty liver disease, and autoimmune hepatitis) or cholangiopathies (primary biliary cirrhosis and primary sclerosing cholangitis) (36). The activation of RelB in cholangiocytes and hepatocytes induces the secretion of LTβ, which activates cholangiocyte RelB in both an autocrine and paracrine manner through the LTβ receptor, thereby stimulating bile duct proliferation. Thus, RelB is essential for cholangiocyte proliferation and the ductular reaction. But so far, there are no drugs targeting RelB yet in clinical, therefore, the design of new drugs for RelB has broad prospects. Accordingly, we first examined the effect of TP on cholangiocyte proliferation *in vitro*. As expected (37), TP (an NF-κB inhibitor) significantly reduced cell proliferation, as well as the expression of RelB and its downstream genes. *In vivo* analysis showed that TP significantly alleviated the BDL-induced upregulation of RelB. This finding suggested that TP reduces cholangiocyte expression of RelB, thus suppressing cholangiocyte proliferation; alleviating the BDL-induced ductular reaction; and reducing liver damage, inflammation, and fibrosis.

RelB is frequently associated with liver fibrosis. In addition to its presence in cholangiocytes, RelB is expressed in Kupffer cells (55) and hepatocytes (36). RelB-regulated TNFSF14 is presumed to promote hepatic stellate cell activation and the resulting liver fibrosis (38). Our assays of serum TNFSF14 levels indicated that TP reduced the BDL-induced increase in the TNFSF14 level; this may partly explain why TP relieves hepatic inflammation and fibrosis.

Finally, TP is a small-molecule drug and may thus act via several mechanisms. We focused on RelB. More detailed clinical and translational studies are needed to substantiate the potential utility of TP as a cholestasis treatment. Careful dosing studies are also essential.

Conclusion

Triptolide (TP) at certain doses improved cholestasis. TP may be useful in the prevention or treatment of cholestasis-induced liver injuries, fibrosis, and other inflammatory diseases.

Data availability statement

The original contributions presented in this study are included in the article/**Supplementary material**, further inquiries can be directed to the corresponding authors.

Ethics statement

The animal study was reviewed and approved by China Pharmaceutical University Experimental Animal Ethics Committee.

Author contributions

ZJ and ZhY designed the overall research experiments. ZhY, JW, HZ, YM, QT, ZqY, and CN performed the experiments. ZhY and JW analyzed the data. ZhY wrote the manuscript. ZJ and QY reviewed the manuscript. All authors contributed to the article and approved the submitted version.

Funding

This study was supported by the Postgraduate Research Practice Innovation Program of Jiangsu Province (KYCX19_0674 to ZhY), the Natural Science Foundation of Jiangsu Province (BK20221526 to ZJ), National Natural Science Foundation of China (81773827 and 82074114 to ZJ), “Double First-Class” University project (CPU2018 GY33 to ZJ), and China Postdoctoral Science Foundation (2020M681786 to QY).

References

- Zollner G, Trauner M. Mechanisms of cholestasis. *Clin Liver Dis.* (2008) 12:1–26. doi: 10.1016/j.cld.2007.11.010
- Cai SY, Boyer JL. Bile infarcts: new insights into the pathogenesis of obstructive cholestasis. *Hepatology.* (2019) 69:473–5. doi: 10.1002/hep.30291
- European Association for the Study of the Liver. EASL clinical practice guidelines: management of cholestatic liver diseases. *J Hepatol.* (2009) 51:237–67. doi: 10.1016/j.jhep.2009.04.009
- Beuers U. Drug insight: mechanisms and sites of action of ursodeoxycholic acid in cholestasis. *Nat Clin Pract Gastroenterol Hepatol.* (2006) 3:318–28. doi: 10.1038/ncpgasthep0521
- Samur S, Klebanoff M, Banken R, Pratt DS, Chapman R, Ollendorf DA, et al. Long-term clinical impact and cost-effectiveness of obeticholic acid for the treatment of primary biliary cholangitis. *Hepatology.* (2017) 65:920–8. doi: 10.1002/hep.28932
- Pellicciari R, Fiorucci S, Camaioni E, Clerici C, Costantino G, Maloney PR, et al. Agonist endowed with anticholestatic. *Society.* (2002) 45:15–8. doi: 10.1021/jm025529g
- Nevens F, Andreone P, Mazzella G, Strasser SI, Bowlus C, Invernizzi P, et al. A placebo-controlled trial of obeticholic acid in primary biliary cholangitis. *N Engl J Med.* (2016) 375:631–43. doi: 10.1056/nejmoa1509840
- Neuschwander-Tetri BA, Loomba R, Sanyal AJ, Lavine JE, Van Natta ML, Abdelmalek MF, et al. Farnesoid X nuclear receptor ligand obeticholic acid for non-cirrhotic, non-alcoholic steatohepatitis (FLINT): a multicentre, randomised, placebo-controlled trial. *Lancet.* (2015) 385:956–65. doi: 10.1016/S0140-6736(14)61933-4
- Crocenzi F, Roma M. Silymarin as a new hepatoprotective agent in experimental cholestasis: new possibilities for an ancient medication. *Curr Med Chem.* (2006) 13:1055–74. doi: 10.2174/092986706776360950
- Wang X, Han L, Bi Y, Li C, Gao X, Fan G, et al. Paradoxical effects of emodin on anit-induced intrahepatic cholestasis and herb-induced hepatotoxicity in Mice. *Toxicol Sci.* (2019) 168:264–78. doi: 10.1093/toxsci/kfy295
- Xiong XL, Ding Y, Chen ZL, Wang Y, Liu P, Qin H, et al. Emodin rescues intrahepatic cholestasis via stimulating FXR/BSEP pathway in promoting the canalicular export of accumulated bile. *Front Pharmacol.* (2019) 10:522. doi: 10.3389/fphar.2019.00522
- Liao M, Zhang R, Wang Y. Corilagin prevents non-alcoholic fatty liver disease via improving lipid metabolism and glucose homeostasis in high fat diet-fed mice. *Front Nutr.* (2022) 9:983450. doi: 10.3389/fnut.2022.983450
- Li XJ, Jiang ZZ, Zhang LY. Triptolide: progress on research in pharmacodynamics and toxicology. *J Ethnopharmacol.* (2014) 155:67–79. doi: 10.1016/j.jep.2014.06.006
- Xia M, Liu D, Liu H, Zhao J, Tang C, Chen G, et al. Based on network pharmacology tools to investigate the mechanism of tripterygium wilfordii against IgA nephropathy. *Front Med.* (2021) 8:794962. doi: 10.3389/fmed.2021.794962
- Zhang X, Zhang X, Wang X, Wang T, Bai B, Zhang N, et al. Efficient delivery of triptolide plus a miR-30-5p inhibitor through the use of near infrared laser responsive or CADY modified MSNs for efficacy in rheumatoid arthritis therapeutics. *Front Bioeng Biotechnol.* (2020) 8:170. doi: 10.3389/fbioe.2020.00170
- Datan E, Minn I, Xu P, He QL, Ahn HH, Yu B, et al. Glucose-triptolide conjugate selectively targets cancer cells under hypoxia. *iScience.* (2020) 23:101536. doi: 10.1016/j.isci.2020.101536
- Fan D, Guo Q, Shen J, Zheng K, Lu C, Zhang G, et al. The effect of triptolide in rheumatoid arthritis: from basic research towards clinical translation. *Int J Mol Sci.* (2018) 19:376. doi: 10.3390/ijms19020376
- Liang D, Mai H, Ruan F, Fu H. The efficacy of triptolide in preventing diabetic kidney diseases: a systematic review and meta-analysis. *Front Pharmacol.* (2021) 12:728758. doi: 10.3389/fphar.2021.728758
- Huang W, He T, Chai C, Yang Y, Zheng Y, Zhou P, et al. Triptolide inhibits the proliferation of prostate cancer cells and down-regulates SUMO-specific protease 1 expression. *PLoS One.* (2012) 7:e37693. doi: 10.1371/journal.pone.0037693
- Yan P, Sun X. Triptolide: a new star for treating human malignancies. *J Cancer Res Ther.* (2018) 14(Suppl.):S271–5. doi: 10.4103/0973-1482.235340

Conflict of interest

The authors declare that the research was conducted in the absence of any commercial or financial relationships that could be construed as a potential conflict of interest.

Publisher's note

All claims expressed in this article are solely those of the authors and do not necessarily represent those of their affiliated organizations, or those of the publisher, the editors and the reviewers. Any product that may be evaluated in this article, or claim that may be made by its manufacturer, is not guaranteed or endorsed by the publisher.

Supplementary material

The Supplementary Material for this article can be found online at: <https://www.frontiersin.org/articles/10.3389/fnut.2022.1032722/full#supplementary-material>

21. Luo D, Ren H, Zhang H, Zhang P, Huang Z, Xian H, et al. The protective effects of triptolide on age-related bone loss in old male rats. *Biomed Pharmacother.* (2018) 98:280–5. doi: 10.1016/j.biopha.2017.12.072
22. Kim SJ, Beak SM, Park SK. Supplementation with triptolide increases resistance to environmental stressors and lifespan in *C. elegans*. *J Food Sci.* (2017) 82:1484–90. doi: 10.1111/1750-3841.13720
23. Li H, Li L, Mei H, Pan G, Wang X, Huang X, et al. Antitumor properties of triptolide: phenotype regulation of macrophage differentiation. *Cancer Biol Ther.* (2020) 21:178–88. doi: 10.1080/15384047.2019.1679555
24. Li H, Xing X, Zhang X, Li L, Jiang Z, Wang T, et al. Effects of triptolide on the sphingosine kinase – Sphingosine-1-phosphate signaling pathway in colitis-associated colon cancer. *Int Immunopharmacol.* (2020) 88:106892. doi: 10.1016/j.intimp.2020.106892
25. Luo JL, Kamata H, Karin M. IKK/NF- κ B signaling: balancing life and death – a new approach to cancer therapy. *J Clin Invest.* (2005) 115:2625–32. doi: 10.1172/JCI26322
26. García-García VA, Alameda JP, Page A, Casanova ML. Role of nf- κ b in ageing and age-related diseases: lessons from genetically modified mouse models. *Cells.* (2021) 10:1906. doi: 10.3390/cells10081906
27. Liu T, Zhang L, Joo D, Sun SC. NF- κ B signaling in inflammation. *Signal Transduct Target Ther.* (2017) 2:17023. doi: 10.1038/sigtrans.2017.23
28. Sabir JSM, El Omri A, Shaik NA, Banaganapalli B, Al-Shaeri MA, Alkenani NA, et al. Identification of key regulatory genes connected to Nf- κ B family of proteins in visceral adipose tissues using gene expression and weighted protein interaction network. *PLoS One.* (2019) 14:e0214337. doi: 10.1371/journal.pone.0214337
29. Yang J, Tang X, Ke X, Dai Y, Shi J. Triptolide suppresses NF- κ B-mediated inflammatory responses and activates expression of Nrf2-mediated antioxidant genes to alleviate caerulein-induced acute pancreatitis. *Int J Mol Sci.* (2022) 23:1252. doi: 10.3390/ijms23031252
30. Yinjun L, Jie J, Yungui W. Triptolide inhibits transcription factor NF- κ B and induces apoptosis of multiple myeloma cells. *Leuk Res.* (2005) 29:99–105. doi: 10.1016/j.leukres.2004.05.014
31. Yoshida T, Yamashita M, Horimai C, Hayashi M. Smooth muscle-selective nuclear factor- κ B inhibition reduces phosphate-induced arterial medial calcification in mice with chronic kidney disease. *J Am Heart Assoc.* (2017) 6:e007248. doi: 10.1161/JAHA.117.007248
32. Sato K, Marziani M, Meng F, Francis H, Glaser S, Alpini G. Ductular reaction in liver diseases: pathological mechanisms and translational significances. *Hepatology.* (2019) 69:420–30. doi: 10.1002/hep.30150
33. Peng ZW, Ikenaga N, Liu SB, Sverdlow DY, Vaid KA, Dixit R, et al. Integrin α v β 6 critically regulates hepatic progenitor cell function and promotes ductular reaction, fibrosis, and tumorigenesis. *Hepatology.* (2016) 63:217–32. doi: 10.1002/hep.28274
34. Hsieh WC, Mackinnon AC, Lu WY, Jung J, Boulter L, Henderson NC, et al. Galectin-3 regulates hepatic progenitor cell expansion during liver injury. *Gut.* (2015) 64:312–21. doi: 10.1136/gutjnl-2013-306290
35. Hayden MS, Ghosh S. Shared principles in NF- κ B signaling. *Cell.* (2008) 132:344–62. doi: 10.1016/j.cell.2008.01.020
36. Elßner C, Goepfert B, Longerich T, Scherr AL, Stindt J, Nanduri LK, et al. Nuclear translocation of RELB is increased in diseased human liver and promotes ductular reaction and biliary fibrosis in mice. *Gastroenterology.* (2019) 156:1190–205.e14. doi: 10.1053/j.gastro.2018.11.018
37. Yuan Z, Yuan Z, Hasnat M, Zhang H, Liang P, Sun L, et al. A new perspective of triptolide-associated hepatotoxicity: the relevance of NF- κ B and NF- κ B-mediated cellular FLICE-inhibitory protein. *Acta Pharm Sin B.* (2020) 10:861–77. doi: 10.1016/j.apsb.2020.02.009
38. Liang QS, Xie JG, Yu CP, Feng ZS, Ma JC, Zhang Y, et al. Splenectomy improves liver fibrosis via tumor necrosis factor superfamily 14 (LIGHT) through the JNK/TGF- β 1 signaling pathway. *Exp Mol Med.* (2021) 53:393–406. doi: 10.1038/s12276-021-00574-2
39. Jiao J, Ooka K, Fey H, Fiel MI, Rahmman AH, Kojima K, et al. Interleukin-15 receptor α on hepatic stellate cells regulates hepatic fibrogenesis in mice. *J Hepatol.* (2016) 65:344–53. doi: 10.1016/j.jhep.2016.04.020
40. Wang X, Lopategi A, Ge X, Lu Y, Kitamura N, Urtasun R, et al. Osteopontin induces ductular reaction contributing to liver fibrosis. *Gut.* (2014) 63:1805–18. doi: 10.1136/gutjnl-2013-306373
41. Wang X, Zhang L, Duan W, Liu B, Gong P, Ding Y, et al. Anti-inflammatory effects of triptolide by inhibiting the NF- κ B signalling pathway in LPS-induced acute lung injury in a murine model. *Mol Med Rep.* (2014) 10:447–52. doi: 10.3892/mmr.2014.2191
42. Li H, Pan GF, Jiang ZZ, Yang J, Sun LX, Zhang LY. Triptolide inhibits human breast cancer MCF-7 cell growth via downregulation of the ER α -mediated signaling pathway. *Acta Pharmacol Sin.* (2015) 36:606–13. doi: 10.1038/aps.2014.162
43. Tang B, Zhu J, Zhang B, Wu F, Wang Y, Weng Q, et al. Therapeutic potential of triptolide as an anti-inflammatory agent in dextran sulfate sodium-induced murine experimental colitis. *Front Immunol.* (2020) 11:592084. doi: 10.3389/fimmu.2020.592084
44. Noel P, Von Hoff DD, Saluja AK, Velagapudi M, Borazanci E, Han H. Triptolide and its derivatives as cancer therapies. *Trends Pharmacol Sci.* (2019) 40:327–41. doi: 10.1016/j.tips.2019.03.002
45. Yuan Z, Zhang H, Hasnat M, Ding J, Chen X, Liang P, et al. new perspective of triptolide-associated hepatotoxicity: liver hypersensitivity upon LPS stimulation. *Toxicology.* (2019) 414:45–56. doi: 10.1016/j.tox.2019.01.005
46. Wang X, Jiang Z, Cao W, Yuan Z, Sun L, Zhang L. Th17/Treg imbalance in triptolide-induced liver injury. *Fitoterapia.* (2014) 93:245–51. doi: 10.1016/j.fitote.2014.01.006
47. Wang X, Jiang Z, Xing M, Fu J, Su Y, Sun L, et al. Interleukin-17 mediates triptolide-induced liver injury in mice. *Food Chem Toxicol.* (2014) 71:33–41. doi: 10.1016/j.fct.2014.06.004
48. Ghonem NS, Assis DN, Boyer JL. Fibrates and cholestasis. *Hepatology.* (2015) 62:635–43. doi: 10.1002/hep.27744
49. Yang M, Ramachandran A, Yan HM, Woolbright BL, Copple BL, Fickert P, et al. Osteopontin is an initial mediator of inflammation and liver injury during obstructive cholestasis after bile duct ligation in mice. *Toxicol Lett.* (2014) 224:186–95. doi: 10.1016/j.toxlet.2013.10.030
50. Whittington PF, Malladi P, Melin-Aldana H, Azzam R, Mack CL, Sahai A. Expression of osteopontin correlates with portal biliary proliferation and fibrosis in biliary atresia. *Pediatr Res.* (2005) 57:837–44. doi: 10.1203/01.PDR.0000161414.99181.61
51. Syn WK, Choi SS, Liaskou E, Karaca GF, Agboola KM, Oo YH, et al. Osteopontin is induced by hedgehog pathway activation and promotes fibrosis progression in nonalcoholic steatohepatitis. *Hepatology.* (2011) 53:106–15. doi: 10.1002/hep.23998
52. Nuñez-García M, Gomez-Santos B, Buqué X, García-Rodríguez JL, Romero MR, Marin JGG, et al. Osteopontin regulates the cross-talk between phosphatidylcholine and cholesterol metabolism in mouse liver. *J Lipid Res.* (2017) 58:1903–15. doi: 10.1194/jlr.M078980
53. Wang Y, Aoki H, Yang J, Peng K, Liu R, Li X, et al. The role of sphingosine 1-phosphate receptor 2 in bile-acid-induced cholangiocyte proliferation and cholestasis-induced liver injury in mice. *Hepatology.* (2017) 65:2005–18. doi: 10.1002/hep.29076
54. Coombes JD, Swiderska-Syn M, Dollé L, Reid D, Eksteen B, Claridge L, et al. Osteopontin neutralisation abrogates the liver progenitor cell response and fibrogenesis in mice. *Gut.* (2015) 64:1120–31. doi: 10.1136/gutjnl-2013-306484
55. Hsu KH, Wei CW, Su YR, Chou T, Lin YL, Yang FC, et al. Upregulation of RelB in the miR-122 knockout mice contributes to increased levels of proinflammatory chemokines/cytokines in the liver and macrophages. *Immunol Lett.* (2020) 226:22–30. doi: 10.1016/j.imlet.2020.06.015



OPEN ACCESS

EDITED BY

Yi Wu,
Nanjing Agricultural University, China

REVIEWED BY

Wenke Feng,
University of Louisville, United States
Grace L Guo,
Rutgers, The State University of New
Jersey, United States

*CORRESPONDENCE

Chunhua Jiao
jch0409@163.com
Lixin Sun
slxcpu@126.com

[†]These authors have contributed
equally to this work and share
first authorship

SPECIALTY SECTION

This article was submitted to
Nutritional Immunology,
a section of the journal
Frontiers in Immunology

RECEIVED 17 August 2022

ACCEPTED 06 October 2022

PUBLISHED 20 October 2022

CITATION

Yang M, Zhang Q, Taha R,
Abdelmotalab MI, Wen Q, Yuan Y,
Zhao Y, Li Q, Liao C, Huang X, Jiang Z,
Chu C, Jiao C and Sun L (2022)
Polysaccharide from *Atractylodes*
macrocephala Koidz. ameliorates DSS-
induced colitis in mice by regulating
the Th17/Treg cell balance.
Front. Immunol. 13:1021695.
doi: 10.3389/fimmu.2022.1021695

COPYRIGHT

© 2022 Yang, Zhang, Taha,
Abdelmotalab, Wen, Yuan, Zhao, Li, Liao,
Huang, Jiang, Chu, Jiao and Sun. This is
an open-access article distributed under
the terms of the [Creative Commons
Attribution License \(CC BY\)](#). The use,
distribution or reproduction in other
forums is permitted, provided the
original author(s) and the copyright
owner(s) are credited and that the
original publication in this journal is
cited, in accordance with accepted
academic practice. No use,
distribution or reproduction is
permitted which does not comply with
these terms.

Polysaccharide from *Atractylodes macrocephala* Koidz. ameliorates DSS-induced colitis in mice by regulating the Th17/Treg cell balance

Mengjiao Yang^{1†}, Qianwen Zhang^{1†}, Reham Taha¹,
Mohammed Ismail Abdelmotalab¹, Qing Wen¹, Yuzhu Yuan¹,
Yongrui Zhao¹, Qingyu Li¹, Chunyu Liao¹, Xin Huang¹,
Zhenzhou Jiang¹, Chenghan Chu¹, Chunhua Jiao^{2*}
and Lixin Sun^{1*}

¹Jiangsu Center for Pharmacodynamics Research and Evaluation, China Pharmaceutical University, Nanjing, China, ²Department of Gastroenterology, The First Affiliated Hospital of Nanjing Medical University, Nanjing, China

Atractylodes macrocephala Koidz. is one of the most frequently used traditional Chinese medicines for the treatment of ulcerative colitis (UC). The beneficial effect of polysaccharide from *Atractylodes macrocephala* Koidz. (PAMK) on UC has been reported, while the underlying mechanism and target remain unclear. In this study, we systematically investigated the therapeutic effect and the underlying mechanism of PAMK in UC based on a mouse model of dextran sodium sulfate (DSS)-induced colitis. PAMK treatment (100 mg/kg, 200 mg/kg and 400 mg/kg) significantly ameliorated DSS-induced colitis, manifested as a reduction in weight loss, disease activity index (DAI), colon shortening, spleen index and histological score. Moreover, PAMK treatment inhibited inflammation and improved the integrity of the intestinal barrier in colitis mice. Mechanistically, microarray analysis determined the critical role of the immunoregulatory effect of PAMK in alleviating UC. Flow cytometry analysis further demonstrated that PAMK treatment regulated the balance between T helper (Th) 17 and regulatory T (Treg) cells in the mesenteric lymph nodes (MLN) and spleen in mice with colitis. In addition, PAMK treatment downregulated the expression of IL-6 and suppressed the phosphorylation of STAT3. Together, these data revealed that PAMK treatment alleviated DSS-induced colitis by regulating the Th17/Treg cell balance, which may be dependent on the inhibition of the IL-6/STAT3 signaling pathway. Our study is the first to elucidate that the underlying mechanism by which PAMK treatment alleviates DSS-induced colitis is associated with an improved Th17/Treg cell balance. Collectively, the study provides evidence for the potential of PAMK to treat UC.

KEYWORDS

polysaccharide from *Atractylodes macrocephala* Koidz., ulcerative colitis, transcriptional profile, Th17/Treg cell balance, IL-6/STAT3

Introduction

Ulcerative colitis (UC), a subtype of inflammatory bowel disease (IBD), is characterized by chronic and relapsing mucosal inflammation initiating in the rectum and extending upward through part or the entire colon in a continuous fashion (1). The worldwide prevalence of UC has increased in the last few decades. Currently, 5-aminosalicylic acid agents, corticosteroids, immunomodulators, and surgery are the main treatments for UC, which are limited in clinical practice due to common nonadherence, serious adverse effects and heavy financial burden (2). Thus, it is imperative to develop new alternative treatments for UC.

Atractylodes macrocephala Koidz. (Baizhu) has been used for improving gastrointestinal function and treating digestive disorders for thousands of years (3), and is currently one of the most frequently used traditional Chinese medicines (TCMs) for the treatment of UC (4). Previous studies demonstrated that combination therapy of a Chinese herbal compound containing Baizhu and mesalazine was more effective in improving the clinical symptoms of UC patients than mesalazine alone (5). Polysaccharide from *Atractylodes macrocephala* Koidz. (PAMK), one of the main components in *Atractylodes macrocephala* Koidz., promoted the proliferation and survival of intestinal epithelial cells *in vitro* (6) and prevented intestinal barrier dysfunction in colitis mice (7). However, the underlying mechanism by which PAMK treatment alleviates colitis remains unclear.

Aberrant immune responses are a hallmark of UC. In UC, large numbers of immune cells are recruited into the inflamed colonic mucosa, and then they produce excessive proinflammatory cytokines, resulting in intestinal barrier impairment, gut microbiota dysbiosis and perpetuation of inflammation (8). Immunotherapy drugs, such as anti-IL-12/IL-23 antibodies, have emerged as important treatments for UC by inhibiting the activation of immune cells and the production of their mediators (9). The immunoregulatory effect of PAMK has been determined in previous studies, including promoting the differentiation of Treg cells *in vitro* (10) and enhancing mucosal immunity in the intestine (11). Thus, we investigated the mechanism of PAMK in a mouse model of dextran sodium sulfate (DSS)-induced colitis and hypothesized that the immunoregulatory function plays a key role in its beneficial effect of PAMK on colitis.

Materials and methods

Drug

Polysaccharide from *Atractylodes macrocephala* Koidz. (PAMK, purity $\geq 98.0\%$) used in our study was purchased from Shanxi Ciyuan Biotechnology Co., Ltd. (Xian, China).

PAMK was extracted from *Atractylodes macrocephala* Rhizoma from Zhejiang Province, China. During the production process, the manufacturer implemented strict process parameters and quality inspection of the intermediates in key processes, such as properties and polysaccharide content. The purity, molecular weight and monosaccharide composition of all final products were investigated. The quality inspection reports offered by the manufacturer showed that there were few differences in the molecular weight and monosaccharide composition between different batches of PAMK, indicating the stable reproducibility of PAMK preparation.

Reagents

Dextran sulfate sodium (DSS, MW 36000-50000) was obtained from MP Biomedicals (CA, USA). The myeloperoxidase (MPO) assay kit was obtained from Jiancheng Bioengineering Institute (Nanjing, China). Zonula occludens protein 1 (ZO-1) and Occludin antibodies were obtained from Affinity (Liyang, China). FITC anti-CD4, PE anti-Foxp3, and PE anti-IL-17A antibodies were obtained from Biolegend (CA, USA). CD3e antibody, APC anti-CD25 antibody, Foxp3/transcription factor staining buffer set and IC fixation buffer were obtained from eBioscienceTM (CA, USA). CD16/CD32 antibody was obtained from BD Biosciences (CA, USA). STAT3 and phospho-STAT3 (p-STAT3) antibodies were obtained from Cell Signaling Technology (MA, USA). The QuantiCyto[®] Mouse TNF- α enzyme-linked immunosorbent assay (ELISA) kit was obtained from NeoBioscience (Shenzhen, China).

Characterization of PAMK

UV spectra analysis

The UV spectrum of PAMK aqueous solution (40 mg/mL) was recorded with a Nanodrop 2000 system in a region of 220-350 nm to detect free proteins and nucleic acids.

Molecular weight analysis

PAMK (11 mg) was dissolved in 1 mL of distilled water and then applied to a gel permeation chromatography system using a PL aquagel-OH MIXED-M column (7.5 \times 300 mm) maintained at a temperature of 40°C. The sample was eluted with 0.1 M NaNO₃ at a flow rate of 1.0 mL/min. The calibration curve was obtained based on the T-series dextran standards of different molecular weights (T-5, T-10, T-40, T-100, T-500, T-1000 and T-2000).

Determination of monosaccharide composition

The monosaccharide composition of PAMK was determined by high-performance liquid chromatography (HPLC). A total of

0.5 mL of 19.4 mg/mL PAMK aqueous solution was hydrolyzed with 0.5 mL of 4 M trifluoroacetic acid (TFA) at 110°C for 2 h. After removal of TFA, the residue was dissolved in 0.5 mL of distilled water, and 200 μ L of the solution was acetylated with 120 μ L of 0.5 M 1-phenyl-3-methyl-5-pyrazolone (PMP) and 120 μ L of 0.3 M sodium hydrate solution in a water bath at 70°C for 2 h. Then, the product was neutralized with 120 μ L of 3 M hydrochloric acid and extracted with 2 mL of chloroform thrice with sufficient blending. The aqueous phase was filtered with a 0.22 μ m microporous filter and analyzed on a Hypersil BDS-C18 chromatographic column (4.6 \times 150 mm, 5 μ m) at 30°C. The mobile phase consisted of phosphate buffer (20 mM, pH 6.7) and acetonitrile as eluents A and B (82:18 v/v). The flow rate was 1.0 mL/min, and the wavelength for UV detection was 250 nm. Eight standard monosaccharides, namely, mannose, rhamnose, glucuronic acid, galacturonic acid, glucose, galactose, arabinose and fucose, were used as references.

Animals

Specific-pathogen-free (SPF)-grade male C57BL/6J mice weighing 20 ± 2 g were obtained from Shanghai Lingchang Biological Technology Co., Ltd. (Shanghai, China, certificate No. SCXK (hu) 2018-0003). The animals were housed in a specific pathogen-free condition (ambient temperature of $22 \pm 2^\circ\text{C}$, relative humidity of $60 \pm 5\%$, and light-dark cycle of 12 h). All animal experimental protocols were approved by the Ethics Committee of China Pharmaceutical University (No. 2021-09-001).

Animal experiment

Mice were fed adaptively for 7 days before the experiment and randomly divided into five groups (Control, DSS, DSS+100 mg/kg PAMK, DSS+200 mg/kg PAMK, and DSS+400 mg/kg PAMK). Acute colitis was induced by distilled water containing 3% DSS for 7 days, and the Control group was only given distilled water. From day 8 to day 14, the mice in the five groups received one of the following treatments: Control group (1 ml/100 g normal saline, i.g.), DSS group (1 ml/100 g normal saline, i.g.), DSS+100 mg/kg PAMK (100 mg/kg PAMK, i.g.), DSS+200 mg/kg PAMK (200 mg/kg PAMK, i.g.), and DSS+400 mg/kg PAMK (400 mg/kg PAMK, i.g.). The experimental scheme is shown in [Figure 2A](#).

Evaluation of colitis severity

The body weight, stool consistency and blood in stool were recorded daily during the whole experimental period, and the

scoring criteria are shown in [Supplementary Table 1](#). The aggregate of all three observations was taken as a disease activity index (DAI). On the 15th day, the mice were sacrificed, and spleen weight and colon length were measured. For histological evaluation, the distal colon tissues were fixed in 10% neutral formaldehyde, dehydrated, and embedded in paraffin. The colon specimens were cut into slices, deparaffinized, stained with hematoxylin and eosin (H&E), and observed under a microscope. The scoring system was based on four independent parameters ([Supplementary Table 2](#)), and the summation of these scores provided a histopathological score.

Determination of TNF- α level in plasma

The content of TNF- α in plasma was determined by an ELISA kit according to the manufacturer's instructions.

Measurement of MPO activity in colon

The weighed colonic tissue was homogenized with PBS to prepare a 5% homogenate and centrifuged at 12,000 rpm for 5 min. Then, the supernatant was collected, and the MPO activity was determined according to the manufacturer's protocol.

Microarray analysis

The Agilent Mouse ceRNA Microarray 2019 (4 \times 180K, Design ID:086242) was used for microarray analysis of the colonic tissues of the Control, DSS and DSS+PAMK (200 mg/kg PAMK, i.g.) groups ($n=3$). RNA was extracted by a mirVanaTM RNA isolation kit following the manufacturer's instructions. The purity and integrity of total RNA were determined with a NanoDrop ND-2000 and Agilent 2100 bioanalyzer, respectively. RNA was transcribed to cDNA, and then cRNA was synthesized and labeled with Cyanine-3-CTP (Cy3). The labeled cRNA was hybridized onto the microarray. Slides were scanned immediately after washing on the Agilent DNA Microarray Scanner (G2505C), and the scanned images were analyzed with Feature Extraction Software 10.7.1.1 (Agilent) to obtain raw data. Raw data were normalized with the quantile algorithm. Differentially expressed genes (DEGs) and differentially expressed mRNAs (DEMs) were identified through a fold change ≥ 2 as well as a $P \leq 0.05$ calculated with a *t* test. Gene Ontology (GO) enrichment and Kyoto Encyclopedia of Genes and Genomes (KEGG) enrichment analyses of DEMs were performed to determine the roles of DEMs based on the hypergeometric distribution.

Quantitative real-time polymerase chain reaction (qRT-PCR) analysis

Total RNA was extracted from colonic tissues with TRIzol reagent. The concentration and purity were measured by a Nanodrop 2000. Then, cDNA was synthesized with HiScript® Q RT Super Mix, and PCRs were performed with AceQ® qPCR SYBR Green Master Mix as directed by the manufacturer's protocols. The expression of genes was normalized to the *Actb* gene on the basis of the $2^{-\Delta\Delta CT}$ algorithm. The primers used in the research are listed in [Supplementary Table 3](#).

Western blotting

The total protein of colonic tissue was extracted using RIPA buffer containing protease inhibitor and phosphatase inhibitor, and the content was determined using a BCA kit. Proteins were separated by SDS-PAGE and transferred to a PVDF membrane. The membrane was blocked with 5% BSA buffer for one hour at room temperature, followed by incubation with p-STAT3 antibody (1:2000) overnight at 4°C and secondary antibodies for an hour at room temperature. The protein bands were visualized by an automated chemiluminescence Western blot detection system. Then, the same blots were stripped and reprobed with STAT3 antibody (1:1000). Densitometry analysis of bands was performed using ImageJ.

Flow cytometry analysis

For T helper (Th) 17 cells staining, cells isolated from the spleen and mesenteric lymph nodes (MLN) were stimulated with phorbol-12-myristate-13-acetate (100 ng/mL), ionomycin (1 µg/mL) and brefeldin A (10 µg/mL) at 37°C for 5 h. After blocking with anti-CD16CD32 antibody, the cells were labeled with FITC anti-CD4 antibody. Then, the cells were fixed and permeabilized, followed by intracellular staining with PE anti-IL-17A antibody. Similarly, the surface markers FITC anti-CD4 and APC anti-CD25 antibodies and the intranuclear marker PE anti-Foxp3 antibody were used to label regulatory T (Treg) cells. The data were analyzed using FlowJo 10 software. The proportions of Th17 and Treg cells, and the ratios of Th17/Treg cell in the spleen and MLN in the DSS group and all PAMK treatment groups were normalized to those in the Control group.

Immunofluorescence staining

The sections of colonic tissues were fixed in 4% paraformaldehyde. For ZO-1 and Occluding staining, the samples were permeabilized with 0.3% Triton X-100 at room

temperature for 15 min and blocked with 5% goat serum buffer. For p-STAT3 staining, the samples were permeabilized with methanol at -20°C for 10 min and blocked with 5% goat serum buffer containing 0.3% Triton X-100. Then, the sections were incubated with ZO-1 (1:200), Occludin (1:200) or p-STAT3 (1:100) antibodies overnight at 4°C. The next day, the secondary antibody and 4,6-diamidino-2-phenylindole (DAPI) were used to stain the samples. The stained sections were observed under a fluorescence microscope.

Statistical analysis

All statistical analyses were performed using GraphPad Prism 8, and the data are presented as the mean ± standard error of the mean (SEM). One-way ANOVA and two-way ANOVA were used for multiple comparisons. A $P < 0.05$ was recognized as statistically significant.

Results

Structural characterization of PAMK

The UV scanning spectrum revealed no apparent light absorption at 260 nm and 280 nm, indicating that free proteins and nucleic acids were not present in PAMK ([Figure 1A](#)). The molecular weight of PAMK was determined to be 2.45×10^3 Da ([Figure 1B](#)). Based on the HPLC retention times of standard sugars, the monosaccharide composition of PAMK mainly consisted of mannose, rhamnose, glucuronic acid, galacturonic acid, glucose, galactose, arabinose and fucose in a molar ratio of 7.64, 0.25, 0.17, 0.13, 70.14, 1.00, 6.59, and 0.23 ([Figures 1C, D](#)).

PAMK treatment ameliorated DSS-induced colitis

The beneficial impacts of PAMK on intestinal functions were examined in a mouse model of DSS-induced colitis. During the experimental process, DSS treatment resulted in weight loss, diarrhea and bloody stool. A significant reduction in weight loss and a marked decrease in the DAI score were observed in all PAMK treatment groups compared with the DSS group ([Figures 2B, C](#)). PAMK treatment significantly inhibited colon shortening and improved splenomegaly in the mice with colitis ([Figures 2D–F](#)). H&E staining was performed to systematically evaluate colonic injury. The mice in the DSS group exhibited serious pathological injury, as evidenced by surface epithelium erosion, inflammatory cell infiltration, mucosal ulceration, crypt loss, and goblet cell depletion. These pathological injuries were significantly relieved, and the histological scores significantly

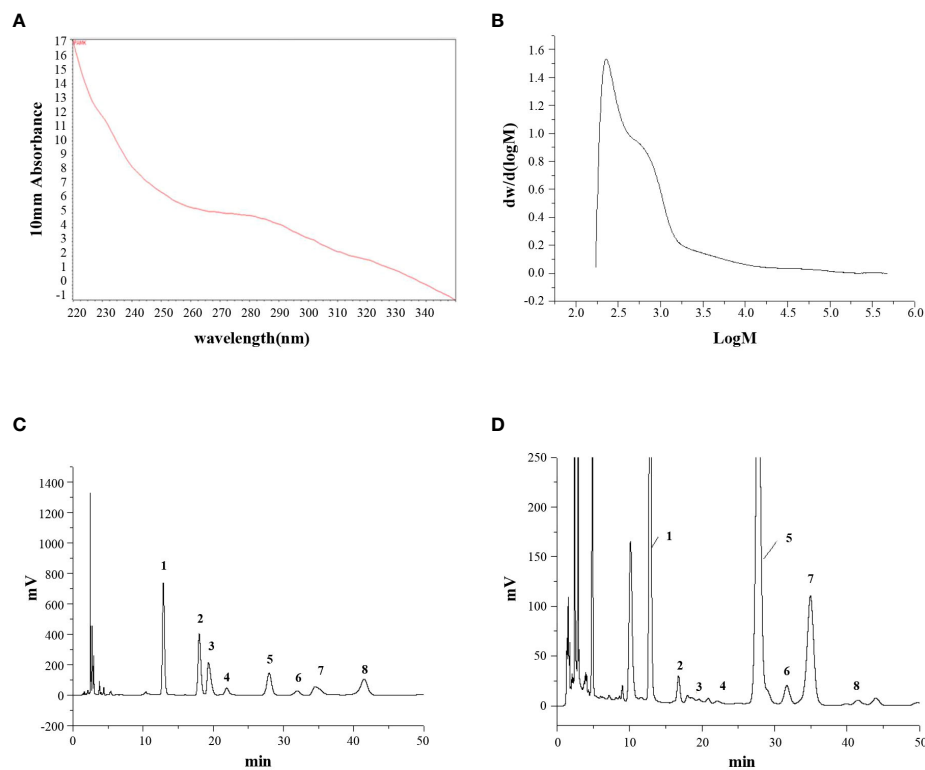


FIGURE 1

The structural characterization of PAMK. (A) UV scan spectrum. (B) Gel permeation chromatography spectrum. (C) HPLC spectrum of standard monosaccharides. (D) HPLC spectrum of PAMK. The peaks numbered 1 to 8 represent mannose, rhamnose, glucuronic acid, galacturonic acid, glucose, galactose, arabinose and fucose, respectively.

decreased after PAMK administration in a dose-dependent manner (Figures 2G, H). Together, these results indicated that PAMK treatment significantly ameliorated DSS-induced colitis.

PAMK treatment inhibited the inflammatory response and improved the intestinal barrier in DSS-induced colitis mice

To further assess the effect of PAMK on colitis, MPO activity in colon tissue, an important biomarker of the extent of neutrophil infiltration, was measured, and the data showed that PAMK treatment could decreased MPO activity in colitis mice (Figure 3A). UC is known to be caused by overstimulation of proinflammatory cytokines. The level of $TNF-\alpha$ in plasma significantly increased in the DSS group and decreased after PAMK treatment (Figure 3B). Similarly, PAMK treatment lowered the expression of proinflammatory cytokines (Figures 3C–F), including *Tnfa*, *Il1b*, *Il18* and *Il23*, which have been reported to be increased in UC patients (12, 13). Among

the various doses used in the study, 200 mg/kg PAMK treatment showed the strongest anti-inflammatory effect. Impaired intestinal barrier is one of the major pathological features of UC, and tight junction proteins, such as ZO-1 and Occludin, contribute to the integrity of the epithelial barrier (14). The immunofluorescence staining results showed that DSS treatment caused damage to the intestinal barrier in mice, as evidenced by lower expression of ZO-1 and Occludin. PAMK treatment significantly increased the expression of the tight junction proteins (Figures 3G, H). The above results indicated that PAMK treatment inhibited inflammation and maintained the integrity of the intestinal barrier in the colon of mice with UC.

PAMK treatment altered the transcriptional profile in DSS-induced colitis mice

Microarray analysis was performed to investigate the underlying mechanism for the therapeutic effect of PAMK on colitis. As shown in the principal component analysis (PCA) of

DEGs, no obvious separation was observed among the Control, DSS and DSS+PAMK groups (Figure 4A). We identified 1144 upregulated DEGs and 484 downregulated DEGs upon comparing the DSS group and Control group. A total of 392 DEGs were upregulated, and 455 DEGs were downregulated in

the DSS+PAMK group compared with the DSS group (Figure 4B; Supplementary Excel Sheet). A Venn diagram showed the DEGs in the comparisons between the DSS vs Control group and the DSS+PAMK vs DSS group (Figure 4C; Supplementary Excel Sheet). Since there was no significant

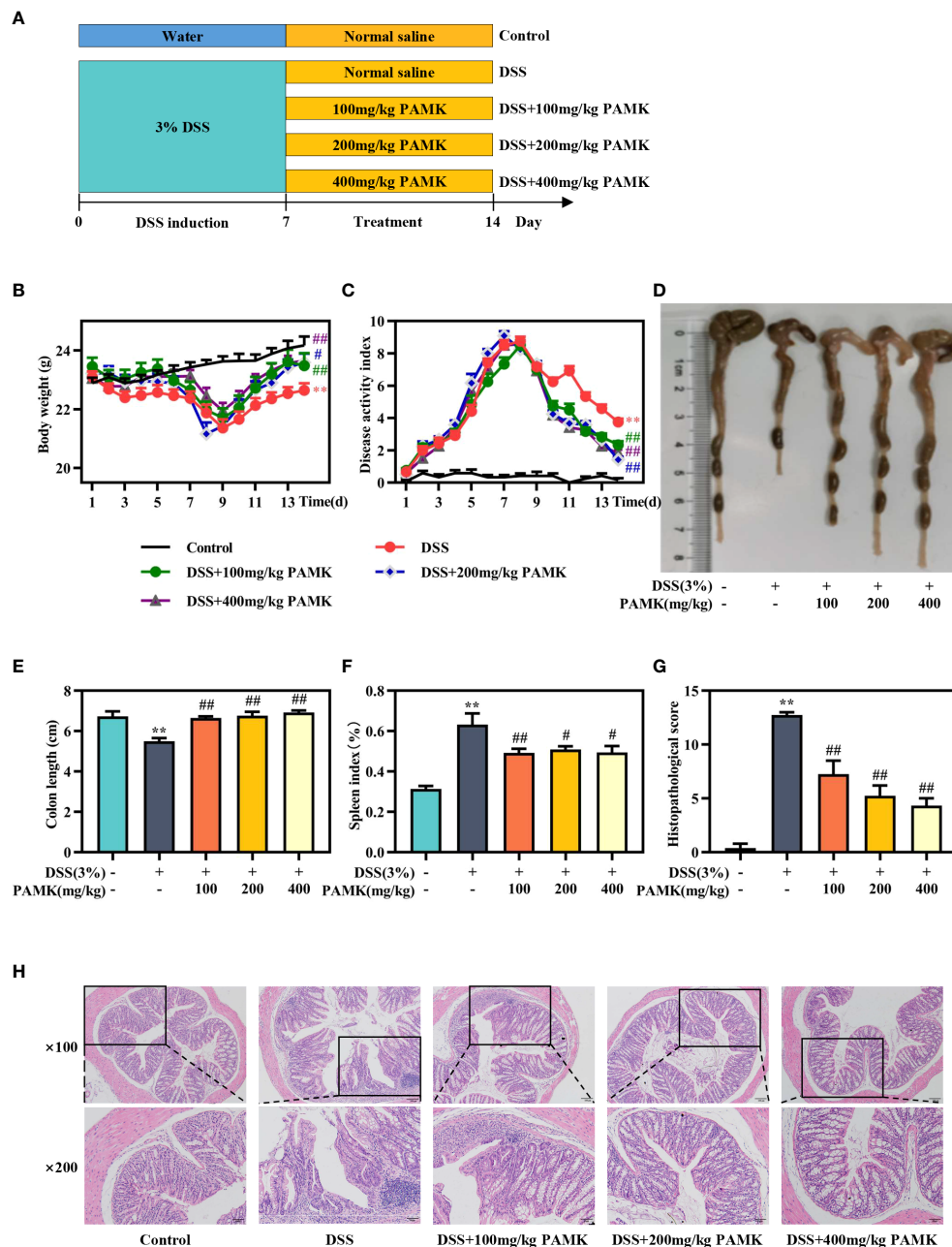


FIGURE 2

PAMK treatment ameliorated DSS-induced colitis. (A) Experimental scheme, (B) Daily body weight, (C) Daily disease activity index (DAI) scores, (D) Representative images of colons, (E) Length of colons, (F) Spleen index, (G) Histopathological scores of colons, (H) Representative images of H&E staining of colon tissue (magnification 100x and 200x). All data are presented as the mean \pm SEM ($n \geq 6$). $^{**}P < 0.01$ vs Control group; $^{#}P < 0.05$, $^{##}P < 0.01$ vs DSS group.

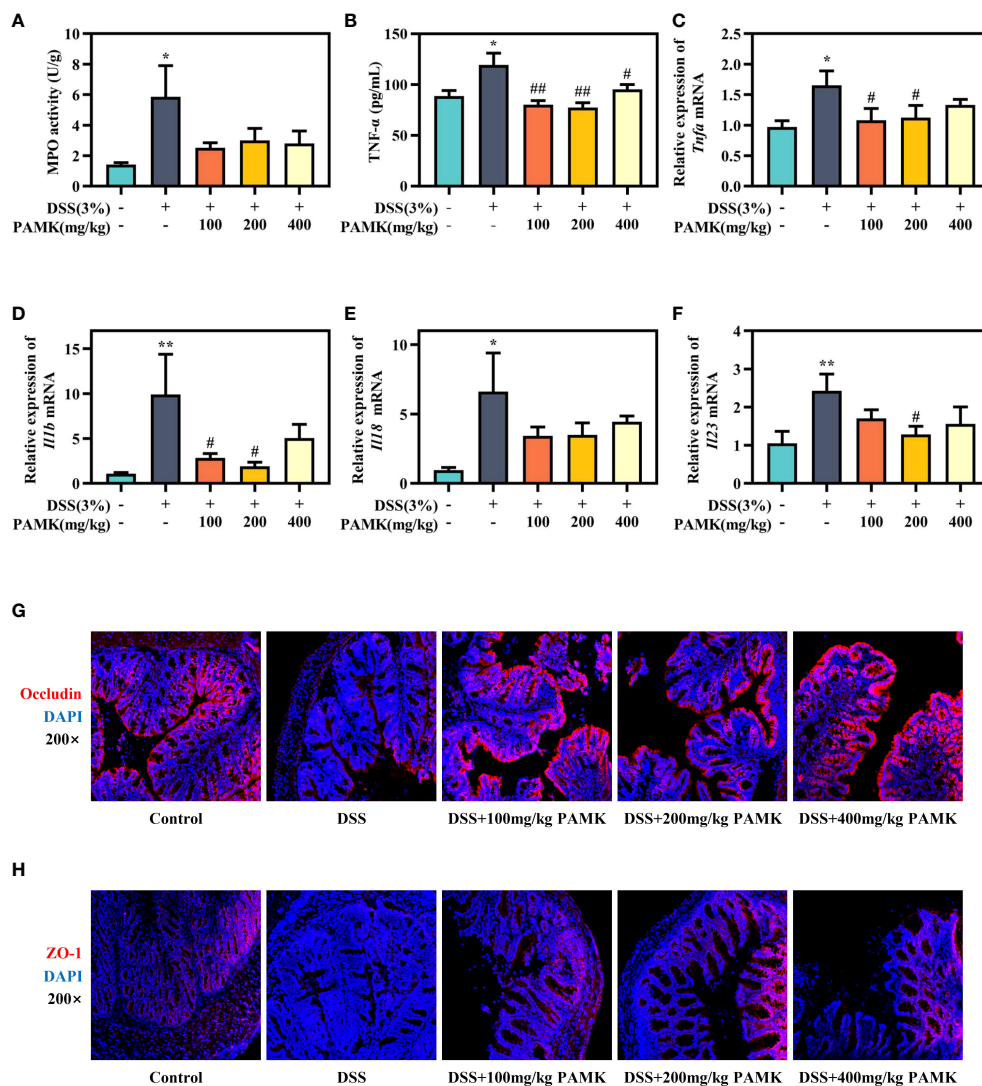


FIGURE 3

PAMK treatment inhibited the inflammatory response and improved the intestinal barrier in DSS-induced colitis mice. (A) MPO activity in the colon. (B) The concentration of TNF- α in plasma. The relative expression of *Tnfa* (C), *Il1b* (D), *Il18* (E) and *Il23* (F) in the colonic tissue. Representative images of immunofluorescence staining of Occludin (G) and ZO-1 (H) in colonic tissue (magnification 200 \times). All data are presented as the mean \pm SEM ($n \geq 6$). * $P < 0.05$, ** $P < 0.01$ vs Control group; # $P < 0.05$, ## $P < 0.01$ vs DSS group.

difference in DEGs between the Control, DSS and DSS+PAMK groups, we focused on the analysis of DEMs. The PCA of DEMs showed that the Control group and DSS group were clearly separated and that the DSS+PAMK group was distinct from the DSS group and tended to be closer to the Control group (Figure 4D). We found that 702 DEMs were upregulated and 103 DEMs were downregulated in the DSS group compared with the Control group. A total of 125 DEMs were upregulated and 204 DEMs were downregulated in the DSS+PAMK group compared with the DSS group (Figure 4E; Supplementary

Excel Sheet). PAMK treatment led to the downregulation of 99 DEMs that were significantly increased in the DSS group and resulted in the upregulation of 10 DEMs that were significantly decreased in the DSS group (Figure 4F; Supplementary Excel Sheet). Thus, 99 upregulated DEMs (DSS vs Control) and 10 downregulated DEMs (DSS vs Control) were considered critical genes reversed by PAMK treatment. The results are presented in the heatmap (Figure 4G). These results indicated that PAMK treatment altered the transcriptional profile in the colonic tissues of DSS-induced colitis mice.

Cluster analysis of DEMs revealed that regulating the Th17/Treg cell balance may be the mechanism of the therapeutic effect of PAMK treatment on DSS-induced colitis

To further investigate the mechanism of the therapeutic effect of PAMK on DSS-induced colitis in mice, we conducted a trend analysis of the microarray data. The total DEMs were clustered into 16 profiles (from profiles 0 to 15) based on the expression patterns of genes using Short Time-series Expression Miner (STEM) software. Among the 16 profiles, profile 14 (reaching the peak in the DSS group and decreasing in the DSS+PAMK group), profile 11 (reaching the peak in the DSS group and remaining in the DSS+PAMK group) and profile 10 (reaching the peak in the DSS group and returning to the level of the Control group in DSS+PAMK group) were identified with significant ($P < 0.05$) expression patterns (Figure 5). Profile 14 and profile 10 were the most representative expression patterns. GO enrichment and KEGG enrichment analyses were performed to evaluate the potential functions of DEMs from profile 14 and profile 10. GO analysis, commonly used to analyze the function of genes, showed that the top 30 enriched GO terms of profiles 14 and 10 included immune system process, inflammatory response, immune response, acute-phase response and innate immune response (Figures 6A, B). The GO analysis indicated that the beneficial effect of PAMK on DSS-induced colitis may rely on the regulation of the immune response. In addition, the KEGG enrichment of profiles 14 and 10 showed multiple immune-related pathways among the top 30 pathways, including the IL-17 signaling pathway, Th17 cell differentiation, Th1 and Th2 cell differentiation, TNF signaling and the chemokine signaling pathway (Figures 6C, D). Therefore, the effect of PAMK on colitis may depend on the immunoregulatory function of PAMK by maintaining Th17/Treg cell homeostasis.

PAMK treatment regulated the Th17/Treg cell balance in the MLN and spleen in DSS-induced colitis mice

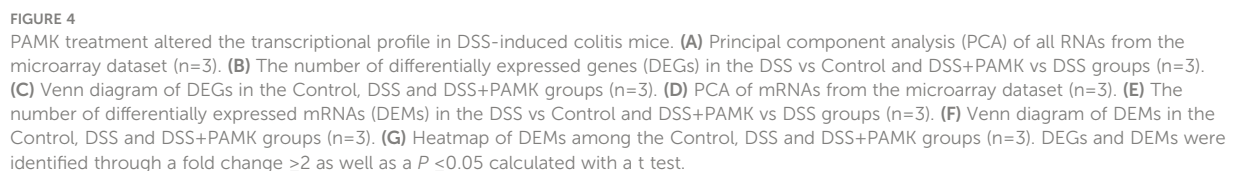
To examine the effect of PAMK on the Th17/Treg cell balance in DSS-induced colitis mice, we measured the proportions of both Th17 cells and Treg cells in the CD4⁺ T cells compartment of the MLN and spleen by flow cytometry. As shown in Figures 7, 8, the proportions of Th17 cells in the MLN and spleen of the DSS group mice were significantly increased compared with those in the Control group mice, and PAMK treatment significantly decreased the proportions of Th17 cells in the MLN and spleen. However, PAMK treatment did not

increase the frequency of Treg cells in the MLN and spleen compared with those in the DSS group. The ratios of Th17/Treg cells in the MLN and spleen were shown to decrease after PAMK administration, supporting the role of PAMK in the resumption of the Th17/Treg cell balance in colitis mice.

Then, Th17- and Treg-specific transcription factors ROR γ t and Foxp3, as well as the associated cytokines IL-17A, IL-10 and TGF- β 1, were analyzed using qRT-PCR to further investigate the regulatory effect of PAMK on the Th17/Treg cell balance. Significantly increased *Rorc* expression was found in colitis mice in comparison with the Control group, and PAMK treatment significantly decreased the mRNA level of *Rorc* (Figure 9A). In addition, the expression of *Foxp3* significantly decreased in colitis and slightly increased in the PAMK treatment groups (Figure 9B). The results showed that the expression of Th17- and Treg- associated cytokines was consistent with that of specific transcription factors. IL-17A is secreted specifically by Th17 cells, and TGF- β 1 and IL-10 are secreted specifically by Treg cells. The expression level of *Il17a* significantly increased in the colon of the DSS group and decreased after PAMK administration (Figure 9C). In contrast, PAMK treatment slightly increased the expression of *Tgfb1* and *Il10* in colitis mice (Figures 9D, E). Collectively, these data confirmed the effect of PAMK on maintaining the homeostasis of Th17 and Treg cells in DSS-induced colitis.

PAMK treatment inhibited the IL-6/STAT3 signaling pathway in DSS-induced colitis mice

The role of the IL-6/STAT3 signaling pathway in the differentiation of Th17 and Treg cells has been reported in multiple studies. Activation of the IL-6/STAT3 signaling pathway drives naïve T cells to differentiate into Th17 cells, resulting in a Th17/Treg cell imbalance (15). Thus, we analyzed the IL-6/STAT3 signaling pathway to explore the mechanism by which PAMK administration modulated the Th17/Treg cell balance. qRT-PCR results showed that the *Il6* mRNA level in colonic tissue was significantly reduced in the PAMK treatment groups compared to the DSS group (Figure 10A). The Western blotting results showed that the level of STAT3 in colonic tissue increased in colitis mice and decreased after PAMK treatment (Figures 10B, C). A comparison of p-STAT3/STAT3 in colonic tissues from the DSS and PAMK treatment groups revealed that PAMK treatment decreased the ratio of p-STAT3/STAT3, indicating that PAMK treatment suppressed the activation of STAT3 (Figure 10D). The immunofluorescence analysis showed a similar result (Figure 10E). Our findings demonstrated that PAMK treatment effectively inhibited the activation of IL-6/STAT3 signaling.



UC, a chronic and recurring intestinal disease, is characterized by abdominal pain, diarrhea and hematochezia, and persistent colitis increases the risk of colorectal cancer (16). 5-aminosalicylic acid (5-ASA) is a first-line therapy for the treatment of UC (17). However, many patients suffer a recurrence after 5-ASA is discontinued, and those patients are

frontiersin.org

frequently used TCMs in 177 Chinese herbal compound prescriptions used in the clinical treatment of UC (4). Thus, we investigated the effect and the underlying mechanism of PAMK on colitis. This study is the first to elucidate the underlying mechanism of the therapeutic effect of PAMK on colitis and determine that the regulation of the Th17/Treg cell balance of PAMK plays a critical role in alleviating colitis.

The common preclinical murine models of UC include the DSS-induced colitis model, trinitrobenzene sulfonic acid (TNBS)-induced colitis model and IL-10-deficient mouse model (20). Various studies have demonstrated that IL-10 suppresses inflammation in colitis by regulating innate and adaptive immune responses, such as promoting the expansion

of Treg cells to suppress the immune response mediated by Th17 cells, which indicates that IL-10-deficient mice were not suitable for the present study (21). TNBS treatment promoted an immune response mediated by Th1 cells, resembling Crohn's disease but not UC in humans (22). The DSS-induced colitis model is the most widely used murine model of colitis due to its reproducibility, controllability and similarities of pathological and clinical manifestations with UC patients (23). In addition, DSS, as a chemical toxin, causes the damage to the epithelial cells and does not directly activate the adaptive immune system (24), supporting that DSS-induced colitis is the most suitable model for this study. The results showed that PAMK treatment significantly ameliorated DSS-induced colitis manifested as

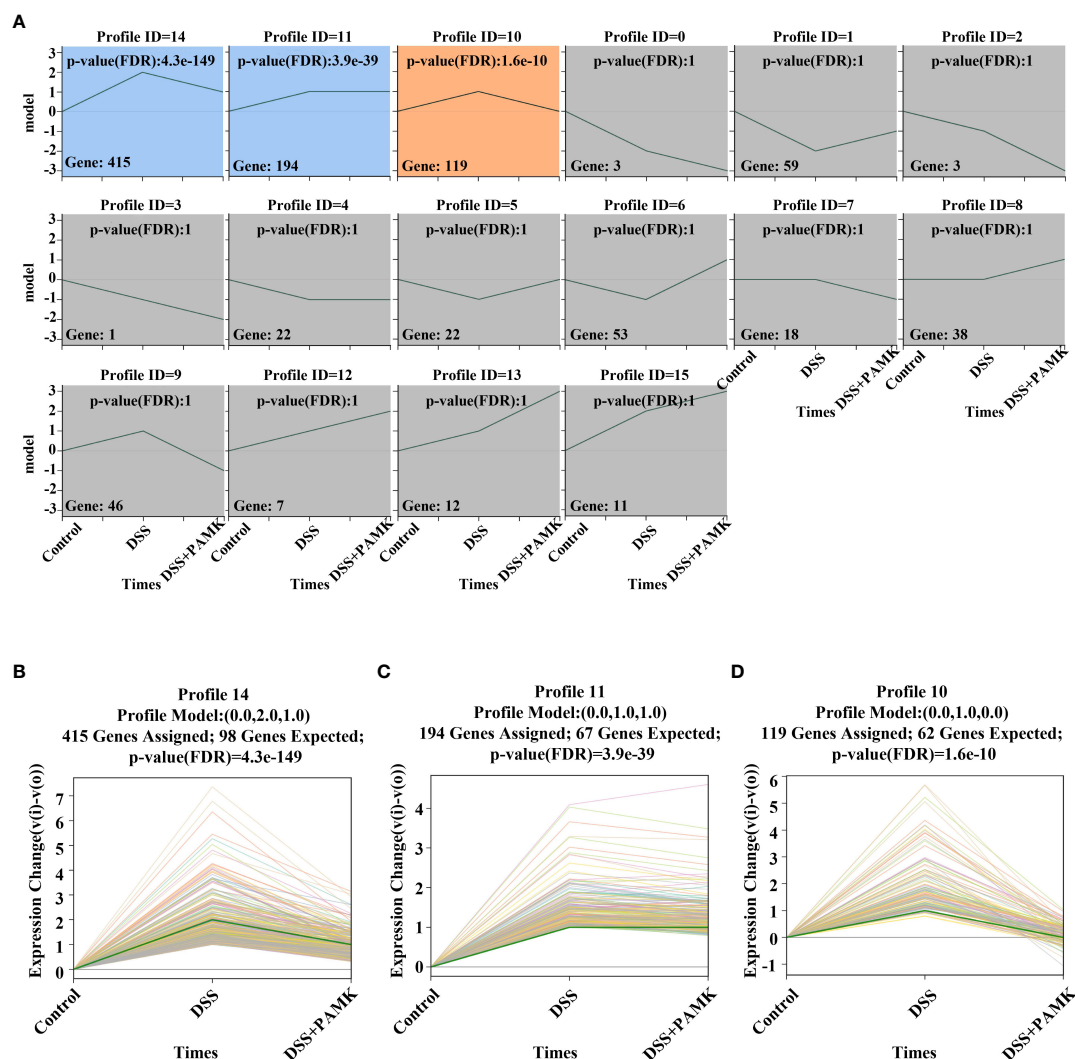


FIGURE 5

Trend analysis of DEMs. (A) Short time-series transcriptomic analysis of DEMs in the Control, DSS and DSS+PAMK groups (n=3). (B–D) The statistically significant profiles ($P < 0.05$) of DEMs in the Control, DSS and DSS+PAMK groups (n=3).

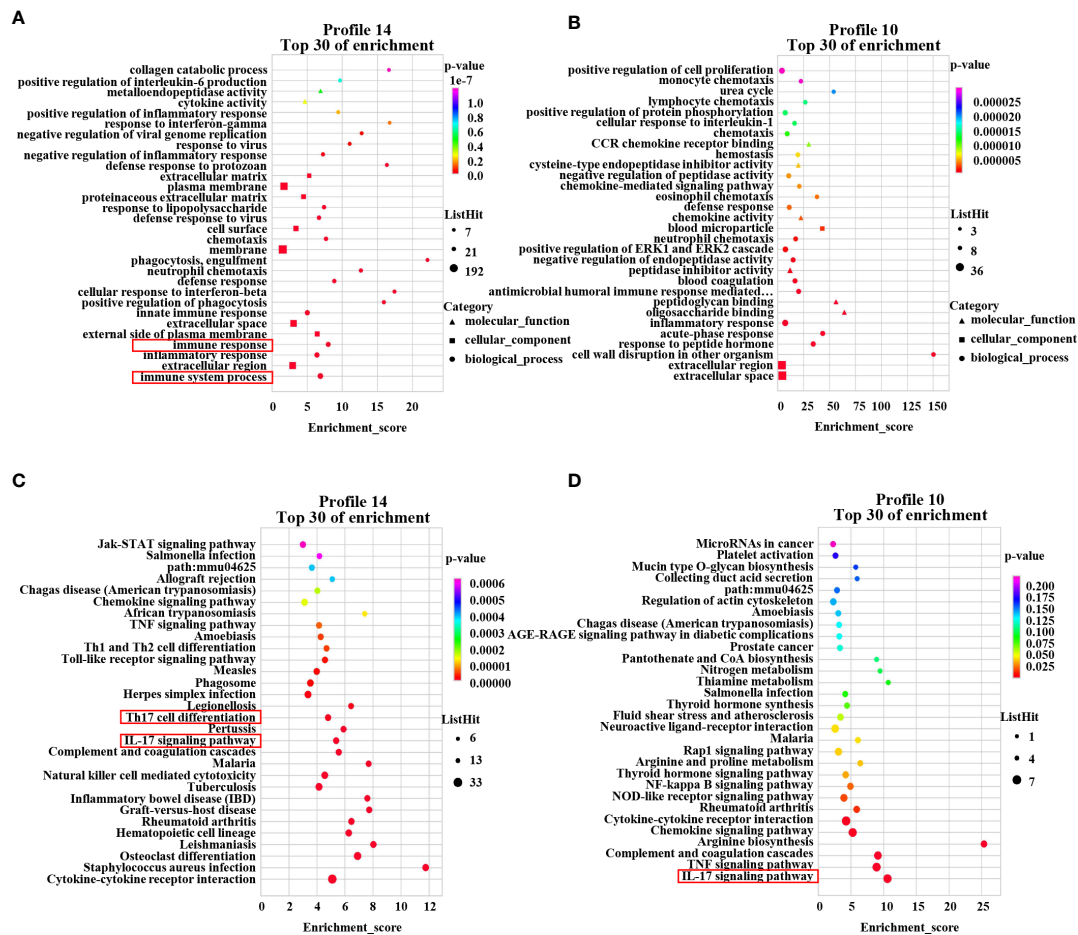


FIGURE 6

GO enrichment and KEGG pathway enrichment of DEMs. The GO analysis from DEMs of profile 14 (A) and profile 10 (B) among the Control, DSS and DSS+PAMK groups (n = 3) showed the top 30 enriched biological functions. The KEGG analysis from DEMs of profile 14 (C) and profile 10 (D) among the Control, DSS and DSS+PAMK groups (n = 3) showed the top 30 enriched signaling pathways.

relief of symptoms, inflammation inhibition and intestinal barrier maintenance.

The effects of polysaccharides are intimately associated with their structural properties, especially monosaccharide composition. Numerous studies have demonstrated that the most common monosaccharides contained in polysaccharides from TCMs include glucose, mannose, galactose and arabinose (25). Consistent with the monosaccharide composition of these polysaccharides, the monosaccharide components of PAMK used in our study are mainly glucose, mannose, arabinose and galactose. The effects of monosaccharide treatment on DSS-induced colitis have been determined in previous studies. For instance, both mannose and arabinose treatment alleviated DSS-induced colitis by suppressing the inflammatory response and improving barrier damage (26–28). Galactose is essential for immune system function, and *Astragalus* polysaccharide with

higher galactose content showed a more beneficial effect on DSS-induced colitis (29). Therefore, we considered that the protective effect of PAMK against colitis may depend on mannose, arabinose and galactose. However, high glucose treatment exacerbated colitis pathogenesis in mice (30), which may explain why 400 mg/kg PAMK treatment did not exert a more beneficial effect on DSS-induced colitis than 200 mg/kg PAMK treatment. In addition, extensive studies have demonstrated that the polysaccharides from TCMs rich in mannose, arabinose and galactose in colitis, such as polysaccharides from *Inonotus obliquus* (31), *Ganoderma lucidum* (32) and *Dendrobium fimbriatum* Hook (33), alleviate DSS-induced colitis by modulating the immune response. Consistent with these results, our study determined the key role of the immunoregulatory effect of PAMK in ameliorating DSS-induced colitis.

The multifactorial pathophysiology of UC includes environmental factors, disordered intestinal flora, impaired epithelial barrier, genetic predisposition and dysregulated immune responses (34). Among them, a dysregulated immune system accelerates the development of UC (1). In UC, the increasing permeability of the colonic mucosal and epithelial barrier lead to the migration of intestinal flora and triggers the activation of the immune system (35). Stimulated by innate immune cells secreting cytokines, naive CD4⁺ T cells are induced to differentiate into effector CD4⁺ T cells, including Th17 cells and Treg cells (36). The KEEG enrichment analysis revealed that the effect of PAMK on colitis was associated to the Th17/Treg cell balance. Under physiological conditions, Th17 cells protect the host against infection and mediate the immune response by secreting inflammatory cytokines. Treg cells maintain immune tolerance and prevent an excessive immune response by secreting anti-inflammatory cytokines (37). In UC patients, Th17 cells infiltrate the gastrointestinal mucosa and produce

excessive inflammatory cytokines, such as IL-17A, initiating a more intense inflammatory response that Treg cells are not able to tolerate (38). Thus, Th17/Treg cell imbalance is a crucial factor in the occurrence and development of UC, and targeting the regulation of the Th17/Treg cell balance has been a promising strategy for treating UC (15). In our study, PAMK treatment significantly decreased the frequency of Th17 cells in the spleen and MLN, and the expression of *Il17a* in colonic tissue in colitis mice. In UC patients, the proportion of Treg cells is decreased in peripheral blood, while it is increased in the inflamed mucosa of the colon, which may be attributed to the active recruitment of Treg cells in inflamed areas to maintain immune tolerance and inhibit the inflammation (39). Consistently, our study also showed that the frequency of Treg cells in the MLN and spleen increased in colitis mice. However, the instability of Foxp3⁺ Treg cells in colitis has been identified, and multiple studies have demonstrated that the expression of Foxp3 in Treg cells isolated from inflammatory sites decreased,

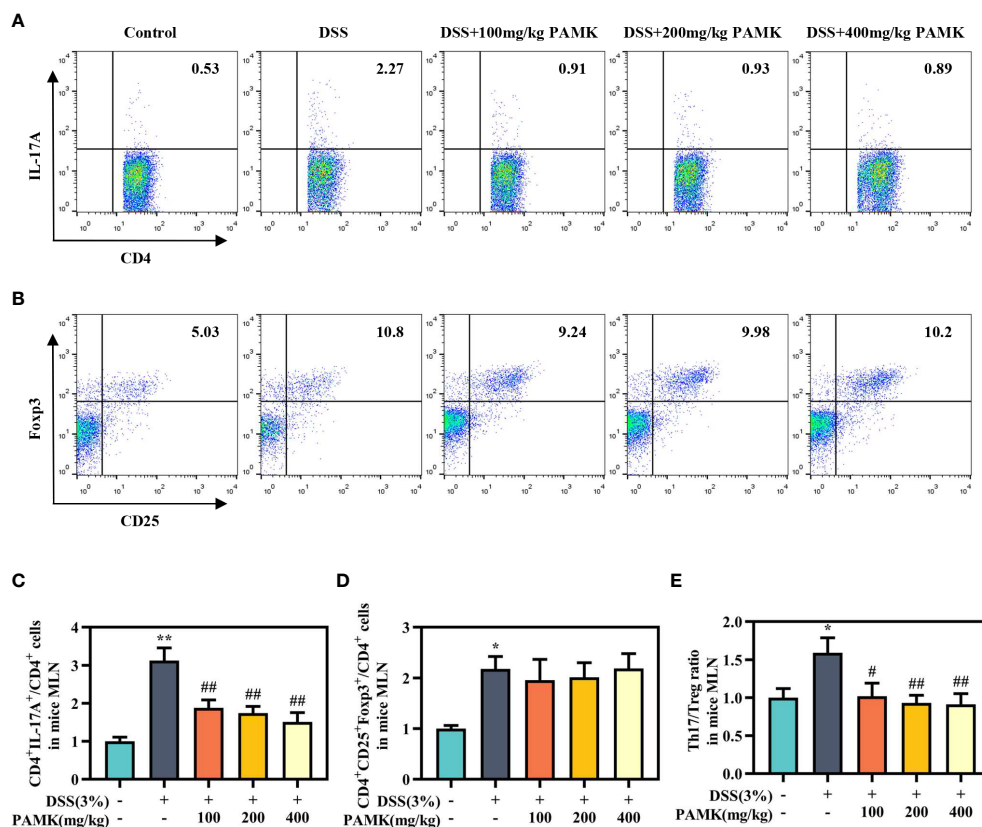


FIGURE 7

PAMK treatment regulated the Th17/Treg cell balance in the MLN of colitis mice. Flow cytometry of Th17 (CD4⁺IL-17A⁺) cells (A) and Treg (CD4⁺CD25⁺Foxp3⁺) cells (B) in the MLN. The frequency of Th17 (C) and Treg cells (D) in the MLN. (E) The Th17/Treg ratio in the MLN. The frequency of Th17 and Treg cells and the ratios of Th17/Treg in the DSS group and PAMK treatment groups were normalized to those in the Control group. All data are presented as the mean \pm SEM ($n \geq 6$). * $P < 0.05$, ** $P < 0.01$ vs Control group; # $P < 0.05$, ## $P < 0.01$ vs DSS group.

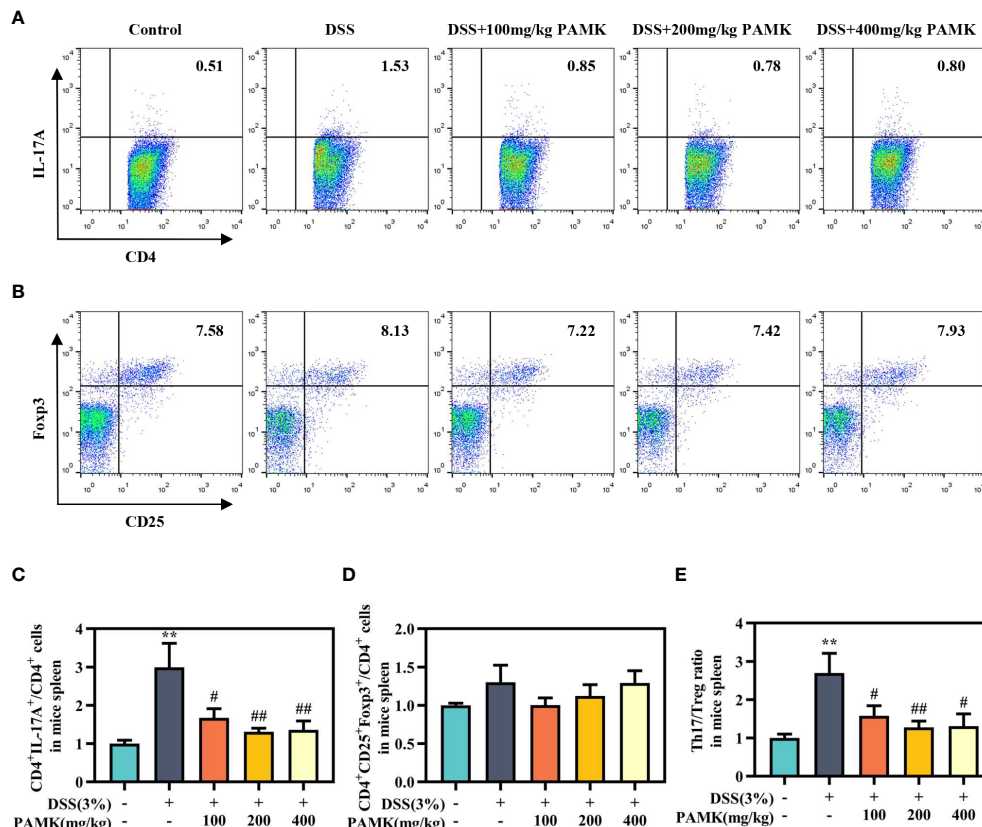


FIGURE 8

PAMK treatment regulated the Th17/Treg cell balance in the spleen of colitis mice. Flow cytometry of Th17 (CD4⁺IL-17A⁺) cells (A) and Treg (CD4⁺CD25⁺Foxp3⁺) cells (B) in the spleen. The frequency of Th17 (C) and Treg cells (D) in the spleen. (E) The Th17/Treg ratio in the spleen. The frequency of Th17 and Treg cells and the ratios of Th17/Treg in the DSS group and PAMK treatment groups were normalized to those in the Control group. All data are presented as the mean \pm SEM ($n \geq 6$). ** $P < 0.01$ vs Control group; # $P < 0.05$, ## $P < 0.01$ vs DSS group.

indicating a loss of Foxp3 expression (40), which may explain why the proportions of Treg cells increased in colitis mice, while the expression of *Foxp3*, *Il10* and *Tgfb1* decreased. The upregulation of *Foxp3*, *Il10* and *Tgfb1* expression in the PAMK treatment groups indicated that PAMK treatment enhanced the activation of Treg cells. Our study indicated that PAMK treatment alleviated DSS-induced colitis by regulating the Th17/Treg cell balance.

Finally, we explored the pathways that promoted differentiation and enhanced the secretion of Th17 cells. Genome-wide association studies have determined that STAT3 is linked to UC susceptibility. STAT3 is expressed in mucosal immune cells, and STAT3 activation enhances the inflammatory response in the intestine (41). IL-6 initiates the phosphorylation of STAT3 by binding the membrane-bound IL-6 receptor (42), and p-STAT3 is an essential mediator of the Th17/Treg cell balance and upregulates the expression of Th17-specific genes, such as IL-17A (38). Thus, the IL-6/STAT3 signaling pathway

plays a pivotal role in the differentiation of Th17 cells. In UC, the phosphorylated STAT3 levels were significantly increased in actively inflamed colons (43, 44). Target blockade of the IL-6/STAT3 signaling pathway, such as blockade with IL-6 antagonists, JAK inhibitors and direct STAT3 inhibitors, can effectively prevent and treat UC (45). Many polysaccharides from TCMs have been demonstrated to inhibit the IL-6/STAT3 pathway in DSS-induced colitis mice (46, 47). Our results showed that the regulatory effect of PAMK on the Th17/Treg balance in colitis may depend on the inhibition of the IL-6/STAT3 pathway.

Conclusion

The study evaluated the effect of PAMK on colitis and determined the underlying mechanism based on a mouse

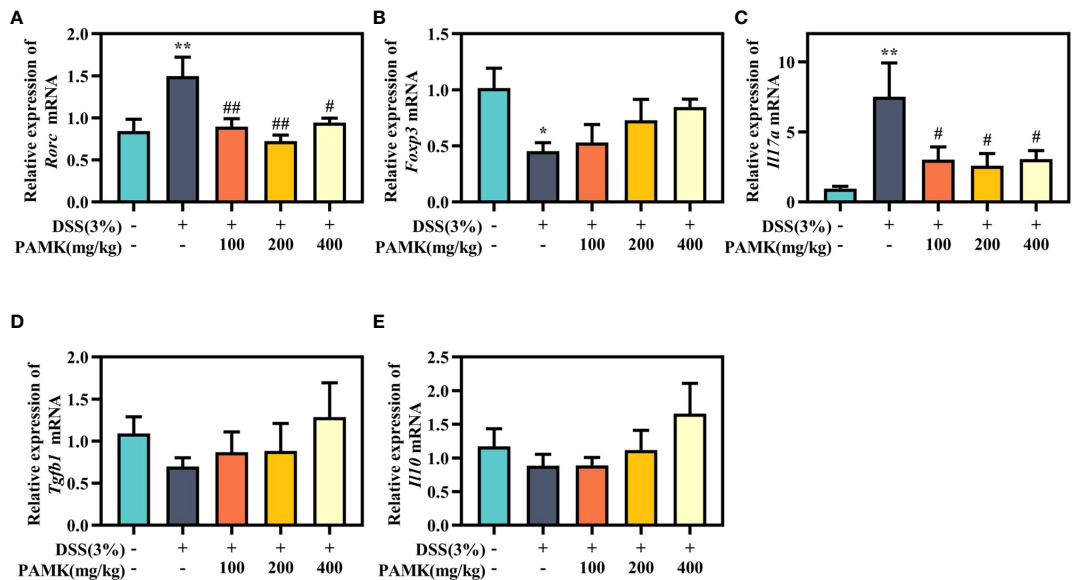


FIGURE 9
PAMK treatment regulated the levels of Th17- and Treg-specific transcription factors and associated cytokines. The relative expression of *Rorc* (A), *Foxp3* (B), *Il17a* (C), *Tgfb1* (D), and *Il10* (E) in the colonic tissue. All data are presented as the mean \pm SEM ($n \geq 6$). * $P < 0.05$, ** $P < 0.01$ vs Control group; # $P < 0.05$, ## $P < 0.01$ vs DSS group.

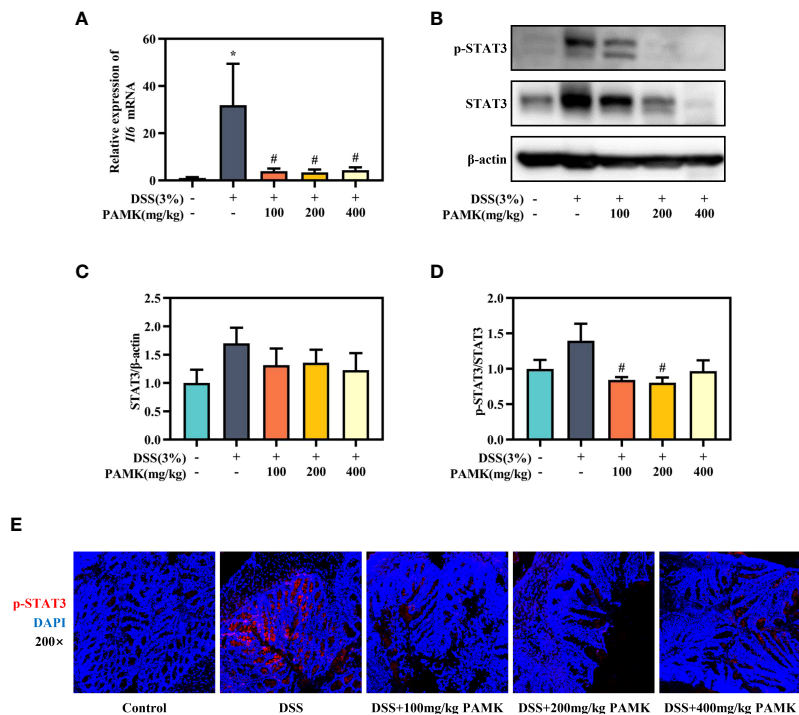


FIGURE 10
PAMK treatment inhibited the IL-6/STAT3 signaling pathway in DSS-induced colitis mice. (A) The relative expression of *Il6* in the colonic tissue. (B) Western blot analysis of STAT3 and p-STAT3 expression levels in colonic tissue. (C) Densitometric analysis of STAT3 expression. (D) Quantitative analysis of p-STAT3/STAT3. (E) Representative images of immunofluorescence staining of p-STAT3 in colonic tissue (magnification 200 \times). All data are presented as the mean \pm SEM. * $P < 0.05$ vs Control group; # $P < 0.05$ vs DSS group.

model of DSS-induced colitis. PAMK improved colitis symptoms, alleviated pathological injury, inhibited the inflammatory response and improved the intestinal barrier in colitis mice. In addition, the beneficial effect of PAMK on colitis depended upon the immunoregulatory effect. Our results suggested that PAMK treatment regulated the Th17/Treg cell balance to attenuate DSS-induced colitis in mice, which may be dependent on the inhibition of the IL-6/STAT3 signaling pathway. These findings provide further evidence for the potential of PAMK for treating UC.

Data availability statement

The datasets presented in this study can be found in online repositories. The names of the repository/repositories and accession number(s) can be found below: <https://www.ncbi.nlm.nih.gov/geo/>, GSE211359.

Ethics statement

The animal study was reviewed and approved by Ethics Committee of China Pharmaceutical University.

Author contributions

LS and CJ conceived and designed the study. QZ and MY performed the experiments. MA, QW, YY and YZ helped with several experiment procedures. QL, CL, ZJ, XH and CC analyzed the data. MY drafted the paper. LS and RT revised the paper. All authors contributed to the article and approved the submitted version.

References

1. Kobayashi T, Siegmund B, Le Berre C, Wei SC, Ferrante M, Shen B, et al. Ulcerative colitis. *Nat Rev Dis Primers* (2020) 6(1):74. doi: 10.1038/s41572-020-0205-x
2. Burri E, Maillard MH, Schoepfer AM, Seibold F, Van Assche G, Rivière P, et al. Treatment algorithm for mild and moderate-to-severe ulcerative colitis: an update. *Digestion* (2020) 101(Suppl 1):2–15. doi: 10.1159/000504092
3. Yang L, Yu H, Hou AJ, Man WJ, Wang S, Zhang JX, et al. A review of the ethnopharmacology, phytochemistry, pharmacology, application, quality control, processing, toxicology, and pharmacokinetics of the dried rhizome of *Atractylodes macrocephala*. *Front Pharmacol* (2021) 12:727154. doi: 10.3389/fphar.2021.727154
4. Jia Y, Wang ZZ, Li XM, Miao MS. Data mining of drug use rules based on traditional Chinese medicine treatment of ulcerative colitis. *China J Chin Mater Med* (2021) 46(10):2594–600. doi: 10.19540/j.cnki.cjcmm.20200911.501
5. Jiao CH, Zhang QW, Yang MJ, Ma JJ, Zhao XJ, Tang NN, et al. Shenling baizhu San ameliorates ulcerative colitis by regulating the gut microbiota and its

Funding

This work was supported by the National Natural Science Foundation of China (82074115, 81873084 and 82174072).

Acknowledgments

We thank the Laboratory of Active Components and Pharmacodynamics of Natural Medicines of China Pharmaceutical University and OE Biotechnology Co., Ltd. for laboratory assistance.

Conflict of interest

The authors declare that the research was conducted in the absence of any commercial or financial relationships that could be construed as a potential conflict of interest.

Publisher's note

All claims expressed in this article are solely those of the authors and do not necessarily represent those of their affiliated organizations, or those of the publisher, the editors and the reviewers. Any product that may be evaluated in this article, or claim that may be made by its manufacturer, is not guaranteed or endorsed by the publisher.

Supplementary material

The Supplementary Material for this article can be found online at: <https://www.frontiersin.org/articles/10.3389/fimmu.2022.1021695/full#supplementary-material>.

tryptophan metabolites: a complementary medicine to mesalamine. *J Ethnopharmacol* (2022) 291:115145. doi: 10.1016/j.jep.2022.115145

6. Zong X, Xiao X, Kai LX, Cheng YZ, Fu J, Xu W, et al. *Atractylodes macrocephala* polysaccharides protect against DSS-induced intestinal injury through a novel lncRNA ltsn1-OT1. *Int J Biol Macromol* (2021) 167:76–84. doi: 10.1016/j.ijbiomac.2020.11.144

7. Kai LX, Zong X, Jiang Q, Lu ZQ, Wang FQ, Wang YZ, et al. Protective effects of polysaccharides from *Atractylodes macrocephala* koidz. against dextran sulfate sodium induced intestinal mucosal injury on mice. *Int J Biol Macromol* (2022) 195:142–51. doi: 10.1016/j.ijbiomac.2021.12.042

8. Neurath MF. Targeting immune cell circuits and trafficking in inflammatory bowel disease. *Nat Immunol* (2019) 20(8):970–9. doi: 10.1038/s41590-019-0415-0

9. Nakase H, Sato N, Mizuno N, Ikawa Y. The influence of cytokines on the complex pathology of ulcerative colitis. *Autoimmun Rev* (2022) 21(3):103017. doi: 10.1016/j.autrev.2021.103017

10. Xue WY, Gao Y, Li QW, Lu QB, Bian ZY, Tang L, et al. Immunomodulatory activity-guided isolation and characterization of a novel polysaccharide from *Atractylodes macrocephalae* koidz. *Int J Biol Macromol* (2020) 161:514–24. doi: 10.1016/j.ijbiomac.2020.06.003
11. Xie F, Sakwiwatkul K, Zhang CR, Wang YM, Zhai LJ, Hu SH. *Atractylodes macrocephalae* koidz. polysaccharides enhance both serum IgG response and gut mucosal immunity. *Carbohydr Polym* (2013) 91(1):68–73. doi: 10.1016/j.carbpol.2012.07.083
12. Francescone R, Hou V, Grivennikov SI. Cytokines, IBD, and colitis-associated cancer. *Inflammation Bowel Dis* (2015) 21(2):409–18. doi: 10.1097/mib.0000000000000236
13. Guan QD, Zhang JG. Recent advances: the imbalance of cytokines in the pathogenesis of inflammatory bowel disease. *Mediators Inflammation* (2017) 2017:4810258. doi: 10.1155/2017/4810258
14. Kaminsky LW, Al-Sadi R, Ma TY. IL-1 β and the intestinal epithelial tight junction barrier. *Front Immunol* (2021) 12:767456. doi: 10.3389/fimmu.2021.767456
15. Ueno A, Jeffery L, Kobayashi T, Hibi T, Ghosh S, Jijon H. Th17 plasticity and its relevance to inflammatory bowel disease. *J Autoimmun* (2018) 87:38–49. doi: 10.1016/j.jaut.2017.12.004
16. Nadeem MS, Kumar V, Al-Abbasi FA, Kamal MA, Anwar F. Risk of colorectal cancer in inflammatory bowel diseases. *Semin Cancer Biol* (2020) 64:51–60. doi: 10.1016/j.semcancer.2019.05.001
17. Le Berre C, Roda G, Nedeljkovic Protic M, Danese S, Peyrin-Biroulet L. Modern use of 5-aminosalicylic acid compounds for ulcerative colitis. *Expert Opin Biol Ther* (2020) 20(4):363–78. doi: 10.1080/14712598.2019.1666101
18. Lamb CA, Kennedy NA, Raine T, Hendy PA, Smith PJ, Limdi JK, et al. British Society of gastroenterology consensus guidelines on the management of inflammatory bowel disease in adults. *Gut* (2019) 68(Suppl 3):s1–s106. doi: 10.1136/gutjnl-2019-318484
19. Hu Y, Ye Z, She YQ, Li LZ, Wu MQ, Qin KH, et al. Efficacy and safety of probiotics combined with traditional Chinese medicine for ulcerative colitis: a systematic review and meta-analysis. *Front Pharmacol* (2022) 13:844961. doi: 10.3389/fphar.2022.844961
20. Katsandegwaza B, Horsnell W, Smith K. Inflammatory bowel disease: a review of pre-clinical murine models of human disease. *Int J Mol Sci* (2022) 23(16):9344. doi: 10.3390/ijms23169344
21. Keubler LM, Buettner M, Häger C, Bleich A. A multihit model: colitis lessons from the interleukin-10-deficient mouse. *Inflammation Bowel Dis* (2015) 21(8):1967–75. doi: 10.1097/mib.0000000000000468
22. Silva I, Pinto R, Mateus V. Preclinical study *in vivo* for new pharmacological approaches in inflammatory bowel disease: a systematic review of chronic model of TNBS-induced colitis. *J Clin Med* (2019) 8(10):1574. doi: 10.3390/jcm8101574
23. Chassaing B, Aitken JD, Malleshappa M, Vijay-Kumar M. Dextran sulfate sodium (DSS)-induced colitis in mice. *Curr Protoc Immunol* (2014) 104:15.25.1–15.25.14. doi: 10.1002/0471142735.im1525s104
24. Eichele DD, Kharbanda KK. Dextran sodium sulfate colitis murine model: an indispensable tool for advancing our understanding of inflammatory bowel diseases pathogenesis. *World J Gastroenterol* (2017) 23(33):6016–29. doi: 10.3748/wjg.v23.i33.6016
25. Wang YJ, Li QM, Zha XQ, Luo JP. Intervention and potential mechanism of non-starch polysaccharides from natural resources on ulcerative colitis: a review. *Int J Biol Macromol* (2022) 210:545–64. doi: 10.1016/j.ijbiomac.2022.04.208
26. Dong LJ, Xie JW, Wang YY, Jiang HL, Chen K, Li DT, et al. Mannose ameliorates experimental colitis by protecting intestinal barrier integrity. *Nat Commun* (2022) 13(1):4804. doi: 10.1038/s41467-022-32505-8
27. Li Y, Pan HO, Liu JX, Li TT, Liu SN, Shi WL, et al. L-arabinose inhibits colitis by modulating gut microbiota in mice. *J Agric Food Chem* (2019) 67(48):13299–306. doi: 10.1021/acs.jafc.9b05829
28. Torretta S, Scagliola A, Ricci L, Mainini F, Di Marco S, Cuccovillo I, et al. D-mannose suppresses macrophage IL-1 β production. *Nat Commun* (2020) 11(1):6343. doi: 10.1038/s41467-020-20164-6
29. Wu JC, Li CY, Bai LS, Wu J, Bo R, Ye MZ, et al. Structural differences of polysaccharides from *Astragalus* before and after honey processing and their effects on colitis mice. *Int J Biol Macromol* (2021) 182:815–24. doi: 10.1016/j.ijbiomac.2021.04.055
30. Khan S, Waliullah S, Godfrey V, Khan MAW, Ramachandran RA, Cantarel BL, et al. Dietary simple sugars alter microbial ecology in the gut and promote colitis in mice. *Sci Transl Med* (2020) 12(567):eaay6218. doi: 10.1126/scitranslmed.aay6218
31. Chen YF, Zheng JJ, Qu C, Xiao Y, Li FF, Jin QX, et al. *Inonotus obliquus* polysaccharide ameliorates dextran sulphate sodium induced colitis involving modulation of Th1/Th2 and Th17/Treg balance. *Artif Cells Nanomed Biotechnol* (2019) 47(1):757–66. doi: 10.1080/21691401.2019.1577877
32. Wei B, Zhang R, Zhai JB, Zhu JF, Yang FL, Yue D, et al. Suppression of Th17 cell response in the alleviation of dextran sulfate sodium-induced colitis by *Ganoderma lucidum* polysaccharides. *J Immunol Res* (2018) 2018:2906494. doi: 10.1155/2018/2906494
33. Wang YJ, Li QM, Zha XQ, Luo JP. *Dendrobium fimbriatum* hook polysaccharide ameliorates dextran-sodium-sulfate-induced colitis in mice via improving intestinal barrier function, modulating intestinal microbiota, and reducing oxidative stress and inflammatory responses. *Food Funct* (2022) 13(1):143–60. doi: 10.1039/d1fo03003e
34. Ramos GP, Papadakis KA. Mechanisms of disease: Inflammatory bowel diseases. *Mayo Clin Proc* (2019) 94(1):155–65. doi: 10.1016/j.mayocp.2018.09.013
35. Kałużna A, Olczyk P, Komosińska-Vasess K. The role of innate and adaptive immune cells in the pathogenesis and development of the inflammatory response in ulcerative colitis. *J Clin Med* (2022) 11(2):400. doi: 10.3390/jcm11020400
36. Tindemans I, Joosse ME, Samsom JN. Dissecting the heterogeneity in T-cell mediated inflammation in IBD. *Cells* (2020) 9(1):110. doi: 10.3390/cells9010110
37. Fasching P, Stradner M, Graninger W, Dejaco C, Fessler J. Therapeutic potential of targeting the Th17/Treg axis in autoimmune disorders. *Molecules* (2017) 22(1):134. doi: 10.3390/molecules22010134
38. Yan JB, Luo MM, Chen ZY, He BH. The function and role of the Th17/Treg cell balance in inflammatory bowel disease. *J Immunol Res* (2020) 2020:8813558. doi: 10.1155/2020/8813558
39. Xia SL, Ying SJ, Lin QR, Wang XQ, Hong WJ, Lin ZJ, et al. Association of ulcerative colitis with FOXP3 gene polymorphisms and its colonic expression in chinese patients. *Gastroenterol Res Pract* (2019) 2019:4052168. doi: 10.1155/2019/4052168
40. Takahashi R, Nishimoto S, Muto G, Sekiya T, Tamiya T, Kimura A, et al. SOCS1 is essential for regulatory T cell functions by preventing loss of Foxp3 expression as well as IFN- γ and IL-17A production. *J Exp Med* (2011) 208(10):2055–67. doi: 10.1084/jem.20110428
41. Li Y, de Haar C, Chen M, Deuring J, Gerrits MM, Smits R, et al. Disease-related expression of the IL6/STAT3/SOCS3 signalling pathway in ulcerative colitis and ulcerative colitis-related carcinogenesis. *Gut* (2010) 59(2):227–35. doi: 10.1136/gut.2009.184176
42. Garbers C, Aparicio-Siegmund S, Rose-John S. The IL-6/gp130/STAT3 signaling axis: recent advances towards specific inhibition. *Curr Opin Immunol* (2015) 34:75–82. doi: 10.1016/j.coi.2015.02.008
43. Mudter J, Weigmann B, Bartsch B, Kiesslich R, Strand D, Galle PR, et al. Activation pattern of signal transducers and activators of transcription (STAT) factors in inflammatory bowel diseases. *Am J Gastroenterol* (2005) 100(1):64–72. doi: 10.1111/j.1572-0241.2005.40615.x
44. Musso A, Dentelli P, Carlino A, Chiusa L, Repici A, Sturm A, et al. Signal transducers and activators of transcription 3 signaling pathway: an essential mediator of inflammatory bowel disease and other forms of intestinal inflammation. *Inflammation Bowel Dis* (2005) 11(2):91–8. doi: 10.1097/00054725-200502000-00001
45. Kasembeli MM, Bharadwaj U, Robinson P, Tweardy DJ. Contribution of STAT3 to inflammatory and fibrotic diseases and prospects for its targeting for treatment. *Int J Mol Sci* (2018) 19(8):2299. doi: 10.3390/ijms19082299
46. Tao JH, Duan JA, Zhang W, Jiang S, Guo JM, Wei DD. Polysaccharides from *Chrysanthemum morifolium* ramat ameliorate colitis rats via regulation of the metabolic profiling and NF- κ B/TLR4 and IL-6/JAK2/STAT3 signaling pathways. *Front Pharmacol* (2018) 9:746. doi: 10.3389/fphar.2018.00746
47. Zong S, Ye ZY, Zhang XM, Chen H, Ye M. Protective effect of *Lachnum* polysaccharide on dextran sulfate sodium-induced colitis in mice. *Food Funct* (2020) 11(1):846–59. doi: 10.1039/c9fo02719j



OPEN ACCESS

EDITED BY

Guiyan Yang,
University of California, Davis,
United States

REVIEWED BY

Dong Zhou,
Northwest A&F University, China
Tingjun Hu,
Guangxi University, China

*CORRESPONDENCE

RuoNan Bo
007309@yzu.edu.cn
JinGui Li
jgli@yzu.edu.cn

†These authors have contributed
equally to this work

SPECIALTY SECTION

This article was submitted to
Nutritional Immunology,
a section of the journal
Frontiers in Nutrition

RECEIVED 28 September 2022

ACCEPTED 20 October 2022

PUBLISHED 10 November 2022

CITATION

Mohamed Husien H, Peng W, Su H,
Zhou R, Tao Y, Huang J, Liu M, Bo R
and Li J (2022) *Moringa oleifera* leaf
polysaccharide alleviates
experimental colitis by inhibiting
inflammation and maintaining
intestinal barrier.
Front. Nutr. 9:1055791.
doi: 10.3389/fnut.2022.1055791

COPYRIGHT

© 2022 Mohamed Husien, Peng, Su,
Zhou, Tao, Huang, Liu, Bo and Li. This
is an open-access article distributed
under the terms of the [Creative
Commons Attribution License \(CC BY\)](#).
The use, distribution or reproduction in
other forums is permitted, provided
the original author(s) and the copyright
owner(s) are credited and that the
original publication in this journal is
cited, in accordance with accepted
academic practice. No use, distribution
or reproduction is permitted which
does not comply with these terms.

Moringa oleifera leaf polysaccharide alleviates experimental colitis by inhibiting inflammation and maintaining intestinal barrier

Hosameldeen Mohamed Husien^{1,2,3†}, WeiLong Peng^{1,2†},
Hongrui Su^{1,2}, RuiGang Zhou^{1,2}, Ya Tao^{1,2}, JunJie Huang^{1,2},
MingJiang Liu^{1,2}, RuoNan Bo^{1,2*} and JinGui Li^{1,2*}

¹College of Veterinary Medicine, Yangzhou University, Yangzhou, China, ²Jiangsu Co-innovation
Center for Prevention and Control of Important Animal Infectious Diseases and Zoonoses,
Yangzhou, China, ³College of Veterinary Medicine, University of Albutana, Albutana, Sudan

The characteristic of ulcerative colitis (UC) is extensive colonic mucosal inflammation. *Moringa oleifera* (*M. oleifera*) is a medicine food homology plant, and the polysaccharide from *M. oleifera* leaves (MOLP) exhibits antioxidant and anti-inflammatory activity. The aim of this study to investigate the potential effect of MOLP on UC in a mouse model as well as the underlying mechanism. Dextran sulfate sodium (DSS) 4% in drinking water was given for 7 days to mice with UC, at the same time, MOLP (25, 50, and 100 mg/kg/day) was intragastric administered once daily during the experiment. Structural analysis revealed that MOLP had an average molecular weight (Mw) of 182,989 kDa and consisted of fucose, arabinose, rhamnose, galactose, glucose, xylose, mannose, galactose uronic acid, glucuronic acid, glucose uronic acid and mannose uronic acid, with a percentage ratio of 1.64, 18.81, 12.04, 25.90, 17.57, 12.01, 3.51, 5.28, 0.55, 1.27, and 1.43%, respectively. In addition, the features of MOLP were identified by Fourier-transform infrared (FT-IR) and spectra, X-ray diffraction (XRD). The results showed that MOLP exhibited protective efficacy against UC by alleviating colonic pathological alterations, decreasing goblet cells, crypt destruction, and infiltration of inflammatory cells caused by DSS. Furthermore, MOLP notably repressed the loss of zonula occludens-1 (ZO-1) and occludin proteins in mucosal layer, as well as up-regulating the mRNA expression of interleukin-10 (IL-10) and peroxisome proliferator-activated receptor- γ (PPAR- γ), whereas down-regulating the activation of Toll-like receptor 4

(TLR4), myeloid differentiation primary response 88 (MyD88), nuclear factor-kappa B (NF- κ B) signaling pathway and the production of pro-inflammatory cytokines. Therefore, these results will help understand the protective action procedure of MOLP against UC, thereby providing significance for the development of MOLP.

KEYWORDS

inflammatory bowel disease, *Moringa oleifera* leaves polysaccharide, intestinal injury, inflammatory signaling pathway, tight junction expression

Introduction

Ulcerative colitis (UC), a common consequence of inflammatory bowel disease (IBD), is a chronic recurring intestinal disease, indicated by abdominal pain, losing weight, and bloody stools (1). Recently, anti-inflammatory drugs (sulfasalazine or mesalazine), common immunosuppressive agents (glucocorticoids, azathioprine, methotrexate, and cyclosporine A), and biological products, such as infliximab and adalimumab, have been shown to help relieve UC symptoms (2, 3). Nevertheless, these treatments are restricted due to their side effects or serious adverse events, such as steroid dependence and secondary infection (4). Consequently, developing effective alternative strategies for preventing and mitigating UC is critical.

Damage to the intestinal mucosal barrier allows external antigens (LPS et al.) and pathogens to infiltrate and activate immune cells in the body's lamina propria. The activated immune cells then initiate an inflammatory cascade marked by elevated levels of pro-inflammatory cytokines such as interleukin-1 β (IL-1 β) and tumor necrosis factor alpha (TNF- α), as well as a reduction in the anti-inflammatory cytokine interleukin-10 (IL-10) (5). Pro-inflammatory factors motivate macrophage and neutrophil infiltration, stimulate mucosal permeability, and reduce tight junction (TJ) proteins, ultimately leading to tissue injury (6).

Moringa oleifera (*M. oleifera*), a perennial plant with considerable nutritional and medicinal benefits, is a component of the Moringa family. It grows widely throughout Southeast Asia, Africa, China's southern region, and even the rest of the world (7). The World Health Organization (WHO) has recommended *M. oleifera* leaves as a highly nutritious

alternative to imported food sources for the treatment of malnutrition (8). The leaves are healthful whether eaten fresh or cooked. Furthermore, *M. oleifera* leaf extracts have a variety of biological characteristics, such as antioxidants activity, hypoglycemic activity, anti-inflammatory activity, and immunomodulatory activity (9, 10).

Recent research indicates that polysaccharides extracted from *M. oleifera* leaves have acquired popularity due to their diverse and excellent biological activity. For example, a novel arabinogalactan (MOP-1) with considerable *in vitro* antioxidant activity was extracted from the leaves of *M. oleifera* (11). Dong et al. obtained another polysaccharide (MOP-2) from the leaves of *M. oleifera* and measured its immunomodulatory activity *in vitro* (12). However, the potential effect of *M. oleifera* leaf polysaccharide (MOLP) against UC and the underlying mechanism unclear.

In this study, we examine the potential protective effect of MOLP on dextran sulfate sodium (DSS)-induced UC in mice by detecting colonic histopathological alterations, Toll-like receptor 4 (TLR4), Myeloid differentiation primary response 88 (MyD88), Nuclear factor-kappa B (NF- κ B) signaling pathways and the corresponding inflammatory cytokines, TNF- α , high mobility group box 1 (HMGB1), peroxisome proliferator-activated receptor- γ (PPAR- γ) and so on. In addition, mucosal permeation related TJ protein levels were also analyzed. These findings can serve as a theoretical foundation for the further development and implementation of MOLP.

Materials and methods

Reagents and materials

M. oleifera leaves were purchased from Yunnan Ruziniu Biotechnology (Yunnan, China). The plant material was identified by Prof. Jingui Li. Dextran sulfate sodium (DSS; product code # 160110; MW: 36000–50,000) was obtained from MP Biomedicals (Solon, USA). Myeloperoxidase (MPO) (Cat No. A044-1-1) was obtained from the Jiancheng Bioengineering Institute of Nanjing (Nanjing, China). LPS (Cat No. 21100201)

Abbreviations: UC, ulcerative colitis; IBD, inflammatory bowel disease; MOLP, *Moringa oleifera* leaves polysaccharide; TNF- α , tumor necrosis factor alpha; DSS, dextran sulfate sodium; MPO, myeloperoxidase; TJ, tight junction; DAI, disease activity index; PPAR- γ , peroxisome proliferator-activated receptor- γ ; HMGB1, High mobility group box 1; ZO-1, zonula occludens-1; TLR4, Toll-like receptor 4; NF- κ B, nuclear factor-kappa B; I κ B α , inhibitor of kappa B alpha; MyD88, myeloid differentiation primary response 88.

was obtained from the Xiamen Bioendo Technology Co., Ltd. Primers and a bicinchoninic acid (BCA) protein assay kit were provided by Solarbio, Beijing, China. Immobilon-P polyvinylidene fluoride (PVDF) membranes (size: 0.45 μm) were obtained from Merck Millipore (Billerica, USA). RNA-easy Isolation Reagent (Cat No. R701) was purchased from Vazyme Biotech Co., Ltd. Hifair® 1st Strand cDNA Synthesis SuperMix for qPCR (gDNA digester plus) (Cat No. 11141ES60) and Hieff® qPCR SYBR Green Master Mix (High Rox Plus) (Cat No. 11201ES08) were the products of Yeasen Biotech Co., Ltd. Antibodies of TLR4 (Cat No. 14358s), MyD88 (Cat No. 4283s), phospho-I κ B α (P-I κ B α) (Cat No. 4812s), phospho-p65 (P-p65) (Cat No. 8242s) and β -actin (Cat No. 4970s) were the products of Cell Signaling Technology Pathways. TLR4 inhibitor (TAK242, Cat No. M4838) was purchased from Abmole (Houston, TX, USA). Primary antibodies against Occludin and claudin-1 (ab242370) were purchased from Abcam (Cambridge, United Kingdom). The corresponding horseradish peroxidase (HRP)-conjugated secondary antibodies (111-035-003 and 115-035-003) were bought from Jackson Immuno Research (West Grove, PA, United States). Secondary antibody which conjugated to fluorescence (ab150077 and ab150116) was bought from Abcam (Cambridge, United Kingdom). ELISA kits for TNF- α (Cat No. ck-E20852), IL-1 β (Cat No. ck-E20174), IL-10 (Cat No. ck-E20162), and HMGB1 (Cat No. ck-E20318) were purchased from Shanghai Beyotime Biotechnology Co., Ltd. (Shanghai, China).

Preparation and extraction of polysaccharide from *Moringa oleifera*

The crude polysaccharide was extracted from the leaf powder of *M. oleifera* using the procedures reported in earlier investigations (13). The polysaccharide was extracted three times using deionized water at a 1:10 (w/v) ratio at 70°C for 90 min, followed by centrifugation at 4,000 rpm for 20 min. Mixing and evaporating the collected supernatants with a rotary evaporator. Following an overnight incubation at 4°C, then the concentrations were precipitated by adding dehydrated ethanol to a final concentration of 80% (v/v). The obtained precipitates were washed with 95% ethanol and dissolved in deionized water following centrifugation. The dialysate solution was freeze-dried, then deproteinated using the sewage method (14). Final solution was freeze-dried to obtain MOLP.

Determination of molecular weight

The weight average molecular weight (Mw) of MOLP was determined using SEC-MALLS-RI, which was described in a previous study (15). A DAWN HELEOS-II laser photometer (Wyatt Technology Co., USA) equipped with three tandem

columns (300 \times 8 mm, Shodex OH-pak SB-805, 804 and 803; Showa Denko K.K., Tokyo, Japan) was utilized for the determination. MOLP solution (1 mg·mL⁻¹) filtered through a filter of 0.45 μm pore size, which was held at 45°C using a model column heater by Sanshu Biotech. Co., Ltd. (Shanghai, China) and flow rate 0.4 mL·min⁻¹ with 0.1 M NaNO₃ aqueous solution containing 0.02% NaN₃. The Mw was calculated by reference to the standard curve of a Dextran series.

Monosaccharide composition analysis

5 mg of sample was hydrolyzed with trifluoroacetic acid (TFA, 2 M) at 121°C for 2 h in a sealed tube. The sample was dried with nitrogen. Add methanol to wash, then blow dry, repeat methanol wash 2–3 times. The monosaccharide standards included fucose, arabinose, rhamnose, galactose, glucose, xylose, mannose, fructose, ribose, galacturonic acid and glucuronic acid. Finally, samples were analyzed by high-performance anion-exchange chromatography (HPAEC) on a CarboPac PA-20 anion-exchange column (3 by 150 mm; Dionex) using a pulsed amperometric detector (PAD; Dionex ICS 5000 system). Flow rate, 0.5 mL/min; injection volume, 5 μL ; solvent system A: (ddH₂O), solvent system B: (0.1 M NaOH), solvent system C: (0.1 M NaOH, 0.2 M NaAc); gradient program, volume ratio of solution A, B, C was 95:5:0 at 0 min, 85:5:10 at 26 min, 85:5:10 at 42 min, 60:0:40 at 42.1 min, 60:40:0 at 52 min, 95:5:0 at 52.1 min, 95:5:0 at 60 min. Data were acquired on the ICS5000 (Thermo Fisher Scientific), and processed using chromeleon 7.2 CDS (Thermo Fisher Scientific).

Fourier transform-infrared spectroscopy

3 mg of MOLP sample was combined with KBr powder (100 mg) and pressed into thin slices, which were then evaluated in a wave number range of 4,000–400 cm⁻¹ using an Fourier transform-infrared (FT-IR) spectrometer (Cary 670-IR + 610-IR, Agilent Company, USA).

X-Ray diffraction

Five milligram of MOLP sample was measured at an angle of 0.8–140° using an X-ray diffractometer (D8 Advance, Bruker AXS, Germany).

Scanning electron microscope

MOLP sample was coated with gold powder, and its structural characteristics were analyzed using a scanning electron microscope (SEM) system (S-4800, Hitachi, Japan).

Animals and experimental design

Male BALB/C mice (6–8 weeks old), weighing 20 ± 2 g, were obtained from Yangzhou University Laboratory Animal Co., Ltd. (Yangzhou, China). Forty mice were housed under standard laboratory conditions (12 h light-dark cycle, $25 \pm 2^\circ\text{C}$ and 60–80% relative humidity), and fed standard laboratory chow and sterile, distilled water *ad libitum* in the animal room. All animal study was reviewed and approved by Institutional Animal Care and Use Committees (IACUC) of Yangzhou University. After 1 week of acclimatization, the mice were randomly categorized into five groups ($n = 8$). The experimental design was illustrated in [Figure 1A](#). All experimental groups were administered distilled water for the first 3 days, control group was administered 0.9% (0.2 mL) sodium chloride (NaCl) from days 4 to 10. DSS group was administered 4% (w/v) DSS from days 4 to 10. DSS + MOLP-L group, DSS + MOLP-M group and DSS + MOLP-H group were given oral administration with different doses of MOLP (25, 50 and 100 mg/kg/day, respectively), along with the oral administration of 4% (w/v) DSS from days 4 to 10 for 7 days. All mice were injected with 0.1% (50 mg/kg, i. p.) pentobarbital sodium and sacrificed after 10-day experimental period. The weight of liver and spleen were measured and recorded. The entire colon was quickly removed and washed with cold phosphate-buffered saline (PBS). The distal part was fixed in 10% buffered formalin for histological analysis, and other parts were then stored at -80°C for immunological assays.

Disease activity index and histological injury analysis

The body weight of mice was recorded using an electronic analytical balance. The following analysis of a disease activity index (DAI) indicator score, which included body weight loss, stool consistency, and blood in the stools, was performed in accordance with the literature (16). Briefly, (a) body weight loss: 0 points = none; 1 points = 1–5% loss; 2 points = 5–10% loss; 3 points = 10–20% loss; 4 points = over 20% loss. (b) Diarrhea: 0 points = normal; 1 point = soft but still formed; 2 points = soft; 3 points = very soft and wet; 4 points = watery diarrhea. (c) Hematochezia: 0 points = negative hemocult; 1 point = weakly positive hemocult; 2 points = positive hemocult; 3 points = blood traces in stool visible; 4 points = gross rectal bleeding.

Using the previously published method (17), paraffin-embedded colonic tissues were sectioned and stained with hematoxylin and eosin (H&E) for evaluation and histopathologic scoring of UC. Briefly, (a) severity of inflammation: 0 points = none; 1 points = mild; 2 points = moderate; 3 points = severe. (b) Extent of inflammation: 0 points = none; 1 points = mucosal; 2

points = mucosal and submucosal; 3 points = transmural. (c) Crypt damage: 0 points = none; 1 points = basal 1/3; 2 points = basal 2/3; 3 points = crypts lost but surface epithelium present; 4 points = crypts and surface epithelium lost.

Determination of myeloperoxidase activity, inflammatory cytokines and lipopolysaccharide content

Myeloperoxidase (MPO) activity, and inflammatory cytokines such as TNF- α , IL-1 β , HMGB1 and IL-10 levels in colonic tissues, and serum lipopolysaccharide (LPS) levels were assessed using ELISA kits in accordance with the manufactures instructions.

Analysis of colon tissues after dextran sulfate sodium-treatment using qRT-PCR

Using Trizol reagent, total RNA was isolated from colon tissue samples and examined using a NanoDrop 2000 UV-vis spectrophotometer (Thermo Fisher Scientific, Wilmington, DE, USA). The Hifair® I1st strand cDNA synthesis SuperMix was used to create the cDNA samples. Utilizing the CFX96™ connect real-time PCR system (Bio-Rad, USA) and SYBR® Green Master Mix Kit, the expression levels of IL-1 β , IL-10, TNF- α , HMGB1 and PPAR-mRNA in colon tissues were determined. GAPDH was designated as the housekeeping gene for the $2^{-\Delta\Delta CT}$ technique to calculate relative mRNA levels. The specific primers for the target genes are shown in [Table 1](#).

Western blotting analysis

The colon tissue was homogenized and lysed in RIPA buffer with a PMSF protease inhibitor on ice, homogenized, and centrifuged at 12,000 rpm for 10 min. The amount of proteins in the supernatant was then measured using a BCA protein assay kit. After boiling with loading buffer, equal quantities of protein from each sample were prepared for electrophoresis on 10% SDS-PAGE under reducing conditions, transferred to the PVDF membrane, blocked for 2 h with 5% skim milk, and then overnight incubated with primary antibodies (1:1,000 dilution) at 4°C (all antibodies were diluted following instructions). The membrane was treated with species-specific secondary antibodies together with horseradish peroxidase (1:1,000 dilution) at room temperature for 1 h after three TBST washes. Using an enhanced chemiluminescence kit, protein signal bands

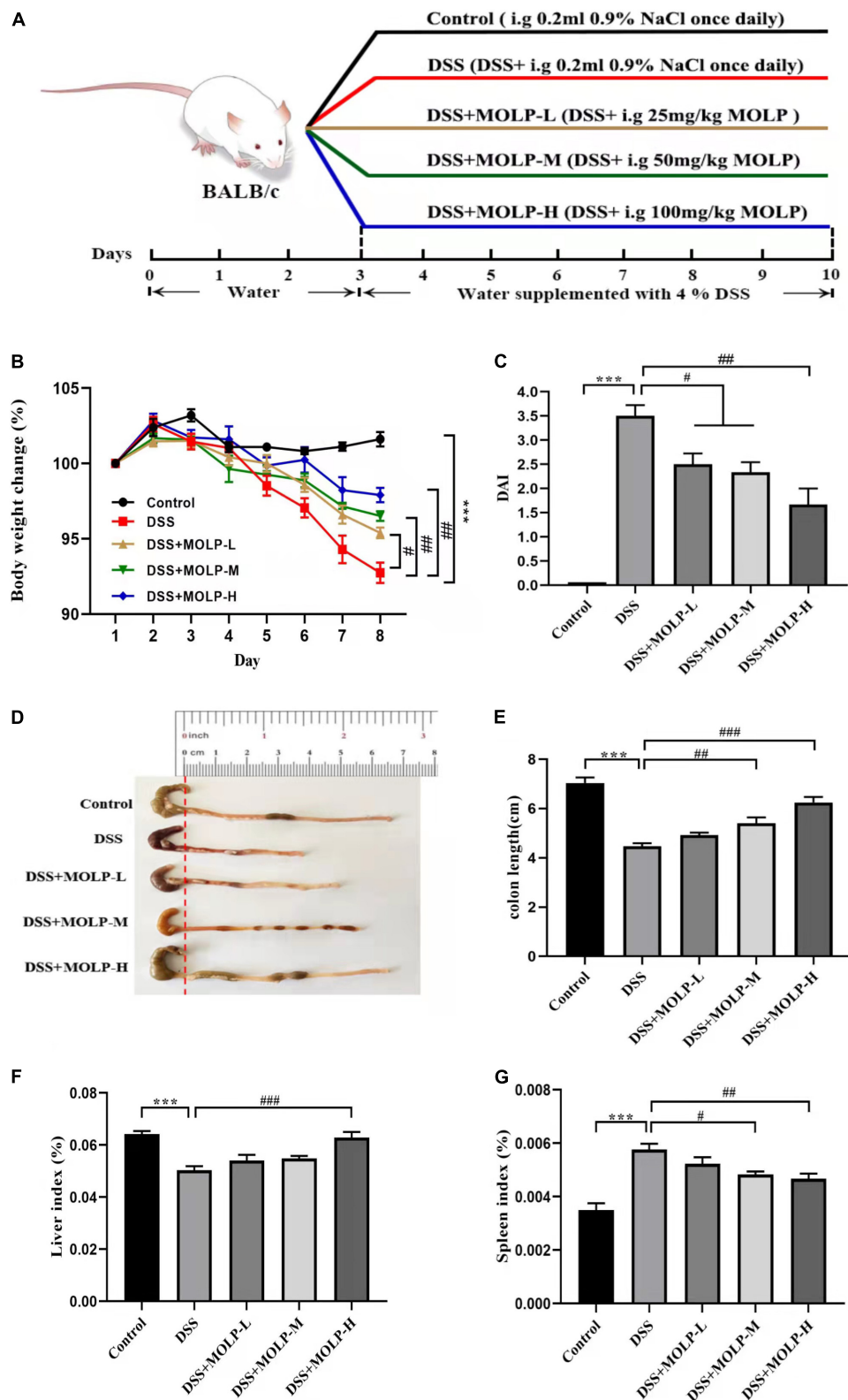


FIGURE 1

Effect of MOLP on the symptoms of mice with ulcerative colitis. The experimental design (A), changes of body weight (B), DAI (C), the status (D) and length (E) of colon, indexes of liver (F) and spleen (G). Data are presented as mean \pm SEM ($n = 8$), *** $P < 0.001$, DSS vs. Control; # $P < 0.05$, ## $P < 0.01$, ### $P < 0.001$, DSS + MOLP-L, DSS + MOLP-M and DSS + MOLP-H vs. DSS.

TABLE 1 List of primer sequences used for qRT-PCR.

Gene	Sense (5'–3')	Antisense (5'–3')
IL-1 β	CCAGCAGGTTATCATCACATCC	ATCTCGCAGCAGCACATCA
IL-10	GGCAGCCTTGTCCTTG	AACATACTGCTAACCGACTCCTT
TNF- α	TGAAGCAGCAGCCAGCAA	GCAGCCTGTCTCCTTCTATGA
HMGB1	ATGGGCAAAGGAGATCCTA	ATTTCATCATCATCTCTTCT
PPAR γ	CCCACCAACTTCGGAATCAG	TGCTGGAGAAATCAACCGTGGTA
GAPDH	CACCATCTTCCAGGAGCGAG	GGGGCCATCCACAGTCTTC

were observed on a Chemidoc XRS (BIO-RAD, Marnes-la-Coquette, France) following three washes with TBST (Merck Millipore, Billerica, USA). and quantified using Image J software.

Immunohistochemistry analysis

Paraffin-embedded slices of colonic tissue were deparaffinized, rehydrated, rinsed with distilled water, and then placed in citrate buffer for antigen thermal retrieval. After that, the cells were washed three times with PBS for 5 min each, incubated for 60 min at room temperature with blocking buffer (3% BSA in PBS), and then incubated overnight at 4°C with anti-zonula occludens-1 (ZO-1) and anti-occludin primary antibodies. The primary antibody was incubated with the secondary antibody for 50 min at room temperature before being rinsed three times with PBS for 5 min each and stained with DAPI for 10 min. After being acquired with a fluorescent microscopy imaging system (Nikon Corporation, Tokyo, Japan), the sections were quantified using Image J software.

Statistical analysis

The data is displayed as the mean \pm standard error of the mean. GraphPad Prism's one-way ANOVA test was utilized for statistical analysis (version 8.0). $P < 0.05$, $P < 0.01$, or $P < 0.001$ indicates statistical significance.

Results and discussion

Molecular weight and monosaccharide composition

The Mw distribution of MOLP was determined by SEC-MALLS-RI. As shown in **Figure 2A**, a single, sharp, and symmetrical peak at 42.95 min was observed, indicating that

MOLP was a homogeneous polysaccharide. The Mw of MOLP was estimated to be 182,989 kDa.

The monosaccharide composition analysis of MOLP was shown in **Figure 2B**, MOLP was composed of fucose, arabinose, rhamnose, galactose, glucose, xylose, mannose, galactose uronic acid, glucuronic acid, glucose uronic acid and mannose uronic acid, with a percentage ratio of 1.64, 18.81, 12.04, 25.90, 17.57, 12.01, 3.51, 5.28, 0.55, 1.27, and 1.43%, respectively. According to the standard curve (**Figure 2D**), the result indicated that MOLP was a hetero-polysaccharide.

Fourier-transform infrared spectroscopy analysis

The FT-IR spectrum of MOLP revealed typical polysaccharide absorption peaks in the ranges of 4,000–400 cm^{-1} . As shown in **Figure 2C**, the strong absorptions at 3401.1 and 2919.4 cm^{-1} showed O–H and C–H stretching vibrations, respectively (18). The absorption peak at 1628.4 cm^{-1} was given the C = O stretching vibration. The absorption peak at 1242.8 cm^{-1} was identified as the source of the S = O stretching vibration. The absorption peak at 1105.8 cm^{-1} was also attributed to the C–O stretching vibration. Additionally, a pyranose ring was discovered by the 848.5 cm^{-1} absorption, it is similar with the previous studies on the polysaccharides extracted from the leaves of *M. oleifera* (19, 20).

X-ray diffraction analysis

An obvious dispersing peak was observed at 19.80° according to the XRD curve of MOLP (**Figure 2E**). However, no obvious characteristic peaks were observed, only a few small dispersing absorption peaks at 29.12° and 35.50°, respectively.

Scanning electron microscope analysis

The SEM image of MOLP was illustrated in **Figure 2F**. The surface of MOLP was smooth and mainly exhibited sheet and needle or rod-like shape.

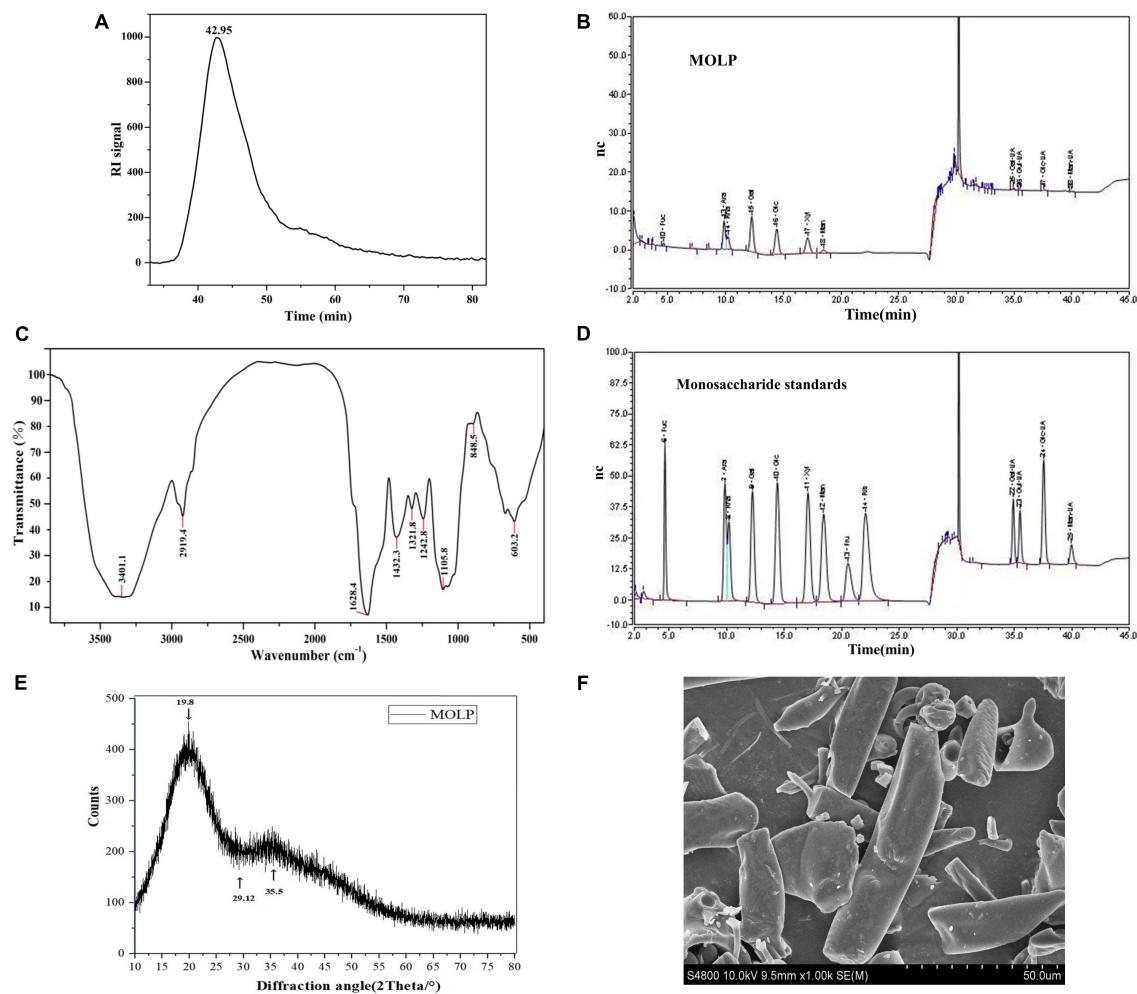


FIGURE 2

Structural characterization of MOLP. The peak at retention time of MOLP (A). The monosaccharide composition analysis of MOLP (B). FT-IR spectrum of MOLP (C). Monosaccharide standards (D). Fuc, fucose; Ara, arabinose; Rha, rhamnose; Gal, galactose; Glc, glucose; Xyl, xylose; Man, mannose; Gal-UA, galacturonic acid; Glu-UA, glucuronic acid; Man-UA, mannose uronic acid. XRD (E), and SEM (F) of MOLP.

TABLE 2 Effects of MOLP on MPO activity and LPS content.

Groups	Control	DSS	DSS + MOLP-L	DSS + MOLP-M	DSS + MOLP-H
MPO (U/g)	0.11 ± 0.03	0.54 ± 0.07**	0.33 ± 0.03	0.29 ± 0.09#	0.15 ± 0.08##
LPS (EU/mL)	1.61 ± 0.06	4.87 ± 0.57***	3.71 ± 0.18	2.53 ± 0.07##	2.37 ± 0.09##

Data are presented as mean ± SEM ($n = 8$), ** $P < 0.01$, *** $P < 0.001$, DSS vs. Control; # $P < 0.05$, ## $P < 0.01$, DSS + MOLP-M and DSS + MOLP-H vs. DSS. MPO, Myeloperoxidase; LPS, Lipopolysaccharide; DSS, Dextran sodium sulfate; MOLP-L, low dose of *Moringa oleifera* leaf polysaccharide; MOLP-M, medium dose of *Moringa oleifera* leaf polysaccharide; MOLP-H, high dose of *Moringa oleifera* leaf polysaccharide.

Moringa oleifera leaves polysaccharide improved colitis symptoms in dextran sulfate sodium-treated mice

The change in body weight was calculated and shown in Figure 1B. The DSS treatment led to a significant weight loss. Nonetheless, MOLP administration had a protective effect and reduced the trend in body weight loss in a dose-dependent

manner, indicating that MOLP reduced body weight loss in DSS-induced UC mice.

DAI scores were used to detect the progression of DSS-induced UC (21). Colonic contraction has been identified as the primary feature of UC, and shortening of colon length is clearly associated with disease severity (22). As illustrated in Figure 1C, DSS treatment significantly increased DAI score in model mice after 10 days. However, MOLP supplementation

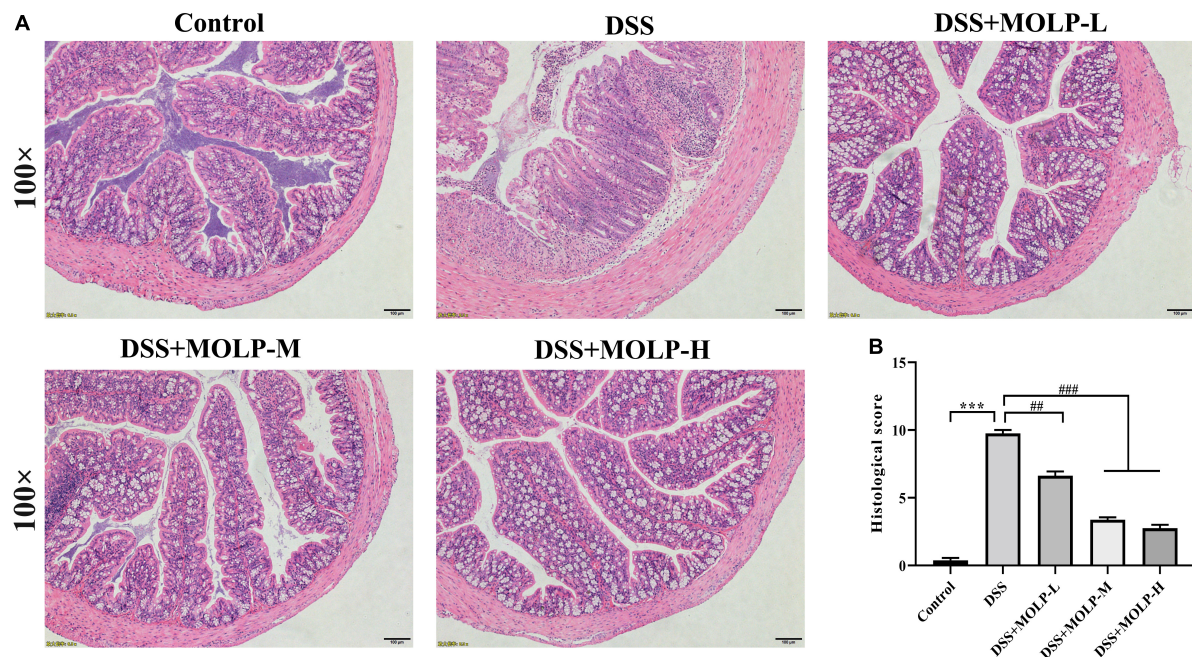


FIGURE 3

Effect of MOLP on histopathological changes of mice with ulcerative colitis. Histology analysis of colon tissues by HE staining (A), histological score (B). Data are presented as mean \pm SEM ($n = 8$), *** $P < 0.001$, DSS vs. Control; ## $P < 0.01$, ### $P < 0.001$, DSS + MOLP-L, DSS + MOLP-M and DSS + MOLP-H vs. DSS.

inhibited the elevation of DAI scores in the low, medium, and high dose groups. In contrast, the DSS group showed a significant contraction in mouse colon length. Nonetheless, intervention with MOLP at medium and high doses effectively prevented colon shortening (Figures 1D,E). Similar to Zhang et al. (23), which indicated that 5-ASA and (MOPE) isolated from *M. oleifera* treatments reduced inflammatory symptoms in the colon of mice. Our results suggested that the MOLP supplementation has a preventative effect on UC induced by DSS.

Spleen index is regarded as a key indicator of immunological function (24). In this study, DSS challenge significantly reduced the liver index while increasing the spleen index when compared to the control. However, the high dose of MOLP significantly increased the liver index while decreasing the spleen index in DSS-induced UC mice (Figures 1F,G). Taken together, all the findings showed that MOLP reduced clinical symptoms and anatomical changes in DSS-induced UC.

Moringa oleifera leaves polysaccharide ameliorated the colonic histopathological changes

As shown in Figure 3, the histology of the control group was normal, with dense columnar epithelium, intact intestinal crypts, and abundant goblet cells. There was epithelial rupture,

irregular crypt architecture, submucosal edema, goblet cell reduction, and neutrophil hyper-infiltration in the DSS group. On the contrary, MOLP intervention significantly improved these DSS-induced histopathological scores. According to previous studies, the impaired function of the intestinal mucosal barrier is directly related to the development of UC (25) and was characterized by epithelial rupture, irregular mucosal and crypt structure, and reduction of goblet cells. And also neutrophils are one of the infiltrating cells that cause inflammation in colitis (26). This is consistent with the findings of Hong et al. (27), which indicated that a high dose of (MOP) extracted and purified a peptide from *M. oleifera* seeds significantly reduced such mucosal damage (including the greater crypt depth), decreased in goblet cells and inflammatory cell infiltration, leading to lower histological scores in DSS-induced UC mice. Therefore, these results showed that MOLP supplementation could improve the histopathological changes in DSS-induced UC.

Moringa oleifera leaves polysaccharide decreased myeloperoxidase activity in colonic tissues and serum lipopolysaccharide level

MPO is a peroxidase that reflects infiltration and inflammation levels directly (28). LPS is another inflammatory

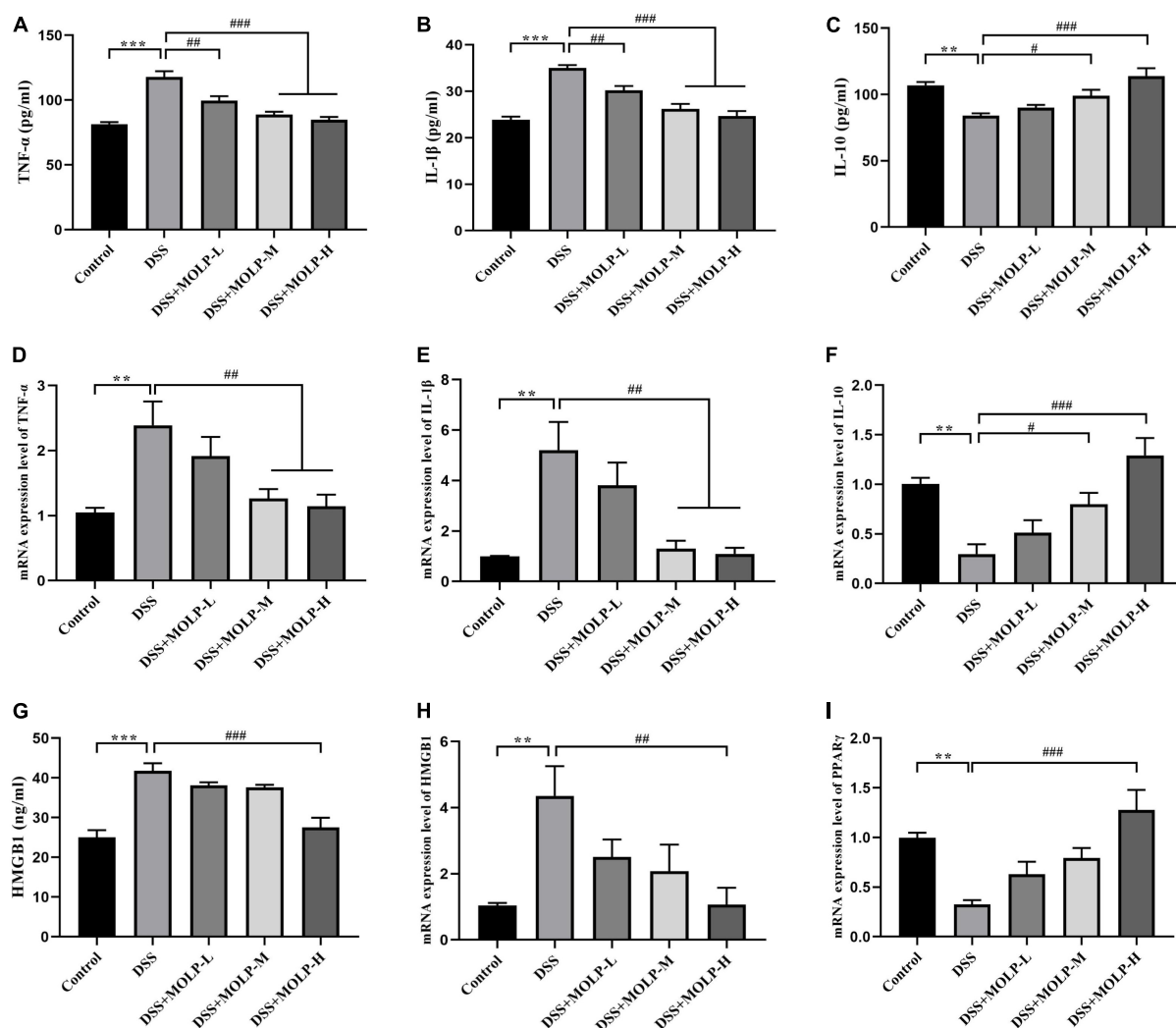


FIGURE 4

Effect of MOLP on serum cytokine levels and colon tissues in mice with ulcerative colitis. The concentrations of TNF- α (A), IL-1 β (B), IL-10 (C) and HMGB1 (G) detected by (ELISA) ($n = 8$). The mRNA expression levels of TNF- α (D), IL-1 β (E), IL-10 (F), HMGB1 (H) and PPAR γ (I) ($n = 5$). Data are presented as mean \pm SEM, ** $P < 0.01$, *** $P < 0.001$, DSS vs. Control; # $P < 0.05$, ## $P < 0.01$, ### $P < 0.001$, DSS + MOLP-L, DSS + MOLP-M and DSS + MOLP-H vs. DSS.

stimulator that promotes the release of pro-inflammatory cytokines, inflammatory signaling, and tissue damage in a range of inflammatory diseases (29). We examined MPO activity in colon tissues and serum LPS levels in DSS-induced UC mice. As shown in Table 2, MPO activity and LPS level raised significantly in the DSS treatment relative to the control group. Additionally, administration reduced tissue MPO activity and serum LPS levels in the DSS + MOLP-M and DSS + MOLP-H groups when compared to the DSS group. This is in line with the results of Hong et al. (27), which indicated that a high dose of (MOP) decreased MPO in the serum of DSS-induced UC mice. These findings suggest that MOLP plays a protective role against DSS-induced UC by inhibiting MPO activity and serum LPS levels.

Anti-inflammatory effect of *Moringa oleifera* leaves polysaccharide in the colon tissues

TNF- α is a major factor promoting damage to the intestinal epithelial barrier, is associated with the development of UC, and has the potential to stimulate the production of IL-1 β (30, 31). The anti-inflammatory cytokine IL-10 can inhibit the production of pro-inflammatory cytokines such as TNF- α and IL-1 β (4). In addition, HMGB1 is a key mediator in the pathogenesis of systemic inflammation in a variety of inflammatory diseases, with a strong ability to trigger inflammatory responses (32). In order to determine whether MOLP intervention might alleviate DSS-induced colonic

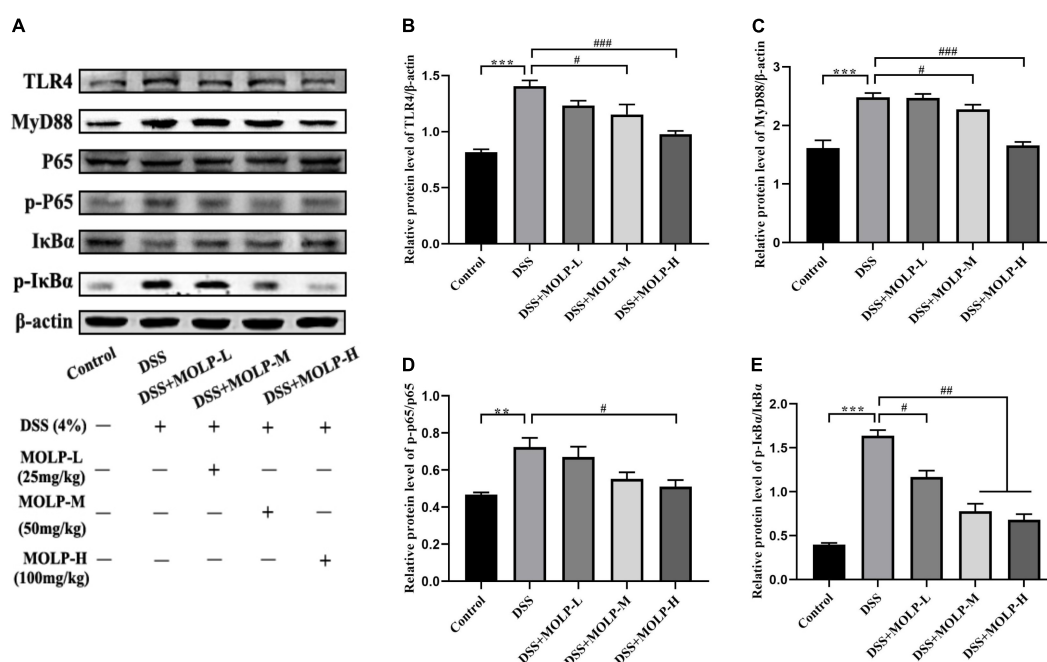


FIGURE 5

Effect of MOLP on colon tissues in mice with ulcerative colitis. Western blot analysis of key signaling proteins in colonic tissue (A), TLR4 (B), MyD88 (C), NF- κ B p65/p-P65 (D) and p-I κ B α /I κ B α (E). Data are presented as mean \pm SEM ($n = 3$), ** $P < 0.01$, *** $P < 0.001$, DSS vs. Control; # $P < 0.05$, ## $P < 0.01$, ### $P < 0.001$, DSS + MOLP-L, DSS + MOLP-M and DSS + MOLP-H vs. DSS.

inflammation by modulating the inflammatory response, the levels of inflammatory cytokines and their mRNA in colon tissues were measured. The expression levels of pro-inflammatory cytokines TNF- α , IL-1 β and HMGB1 were up-regulated after oral administration of DSS compared with the control group (Figure 4). However, the expression levels of TNF- α , and IL-1 β were dramatically reduced in the colon tissue of colitis mice after MOLP intervention at all doses (Figures 4A,B). While, the IL-10 expression level in colon tissues was up-regulated after the medium and high doses of MOLP treatment (Figure 4C). Only at the high dose of MOLP intervention was the level of HMGB1 significantly lower than in the DSS group (Figure 4G).

Similar trends were shown in terms of mRNA expression levels of inflammatory cytokines in colon tissues. The mRNA expression levels of TNF- α , IL-1 β and HMGB1 were significantly up-regulated by DSS challenge. In contrast, the mRNA expressions levels of TNF- α and IL-1 β were significantly down-regulated by MOLP administration at the medium and high dosages (Figures 4D,E). And the level of HMGB1 mRNA expression in the DSS + MOLP-H group was significantly lower than that in the DSS group (Figure 4H). However, the IL-10 mRNA expression levels were significantly increased in the DSS + MOLP-M and DSS + MOLP-H groups (Figure 4F). Previous studies reported that polysaccharides play important roles in cytokine homeostasis by regulating inflammatory factor levels (33, 34).

PPAR- γ is highly expressed in intestinal and colonic mucosal epithelial cells, as well as macrophages (35). The level of PPAR- γ mRNA expression in colon tissue was investigated. As showed in Figure 4I, DSS treatment alone significantly down-regulated the PPAR- γ mRNA expression level. However, the DSS-induced change in mice may incrementally revert to normal level by the high dose of MOLP administration. Previous studies reported that mRNA PPAR- γ expression were decreased in active UC compared to the UC in remission (36), and also its expression were significantly lower in comparison to healthy controls (37). According to Li et al. (13) MOP supplementation effectively suppressed serum concentration levels of TNF- α and IL-1 β , and regulated the mRNA expression level of PPAR γ in high-fat diet (HFD)-induced C57BL/6J mice. Our findings suggested that MOLP supplementation regulated inflammatory responses in DSS-induced UC by suppressing anti-inflammatory cascades.

Moringa oleifera leaves polysaccharide inhibited the TLR4/MyD88/NF- κ B signaling pathway in colonic tissues

NF- κ B signaling pathway is important in the development of UC (38, 39). In comparison to the DSS group, medium and high doses of MOLP supplementation effectively reduced

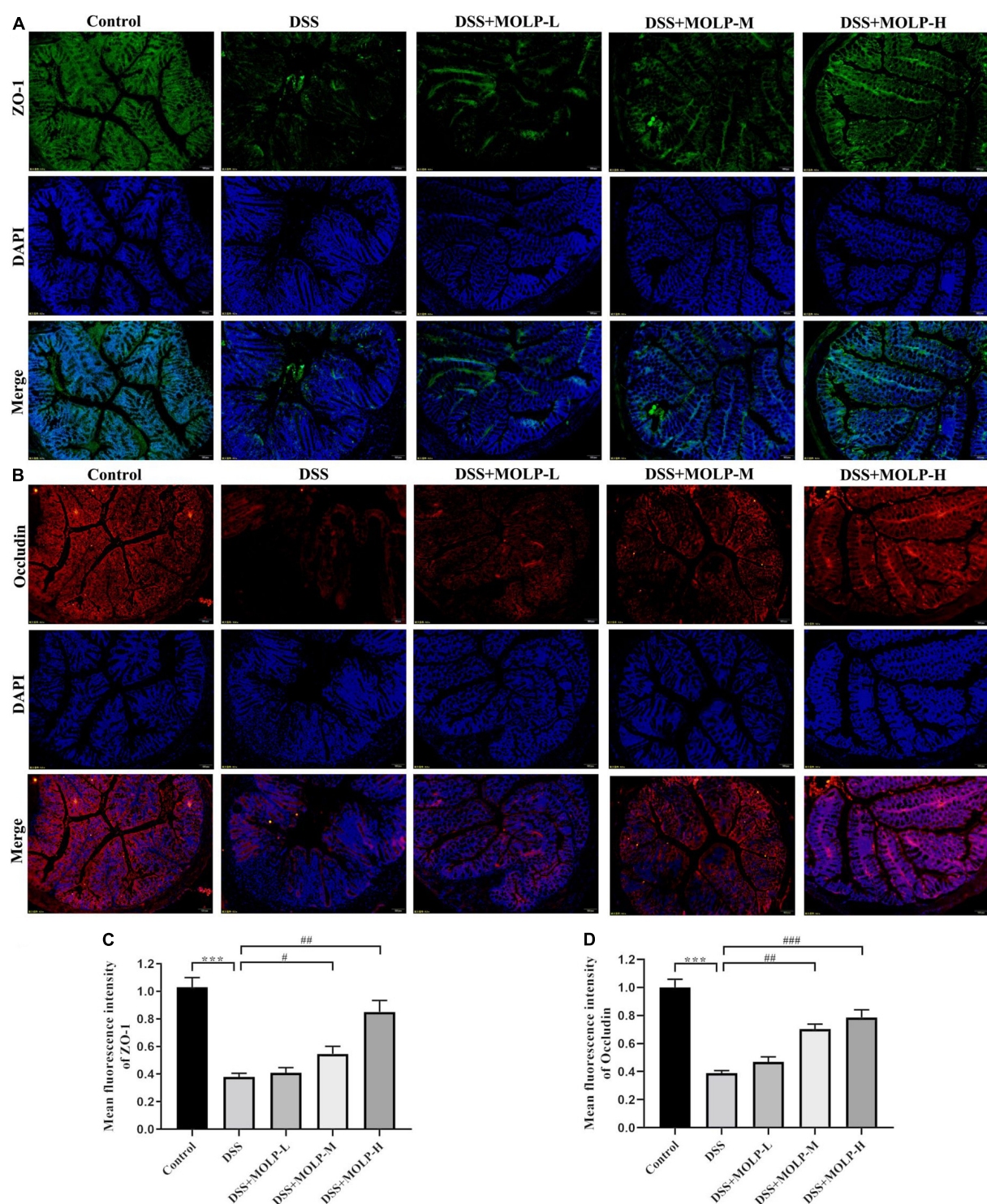
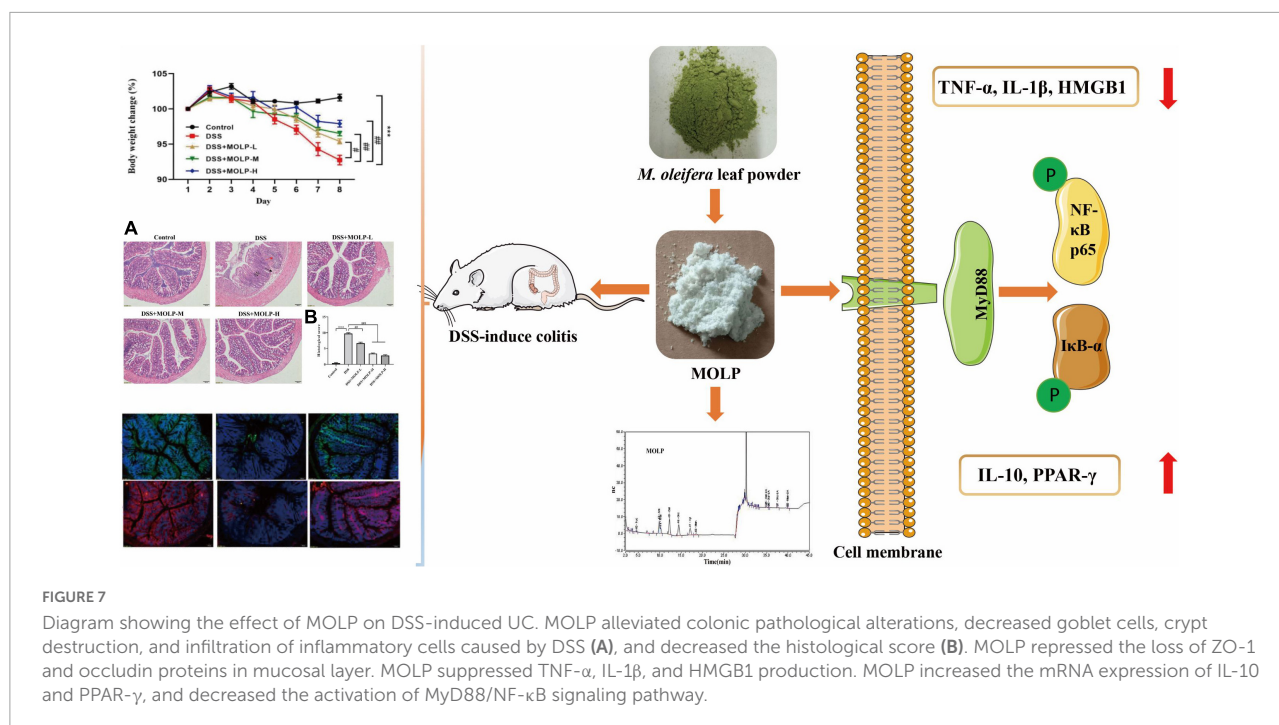


FIGURE 6
Effect of MOLP on the tight junction of mice with ulcerative colitis. Sections of colon tissues were immunostained with DAPI and antibodies and then observed under 200 × fluorescence microscope. The green fluorescence represents the amount of ZO-1 (A). The red fluorescence represents the amount of occludin (B). The blue fluorescence is the nucleus stained by DAPI. (C) quantified results from (A), (D) quantified results from (B). Data are presented as mean ± SEM (n = 3), ***P < 0.001, DSS vs. Control; #P < 0.05, ###P < 0.01, ####P < 0.001, DSS + MOLP-M and DSS + MOLP-H vs. DSS.



the up-regulation of TLR4 and MyD88 expression in colonic tissues induced by DSS (Figures 5B,C). Oral administration with DSS resulted in a marked increase in I κ B α phosphorylation (p-I κ B α), I κ B α is a key inhibitor of NF- κ B activation, and MOLP inhibited p-I κ B α (Figure 5E). Furthermore, elevated phosphorylation of NF- κ B p65 (p-NF- κ B p65) was observed in colon tissue after DSS challenge, whereas high-dose MOLP supplementation significantly blocked DSS-induced p-NF- κ B p65 (Figure 5D). Previous studies found that MOPE reduced the protein expression of NF- κ B p65 and p-I κ B α while increasing the expression of I κ B α (23). Therefore, these results suggested that MOLP may suppress inflammatory responses by inhibiting TLR4/MyD88/NF- κ B signaling pathways (Figure 5A), thereby reducing DSS-induced UC in mice.

Moringa oleifera leaves polysaccharide attenuated dextran sodium sulfate-induced loss to colonic epithelial tight junction proteins

The intercellular TJ proteins are essential components of the intestinal mechanical barrier and are responsible for epithelial permeability, paracellular spreading, and intercellular adhesion (40, 41). TJs, including ZO-1 and occludin, are essential to maintain intestinal integrity (42). However, natural extracts have been shown in clinical studies to improve the expression of TJ proteins, thereby maintaining the intestinal barrier and preventing the development of UC (43). Previously, alterations in the TJ protein of colonic epithelial cells exacerbate colitis

(44). In this study, immunofluorescence staining was used in the colons of mice to detect the distribution and expression of the intracellular scaffold protein ZO-1 and the transmembrane TJ protein occludin to see whether physiological changes in the barrier were related to changes in TJ protein distribution. As showed in the Figure 6, the fluorescence intensity of ZO-1 was significantly attenuated in DSS treated mice, and similar to the changes in the occludin expression. However, the medium and high doses of MOLP administration maintained the expression and distribution of these two proteins. Previous research (27) found that MOP reduced the levels of occludin and ZO-1 in DSS-induced UC mice. These findings indicated that the protective roles of MOLP in the intestinal epithelium may be associated with its ability to improve compromised TJs in DSS-induced UC.

Taken together, MOLP alleviated colonic pathological alterations, decreased goblet cells, crypt destruction, and infiltration of inflammatory cells caused by DSS. MOLP suppressed the loss of ZO-1 and occludin proteins in mucosal layer and the production of TNF- α , IL-1 β and HMGB1. Furthermore, MOLP increased the mRNA expression of IL-10 and PPAR- γ , and decreased the activation of TLR4, MyD88, NF- κ B signaling pathway (Figure 7).

Conclusion

Our study confirmed that the polysaccharide obtained from *M. oleifera* leaf exhibited prophylactic efficacies on DSS-induced UC by reducing intestinal damage, suppressing the activation of

TLR4/MyD88/NF- κ B signaling pathway, as well as the release of cytokines that promote inflammation, whereas maintaining the goblet cells and expression of TJ proteins. These findings will make a better understanding of the protective action of MOLP against UC, thereby providing a rationale for the development of MOLP.

Data availability statement

The original data presented in this study are included in the **Supplementary material**, further inquiries can be directed to the corresponding authors.

Ethics statement

This animal study was reviewed and approved by the Institutional Animal Care and Use Committees (IACUC) of Yangzhou University.

Author contributions

HM: conceptualization, methodology, software, data curation, and writing—original draft. WP: conceptualization, methodology, investigation, software, data curation, writing—original draft, and visualization. HS and RZ: methodology, investigation, and writing—original draft. YT: investigation and software. JH: visualization and investigation. ML: supervision. RB and JL: conceptualization, methodology, project administration, and funding acquisition. All authors contributed to the article and approved the submitted version.

Funding

This work was supported by the National Natural Science Foundation of China (Grant Nos. 32072911 and 32002324),

the Natural Science Foundation of Jiangsu Province (Grant No. BK2020945), the Innovation and entrepreneurship training program for college students of Yangzhou University (C202211117026Y), and the Priority Academic Program Development of Jiangsu Higher Education Institutions (PAPD).

Acknowledgments

We are grateful to all of the other staff members and students at the department of Traditional Chinese Veterinary Medicine (TCVM) at Yangzhou University for their assistance in the experiments.

Conflict of interest

The authors declare that the research was conducted in the absence of any commercial or financial relationships that could be construed as a potential conflict of interest.

Publisher's note

All claims expressed in this article are solely those of the authors and do not necessarily represent those of their affiliated organizations, or those of the publisher, the editors and the reviewers. Any product that may be evaluated in this article, or claim that may be made by its manufacturer, is not guaranteed or endorsed by the publisher.

Supplementary material

The Supplementary Material for this article can be found online at: <https://www.frontiersin.org/articles/10.3389/fnut.2022.1055791/full#supplementary-material>

References

1. Niu W, Chen X, Xu R, Dong H, Yang F, Wang Y, et al. Polysaccharides from natural resources exhibit great potential in the treatment of ulcerative colitis: a review. *Carbohydr Polym.* (2021) 254:117189. doi: 10.1016/j.carbpol.2020.117189
2. Bernstein CN. Treatment of IBD: where we are and where we are going. *Am J Gastroenterol.* (2015) 110:114–26. doi: 10.1038/ajg.2014.357
3. Alex PNC, Zachos T, Nguyen L, Gonzales TE, Chen LS, Conklin M, et al. Distinct cytokine patterns identified from multiplex profiles of murine DSS and TNBS-induced colitis. *Inflamm Bowel Dis.* (2009) 15:341–52. doi: 10.1002/ibd.20753
4. Pithadia AB, Jain S. Treatment of inflammatory bowel disease (IBD). *Pharmacol Rep.* (2011) 63:629–42. doi: 10.1016/S1734-1140(11)70575-8
5. Vargas-Robles H, Castro-Ochoa KF, Nava P, Olivares AS, Schnoor M. Beneficial effects of nutritional supplements on intestinal epithelial barrier functions in experimental colitis models in vivo. *World J Gastroenterol.* (2019) 25:4181–98. doi: 10.3748/wjg.v25.i30.4181
6. Piechota-Polanczyk A, Fichna J. Review article: the role of oxidative stress in pathogenesis and treatment of inflammatory bowel diseases. *Naunyn Schmiedeberg Arch Pharmacol.* (2014) 387:605–20. doi: 10.1007/s00210-014-0985-1
7. Cui C, Chen S, Wang X, Yuan G, Jiang F, Chen X, et al. Characterization of *Moringa oleifera* roots polysaccharide MRP-1 with anti-inflammatory effect. *Int J Biol Macromol.* (2019) 132:844–51. doi: 10.1016/j.ijbiomac.2019.03.210

8. Yassa HD, Tohamy AF. Extract of *Moringa oleifera* leaves ameliorates streptozotocin-induced diabetes mellitus in adult rats. *Acta Histochem.* (2014) 116:844–54. doi: 10.1016/j.acthis.2014.02.002
9. Sharma K, Kumar M, Waghmare R, Suhag R, Gupta OP, Lorenzo J, et al. *Moringa (Moringa oleifera Lam.) polysaccharides: extraction, characterization, bioactivities, and industrial application.* *Int J Biol Macromol.* (2022) 209:763–78. doi: 10.1016/j.ijbiomac.2022.04.047
10. Yang M, Tao L, Kang XR, Li LF, Zhao CC, Wang ZL, et al. Recent developments in *Moringa oleifera* Lam. polysaccharides: a review of the relationship between extraction methods, structural characteristics and functional activities. *Food Chem X.* (2022) 14:100322. doi: 10.1016/j.fochx.2022.100322
11. He T, Huang Y, Huang Y, Wang X, Hu J, Sheng J. Structural elucidation and antioxidant activity of an arabinogalactan from the leaves of *Moringa oleifera*. *Int J Biol Macromol.* (2018) 112:126–33. doi: 10.1016/j.ijbiomac.2018.01.110
12. Dong Z, Li C, Huang Q, Zhang B, Fu X, Liu RH. Characterization of a novel polysaccharide from the leaves of *Moringa oleifera* and its immunostimulatory activity. *J Funct Foods.* (2018) 49:391–400. doi: 10.1016/j.jff.2018.09.002
13. Li L, Ma L, Wen Y, Xie J, Yan L, Ji A, et al. Crude polysaccharide extracted from *Moringa oleifera* leaves prevents obesity in association with modulating gut microbiota in high-fat diet-fed mice. *Front Nutr.* (2022) 9:861588. doi: 10.3389/fnut.2022.861588
14. Zhang YJ, Zhang LX, Yang JF, Liang ZY. Structure analysis of water-soluble polysaccharide CPPS3 isolated from *Codonopsis pilosula*. *Fitoterapia.* (2010) 81:157–61. doi: 10.1016/j.fitote.2009.08.011
15. Zheng Z, Huang Q, Ling C. Water-soluble yeast β -glucan fractions with different molecular weights: extraction and separation by acidolysis assisted-size exclusion chromatography and their association with proliferative activity. *Int J Biol Macromol.* (2018) 123:269–79. doi: 10.1016/j.ijbiomac.2018.11.020
16. Cooper HS, Murthy SN, Shah RS, Sedergran DJ. Clinicopathologic study of dextran sulfate sodium experimental murine colitis. *Lab Invest.* (1993) 69:238–49. doi: 10.1016/S0021-5198(19)41298-5
17. Cai X, Han Y, Gu M, Song M, Wu X, Li Z, et al. Dietary cranberry suppressed colonic inflammation and alleviated gut microbiota dysbiosis in dextran sodium sulfate-treated mice. *Food Funct.* (2019) 10:6331–41. doi: 10.1039/c9fo01537j
18. Yu Y, Zhang Y, Hu C, Zou X, Lin Y, Xia Y, et al. Chemistry and immunostimulatory activity of a polysaccharide from *Undaria pinnatifida*. *Food Chem Toxicol.* (2019) 128:119–28. doi: 10.1016/j.fct.2019.03.042
19. Chen C, Zhang B, Huang Q, Fu X, Liu RH. Microwave-assisted extraction of polysaccharides from *Moringa oleifera* Lam. leaves: characterization and hypoglycemic activity. *Indust Crops Prod.* (2017) 100:1–11. doi: 10.1016/j.indcrop.2017.01.042
20. Li C, Dong Z, Zhang B, Huang Q, Liu G, Fu X. Structural characterization and immune enhancement activity of a novel polysaccharide from *Moringa oleifera* leaves. *Carbohydr Polym.* (2020) 234:115897. doi: 10.1016/j.carbpol.2020.115897
21. Yu D, Yan Y, Dan C, Ran L, Mi J, Lu L, et al. Modulating effects of polysaccharides from the fruits of *Lycium barbarum* on immune response and gut microbiota in cyclophosphamide-treated mice. *Food Funct.* (2019) 10:3671. doi: 10.1039/C9FO00638A
22. Tian M, Ma P, Zhang Y, Mi Y, Fan D. Ginsenoside Rk3 alleviated DSS-induced ulcerative colitis by protecting colon barrier and inhibiting NLRP3 inflammasome pathway. *Int Immunopharmacol.* (2020) 85:106645. doi: 10.1016/j.intimp.2020.106645
23. Zhang YJ, Peng L, Li WY, Dai TY, Nie L, Xie J, et al. Polyphenol extract of *Moringa oleifera* leaves alleviates colonic inflammation in dextran sulfate sodium-treated mice. *Evid Based Complement Alternat Med.* (2020) 2020:6295402. doi: 10.1155/2020/6295402
24. Chen C, Su X, Hu Z. Immune promotive effect of bioactive peptides may be mediated by regulating the expression of SOCS1/miR-155. *Exp Ther Med.* (2019) 18:1850–62. doi: 10.3892/etm.2019.7734
25. Sheng K, Zhang G, Sun M, He S, Kong X, Wang J, et al. Grape seed proanthocyanidin extract ameliorates dextran sulfate sodium-induced colitis through intestinal barrier improvement, oxidative stress reduction, and inflammatory cytokines and gut microbiota modulation. *Food Funct.* (2020) 11:7817–29. doi: 10.1039/d0fo01418d
26. Fournier BM, Parkos CA. The role of neutrophils during intestinal inflammation. *Mucosal Immunol.* (2012) 5:354–66. doi: 10.1038/mi.2012.24
27. Hong ZS, Xie J, Wang XF, Dai JJ, Mao JY, Bai YY, et al. *Moringa oleifera* Lam. peptide remodels intestinal mucosal barrier by inhibiting JAK-STAT activation and modulating gut microbiota in colitis. *Front Immunol.* (2022) 13:924178. doi: 10.3389/fimmu.2022.924178
28. Aratani Y. Myeloperoxidase: its role for host defense, inflammation, and neutrophil function. *Arch Biochem Biophys.* (2018) 640:47–52. doi: 10.1016/j.abb.2018.01.004
29. Santos-Oliveira JR, Regis EG, Leal CRB, Cunha RV, Bozza PT, Da Cruz AM. Evidence that lipopolysaccharide may contribute to the cytokine storm and cellular activation in patients with visceral leishmaniasis. *PLoS Negl Trop Dis.* (2011) 5:e1198. doi: 10.1371/journal.pntd.0001198
30. Chelakkot C, Ghim J, Ryu SH. Mechanisms regulating intestinal barrier integrity and its pathological implications. *Exp Mol Med.* (2018) 50:1–9. doi: 10.1038/s12276-018-0126-x
31. Pugliese D, Felice C, Papa A, Gasbarrini A, Rapaccini G, Guidi L, et al. Anti TNF- α therapy for ulcerative colitis: current status and prospects for the future. *Expert Rev Clin Immunol.* (2017) 13:223–33. doi: 10.1080/1744666X.2017.1243468
32. Al-kuraishy HM, Al-Gareeb AI, Alkazmi L, Habotta OA, Batiha GE. High-mobility group box 1 (HMGB1) in COVID-19: extrapolation of dangerous liaisons. *Inflammopharmacol.* (2022) 30:811–20. doi: 10.1007/s10787-022-00988-y
33. Yin S, Yang H, Tao Y, Wei S, Li L, Liu M, et al. Artesunate ameliorates DSS-induced ulcerative colitis by protecting intestinal barrier and inhibiting inflammatory response. *Inflammation.* (2020) 43:765–76. doi: 10.1007/s10753-019-01164-1
34. Simon JM, Davis JP, Lee SE, Schaner MR, Gipson GR, Weiser M, et al. Alterations to chromatin in intestinal macrophages link IL-10 deficiency to inappropriate inflammatory responses. *Eur J Immunol.* (2016) 46:1912–25. doi: 10.1002/eji.201546237
35. Decara J, Rivera P, López-Gamero AJ, Serrano A, Pavón FJ, Baixeras E, et al. Peroxisome proliferator-activated receptors: experimental targeting for the treatment of inflammatory bowel diseases. *Front Pharmacol.* (2020) 11:730. doi: 10.3389/fphar.2020.00730
36. Yamamoto-Furusho JK, Peñaloza-Coronel A, Sánchez-Muñoz F, Barreto-Zuniga R, Dominguez-Lopez A. Peroxisome proliferator-activated receptor-gamma (PPAR- γ) expression is down-regulated in patients with active ulcerative colitis. *Inflamm Bowel Dis.* (2011) 17:680–1. doi: 10.1002/ibd.21322
37. Dubuquoy L, Jansson EA, Deeb S, Rakotobe S, Karoui M, Colombel JF, et al. Impaired expression of peroxisome proliferator-activated receptor- γ in ulcerative colitis. *Gastroenterology.* (2003) 124:1265–76. doi: 10.1016/S0016-5085(03)00271-3
38. Li J, Zhong W, Wang W, Hu S, Yuan J, Zhang B, et al. Ginsenoside metabolite compound K promotes recovery of dextran sulfate sodium-induced colitis and inhibits inflammatory responses by suppressing NF- κ B activation. *PLoS One.* (2014) 9:e87810. doi: 10.1371/journal.pone.0087810
39. Sahu BD, Kumar J, Sistla M, Fisetin R. A dietary flavonoid, ameliorates experimental colitis in mice: relevance of NF- κ B signaling. *J Nutr Biochem.* (2016) 28:171–82. doi: 10.1016/j.jnutbio.2015.10.004
40. Otani T, Furuse M. Tight junction structure and function revisited. *Trends Cell Biol.* (2020) 30:805–17. doi: 10.1016/j.tcb.2020.10.001
41. Tsukita S, Tanaka H, Tamura A. The Claudins: from tight junctions to biological systems. *Trends Biochem Sci.* (2019) 44:141–52. doi: 10.1016/j.tibs.2018.09.008
42. Alizadeh A, Akbari P, Garssen J, Fink-Gremmels J, Braber S. Epithelial integrity, junctional complexes, and markers associated with intestinal functions. *Tissue Barriers.* (2021) 10:1996830. doi: 10.1080/21688370.2021.1996830
43. Xu Z, Chen W, Deng Q, Huang Q, Wang X, Yang C, et al. Flaxseed oligosaccharides alleviate DSS-induced colitis through modulation of gut microbiota and repair of the intestinal barrier in mice. *Food Funct.* (2020) 11:8077–88. doi: 10.1039/D0FO01105C
44. Nunes C, Freitas V, Almeida L, Laranjinha J. Red wine extract preserves tight junctions in intestinal epithelial cells under inflammatory conditions: implications for intestinal inflammation. *Food Funct.* (2019) 10:1364–74. doi: 10.1039/C8FO02469C



OPEN ACCESS

EDITED BY

Yi Wu,
Nanjing Agricultural University, China

REVIEWED BY

Mingchao Liu,
Agricultural University of Hebei, China
Helen Fu,
Jiangsu Provincial Hospital of
Traditional Chinese Medicine, China

*CORRESPONDENCE

Hao-Yu Liu
haoyu.liu@yzu.edu.cn
Demin Cai
demincai@yzu.edu.cn

[†]These authors have contributed
equally to this work

SPECIALTY SECTION

This article was submitted to
Nutritional Immunology,
a section of the journal
Frontiers in Immunology

RECEIVED 29 October 2022

ACCEPTED 21 November 2022

PUBLISHED 06 December 2022

CITATION

Zhu C, Li K, Peng X-X, Yao T-J,
Wang Z-Y, Hu P, Cai D and Liu H-Y
(2022) Berberine a traditional Chinese
drug repurposing: Its actions in
inflammation-associated ulcerative
colitis and cancer therapy.
Front. Immunol. 13:1083788.
doi: 10.3389/fimmu.2022.1083788

COPYRIGHT

© 2022 Zhu, Li, Peng, Yao, Wang, Hu,
Cai and Liu. This is an open-access
article distributed under the terms of
the [Creative Commons Attribution
License \(CC BY\)](#). The use, distribution
or reproduction in other forums is
permitted, provided the original
author(s) and the copyright owner(s)
are credited and that the original
publication in this journal is cited, in
accordance with accepted academic
practice. No use, distribution or
reproduction is permitted which does
not comply with these terms.

Berberine a traditional Chinese drug repurposing: Its actions in inflammation-associated ulcerative colitis and cancer therapy

Cuipeng Zhu^{1†}, Kaiqi Li^{1†}, Xiao-Xu Peng¹, Tong-Jia Yao¹,
Zi-Yu Wang¹, Ping Hu¹, Demin Cai^{1*} and Hao-Yu Liu^{1,2*}

¹College of Animal Science and Technology, Yangzhou University, Yangzhou, China, ²Joint International Research Laboratory of Agricultural & Agri-Product Safety, The Ministry of Education of China, Yangzhou University, Yangzhou, China

Berberine (BBR), an isoquinoline alkaloid extracted from *Coptidis Rhizoma*, has a long history of treating dysentery in the clinic. Over the past two decades, the polytrophic, pharmacological, and biochemical properties of BBR have been intensively studied. The key functions of BBR, including anti-inflammation, antibacterial, antioxidant, anti-obesity, and even antitumor, have been discovered. However, the underlying mechanisms of BBR-mediated regulation still need to be explored. Given that BBR is also a natural nutrition supplement, the modulatory effects of BBR on nutritional immune responses have attracted more attention from investigators. In this mini-review, we summarized the latest achievements of BBR on inflammation, gut microbes, macrophage polarization, and immune responses associated with their possible tools in the pathogenesis and therapy of ulcerative colitis and cancer in recent 5 years. We also discuss the therapeutic efficacy and anti-inflammatory actions of BBR to benefit future clinical applications.

KEYWORDS

berberine, ulcerative colitis, inflammation, microbes, cancer

Introduction

In modern medicine, natural products are closely linked to numerous health complications treatment and great therapeutic approaches. In particular, the functional metabolites derived from plants are suggested to perform various biological activities involving anti-obesity, anti-inflammation, antibacterial, anti-fatty liver, and anti-cancer (1, 2). Alkaloids act as the chemical defense in plants when producing secondary metabolites with beneficial pharmacological roles and account for 3/5 of plant-derived

medicals. The bioactive components of alkaloids have been used for immunomodulatory therapeutic potentials and anti-inflammation (3). Among them, berberine (BBR) is an isoquinoline alkaloid purified from Chinese herbs and a naturally occurring compound extracted from *Coptidis Rhizoma* (4). In recent years, a series of actions of BBR-mediated anti-intestinal diseases, anti-cancer, antioxidative stress, and anti-inflammatory has been reported *in vivo* and *in vitro* (5–7). Indeed, intestinal disorders and cancer are tightly associated and always characterized by inflammation, oxidative stress, and a couple of immune outputs (8). Inflammation response of the body would benefit the recovery when exposed to infection or invasion events. In this process, immune cells are stimulated by BBR to fight the inflammatory responses in these diseases (9). It has been reported that the potential mechanisms of the anti-inflammation of alkaloids would be attributed to the inhibition of several pro-inflammatory enzyme complexes enrolled in inflammatory signaling processes (10). Moreover, evidence indicates that BBR could ameliorate intestinal lesions and tumor development by reducing macrophage and oxidative stress inflammatory responses (11). The possible underlying mechanisms, in particular, of signaling pathways, have been documented (12). It is plausible that at least part of the observed anti-inflammation roles is due to the activations of classic inflammatory signaling factors, including adenosine monophosphate-activated protein kinase (AMPK) and Wnt/ β -catenin (13). Additionally, the extracellular signal-regulated protein kinase 1/2 (ERK1/2) (14), signal transducer and activator of transcription 1 (STAT1), protein kinase B (AKT), nuclear factor kappa-light-chain-enhancer of activated B cells (NF- κ B), and nitric oxide (NO), prostaglandin E2 (PGE2), along with chemokines and cytokines (15–18) have also been illustrated. Again, the modulation of gut microbes and microphage polarization has previously been registered in BBR-mediated inflammatory regulation (19). This mini-review aims to collect updated information on BBR in the fields of inflammation and immune responses for a better understanding of the potential mechanisms in the pathogenesis process of various human and animal ulcerative colitis (UC) and cancer research. This will encourage researchers to explore further addressing all aspects of the utilization of BBR for new treatments and therapeutic strategies.

BBR in ulcerative colitis-the anti-inflammatory, immunomodulatory effects and potential mechanisms

Ulcerative colitis (UC) is a chronic inflammatory disease of the bowel with unclear etiology. It is characterized by mucous purulent, abdominal pain, and recurrent diarrhea and is a modern refractory disease with an extremely high risk of colorectal cancer (CRC) (20). Currently, immunosuppressants,

anti-inflammatory drugs, and biological agents are the main therapeutic approaches for UC. However, it is still difficult to cure because none of the approaches can reverse the colon injury, and a proportion of patients will have recurrent attacks once ceasing the treatments (21). Emerging evidence suggests that traditional Chinese medicine has positive clinical outputs for UC, including reducing recurrent diarrhea, ameliorating intestinal inflammatory responses, and improving the patient's life quality (22, 23). Given that BBR has a long history in Chinese medicine used as an antibacterial agent to treat dysentery, it is promising to repurpose BBR for UC and other inflammatory-associated diseases. Tang and coworkers have recently demonstrated in a rodent model that oral administration of BBR effectively alleviates animals' colitis symptoms when combined with another Chinese herb *Atractylodes macrocephala* Koidz (24). The underlying mechanisms involve local- and systemic regulations of the immune system, including the reduced pro-inflammatory cytokines IL-4, IL-6, IL-1 β , TNF- α , and myeloperoxidase (MPO), and IgA, IgG levels. Indeed, large-scale genome-wide association studies (GWAS) revealed hundreds of loci associated with UC and implicated genes and core cytokines pathways underlying inflammatory pathology. Such as IFN- γ , IL-17, and IL-13, *etc.*, by which immune cells coordinate their functions and intercellular communications (25). In the dextran sulfate sodium (DSS)-induced colitis mice model, treatment of BBR attenuated all pathologic alterations, especially the suppression of the IFN- γ signaling pathway. BBR treatment consistently down-regulated the IFN- γ targeted genes (*e.g.*, *IRF8*, *IRF1*, *Ifit1* and *Ifit3*) in UC mice. In addition, BBR markedly decreased serum pro-inflammatory cytokines/chemokines IL-17, TNF- α , CXCL1, and CXCL9 levels (26). In contrast, studies demonstrate that BBR can block the excessive pro-inflammatory cytokine production in UC rodents *via* the IL-6/STAT3/NF- κ B signaling pathway (27, 28). Following this signaling, BBR exerts antiseptis and antioxidative stress activities by affecting mucosal immunity while improving gut barrier function (27–29). Moreover, the Wnt/ β -catenin signaling is pivotal for intestinal epithelial homeostasis and tissue regeneration and is dysregulated during inflammatory responses (30). In line with this, Dong et al. demonstrated that BBR acts as an effective drug for UC treatment in a Wnt/ β -catenin signaling-dependent manner (31) where BBR administration maintained intestinal mucosal barrier homeostasis and modulated the colonic T cell response, including the transcription and populations of Th17 and regulatory T cells (Treg).

Notably, in the phase I clinical trial, BBR is shown to lower the Geboes Score (GS, a histological score as a UC indicator) in UC patients from a Chinese cohort (32). Accordingly, it suggests that the GS lowering, inflammation suppression, and tissue-repairing effects of BBR in UC may be mediated *via* the chemosensory Tuft cells-controlled IL-25/C2/13 immune pathway in the colon tissues (33). Meanwhile, Li et al. reported that BBR reduces the colonic infiltration of neutrophils,

macrophage and dendritic cells, and innate lymphoid cells (ILCs) and decreases NK cell activation in UC (34). It impedes the colitis from further advancing *via* the JAK-STAT, ERK, and AKT signaling in intestinal stromal cells. Moreover, a protective effect is observed where BBR preserves the colonic mucosal tight junction and modifies the Th17/Treg dynamic equilibrium in DSS-induced colitis mice (35). In addition, the crosstalk of enteric glial-intestinal epithelium-immune cells has been suggested in the BBR regulation of colitis, where Th17 inhibition is a key component (36, 37). With a similar pathway, in another intestinal lesion model induced by cecal ligation and puncture, BBR is demonstrated to exert a protective effect on cecal ligation and puncture (CLP)-induced intestinal injury by reducing the pro-inflammatory response (38). The mechanisms of BBR's mediation should result from the accumulated proportion of Treg cells and CTLA-4 linked cell-cell contact pathway. Shaping of intestinal macrophage function is a key element of infection resistance and tissue reparation. Therefore, it plays a dominant role in UC pathogenesis and regulation. In this regard, maintaining macrophage polarization homeostasis is critical for UC treatment (22). It is worth mentioning that BBR has been validated to target macrophage polarization and its downstream regulation in health and inflammation; therefore could be a potential therapeutic approach for UC (20, 39, 40).

Microbiology studies in human and animal models have shown that UC stems from skewed immune responses toward one's commensal microflora or microbiota dysbiosis. In contrast, numerous studies indicate that maintaining gut microbiota homeostasis or providing beneficial microbes/probiotics can substantially improve mucosal barrier function and ameliorate UC (20, 41). Intriguingly, BBR regulates intestinal microbiota, possibly *via* boosting *Blautia* sp., *Lactobacillus* sp., *Bacteroides* sp., *Bifidobacterium* sp., and *Akkermansia* sp. growth while inhibiting the pathogenic bacteria *Enterococci* sp. and *Escherichia coli* in mice with inflammation (42). It is worth noting that BBR has been shown to improve gut tight junction (TJ) protein expression and reduce the Th17/Treg ratio in DSS-induced colitis by promoting intestinal *Bacteroides fragilis* and the associated IL-6 inhibition (35). Again, BBR could modulate intestinal microecology by boosting specific microflora (*e.g.*, *bifidobacteria*), and enriching bacterial fermentation. Therefore, BBR-promoted gut microbiota balance facilitates its protection of intestinal mucosa and barrier integrity in UC (33). Because gut microbiota is vulnerable to high-fat diets, BBR effectively ameliorates the expression of genes involved in short-chain fatty acids synthesis, improves mucosal immunity, and enhances the host inflammatory response against gut lesions induced by the high-fat challenge (43). In contrast, BBR-mediated actions are sensitized to the gut microbiome. For example, BBR weakens the generation of trimethylamine by microbiota to lessen choline-induced atherosclerosis in mice (44). With the enrichment of quote-generating gut microbiome, BBR attenuates ovariectomy-triggered anxiety-like illness. In a human study, BBR exhibits an antidiabetic function in type 2 diabetes by reducing secondary bile acid by repressing

Ruminococcus bromii growth (45). These studies provide clues of BBR-derived regulations *via* gut microbiome in inflammatory-associated diseases. However, the deep mechanism of BBR on the interaction between gut microbiota and colitis still needs to be explored.

The anti-tumor activity of BBR and its potential roles in cancer therapy

The antitumor actions of BBR mainly include inducing tumor cell apoptosis, suppressing cancer cell proliferation *via* cell cycle arrest, autophagy, scavenging free radicals, and inhibiting the metastasis of tumor cells without causing overt side effects on normal cells (46, 47). In comparison, a number of pathways of these actions have been studied such as inhibition of the PI3K/AKT/mTOR, Wnt/ β -catenin, MAPK/ERK, EGF receptor, Her2/neu, and the VEGF receptor signaling along with induction of Cip1/p21, Rb expression, p53, and Kip1/p27. These are associated with BBR's anti-inflammation and antioxidant properties (46, 48). It is well-known that chronic inflammation is one of the main factors to cause human cancers (49). And cancer-linked inflammation indicates the seventh hallmark of cancer development and progress (49). In this process, tumor-infiltrating immune cells produce inflammatory mediators involving cytokines, reactive oxygen species (ROS), and free radicals, resulting in a pre-malignant state (50). Subsequently, the released pro-inflammatory cytokines and growth factors stimulate signaling pathways like PI3K/AKT/mTOR, MAPK/ERK, STAT3, and NF- κ B. By inhibiting these cascades, medicinal plants or their bioactive extracts, including BBR, can have a preventative effect on tumor onsets (51).

Cancer development is observed when AKT/PI3K/mTOR pathway is activated. At the same time, BBR performs a vital function in tumor management by strongly suppressing the PI3K/AKT/mTOR signaling (46). In a study of gastric cancer, BBR is validated to increase cellular apoptosis, blocks PI3K/AKT/mTOR, and causes the dephosphorylation of the AKT and p38 pathways (52). Inflammation-linked cancer could produce several chemokines and cytokines *via* NF- κ B, which directly binds to the specific gene promoters (53). BBR administration efficiently decreases the NF- κ B signaling accompanied by pro-inflammatory cytokines IL-1, IL-6, and TNF- α productions (54). It has been noted that BBR drastically suppresses lung cancer cell proliferation *via* NF- κ B/COX-2 (55). Furthermore, BBR reduces the activation of the NF- κ B pathway *via* enhancing I κ B α and inhibits the elevated phosphorylation of c-Fos/Jun in the scratched cancer cells MDA-MB-231 (56). Again, the pro-inflammatory cytokines, interleukins and TNF- α are all suppressed in response to BBR treatment in TNBC cells, this would further inhibit the tumor metastasis (57). Moreover, BBR blunts cancer metastasis of melanoma cells by the reduction of ERK signaling and the activation of the AMPK pathway (58). In

agreement, BBR-activated AMPK is a dominant reason to inhibit colorectal carcinogenesis, which could suppress the growth of a colon xenograft tumor when AMPK is activated *via* phosphating AMPK signaling at Thr172 (59). Interestingly, p53 and p38 AMPK are also reported functioning in antitumor processes with BBR treatment (60, 61). In contrast, when BBR inhibits the MAPK/mTOR/p70-S6K pathway, gastric cancer cell growth is markedly suppressed due to cytostatic autophagy (62). It is noteworthy that Wnt/ β -catenin signaling activation is strongly associated with CRC initiation (63). BBR presents a strong cytostatic efficiency against human CRC *via* blocking the Wnt/ β -catenin pathway to stimulate the caspase-dependent apoptosis and diminish cancer cell survival (64). This further inhibits the metastasis of CRC because of the cell cycle arrest at G1/S and G2/M phases, DNA damage, and topoisomerase poisoning in colon tumor cells (65).

It suggests that macrophages play complicated roles in cancer depending on cytokines derived from the microenvironment (20). Notably, it has been reported that BBR manipulates the macrophage polarization, reducing the IL-10 and TGF- β pathways in a mouse melanoma model to reinstall their anti-tumor immune responses (66). By increasing the MHC-II and CD40 expression on macrophages, BBR also activates the cytotoxic T lymphocytes (CTL) activity and stimulates the CD4⁺ T-cells derived IFN- γ production (66). Furthermore, BBR performs anti-tumor roles in diffuse large B cell lymphoma (DLBCL) related to rituximab-based immunochemotherapy and CD47-targeted immunotherapy (67). BBA exerts a remarkable synergistic action to enhance the CD47 inhibition resultant-tumor

repression by c-myc and promote the phagocytosis of macrophages (67). Finally, BBR could prevent lung cancer by modulating the peptidylarginine deiminase 4 (PADI4)-related macrophage inflammatory responses by up-regulating CD86 and decreasing CD163 and CD206 in the PADI4 overexpressed macrophages (68).

Gut bacteria are tightly linked to cancer oncogenesis and progression, while BBR has exhibited therapeutic potential in bacteria-induced cancer (69). BBR maintains *Fusobacterium nucleatum*-induced intracellular signaling pathways and reduces the secretion of mucosal immune factors, including IL-21, IL-22, IL-31, and CD40 (70). Therefore, BBR facilitates intestinal microbiota homeostasis by increasing *Tenericutes* and *Verrucomicrobia* populations and reduces *F. nucleatum* colonization. BBR modulates the intestinal microbiome by regulating sodium butyrate production and inhibits colon cancer (71). BBR boosts the α and β diversity of microbiota, and the abundance of Bacteroidetes and Proteobacteria, whereas alters the biomarkers and metabolic outputs of the intestinal microbe and decreases the abundance of *Ruminococcus* (71). Given that immunotherapy is a critical part of cancer treatment, BBR has been validated to function on the immune system, showing great potential in cancer immunotherapy (72). For instance, BBR serves as a dopamine D1- and D2-like receptor antagonist to diminish IL-6, IL-1 β , IFN- γ , and TNF- α production in the LPS-stimulated lymphocytes (73). It is also addressed that BBR boosts autoimmune neuropathy *via* decreasing IL-1 and TNF- α concentrations together with suppressing CD4⁺ T cell

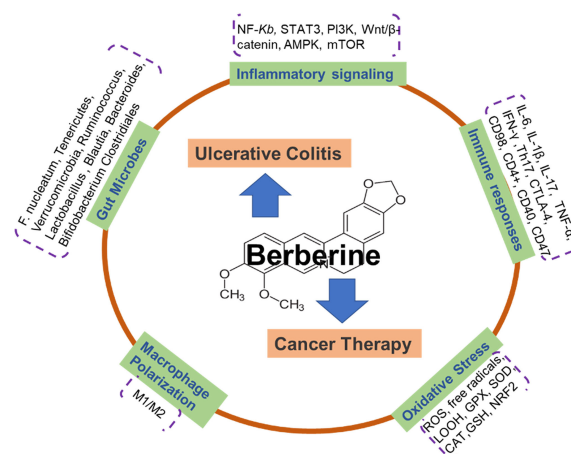


FIGURE 1

Schematic illustration depicting that berberine actions on ulcerative colitis and cancer therapy *via* multiple mechanisms. Berberine is an isoquinoline alkaloid purified from Chinese herbs and a naturally occurring compound extracted from *Coptidis Rhizoma*. There are 5 potential functions of BBR on the treatment of ulcerative colitis and cancer, including: inflammatory signaling pathways (NF- κ B, STAT3, PI3K, Wnt/ β -catenin, AMPK, mTOR); gut microbes (*F. nucleatum*, *Tenericutes*, *Verrucomicrobia*, *Ruminococcus*, *Lactobacillus*, *Blautia*, *Bacteroides*, *Bifidobacterium*, *Clostridiales*); immune responses (IL-6, IL-1 β , IL-17, TNF- α , IFN- γ , Th17, CTLA-4, CD98, CD4⁺, CD40, CD47); macrophage polarization; Oxidative Stress (ROS, free radicals, LOOH, GPX, SOD, CAT, GSH, NRF2).

proliferation (74). Again, IFN- γ -induced indoleamine-2,3-dioxygenase 1 (IDO1) expression is reduced when BBR causes the inhibition of STAT1 phosphorylation (75). Moreover, BBR inhibits the PD-1/PD-L1 pathway by inactivating CSN5 deubiquitination in non-small-cell lung carcinoma (NSCLC) and improves anti-cancer T-cell immunity (9). It suggests a rationale for the therapeutic potential of BBR, which can be used as an efficient antagonist of PD-L1 in cancer immunotherapy.

Conclusions and perspectives

In the past several decades, we have witnessed a tremendous advance in exploring the potential mechanisms behind the pathogenesis of ulcerative colitis and cancer therapy. Nevertheless, the therapeutic approaches are still waiting for the findings of more reliably targetable players and available administrators. BBR is a multi-functional herbal medicine. The characteristics of BBR offer it a pivotal candidate for inflammation-associated UC and cancer treatment and attract more attention to study its targets and modes. In this mini-review, we summarized the latest advances in the main actions of BBR on inflammation and immune responses in UC and cancer research. As shown in the schematic diagram (Figure 1), inflammatory and immune factors include the signaling pathways of MAPK, NF- κ B, Akt, AMPK, and Wnt/ β -catenin interleukins, TNF- α , CD4⁺, CD40, and gut microbes, as well as macrophage polarization, are addressed. Although BBR exerts the marked repression of various targets as aforementioned in basic research, the preventive and therapeutic use of BBR against UC and cancer must be explored and validated in clinical studies.

References

- Chen SR, Dai Y, Zhao J, Lin L, Wang Y, Wang Y. A mechanistic overview of triptolide and celastrol, natural products from tripterygium wilfordii hook f. *Front Pharmacol* (2018) 9:104. doi: 10.3389/fphar.2018.00104
- Ma L, Sun Z, Zeng Y, Luo M, Yang J. Molecular mechanism and health role of functional ingredients in blueberry for chronic disease in human beings. *Int J Mol Sci* (2018) 19(9):2785. doi: 10.3390/ijms19092785
- Song Z, Gao C, Jiang Q, Xu J, Xiong L, Liu K, et al. Diterpenoid alkaloids from delphinium forrestii var. viride and their anti-inflammation activity. *Phytochemistry* (2021) 192:112971. doi: 10.1016/j.phytochem.2021.112971
- Xu Z, Feng W, Shen Q, Yu N, Yu K, Wang S, et al. Rhizoma coptidis and berberine as a natural drug to combat aging and aging-related diseases via anti-oxidation and AMPK activation. *Aging Dis* (2017) 8(6):760–77. doi: 10.14336/AD.2016.0620
- Song D, Hao J, Fan D. Biological properties and clinical applications of berberine. *Front Med* (2020) 14(5):564–82. doi: 10.1007/s11684-019-0724-6
- Zhang W, Xu JH, Yu T, Chen QK. Effects of berberine and metformin on intestinal inflammation and gut microbiome composition in db/db mice. *BioMed Pharmacother* (2019) 118:109131. doi: 10.1016/j.biopha.2019.109131
- Zhang L, Wu X, Yang R, Chen F, Liao Y, Zhu Z, et al. Effects of berberine on the gastrointestinal microbiota. *Front Cell Infect Microbiol* (2020) 10:588517. doi: 10.3389/fcimb.2020.588517
- Han M, Jung YS, Kim WH, Cheon JH, Park S. Cancer risk in patients with intestinal behcet's disease: A nationwide population-based study. *Gut Liver* (2018) 12(4):433–9. doi: 10.5009/gnl17324
- Liu Y, Liu X, Zhang N, Yin M, Dong J, Zeng Q, et al. Berberine diminishes cancer cell PD-L1 expression and facilitates antitumor immunity via inhibiting the deubiquitination activity of CSN5. *Acta Pharm Sin B* (2020) 10(12):2299–312. doi: 10.1016/j.apsb.2020.06.014
- Angelidis C, Kotsialou Z, Kossyvakis C, Vrettou AR, Zacharoulis A, Kolokathis F, et al. Colchicine pharmacokinetics and mechanism of action. *Curr Pharm Des* (2018) 24(6):659–63. doi: 10.2174/1381612824666180123110042
- Yarmohammadi F, Hayes AW, Karimi G. The therapeutic effects of berberine against different diseases: A review on the involvement of the endoplasmic reticulum stress. *Phytother Res* (2022) 36(8):3215–31. doi: 10.1002/ptr.7539
- Pang B, Zhao LH, Zhou Q, Zhao TY, Wang H, Gu CJ, et al. Application of berberine on treating type 2 diabetes mellitus. *Int J Endocrinol* (2015) 2015:905749. doi: 10.1155/2015/905749
- Vishnoi K, Ke R, Saini KS, Viswakarma N, Nair RS, Das S, et al. Berberine represses beta-catenin translation involving 4E-BPs in hepatocellular carcinoma cells. *Mol Pharmacol* (2021) 99(1):1–16. doi: 10.1124/molpharm.120.000029

Author contributions

DC and H-YL: conceptualization. CZ, KL, PH, XP, ZW, and T-JY: writing the original draft. H-YL, and DC: review and editing. All authors contributed to the article and approved the submitted version.

Funding

This work was supported by the Postgraduate Research & Practice Innovation Program of Yangzhou University (X20211025), the Natural Science Foundation of Jiangsu Province (BK20200932, BK20220582), the Priority Academic Program Development of Jiangsu Higher Education Institutions (PAPD).

Conflict of interest

The authors declare that the research was conducted in the absence of any commercial or financial relationships that could be construed as a potential conflict of interest.

Publisher's note

All claims expressed in this article are solely those of the authors and do not necessarily represent those of their affiliated organizations, or those of the publisher, the editors and the reviewers. Any product that may be evaluated in this article, or claim that may be made by its manufacturer, is not guaranteed or endorsed by the publisher.

14. Ma CY, Shi XY, Wu YR, Zhang Y, Yao YH, Qu HL, et al. Berberine attenuates atherosclerotic lesions and hepatic steatosis in ApoE(-/-) mice by down-regulating PCSK9 via ERK1/2 pathway. *Ann Transl Med* (2021) 9(20):1517. doi: 10.21037/atm-20-8106
15. Li C, Xi Y, Li S, Zhao Q, Cheng W, Wang Z, et al. Berberine ameliorates TNBS induced colitis by inhibiting inflammatory responses and Th1/Th17 differentiation. *Mol Immunol* (2015) 67(2 Pt B):444–54. doi: 10.1016/j.molimm.2015.07.013
16. Zhu L, Han J, Yuan R, Xue L, Pang W. Berberine ameliorates diabetic nephropathy by inhibiting TLR4/NF-kappaB pathway. *Biol Res* (2018) 51(1):9. doi: 10.1186/s40659-018-0157-8
17. Zhou Y, Liu SQ, Yu L, He B, Wu SH, Zhao Q, et al. Berberine prevents nitric oxide-induced rat chondrocyte apoptosis and cartilage degeneration in a rat osteoarthritis model via AMPK and p38 MAPK signaling. *Apoptosis* (2015) 20(9):1187–99. doi: 10.1007/s10495-015-1152-y
18. Wang Y, Zhang S. Berberine suppresses growth and metastasis of endometrial cancer cells via miR-101/COX-2. *BioMed Pharmacother* (2018) 103:1287–93. doi: 10.1016/j.biopha.2018.04.161
19. Wang S, Ren H, Zhong H, Zhao X, Li C, Ma J, et al. Combined berberine and probiotic treatment as an effective regimen for improving postprandial hyperlipidemia in type 2 diabetes patients: a double blinded placebo controlled randomized study. *Gut Microbes* (2022) 14(1):2003176. doi: 10.1080/19490976.2021.2003176
20. Guo F, Cai D, Li Y, Gu H, Qu H, Zong Q, et al. How early-life gut microbiota alteration sets trajectories for health and inflammatory bowel disease? *Front Nutr* (2021) 8:690073. doi: 10.3389/fnut.2021.690073
21. Zhang T, Zhang B, Tian W, Wang F, Zhang J, Ma X, et al. Research trends in ulcerative colitis: A bibliometric and visualized study from 2011 to 2021. *Front Pharmacol* (2022) 13:951004. doi: 10.3389/fphar.2022.951004
22. Yang Z, Lin S, Feng W, Liu Y, Song Z, Pan G, et al. A potential therapeutic target in traditional Chinese medicine for ulcerative colitis: Macrophage polarization. *Front Pharmacol* (2022) 13:999179. doi: 10.3389/fphar.2022.999179
23. Yin J, Wei L, Wang N, Li X, Miao M. Efficacy and safety of adjuvant curcumin therapy in ulcerative colitis: A systematic review and meta-analysis. *J Ethnopharmacol* (2022) 289:115041. doi: 10.1016/j.jep.2022.115041
24. Tang X, Yang M, Gu Y, Jiang L, Du Y, Liu J. Orally deliverable dual-targeted pellets for the synergistic treatment of ulcerative colitis. *Drug Des Devel Ther* (2021) 15:4105–23. doi: 10.2147/DDDT.S322702
25. Graham DB, Xavier RJ. Pathway paradigms revealed from the genetics of inflammatory bowel disease. *Nature* (2020) 578(7796):527–39. doi: 10.1038/s41586-020-2025-2
26. Yang T, Ma X, Wang R, Liu H, Wei S, Jing M, et al. Berberine inhibits IFN-gamma signaling pathway in DSS-induced ulcerative colitis. *Saudi Pharm J* (2022) 30(6):764–78. doi: 10.1016/j.jsps.2022.03.015
27. Zhang LC, Wang Y, Tong LC, Sun S, Liu WY, Zhang S, et al. Berberine alleviates dextran sodium sulfate-induced colitis by improving intestinal barrier function and reducing inflammation and oxidative stress. *Exp Ther Med* (2017) 13(6):3374–82. doi: 10.3892/etm.2017.4402
28. Zhu L, Gu P, Shen H. Protective effects of berberine hydrochloride on DSS-induced ulcerative colitis in rats. *Int Immunopharmacol* (2019) 68:242–51. doi: 10.1016/j.intimp.2018.12.036
29. Wang Y, Du P, Jiang D. Berberine functions as a negative regulator in lipopolysaccharide -induced sepsis by suppressing NF-kappaB and IL-6 mediated STAT3 activation. *Pathog Dis* (2020) 78(7):ftaa047. doi: 10.1093/femspd/ftaa047
30. Moparthi L, Koch S. Wnt signaling in intestinal inflammation. *Differentiation* (2019) 108:24–32. doi: 10.1016/j.diff.2019.01.002
31. Dong Y, Fan H, Zhang Z, Jiang F, Li M, Zhou H, et al. Berberine ameliorates DSS-induced intestinal mucosal barrier dysfunction through microbiota-dependence and wnt/beta-catenin pathway. *Int J Biol Sci* (2022) 18(4):1381–97. doi: 10.7150/ijbs.65476
32. Xu L, Zhang Y, Xue X, Liu J, Li ZS, Yang GY, et al. A phase I trial of berberine in Chinese with ulcerative colitis. *Cancer Prev Res (Phila)* (2020) 13(1):117–26. doi: 10.1158/1940-6207.CAPR-19-0258
33. Xiong X, Cheng Z, Wu F, Hu M, Liu Z, Dong R, et al. Berberine in the treatment of ulcerative colitis: A possible pathway through tuft cells. *BioMed Pharmacother* (2021) 134:111129. doi: 10.1016/j.biopha.2020.111129
34. Li H, Feng C, Fan C, Yang Y, Yang X, Lu H, et al. Intervention of oncostatin m-driven mucosal inflammation by berberine exerts therapeutic property in chronic ulcerative colitis. *Cell Death Dis* (2020) 11(4):271. doi: 10.1038/s41419-020-2470-8
35. Zheng C, Wang Y, Xu Y, Zhou L, Hassan S, Xu G, et al. Berberine inhibits dendritic cells differentiation in DSS-induced colitis by promoting bacteroides fragilis. *Int Immunopharmacol* (2021) 101(Pt A):108329. doi: 10.1016/j.intimp.2021.108329
36. Li YH, Xiao HT, Hu DD, Fatima S, Lin CY, Mu HX, et al. Berberine ameliorates chronic relapsing dextran sulfate sodium-induced colitis in C57BL/6 mice by suppressing Th17 responses. *Pharmacol Res* (2016) 110:227–39. doi: 10.1016/j.phrs.2016.02.010
37. Li H, Fan C, Lu H, Feng C, He P, Yang X, et al. Protective role of berberine on ulcerative colitis through modulating enteric glial cells-intestinal epithelial cells-immune cells interactions. *Acta Pharm Sin B* (2020) 10(3):447–61. doi: 10.1016/j.apsb.2019.08.006
38. He Y, Yuan X, Zuo H, Sun Y, Feng A. Berberine exerts a protective effect on gut-vascular barrier via the modulation of the Wnt/Beta-catenin signaling pathway during sepsis. *Cell Physiol Biochem* (2018) 49(4):1342–51. doi: 10.1159/000493412
39. Noh JW, Jun MS, Yang HK, Lee BC. Cellular and molecular mechanisms and effects of berberine on obesity-induced inflammation. *Biomedicines* (2022) 10(7):1739. doi: 10.3390/biomedicines10071739
40. Liu YC, Hsiao YY, Ku KL, Liao HF, Chao WC. Mahonia oiwakensis extract and its bioactive compounds exert anti-inflammatory activities and VEGF production through M2-macrophagic polarization and STAT6 activation. *J Med Food* (2018) 21(7):654–64. doi: 10.1089/jmf.2017.4084
41. Shen ZH, Zhu CX, Quan YS, Yang ZY, Wu S, Luo WW, et al. Relationship between intestinal microbiota and ulcerative colitis: Mechanisms and clinical application of probiotics and fecal microbiota transplantation. *World J Gastroenterol* (2018) 24(1):5–14. doi: 10.3748/wjg.v24.i1.5
42. Neyrinck AM, Sanchez CR, Rodriguez J, Cani PD, Bindels LB, Delzenne NM. Prebiotic effect of berberine and curcumin is associated with the improvement of obesity in mice. *Nutrients* (2021) 13(5):1436. doi: 10.3390/nu13051436
43. Li J, Li J, Ni J, Zhang C, Jia J, Wu G, et al. Berberine relieves metabolic syndrome in mice by inhibiting liver inflammation caused by a high-fat diet and potential association with gut microbiota. *Front Microbiol* (2021) 12:752512. doi: 10.3389/fmicb.2021.752512
44. Li X, Su C, Jiang Z, Yang Y, Zhang Y, Yang M, et al. Berberine attenuates choline-induced atherosclerosis by inhibiting trimethylamine and trimethylamine-n-oxide production via manipulating the gut microbiome. *NPJ Biofilms Microbiomes* (2021) 7(1):36. doi: 10.1038/s41522-021-00205-8
45. Chou S, Zhang S, Guo H, Chang YF, Zhao W, Mou X. Targeted antimicrobial agents as potential tools for modulating the gut microbiome. *Front Microbiol* (2022) 13:879207. doi: 10.3389/fmicb.2022.879207
46. Li G, Zhang C, Liang W, Zhang Y, Shen Y, Tian X. Berberine regulates the Notch1/PTEN/PI3K/AKT/mTOR pathway and acts synergistically with 17-AAG and SAHA in SW480 colon cancer cells. *Pharm Biol* (2021) 59(1):21–30. doi: 10.1080/13880209.2020.1865407
47. Tai CJ, Jassey A, Liu CH, Tai CJ, Richardson CD, Wong SH, et al. Targeting autophagy augments BBR-mediated cell death in human hepatoma cells harboring hepatitis c virus RNA. *Cells* (2020) 9(4):908. doi: 10.3390/cells9040908
48. Hesari A, Ghasemi F, Cicero AFG, Mohajeri M, Rezaei O, Hayat SMG, et al. Berberine: A potential adjunct for the treatment of gastrointestinal cancers? *J Cell Biochem* (2018) 119(12):9655–63. doi: 10.1002/jcb.27392
49. Singh N, Baby D, Rajguru JP, Patil PB, Thakkannavar SS, Pujari VB. Inflammation and cancer. *Ann Afr Med* (2019) 18(3):121–6. doi: 10.4103/aam.aam_56_18
50. Kennel KB, Greten FR. Immune cell - produced ROS and their impact on tumor growth and metastasis. *Redox Biol* (2021) 42:101891. doi: 10.1016/j.redox.2021.101891
51. Xia Y, Chen S, Cui J, Wang Y, Liu X, Shen Y, et al. Berberine suppresses bladder cancer cell proliferation by inhibiting JAK1-STAT3 signaling via upregulation of miR-17-5p. *Biochem Pharmacol* (2021) 188:114575. doi: 10.1016/j.bcp.2021.114575
52. Kou Y, Tong B, Wu W, Liao X, Zhao M. Berberine improves chemosensitivity to cisplatin by enhancing cell apoptosis and repressing PI3K/AKT/mTOR signaling pathway in gastric cancer. *Front Pharmacol* (2020) 11:616251. doi: 10.3389/fphar.2020.616251
53. Filippi I, Carraro F, Naldini A. Interleukin-1beta affects MDAMB231 breast cancer cell migration under hypoxia: Role of HIF-1alpha and NFkappaB transcription factors. *Mediators Inflammation* (2015) 2015:789414. doi: 10.1155/2015/789414
54. Almatroodi SA, Alsahli MA, Rahmani AH. Berberine: An important emphasis on its anticancer effects through modulation of various cell signaling pathways. *Molecules* (2022) 27(18):5889. doi: 10.3390/molecules27185889
55. Fu L, Chen W, Guo W, Wang J, Tian Y, Shi D, et al. Berberine targets AP-2/hTERT, NF-kappaB/COX-2, HIF-1alpha/VEGF and cytochrome-c/Caspase signaling to suppress human cancer cell growth. *PloS One* (2013) 8(7):e69240. doi: 10.1371/journal.pone.0069240
56. Zhao L, Zhang C. Berberine inhibits MDA-MB-231 cells by attenuating their inflammatory responses. *BioMed Res Int* (2020) 2020:3617514. doi: 10.1155/2020/3617514

57. Yao M, Fan X, Yuan B, Takagi N, Liu S, Han X, et al. Berberine inhibits NLRP3 inflammasome pathway in human triple-negative breast cancer MDA-MB-231 cell. *BMC Complement Altern Med* (2019) 19(1):216. doi: 10.1186/s12906-019-2615-4
58. Liu JF, Lai KC, Peng SF, Maraming P, Huang YP, Huang AC, et al. Berberine inhibits human melanoma A375.S2 cell migration and invasion via affecting the FAK, uPA, and NF-kappaB signaling pathways and inhibits PLX4032 resistant A375.S2 cell migration *in vitro*. *Molecules* (2018) 23(8):2019. doi: 10.3390/molecules23082019
59. Li W, Hua B, Saud SM, Lin H, Hou W, Matter MS, et al. Berberine regulates AMP-activated protein kinase signaling pathways and inhibits colon tumorigenesis in mice. *Mol Carcinog* (2015) 54(10):1096–109. doi: 10.1002/mc.22179
60. Zhang X, Gu L, Li J, Shah N, He J, Yang L, et al. Degradation of MDM2 by the interaction between berberine and DAXX leads to potent apoptosis in MDM2-overexpressing cancer cells. *Cancer Res* (2010) 70(23):9895–904. doi: 10.1158/0008-5472.CAN-10-1546
61. Wang ZS, Lu FE, Xu LJ, Dong H. Berberine reduces endoplasmic reticulum stress and improves insulin signal transduction in hep G2 cells. *Acta Pharmacol Sin* (2010) 31(5):578–84. doi: 10.1038/aps.2010.30
62. Zhang Q, Wang X, Cao S, Sun Y, He X, Jiang B, et al. Berberine represses human gastric cancer cell growth *in vitro* and *in vivo* by inducing cytostatic autophagy via inhibition of MAPK/mTOR/p70S6K and akt signaling pathways. *BioMed Pharmacother* (2020) 128:110245. doi: 10.1016/j.biopha.2020.110245
63. Bian J, Dannappel M, Wan C, Firestein R. Transcriptional regulation of wnt/beta-catenin pathway in colorectal cancer. *Cells* (2020) 9(9):2125. doi: 10.3390/cells9092125
64. Jiang X, Jiang Z, Jiang M, Sun Y. Berberine as a potential agent for the treatment of colorectal cancer. *Front Med (Lausanne)* (2022) 9:886996. doi: 10.3389/fmed.2022.886996
65. Liu Y, Hua W, Li Y, Xian X, Zhao Z, Liu C, et al. Berberine suppresses colon cancer cell proliferation by inhibiting the SCAP/SREBP-1 signaling pathway-mediated lipogenesis. *Biochem Pharmacol* (2020) 174:113776. doi: 10.1016/j.bcp.2019.113776
66. Shah D, Challagundla N, Dave V, Patidar A, Saha B, Nivsarkar M, et al. Berberine mediates tumor cell death by skewing tumor-associated immunosuppressive macrophages to inflammatory macrophages. *Phytomedicine* (2021) 99:153904. doi: 10.1016/j.phymed.2021.153904
67. Ren S, Cai Y, Hu S, Liu J, Zhao Y, Ding M, et al. Berberine exerts antitumor activity in diffuse large b-cell lymphoma by modulating c-myc/CD47 axis. *Biochem Pharmacol* (2021) 188:114576. doi: 10.1016/j.bcp.2021.114576
68. Gu W, Zhang M, Gao F, Niu Y, Sun L, Xia H, et al. Berberine regulates PADI4-related macrophage function to prevent lung cancer. *Int Immunopharmacol* (2022) 110:108965. doi: 10.1016/j.intimp.2022.108965
69. Chen H, Ye C, Cai B, Zhang F, Wang X, Zhang J, et al. Berberine inhibits intestinal carcinogenesis by suppressing intestinal pro-inflammatory genes and oncogenic factors through modulating gut microbiota. *BMC Cancer* (2022) 22(1):566. doi: 10.1186/s12885-022-09635-9
70. Li S, Liu J, Zheng X, Ren L, Yang Y, Li W, et al. Tumorigenic bacteria in colorectal cancer: mechanisms and treatments. *Cancer Biol Med* (2021) 19(2):147–162. doi: 10.20892/j.issn.2095-3941.2020.0651
71. Huang C, Sun Y, Liao SR, Chen ZX, Lin HF, Shen WZ. Suppression of berberine and probiotics (*in vitro* and *in vivo*) on the growth of colon cancer with modulation of gut microbiota and butyrate production. *Front Microbiol* (2022) 13:869931. doi: 10.3389/fmicb.2022.869931
72. Wang YX, Pang WQ, Zeng QX, Deng ZS, Fan TY, Jiang JD, et al. Synthesis and biological evaluation of new berberine derivatives as cancer immunotherapy agents through targeting IDO1. *Eur J Med Chem* (2018) 143:1858–68. doi: 10.1016/j.ejmech.2017.10.078
73. Kawano M, Takagi R, Kaneko A, Matsushita S. Berberine is a dopamine D1- and D2-like receptor antagonist and ameliorates experimentally induced colitis by suppressing innate and adaptive immune responses. *J Neuroimmunol* (2015) 289:43–55. doi: 10.1016/j.jneuroim.2015.10.001
74. Li H, Li XL, Zhang M, Xu H, Wang CC, Wang S, et al. Berberine ameliorates experimental autoimmune neuritis by suppressing both cellular and humoral immunity. *Scand J Immunol* (2014) 79(1):12–9. doi: 10.1111/sji.12123
75. Sharma A, Tirpude NV, Bhardwaj N, Kumar D, Padwad Y. Berberis lycium fruit extract and its phytoconstituents berberine and rutin mitigate collagen-CFA-induced arthritis (CIA) via improving GSK3beta/STAT/Akt/MAPKs/NF-kappaB signaling axis mediated oxi-inflammation and joint articular damage in murine model. *Inflammopharmacology* (2022) 30(2):655–66. doi: 10.1007/s10787-022-00941-z



OPEN ACCESS

EDITED BY

Guiyan Yang,
University of California, Davis,
United States

REVIEWED BY

Nagmeldin A Omer,
University of Gezira, Sudan
Dandan Han,
China Agricultural University, China

*CORRESPONDENCE

Demin Cai
✉ demincai@yzu.edu.cn
Wenbin Bao
✉ wbbao@yzu.edu.cn
Hao-Yu Liu
✉ haoyu.liu@yzu.edu.cn

SPECIALTY SECTION

This article was submitted to
Nutritional Immunology,
a section of the journal
Frontiers in Immunology

RECEIVED 18 November 2022

ACCEPTED 09 December 2022

PUBLISHED 04 January 2023

CITATION

Qu H, Zong Q, Hu P, Li Z, Wang H,
Wu S, Liu H-Y, Bao W and Cai D
(2023) Desmosterol: A natural product
derived from macroalgae modulates
inflammatory response and oxidative
stress pathways in intestinal
epithelial cells.
Front. Immunol. 13:1101643.
doi: 10.3389/fimmu.2022.1101643

COPYRIGHT

© 2023 Qu, Zong, Hu, Li, Wang, Wu,
Liu, Bao and Cai. This is an open-access
article distributed under the terms of
the [Creative Commons Attribution
License \(CC BY\)](#). The use, distribution
or reproduction in other forums is
permitted, provided the original
author(s) and the copyright owner(s)
are credited and that the original
publication in this journal is cited, in
accordance with accepted academic
practice. No use, distribution or
reproduction is permitted which does
not comply with these terms.

Desmosterol: A natural product derived from macroalgae modulates inflammatory response and oxidative stress pathways in intestinal epithelial cells

Huan Qu¹, Qiufang Zong¹, Ping Hu¹, Zhaojian Li¹,
Haifei Wang^{1,2}, Shenglong Wu^{1,2}, Hao-Yu Liu^{1,2*},
Wenbin Bao^{1,2*} and Demin Cai^{1,2*}

¹College of Animal Science and Technology, Yangzhou University, Yangzhou, China, ²Joint International Research Laboratory of Agriculture & Agri-Product Safety, Yangzhou University, Yangzhou, Jiangsu, China

The serum level of cholesterol and its biosynthetic intermediates are critical indicators to access metabolism-related disorders in humans and animals. However, the molecular actions of these intermediates on gene functions and regulation remained elusive. Here, we show that desmosterol (DES) is the most abundant intermediate involved in cholesterol biosynthesis and is highly enriched in red/brown algae. It exerts a pivotal role in modulating core genes involved in oxidative stress and inflammatory response processes in the ileum epithelial cells (IPI-2I). We observed that the DES extracted from red algae did not affect IPI-2I cell growth or survival. A transcriptomic measurement revealed that the genes enrolled in the oxidative process and cholesterol homeostasis pathway were significantly down-regulated by DES treatment. Consistent with this notion, cellular reactive oxygen species (ROS) levels were markedly decreased in response to DES treatment. In contrast, key inflammatory genes including *IL-6*, *TNF- α* , and *IFN- γ* were remarkably upregulated in the RNA-seq analysis, as further confirmed by qRT-PCR. Given that DES is a specific agonist of nuclear receptor ROR γ , we also found that DES caused the elevated expression of ROR γ at mRNA and protein levels, suggesting it is a potential mediator under DES administration. Together, these results underscore the vital physiological actions of DES in inflammatory and oxidative processes possibly via ROR γ , and may be helpful in anti-oxidation treatment and immunotherapy in the future.

KEYWORDS

desmosterol, algae extracts, inflammatory response, oxidative stress, ROR γ

1 Introduction

Red algae are ubiquitous marine macroalgae that have developed bioactive plasticity and compound diversity. It is known that desmosterol (DES) is a dominating sterol in red macroalgae with 87–93% of total sterol contents (187–337 $\mu\text{g/g}$ dry weight) (1). Sterols are fundamental components of cell membranes' phospholipid bilayer that include molecules (such as cholesterol and DES) and are responsible for structural and functional roles. DES, a biosynthetic cholesterol intermediate of the Bloch pathway, plays essential roles in some specific circumstances. DES may contribute to cell membrane fluidity and promote sperm maturation. For instance, DES accounts for 25% of sperm sterol in males (2), and the proportion reaches 60% in several animals (3). Furthermore, DES maintains cell proliferation and survival with or without cholesterol supplementation in *Dhcr24*-defective J774 cells (4). Interestingly, DES acts as a precursor of steroidogenesis even better than cholesterol (4). Additionally, biosynthetic DES is an emergent regulator of macrophages during the process of lipid overload (5). Although a number of biological functions have been reported, the molecular actions of DES on gene functions and its direct regulation have remained elusive.

Cholesterol deposition or prolongation facilitates a progressive inflammatory response and immune response associated with disease development (6). Specifically, the innate immune system amplifies the inflammatory signal by modulating cholesterol homeostasis (6). Notably, the balance of cholesterol metabolism protects cells from oxidative stress by reinforcing cell membranes to limit oxygen availability (7). Interleukin-17 (IL-17)-producing T helper 17 (Th17) cells fulfill an essential role in immune induction and mediation of tissue-resident homeostasis (8). In the intestine, Th17 cells contribute to maintaining the integrity of the intestinal barrier (9) and are implicated in oxidative stress generated by imbalanced oxidative phosphorylation (OXPHOS) (8). As the last intermediate in cholesterol biosynthesis, DES may have alternative effects to cholesterol due to their similar molecular structure. Accordingly, besides involving cholesterol-mediated oxidative stress and inflammatory responses, DES also functions as an endogenous ligand for Th17-targeted key transcription factor ROR γ t (10). Therefore, the effects of DES on intestinal cell inflammation and oxidative stress pathways deserve further attention.

To explore the molecular regulation actions in the gut, we investigated the potential of DES in core genes involved in the inflammatory response and oxidative stress in the porcine ileum epithelial cells (IPI-2I). We isolated and extracted DES from red macroalgae to generate the natural compounds for cell treatment. The transcriptomic analysis and molecular biological validations were used to evaluate the transcriptional modulation of DES in IPI-2I. Pigs are biomedical models for humans owing to the similarities in physiology and metabolism (11). Thus, our study would provide new insights for further understanding DES physiological functions to benefit human intestinal health through anti-oxidation or immunotherapy.

2 Materials and methods

2.1 Samples, chemicals, and standards

For sample preparation, the amounts of crude powders (500 g) of macroalgae were sieved and placed into a conical flask, and 95% ethanol was added. Then, the mixed solution was extracted by ultrasound at 60°C for 1 h. Continuous extraction and concentration until ethanol is wholly volatilized. Next, the concentrated extract was successively extracted with an equal volume of petroleum ether, dichloromethane, ethyl acetate, and n-butanol. Further, the organic phase of ethyl acetate was collected and concentrated for DES extraction.

All solvents and reagents were analytical grade or better: 95% ethanol, petroleum ether, dichloromethane, ethyl acetate, n-butanol, methanol, formic acid, acetonitrile, and DES standards (GlpBio, Shanghai, China). The stock solution concentration was calculated considering the purity of commercial standards. Work standard solutions were prepared from the stock solution and diluted with methanol before analysis. Stock solutions containing 1 mL of ethyl acetate were prepared in HPLC-grade methanol. Linear calibration curves ($y=189476x+24442$) were obtained in the tested concentration ranges for the samples.

2.2 LC-MS evaluation of DES content in ethyl acetate extraction solution

DES extractions from macroalgae were determined by a triple quadrupole mass spectrometer LCMS-8050 (Shimadzu, Kyoto, Japan). HSS T3 analytical columns (2.1 mm \times 50 mm, 1.8 μm) were used by chromatographic separation, along with 0.4 mL/min flow rate at 40°C. Formic acid in water (0.1%, v/v, solvent A) and acetonitrile (solvent B) were performed as the mobile phase. Solvent A gradient of 0.5 min 25% solvent B, 2 min 25–95% solvent B, 1 min 95% solvent B, 0.1 min 95–25% solvent B, and 2.4 min 25% solvent B was used. The optimized mass parameters: nebulizing gas flow (3 L/min), drying gas flow (15 L/min), interface voltage (3.5 kV), collision-induced dissociation argon gas pressure (270 kPa), desolvation line temperature (250°C), and heat block temperature (400°C). The mass transition for DES was set as m/z 383.25 $>$ 113.20 (-).

2.3 Cell culture and cell counting experiment

IPI-2I is obtained from the European Collection of Authenticated Cell Cultures (ECACC). IPI-2I cells were maintained in regular RPMI-1640 medium (Hyclone, UT, USA) supplemented with 10% FBS (Gibco, NY, USA) and 100 mg/mL penicillin-streptomycin (Solarbio, Beijing, China) at 37°C in a 5% CO₂ humidified atmosphere.

IPI-2I cells were seeded in the 12-well culture plates at a density of 1.5×10^5 cells/well for 12 h and divided into the vehicle group and DES group. The concentration of 5 μ M/10 μ M DES or DMSO was treated in the indicated wells for another 72 h. The viable cell numbers were counted at 0, 24, 48, and 72 h with a hemocytometer chamber under the microscope.

2.4 Cell counting kit-8 assay

To further assess cell viability, cells were seeded in 96-well culture plates at approximately 5×10^3 cells/well in 100 μ L of the medium. After 3 days of indicated treatment, 10 μ L CCK-8 solution (Dojindo Molecular Technologies Inc., Kumamoto, Japan) and 90 μ L Opti-MEM (Gibco, NY, USA) were added to each well with incubation at 37°C for 3 h. Then, a multimode microplate reader determined the absorbance at 450 nm (Spark™ 10M, Tecan GmbH, Austria).

2.5 Real-time quantitative PCR

Total RNA extracted from IPI-2I cells using TRIzol Reagent (Takara Biotech, Dalian, China) was reverse-transcribed into cDNA using HiScript® II Q Select R.T. SuperMix (Vazyme, Nanjing, China) according to the manufacturer's instructions and previous

report (12, 13). qRT-PCR analysis was performed by an ABI StepOne Plus Real-Time PCR System (Applied Biosystems, CA, USA) using AceQ® qPCR SYBR Green Master Mix (Vazyme, Nanjing, China). The sequences of primers are exhibited in Table 1. The results of relative gene expression were normalized to *GAPDH* and were calculated using the $2^{-\Delta\Delta CT}$ method.

2.6 RNA-seq analysis

Total RNA was extracted from the IPI-2I cells in the vehicle and DES groups. The concentration of RNA was measured with a NanoDrop 2000 spectrophotometer (ThermoFisher Scientific, CA, USA), and its quality was evaluated with an Agilent Bioanalyzer 2100 system (Agilent Technologies, CA, USA). The RNA-seq libraries were constructed using Illumina TruSeq RNA Sample Prep Kit (Illumina, CA, USA). The libraries were deeply sequenced using an Illumina HiSeq 2000 sequencer at BGI Tech (Wuhan, China), according to the manufacturer's instructions. Clean reads with higher quality were aligned to Sscrofa11.1 using TopHat2. For subsequent analysis, the cufflinks software was performed to obtain the quantitative fragments per kilobase of exon model per million mapped fragments (FPKM) values. DESeq 2 software was utilized to perform differential expression of genes between the DES and vehicle groups. The differentially expressed threshold for genes was set as $|\text{Log}_2(\text{fold change})| > 1$ and adjusted $P < 0.05$.

TABLE 1 Real-time PCR primer sequences.

Name	Primer sequences (5'-3')	Products Length(bp)
<i>IL-1β</i>	F: AAGAAAGTGC GCGGAAAGTA R: CCACAGAAGTCCCATCCTTAC	177
<i>IL-6</i>	F: ATCTGGGTTCATCAGGAGACCT R: ATTTGTGGTGGGGTTAGGGG	208
<i>TNF-α</i>	F: CCTACTGCACITTCGAGGTTATC R: GCATACCCACTCTGCCATT	158
<i>IFN-γ</i>	F: CAGCTTTGCGTGACTTTGTG R: GATGAGTTCAGTGATGGCTTT	381
<i>CAT</i>	F: GCTGGTTAATGCGAGTGGAGAGG R: GGGAAAGTCGTGCTGCGTCTTC	101
<i>SQLE</i>	F: ATGTGGACCTTTCTCGGCATTGC R: GGTAGCGACAGCGGTAGGACAG	145
<i>LRP1</i>	F: TCTACCACGCGGCGTCAG R: CAGCAGGCAGATGTCAGAGCAG	95
<i>STAT3</i>	F: TGGAGAAGGACATCAGCGGTAAGAC R: AGGTAGACCAGCGGAGACACAAG	148
<i>NOD1</i>	F: GACAACTTGCTGCACAACGACTAC R: ACGAAGAAGTCCGACACCTCCTC	137
<i>RORC</i>	F: CAATGGAAGTGGTGCTGGTCAGG R: GGGAGCGGAGAGAAGTCAAAGATG	150
<i>GAPDH</i>	F: ACATCATCCCTGCTTCTACTGG R: CTCGGACGCCTGCTTCAC	187

2.7 Kyoto encyclopedia of genes and genomes and gene ontology analysis

Gene Set Enrichment Analysis (GSEA 4.1.0) software was used to identify GO terms enriched in differentially expressed genes (DEGs). Furthermore, statistically enriched biological processes or pathways of DEGs were ranked and classified by the Metascape database (<http://metascape.org/>) for GO and KEGG pathways. KEGG pathway plot, Volcano plot, and Venn diagram were plotted by an online platform for data analysis and visualization (<http://www.bioinformatics.com.cn>).

2.8 Western blot assay

The cells were seeded in 6-well culture plates and treated as described above (vehicle and DES groups). After washing thrice with cold PBS, cells were lysed on ice with 300 μ L RIPA buffer (Beyotime, Shanghai, China) containing protease inhibitors. Cellular proteins were obtained by centrifugation at $12000 \times g$ for 10 min at 4°C and determined using the BCA Protein Assay Kit (CWBiotech, Beijing, China). Proteins were separated in 8–10% SDS-PAGE gels and transferred onto PVDF membranes (Millipore, MA, USA). The membranes were blocked with 5% skim milk and incubated with ROR γ primary antibody (Invitrogen, MA, USA, 14-6988-82, 1:1000) and GAPDH primary antibody (Proteintech Ltd, Wuhan, China, 10494-1-AP, 1:1000) overnight at 4°C. Then the membranes were incubated with HRP-conjugated secondary antibodies. Finally, the membranes were visualized with an Enhanced ECL Chemiluminescent Detection kit (Vazyme, Nanjing, China) using the automatic chemiluminescence imaging analysis system (Tanon, Shanghai, China). The relative integrated density was normalized against GAPDH expression. Western blot bands were quantified using the Image J software.

2.9 ELISA detection

The concentrations of pro-inflammatory cytokines (IL-1 β , IL-6, TNF- α , and IFN- γ) in the cell supernatant were determined using porcine ELISA kits (Solarbio, Beijing, China) according to the manufacturer's instructions.

2.10 Reactive oxygen species determination

Intracellular ROS abundance was determined by the ROS assay kit (Solarbio, Beijing, China). After the DES treatment, the cells were incubated with DCFH-DA probes at 37°C for 30 min, according to the manufacturer's instructions. Thereafter, the collected cells were measured using a microplate reader (SparkTM

10M, Tecan GmbH, Austria). The relative fluorescence intensity (RFI) was measured at 488/525 nm.

2.11 Statistical analysis

Statistical analysis was performed with GraphPad Prism 8.0 software by Student's *t*-test to compare the means, and data were shown as mean \pm SD. The differences were considered significant at *P* < 0.05. All figures were displayed with GraphPad Prism 8.0 software. All data were repeated at least 3 times.

3 Results

3.1 Linear calibration curves construction and contents detection

In this study, LC-MS analysis and MRM workflow were performed to quantify the contents of DES extractions (Figures 1A, B). An internal standard calibration curve was constructed with standard solutions of DES ranging from 0.025 to 0.25 μ g/mL. As shown in Figures 1C, D, the linear regression equation $y=189476x+24442$ was used to determine the content of DES in the pretreatment sample as 125 μ g/mL. These results provide the processes of DES extraction and content measurement.

3.2 DES does not affect cell growth and survival in IPI-2I cells

To investigate the protective function of DES in intestinal epithelial cells, cell proliferation assay was performed in IPI-2I and IPEC-J2 cells with different concentrations of DES (0, 2.5, 5, and 10 μ M). The result of cell viability showed that DES treatment had no effects on cell proliferation in IPI-2I at the indicated time (0, 24, 48, and 72 h), compared to that in the vehicle (Figure 1E). Consistently, DES also had no effects on the cell counting analysis ranging from 0 to 72 h (Figure 1F). Similarly, the effects of DES on IPI-2I and IPEC-J2 were further evidenced by the inconspicuous changes in cell morphology and cell number (Supplementary Figures 1A, B). These results demonstrated that DES does maintain the physiology of the intestinal epithelial cells.

3.3 DES drives inflammatory response and alleviates oxidative stress

To identify the key transcriptional pathway regulated by DES, transcriptome analysis was performed using the IPI-2I cells treated with or without DES (5 μ M/10 μ M). In total, we identified 441 DEGs ($|\log_2(\text{fold change})| > 1$, *P* < 0.05) between DES (10 μ M) and vehicle groups, comprising 224 upregulated and 217 downregulated

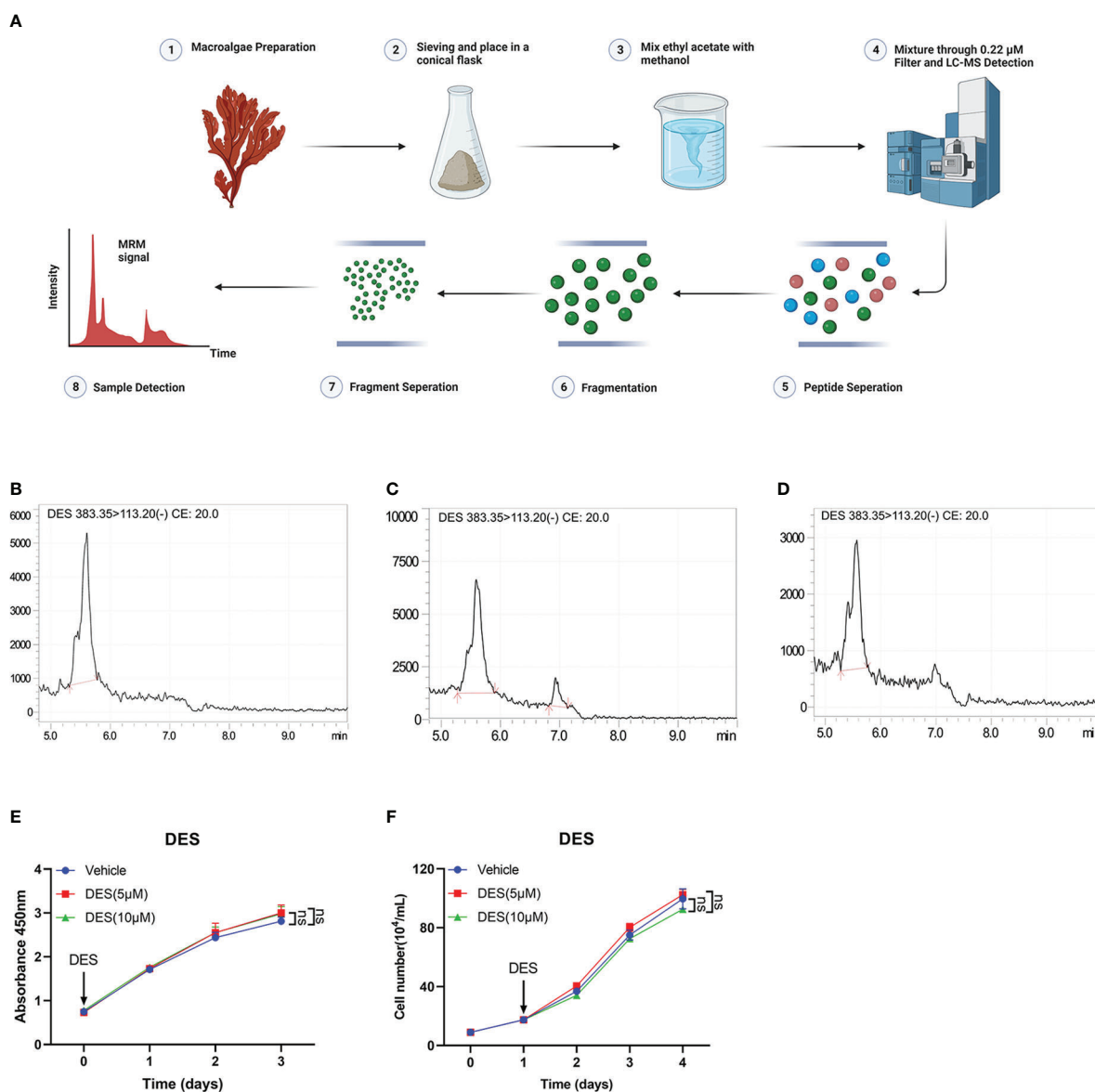


FIGURE 1

DES does not affect cell growth and survival in IPI-2I cells. (A) Overview of sample preparation and detection workflow. (B) DES was determined by LC-MS and quantified with multiple reaction monitoring (MRM) mode. MRM chromatograms of DES standards in 250 μg/mL (C) and 25 μg/mL (D) determined by LC-MS. (E) DES (5 μM/10 μM) treatment in IPI-2I cells for 0, 24, 48, and 72 h by CCK-8 detection. (F) Cell counting analysis at the indicated time. The data are shown as the means ± SD, $n \geq 3$ per group. The experiments were repeated 3 times. ns, represents differences not significant, using Student's *t*-test analysis.

genes (Figure 2A, Table S1). Further function annotations of transcripts are shown in Figures 2B, C and Table S2. The GO and KEGG pathway enrichment analysis of DEGs revealed that genes were most enriched in the inflammatory response and OXPHOS pathways. Further analysis by GSEA also demonstrated that the signatures involving OXPHOS, ROS, and cholesterol homeostasis pathways were strongly downregulated by DES (Figure 2D, Table S3). In association with the GO and KEGG pathway enrichment, the pathway-focused genes subset indicated

that a vast majority of the OXPHOS, inflammatory response, and cholesterol homeostasis pathways were significantly altered (Figures 2E–L, Table S4). It indicated their roles in response to the pro-inflammatory and anti-oxidative stress effects of DES. Intriguingly, the DES (5 μM) treatment showed a similar alteration of these pathways (Supplementary Figures 2A–E, Tables S5–8). Collectively, these findings indicated that inflammatory response and oxidative stress regulated by DES treatment might be the predominant processes in IPI-2I cells.

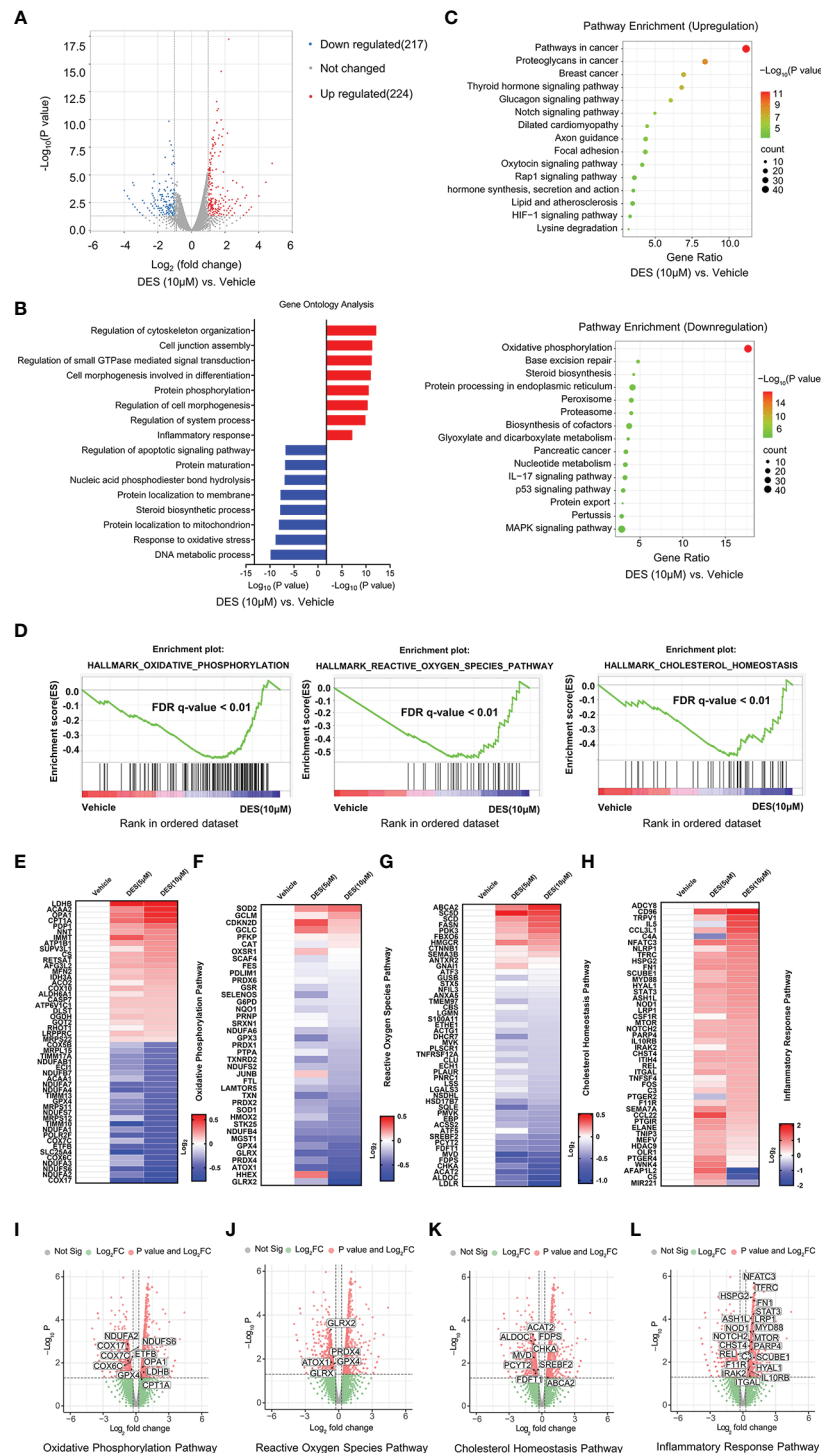


FIGURE 2

DES drives inflammatory response and alleviates oxidative stress pathways in IPI-2I cells. (A) Volcano plot visualization of the differential gene expression profiles between the DES (10 μ M) and vehicle group by transcriptome analysis. (B) Genes expression involved in the inflammatory response pathway were among the most enriched pathways analyzed by GO. (C) DEGs involved in the OXPHOS pathway were the most abundant downregulated enrichments analyzed by the KEGG. (D) The GSEA depicting the enrichment of DEGs downregulated in the cholesterol homeostasis, OXPHOS, and ROS pathways from DES (10 μ M) versus vehicle in IPI-2I. FDR, false-discovery rate. (E–H) Heatmaps of mRNA expression (RNA-seq, \log_2 transformed) changes of the aforementioned (B–D) pathways. (I–L) Volcano plot visualization of DEGs in the aforementioned (B–D) pathways from DES (10 μ M) versus vehicle in IPI-2I.

3.4 ROR γ acts as a key factor to regulate inflammatory response and ROS

Having shown the potential pathway enrichment of DES in the IPI-2I cells, we further explored which DEGs exert critical roles in the pathways mentioned above. Accordingly, 23 upregulated DEGs in the inflammatory response pathway were identified with DES (5 μ M/10 μ M) supplementation in the Venn diagram (Figure 3A). Moreover, a critical anti-oxidative stress gene *GPX4* involved in both OXPHOS and ROS pathways was highly enriched with DES (5 μ M/10 μ M) addition (Figure 3B). To further validate the expression pattern of DEGs, 9 genes (*LRP1*, *STAT3*, *NOD1*, *IL-6*, *TNF- α* , *IFN- γ* , *IL-1 β* , *CAT*, *SQLE*) were quantified by qRT-PCR (Figure 3C). Similarly, the expression patterns of detected genes showed a high concordance with differential analysis results of RNA-seq. In line with the mRNA expression, pro-inflammatory cytokines (*IL-6*, *TNF- α* , and *IFN- γ*) in the supernatant were also significantly elevated by the DES treatment (Figure 3D, $P < 0.05$). In contrast, ROS abundance was significantly reduced by DES (10 μ M) (Figure 3E). Notably, nuclear receptor ROR γ is a promising therapeutic target of the inflammatory response and has a mechanistic link with oxidative stress. We found that the mRNA (Figure 3F) and protein expressions (Figures 3G, H) of ROR γ were upregulated by DES. Interestingly, STRING-ELIXIR analysis demonstrated that the putative transcriptional activators *STAT3*, *IL-6*, and *GPX4* interacted with ROR γ (Figure 3I, Table S9). Taken together, these results suggest that DES promotes the ROR γ pivotal regulation associated with genes involved in the inflammatory response and oxidative stress.

4 Discussion

In recent years, increasing attention has been devoted to the influences of inflammation and immune regulation by cholesterol metabolism. Three essential possibilities have been proposed to explain the cholesterol potential roles: (1) as an important precursor to steroid hormones that regulate immune response (14); (2) as an endogenous intermediate in the bile acids conversion to activate innate immune signaling (15); (3) as metabolites in bile acids that regulate their derivatives (isoallothocholic acid) on differentiation of anti-inflammatory regulatory T cells (Treg) (16). As described by Hu et al. (10) and Santori et al. (17), cholesterol precursor (DES) has been proven to bind to ROR γ and directly regulate its immunoactivity in Th17 cells. In the present study, we analyzed the main regulatory effects of DES in porcine intestinal epithelial cells, involving cholesterol homeostasis, ROR γ expression, OXPHOS, ROS, and inflammatory response pathways. A graphic illustration of the DES-mediated transcriptional regulation of DES in pro-inflammatory and oxidative stress is the process shown in Figure 4. ROR γ , an orphan nuclear receptor, can directly bind to intermediates of cholesterol biosynthesis or interact with SREBP2 to

facilitate cholesterol synthesis (18, 19). Meanwhile, as a nuclear hormone receptor, the activity of ROR γ is also influenced and tightly regulated by endogenous ligands (20). Here we show that DES administration significantly increases ROR γ expression in IPI-2I cells. Upregulated expression of ROR γ further causes the activation of endogenous cholesterol synthesis. Indeed, increased cholesterol contents lead to the inhibition of OXPHOS pathways. Moreover, ROR γ expression improves pro-inflammatory cytokine expression and attenuates ROS abundance by interacting with anti-oxidative genes. Therefore, a logical hypothesis will be that by DES co-option effectively enforce their immunity-activation response and anti-oxidative stress program with activated ROR γ in IPI-2I cells.

The role of cytokines has been implicated in both maintaining homeostasis and inflammatory intestinal disorders (21). Among them, pro-inflammatory cytokines as classical regulators that modulate inflammatory responses and facilitate intestinal homeostasis (22). In the present study, we found that cell supernatant concentration of *IL-6*, *TNF- α* , and *IFN- γ* was increased by DES treatment. Notably, apart from producing the classical cytokines in response to inflammation, DES also mediates inflammatory response by activating some non-typical genes (such as *STAT3*, *NOD1*, and *LRP1*) expression. Elevated *IL-6* levels are observed in inflammatory processes, stimulating the JAK/STAT3 signaling hyperactivation and inducing immunosuppression (23). Furthermore, the *NOD1*/NF- κ B signaling pathway is activated by LPS to produce the pro-inflammatory cytokines, resulting in inflammation (24). *LRP1* can reduce oxidative stress-induced apoptosis to alleviate pathological damage (25). We observed that these factors involved in the inflammatory response pathway are upregulated following DES treatment. It may be a protective response to exogenous stimuli. Indeed, CYP27A1-27hydroxycholesterol-modulated reduction of cholesterol density inhibits the activation of *IL6*-JAK-STAT signaling pathway (26). Our results further provide evidence that the genes enriched in the inflammatory response are related to oxidative stress and cholesterol homeostasis pathways in the STRING-ELIXIR analysis. Increased expression of ROR γ may result from Th17 cell differentiation, which enhances defensive inflammation response. The different cytokines facilitate activated T-cell differentiation into various lineages of effectors (10). In agreement with this notion, Tregs are also crucial for immune tolerance and homeostasis (27). There is evidence that the depletion of Treg can provoke and enhance immune response (27). However, other regulation processes could be beyond the pathways mentioned above, which is a limitation and warrants further investigation.

The influences of marine algae extract, such as amino acids, fatty acids, polyphenolic compounds, and vitamins, on inflammation and ROS have already been reported in different models (28–30). We found that DES, a red algae extract, can also function as a pro-inflammatory and anti-oxidant scavenger. This versatility and capability to act directly or indirectly to improve immunity make natural DES extract highly appealing for

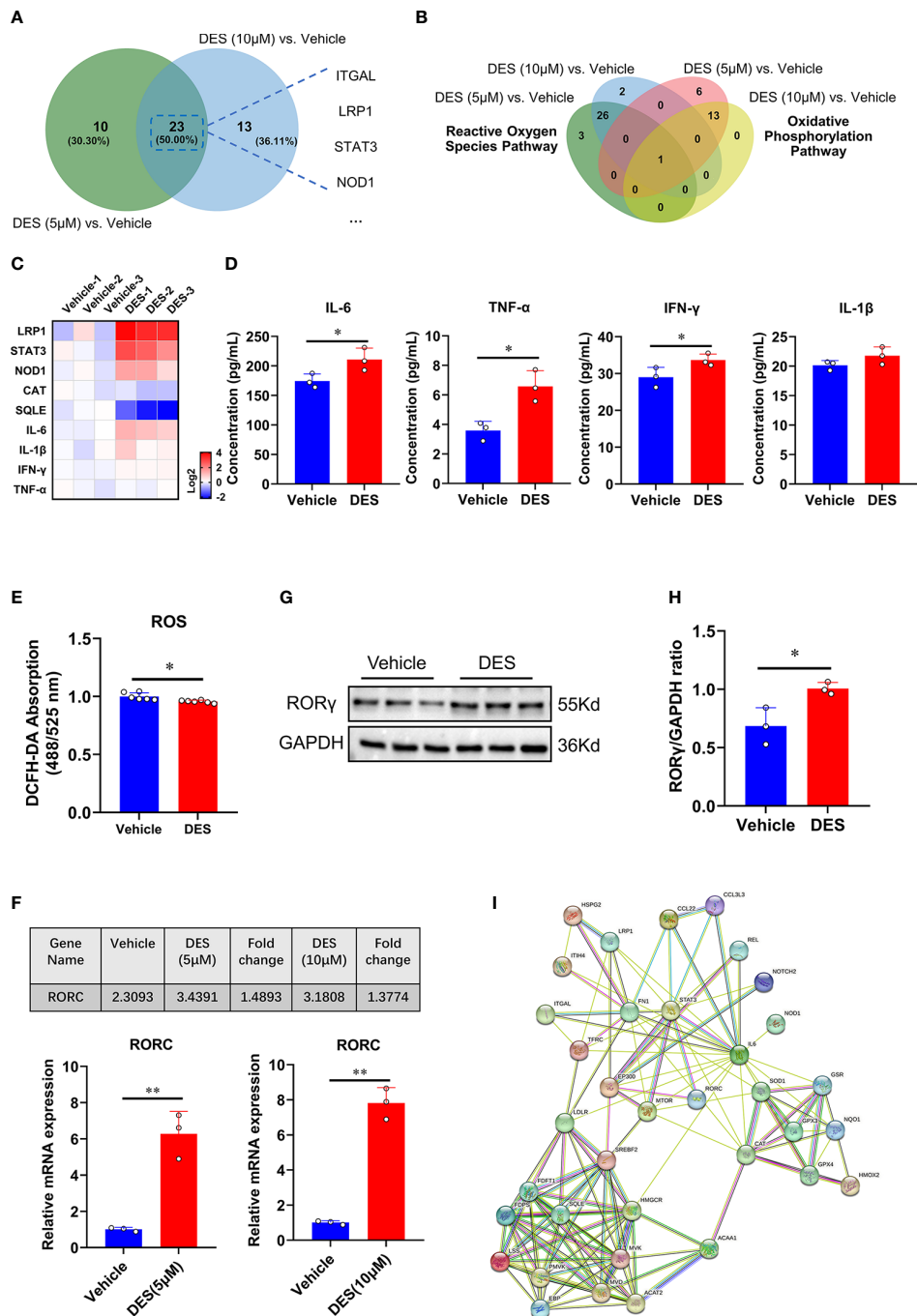


FIGURE 3
RORγ acts as a potential factor to regulate inflammatory response and oxidative stress pathways. **(A)** Venn diagram of the genes with significantly differential expression (Log_2 fold change > 0.5) shared by DES (5 μM) versus vehicle and DES (10 μM) versus vehicle in inflammatory response pathway. **(B)** Venn diagram of the genes with significantly differential expression (Log_2 fold change < -0.5) shared by DES (5 μM) versus vehicle and DES (10 μM) versus vehicle in ROS and OXPHOS pathways. **(C)** A heatmap shows fold change (in Log_2) of 9 genes determined by qRT-PCR analysis in IPI-2I treated with DES (10 μM) for 72 h **(D)** Protein levels of IL-6, TNF- α , IFN- γ , and IL-1 β in the cell supernatant. **(E)** Measurement of ROS (DCFH-DA) fluorescence abundances with DES (10 μM) treatment. **(F)** RNA-seq (FPKM value) and qRT-PCR analysis of RORC gene expression by DES (5 μM /10 μM) treatment. **(G)** Western blot analysis of RORγ protein expression in the DES (10 μM) group. **(H)** The relative protein expression of RORγ was normalized to the GAPDH. **(I)** The interactions among inflammatory response, ROS, and cholesterol homeostasis pathway key proteins involved in RORγ transcriptional regulation were predicted by STRING-ELIXIR analysis. The data are shown as the means \pm SD, $n \geq 3$ per group. The experiments were repeated 3 times. * $P < 0.05$, ** $P < 0.01$, using Student's t -test analysis.

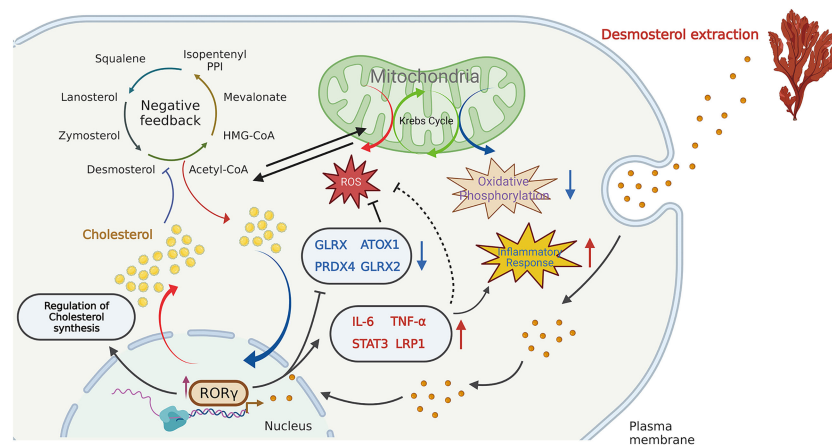


FIGURE 4

Schematic illustration of the DES-mediated transcriptional regulation in cholesterol biosynthesis, pro-inflammatory and oxidative stress. DES causes the highly expressed ROR γ in the IPI-2I and facilitates cholesterol production. The increased cholesterol inhibits the endogenous cholesterol *de novo* synthesis in a negative feedback loop. Again, DES exerts anti-oxidative effects by downregulating oxidative stress-regulated gene expression (GLRX, PRDX4, ATOX1, GLRX2, etc.). Moreover, DES also upregulated the expression of inflammation-related genes (IL-6, TNF- α , STAT3, LRP1, etc.) to activate the immune response.

nutraceutical development. As safe and healthy products, DES can enhance disease resistance and has excellent application prospects for humans and animals. Next, we would focus on toxicity evaluation, and safety validation of DES extract in animals to refine the overall exploration of its function. It is noteworthy that we also have provided a reliable extraction method for both marine algae and other sterols.

Collectively, supplementation of the DES provides a set of negative feedback signals leading to changes in cholesterol metabolism and then action on the inflammatory processes, immune response, and oxidative stress. DES-triggered biological events are probably *via* the activation of ROR γ -mediated transcription. Although primarily descriptive, we provide evidence that DES is a natural candidate for nutraceutical and health product development.

Data availability statement

The data presents in the study are deposited in the NCBI Sequence Read Archive repository, and the accession number is SRR22526287, SRR22526288, and SRR22526289, respectively.

Author contributions

DC and WB conceived the study; HQ and QZ performed most of the experiments; HW and SW participated in the experiments; HQ, QZ, H-YL, and DC participated in its design and coordination and wrote the manuscript. All authors contributed to the article and approved the submitted version.

Funding

This work was supported by the National Natural Science Foundation of China (32002243), Natural Science Foundation of Jiangsu Province (BK20200932, BK20220582), the Priority Academic Program Development of Jiangsu Higher Education Institutions (PAPD).

Conflict of interest

The authors declare that the research was conducted in the absence of any commercial or financial relationships that could be construed as a potential conflict of interest.

Publisher's note

All claims expressed in this article are solely those of the authors and do not necessarily represent those of their affiliated organizations, or those of the publisher, the editors and the reviewers. Any product that may be evaluated in this article, or claim that may be made by its manufacturer, is not guaranteed or endorsed by the publisher.

Supplementary material

The Supplementary Material for this article can be found online at: <https://www.frontiersin.org/articles/10.3389/fimmu.2022.1101643/full#supplementary-material>

References

1. Sánchez M, López-Hernández J, Paseiro-Losada P, López-Cervantes J. An HPLC method for the quantification of sterols in edible seaweeds. *Biomed Chromatogr* (2004) 18(3):183–90. doi: 10.1002/bmc.316
2. Sion B, Grizard G, Boucher D. Quantitative analysis of desmosterol, cholesterol and cholesterol sulfate in semen by high-performance liquid chromatography. *J Chromatogr* (2001) 935(1-2):256–65. doi: 10.1016/S0021-9673(01)01105-0
3. Lin DS, Connor WE, Wolf DP, Neuringer M, Hachey DL. Unique lipids of primate spermatozoa: desmosterol and docosaheptaenoic acid. *J Lipid Res* (1993) 34:491–99. doi: 10.1016/0162-0134(93)80064-G
4. Arthur JR, Blair HA, Boyd GS, Mason JI, Suckling KE. Oxidation of cholesterol and cholesterol analogues by mitochondrial preparations of steroid-hormone-producing tissue. *Biochem J* (1976) 158:47–51. doi: 10.1042/bj1580047
5. Zhang X, McDonald JG, Aryal B, Canfran-Duque A, Goldberg EL, Araldi E, et al. Desmosterol suppresses macrophage inflammasome activation and protects against vascular inflammation and atherosclerosis. *Proc Natl Acad Sci USA* (2021) 118(47):e2107682118. doi: 10.1073/pnas.2107682118
6. Tall AR, Yvan-Charvet L. Cholesterol, inflammation and innate immunity. *Nat Rev Immunol* (2015) 15:104–16. doi: 10.1038/nri3793
7. Galea AM, Brown AJ. Special relationship between sterols and oxygen: Were sterols an adaptation to aerobic life? *Free Radical Biol Med* (2009) 47:880–9. doi: 10.1016/j.freeradbiomed.2009.06.027
8. Omenetti S, Bussi C, Metidji A, Iseppon A, Lee S, Tolaini M, et al. The intestine harbors functionally distinct homeostatic tissue-resident and inflammatory Th17 cells. *Immunity* (2019) 51:77–89. doi: 10.1016/j.immuni.2019.05.004
9. Schnell A, Huang L, Singer M, Singaraju A, Barilla RM, Regan B, et al. Stem-like intestinal Th17 cells give rise to pathogenic effector T cells during autoimmunity. *Cell* (2021) 184:6281–98. doi: 10.1016/j.cell.2021.11.018
10. Hu X, Wang Y, Hao LY, Liu X, Lesch CA, Sanchez BM, et al. Sterol metabolism controls TH17 differentiation by generating endogenous ROR γ agonists. *Nat Chem Biol* (2015) 11:141–7. doi: 10.1038/nchembio0915-741b
11. Lunney JK, Van Goor A, Walker KE, Hailstock T, Franklin J, Dai C. Importance of the pig as a human biomedical model. *Sci Transl Med* (2021) 13(621):d5758. doi: 10.1126/scitranslmed.abd5758
12. Liu HY, Hu P, Li Y, Sun M-A, Qu H, Zong Q, et al. Targeted inhibition of PPAR α ameliorates CLA-induced hypercholesterolemia via hepatic cholesterol biosynthesis reprogramming. *Liver Int* (2022) 42(6):1449–66. doi: 10.1111/liv.15199
13. Li Y, Gu F, Gu H, Hu P, Liu H-Y, Cai D, et al. Lithocholic acid alleviates deoxynivalenol-induced lethal cholesterol metabolic abnormalities in IPI-2I cells. *Metabolites* (2022) 12(7):659. doi: 10.3390/metabo12070659
14. Chiang J, Ferrell JM. Bile acids as metabolic regulators and nutrient sensors. *Annu Rev Nutr* (2019) 39:175–200. doi: 10.1146/annurev-nutr-082018-124344
15. de Aguiar Vallim TQ, Tarling EJ, Edwards PA. Pleiotropic roles of bile acids in metabolism. *Cell Metab* (2013) 17:657–69. doi: 10.1016/j.cmet.2013.03.013
16. Li W, Hang S, Fang Y, Bae S, Zhang Y, Zhang M, et al. A bacterial bile acid metabolite modulates treg activity through the nuclear hormone receptor NR4A1. *Cell Host Microbe* (2021) 29:1366–77. doi: 10.1016/j.chom.2021.07.013
17. Santori FR, Huang P, van de Pavert SA, Douglass EF, Leaver DJ, Haubrich BA, et al. Identification of natural ROR γ ligands that regulate the development of lymphoid cells. *Cell Metab* (2015) 21:286–98. doi: 10.1016/j.cmet.2015.01.004
18. Cai D, Wang J, Gao B, Li J, Wu F, Zou JX, et al. ROR γ is a targetable master regulator of cholesterol biosynthesis in a cancer subtype. *Nat Commun* (2019) 10(1):4621. doi: 10.1038/s41467-019-12529-3
19. Li K, Li H, Zhang K, Zhang J, Hu P, Li Y, et al. Orphan nuclear receptor ROR γ modulates the genome-wide binding of the cholesterol metabolic genes during mycotoxin-induced liver injury. *Nutrients* (2021) 13(8):2539. doi: 10.3390/nu13082539
20. Hu X, Liu X, Moisan J, Wang Y, Lesch CA, Spooner C, et al. Synthetic ROR γ agonists regulate multiple pathways to enhance antitumor immunity. *Oncoimmunology* (2016) 5:e1254854. doi: 10.1080/2162402X.2016.1254854
21. Pizarro TT, Dinarello CA, Cominelli F. Editorial: cytokines and intestinal mucosal immunity. *Front In Immunol* (2021) 12:698693. doi: 10.3389/fimmu.2021.698693
22. Salas A, Hernandez-Rocha C, Duijvestein M, Faubion W, McGovern D, Vermeire S, et al. JAK-STAT pathway targeting for the treatment of inflammatory bowel disease. *Nat Rev Gastroenterol Hepatol* (2020) 17(6):323–37. doi: 10.1038/s41575-020-0273-0
23. Kumari N, Dwarakanath BS, Das A, Bhatt AN. Role of interleukin-6 in cancer progression and therapeutic resistance. *Tumor Biol* (2016) 37:11553–72. doi: 10.1007/s13277-016-5098-7
24. Xu M, Zhuo R, Tao S, Liang Y, Liu C, Liu Q, et al. M(6)A RNA methylation mediates NOD1/NF- κ B signaling activation in the liver of piglets challenged with lipopolysaccharide. *Antioxidants (Basel)* (2022) 11(10):1954–70. doi: 10.3390/antiox11101954
25. He Y, Zheng Z, Liu C, Li W, Zhao L, Nie G, et al. Inhibiting DNA methylation alleviates cisplatin-induced hearing loss by decreasing oxidative stress-induced mitochondria-dependent apoptosis via the LRP1-PI3K/AKT pathway. *Acta Pharm Sin B* (2022) 12:1305–21. doi: 10.1016/j.apsb.2021.11.002
26. Dambal S, Alfaqih M, Sanders S, Maravilla E, Ramirez-Torres A, Galvan GC, et al. 27-hydroxycholesterol impairs plasma membrane lipid raft signaling as evidenced by inhibition of IL6-JAK-STAT3 signaling in prostate cancer cells. *Mol Cancer Res* (2020) 18:671–84. doi: 10.1158/1541-7786.MCR-19-0974
27. Goschl L, Scheinecker C, Bonelli M. Treg cells in autoimmunity: from identification to treg-based therapies. *Semin In Immunopathol* (2019) 41:301–14. doi: 10.1007/s00281-019-00741-8
28. Lordan S, Ross RP, Stanton C. Marine bioactives as functional food ingredients: potential to reduce the incidence of chronic diseases. *Mar Drugs* (2011) 9:1056–100. doi: 10.3390/md9061056
29. Ruxton C, Reed S M, Millington KJ. The health benefits of omega-3 polyunsaturated fatty acids: a review of the evidence. *J Hum Nutr Diet* (2010) 17(5):449–59. doi: 10.1111/j.1365-277X.2004.00552.x
30. Bravo L. Polyphenols: chemistry, dietary sources, metabolism, and nutritional significance. *Nutr Rev* (1998) 56:317–33. doi: 10.1111/j.1753-4887.1998.tb01670.x



OPEN ACCESS

EDITED BY

Yi Wu,
Nanjing Agricultural University, China

REVIEWED BY

Yun peng Fan,
Northwest A&F University, China
Feng Zhang,
Nanjing University of Chinese
Medicine, China

*CORRESPONDENCE

Li Wang
wanglihuina@163.com
Xia Ma
maxia801010@126.com
Bingji Ma
mbj123@sina.com

[†]These authors have contributed
equally to this work

SPECIALTY SECTION

This article was submitted to
Nutritional Immunology,
a section of the journal
Frontiers in Immunology

RECEIVED 15 July 2022

ACCEPTED 23 August 2022

PUBLISHED 11 January 2023

CITATION

Li X, Zhang Z, Wang L, Zhao H, Jia Y,
Ma X, Li J, Wang Y and Ma B (2023)
Three-phase extraction of
polysaccharide from *Stropharia
rugosoannulata*: Process
\optimization, structural
characterization and bioactivities.
Front. Immunol. 13:994706.
doi: 10.3389/fimmu.2022.994706

COPYRIGHT

© 2023 Li, Zhang, Wang, Zhao, Jia, Ma,
Li, Wang and Ma. This is an open-access
article distributed under the terms of
the [Creative Commons Attribution
License \(CC BY\)](#). The use, distribution
or reproduction in other forums is
permitted, provided the original
author(s) and the copyright owner(s)
are credited and that the original
publication in this journal is cited, in
accordance with accepted academic
practice. No use, distribution or
reproduction is permitted which does
not comply with these terms.

Three-phase extraction of polysaccharide from *Stropharia rugosoannulata*: Process optimization, structural characterization and bioactivities

Xinxin Li^{1,2,3†}, Zhiqiang Zhang^{2†}, Li Wang^{1*}, Haoqiang Zhao¹,
Yahui Jia¹, Xia Ma^{3*}, Jinzhan Li⁴, Yi Wang⁵ and Bingji Ma^{1*}

¹Department of Traditional Chinese Medicine, Henan Agricultural University, Zhengzhou, China,

²School of Pharmacy, Henan University of Chinese Medicine, Zhengzhou, China, ³College of
Animal medicine, Henan University of Animal husbandry and Economy, Zhengzhou, China, ⁴Henan
Jinlong Mushroom Industry Co. LTD, Shangqiu, China, ⁵Business Development, GeneGenieDx
Corporation, San Jose, CA, United States

The isolation of *Stropharia rugosoannulata* polysaccharide (SRP) by three-phase extraction was optimized, and its structure and biological activities were identified. The optimal extraction conditions were: mass fraction of ammonium sulfate, 20%; volume ratio of sample solution to t-butanol, 1:1.5; extraction temperature, 35°C. Under these conditions, the yield of SRP was 6.85% ± 0.13%. SRP was found to be composed of glucose (35.79%), galactose (26.80%), glucuronic acid (9.92%), fructose (8.65%), xylose (7.92%), fucose (4.19%), arabinose (3.46%) and rhamnose (3.26%), with the molecular weight of 27.52 kDa. The results of DPPH, hydroxyl, ABTS⁺ radical scavenging and reducing power tests showed that SRP had good antioxidant capacities. SRP had no cytotoxic effect on RAW264.7 macrophages at the concentrations of 25–200 µg/mL, and could significantly promote phagocytosis activity and cell migration according to CCK-8 assay, phagocytosis assay and cell scratch experiment. SRP can significantly stimulate the transcript expression levels of TNF-α, IL-1β and IL-6, as determined by RT-PCR and Western blot assays. SRP activated the TLR4/NF-κB signaling pathway, and autophagy also occurred. These results suggest that SRP is a safe antioxidant and immunomodulator, and that it can be used in the development of functional foods and/or pharmaceuticals.

KEYWORDS

Stropharia rugosoannulata, polysaccharide, three-phase extraction, structure, bioactivities

1 Introduction

Stropharia rugosoannulata Farlow (SR) is a mushroom, also known as wine cap stropharia. It is one of the mushrooms recommended by the Food and Agriculture Organization of the United Nations (FAO) for cultivating, so it is now grown in many developing countries (1). The fruiting body of SR has been reported to include multiple beneficial components, such as flavonoids, vitamins, polysaccharides, and protein. Thus it has potential medicinal value (2).

Fungal polysaccharides have been isolated from fruiting bodies or from fungal mycelia in fermentation broth. Researches have demonstrated that fungal polysaccharides have anti-virus (3), anti-tumor (4), immunomodulatory and anti-aging activities (5). Many have already been developed into a variety of drugs and functional food additives (6). Recently, fungal polysaccharides and their complexes have attracted more attention. *S. rugosoannulata* polysaccharide is one of many fungal polysaccharides and its medicinal value has been gradually recognized. Many studies have shown that polysaccharides from mushrooms have immunomodulatory activity and are good natural immunomodulatory adjuvants (3, 5).

The method of extracting polysaccharides from fungal mycelia affects not only yield but also the structure and biological activities of the polysaccharides extracted. At present, the conventional extraction method is water extraction followed by ethanol precipitation (7). This method has the shortcomings of long time and low efficiency. Three-phase extraction is a new method to extract active ingredients. It has the advantages of high efficiency and environmental sustainability. Recently, this method has been applied to extract polysaccharides from animal material (e.g., shrimp shell (8); *Corbicula fluminea* (9)), plant material (e.g., aloe (10)), and microorganisms. However, there are few reports of using it to isolate polysaccharides from edible or medicinal fungi.

In this research, the polysaccharides of *S. rugosoannulata* were extracted by three-phase extraction. Physicochemical properties such as molecular weight and monosaccharide composition were determined. Scanning electron microscopy (SEM) was used for morphological studies. Antioxidant and immunomodulatory properties were evaluated comprehensively through *in vitro* antioxidant experiments and cell models. The results provide information for the development of SRP as a functional component in foods or medicine.

2 Materials and methods

2.1 Reagents

S. rugosoannulata was collected from a field in Yucheng County, Henan Province, China. Trypsin and RPMI1640 were

purchased from Gibco (Grand Island, NY, United States). The Cell counting kit-8 (CCK-8) was purchased from Han Heng Biotechnology Co., Ltd. (Shanghai, China). Lipopolysaccharide (LPS) was purchased from Sigma Chemical Co. (St. Louis, MO, USA). The remaining chemicals or reagents were all of laboratory or analytical quality.

2.2 Extraction and preparation of SRP

Referring to the method of Yan (9), we made minor modifications. The fruiting body of SR was dried at 45°C in the air-drying box and then ground into powder with a grinder. Then, 95% ethanol (1:200, g/mL) was refluxed 5 hours, repeated 3 times, which was designed to skim and decolorize. Distilled water was added according to the ratio of 1:30 (w/v), and extracted by stirring in a water bath at 100°C for 2 hours. After continuous extraction for two times, the filtrate was merged for two times and concentrated. Added 15–35% (NH₄)₂SO₄ (w/v) to SR powder and vortexed gently. The suspension was then diluted with t-butanol at a ratio of 1.5:1 to 1:2.5 (v/v). Kept the combination at 20–40°C for an hour. Then, the mixture was placed in a centrifuge at 4000 RPM/separation center for 10 minutes to accelerate three-phase extraction. After centrifugation, the three phases formed were carefully separated. The lower phase is mainly ammonium sulfate and polysaccharides, and polysaccharides were freeze-dried after removing inorganic salts by molecular dialysis (3500 Da).

2.3 Structural characterization and molecular morphology

2.3.1 Physicochemical characterizations of SRP

The basic components of carbohydrate, protein and polyphenol were detected according to our previous methods (11, 12).

2.3.2 Molecular weight determination

Gel permeability chromatography (GPC) was used to determine the molecular weight distribution of SRP using a Sugar KS805 column fitted with an Agilent refractive index detector.

2.3.3 Studies on the composition of monosaccharides

Using high-performance anion exchange chromatography (HPAEC) coupled with a pulse ammeter detector, we determined the monosaccharide composition of SRP. Gas chromatography (GC) was used to determine the monosaccharide composition of SRP following the procedure described by Yang (13). 5 mg of SRP was dissolved in 1 mL 2.5 M

trifluoroacetic, and was mixed by the vortex. The sample was placed in the oven for 1.5 hours at 121°C, during which the sample was vortexed every 30 minutes. Once the SRP were hydrolyzed, they were diluted, filtered, and injected into an HPAEC system (Dionex, ICS-5000+, USA) using an ASAP automatic sampler and a calcium carbonate PA-20 column (3×150 mm, Dionex). The monosaccharides in SRP were determined by eight different monosaccharides.

2.3.4 X-ray diffraction test

Empyrean X-ray diffractometer (panalit LTD., Netherlands) was used to record the diffraction patterns of SRP at 40kV and 15 mA. The scanning speed was 3°/min, the step size was 0.01, and the 2 range was 2 to 40°.

2.3.5 SEM analysis

An SEM Model S-4800 II FESEM (Hitachi, Japan) was used to study the molecular morphologies of SRP. A layer of gold foil was laid on the sample and then placed on the substrate. Under a high vacuum and 10.0 kV voltage, the image was observed by a magnification of 100× or 500× fold.

2.4 Antioxidant activities analysis *in vitro* of SRP

2.4.1 Analysis of DPPH free radical scavenging

The DPPH radicals scavenging activity of SRP was determined according to the method of Wang et al. (11). 500 μL different concentrations of SRP (0.05, 0.1, 0.5, 1, 2, 4, 6, 8, 10 mg/mL) were mixed with the newly configured 2-diphenyl-1-picrylhydrazyl (DPPH) solution (dissolved in ethanol) in equal volume, and the reaction solution was left in a dark place at 26°C for half an hour. The blank group consisted of the same volume of distilled water as the sample solution, and the positive control had the same concentration of Vc. The absorbance of the reaction mixture was determined at 517 nm. Scavenging activity (percent) against DPPH was calculated by using the following equation:

$$\text{Scavenging ability (\%)} = [1 - (A_X - A_{X0})/A_0] \times 100$$

Where A_0 was the absorbance of the blank control; A_X was the absorbance of the sample solution; A_{X0} was the background absorbance of the sample solution.

2.4.2 Analysis of hydroxyl free radical scavenging

Added 400 μL FeSO_4 solution to 400 μL different concentrations of SRP (0.05, 0.1, 0.5, 1, 2, 4, 6, 8, 10 mg/mL). After adding 800 μL of H_2O_2 solution, the reaction was started and the solution was left to react at 37°C for 30 minutes. The blank group consisted of the same amount of distilled water that was used to replace the sample solution as the positive control had the

same concentration of Vc. The 510 nm wavelength of the reaction solution was measured. To determine the hydroxyl scavenging capacity (in percent), the following equation was used:

$$\text{Scavenging ability (\%)} = [1 - (A_X - A_{X0})/A_0] \times 100$$

Where A_0 was the absorbance of the blank control; A_X was the absorbance of the sample solution; A_{X0} was the background absorbance of the sample solution.

2.4.3 Analysis of ABTS⁺ free radical scavenging

ABTS⁺ radicals removing capacity of SRP was according to the work of Qiu et al. (14). The ABTS⁺ working solution was made by reacting 7 mmol/L of ABTS⁺ solution with 2.45 mmol/L of $\text{K}_2\text{S}_2\text{O}_8$ solution at 26°C for 16 hours in the dark. When using, adjust the absorbance of the ABTS⁺ working solution at 734 nm. Then, took 100 μL different concentrations of SRP (0.05, 0.1, 0.5, 1, 2, 4, 6, 8, 10 mg/mL), added 0.6 mL ABTS⁺ solution, mixed evenly and placed at 26°C for 10 minutes. The same concentration of Vc solution as the positive group. The reaction solution's absorbance at 734 nm was measured. Using these formulae, we were able to determine the ABTS⁺ scavenging efficiency (in percentage):

$$\text{Scavenging ability (\%)} = [1 - (A_X - A_{X0})/A_0] \times 100$$

Where A_0 was the absorbance of the blank control; A_X was the absorbance of the sample solution; A_{X0} was the background absorbance of the sample solution.

2.4.4 Analysis of reducing ability

The method of Gao et al. (15) was used for sample reduction force detection, and some modifications were made. In brief, 200 μL different concentrations of SRP (0.05, 0.1, 0.5, 1, 2, 4, 6, 8, 10 mg/mL) were taken and 500 μL PBS and 100 μL 1% (w/v) iron oxide clock solution was added, then the reaction system was incubated in 50°C for 20 minutes. After quick cooling, it was combined with a 500 μL 10 percent (w/v) trichloroacetic acid solution, and then centrifuged. Next, took 500 μL supernatant, added 500 μL distilled water and 100 μL 0.1% (w/v) FeCl_3 solution successively, then mixed them evenly at 26°C. The absorbance of the reaction solution was measured at 700 nm and a standard solution with the same quantity of Vc was employed as the positive control. The sample's reducing power is proportional to its absorbance value, which measures the reaction system's efficiency.

2.5 Immunomodulatory activity assay of SRP

2.5.1 Cell culture

RAW 264.7 macrophages were grown in an incubator with 5% CO_2 at 37°C in RPMI1640 media supplemented with 10% fetal bovine serum, 100 U/mL penicillin, and 100 g/mL streptomycin. Every 2-3 days, new media will be added.

2.5.2 Cell viability

The cell viability of SRP was detected by the CCK-8 method (16). RAW 264.7 macrophages were placed onto a 96-well plate with 100 μ L/well cell suspension and cultured in the cell incubator for 24 hours. 10 μ L varying quantities of SRP (25, 50, 100, 200, 400, 600, 800 μ g/mL) and LPS (1 μ g/mL) were set as normal group and positive group, each group was set up with 4 multiple wells, and blank medium group was put in a 37°C, 5 percent CO₂ cell incubator for a length of time. Then, CCK-8 with 1/10 volume of cell culture media was added to it, and the absorbance of the reaction solution was measured at 450 nm after incubation in a constant temperature incubator.

2.5.3 Assay of phagocytosis

When the confluence of RAW264.7 macrophages reached 80%, the medium was used to dilute the cell density to 1×10^4 cells/mL. A 96-well plate containing a cell suspension of RAW 264.7 macrophages at a concentration of 100 μ L/well was placed in a cell incubator for 24 hours. 100 μ L varied doses of SRP (25, 50, 100, 200 μ g/mL) and LPS (1 μ g/mL) were added and cultured in a cell incubator for 24 hours, adding 100 μ L 0.1 percent of the neutral red to each well, and the final concentration of neutral red in each well is 1 μ g/mL. After washing with PBS, 100 μ L cell lysis solution was added to each well and gently shaken for 15 seconds, then left the plate at 37°C for 2 hours. The absorbance of the reaction solution was measured at 540 nm.

2.5.4 Cell scratch experiment

Cell scratch experiment was detected and the method was according to the report of Zubair et al. (17). RAW264.7 macrophages were seeded at a density of 1×10^6 cells per well and cultured in a 6-well plate for 24 hours before being scratched with the tip of a 200 μ L pistol to ensure even damage. Then washing with PBS for 3 times to remove the scratched cells, and the medium with different concentrations of SRP (25, 50, 100, 200 μ g/mL) and LPS (1 μ g/mL) were added and incubated for 24 hours. The medium without drugs was used as the blank control group. The samples were taken and the migration of cells at the same location was recorded.

2.5.5 Extraction of mRNA and RT-PCR

Table 1 displayed primer sequences that were developed using real-time PCR primer design concepts. Total RNA was

isolated using the Trizol procedure, and its concentration and quality were evaluated using a Nanodrop 8000. Then, the obtained RNA were used as templates, cDNA were synthesized by reverse transcription using qPCR (+gDNA) of HiScriptIII RT SuperMix. The fluorescence quantitative reaction system was prepared according to Taq Pro Universal SYBR qPCR Master Mix. After the reaction, the relative gene expression changes were recorded by the $2^{-\Delta\Delta CT}$ method.

2.5.6 Western blot analysis

Total cell protein was isolated using a protein lysate. Protein was quantified using a kit (Bicinchoninic acid, BCA method), transferred to a PVDF membrane using SDS-PAGE gel electrophoresis, blocked in skim milk for 2 hours, and then incubated at 4°C overnight with a diluted primary antibody. The next day, we washed away the residual primary antibody with TBST solution, added the appropriate secondary antibody, and incubated everything at 26°C for 2 hours. After three washes in TBST buffer solution, any lingering secondary antibodies were removed, and an ECL luminous reagent was poured into an automated chemiluminescence imager. Image J was used to save and examine the data.

2.5.7 Statistical analysis

SPSS 21.0 was used to conduct the statistical analysis, and one-way analysis of variance (ANOVA) was employed for the multiple comparisons. In this study, significant differences were defined as those with a probability level of less than 0.05 (represented as “mean \pm standard deviation”).

3 Results and analysis

3.1 Univariate experiments

3.1.1 Effect of ammonium sulfate concentration on SRP yield

As shown in Figure 1A, as the concentration of ammonium sulfate rose from 15%-35%, the yield of SRP increased first and then decreased. When the mass fraction of ammonium sulfate was 20%, the yield reached the maximum value of 7.20%. The

TABLE 1 Sequences for RT-PCR primers.

Primer	Forward (5'-3')	Reverse (5'-3')
TNF- α	GACGTGGAAGTGGCAGAAGAG	TTGGTGGTTTGTGAGTGTGAG
IL-1 β	GGGCCTCAAAGGAAAGAATC	TACCAGTTGGGGAAGTCTGC
IL-6	AGTTGCCTTCTTGGGACTG	CAGAATTGCCATTGCACAA
β -actin	ACCCAGCAAGGACACTGAGCAAG	GGCCCCCTCTGTTATTATGGGGGT

extraction yield of polysaccharides was diminished because of the high salt concentration's potential to disrupt the hydrogen-bond network between SRP and water molecules. Similar to our study, Wang et al. also showed that the extraction efficiency of rice bran polysaccharides decreased with the increase of the concentration of ammonium sulfate (18).

3.1.2 Effect of the sample solution to t-butanol ratio on SRP yield

As shown in Figure 1B, the yield of SRP increased gradually with the increasing proportion of t-butanol volume up to a certain point; this was presumably due to increased interaction between increased t-butanol and ammonium sulfate (19). When the ratio of sample solution to t-butanol was 1:1.5 (v/v), the yield reached the maximum value of 7.0%. With further increase of t-butanol, however, the yield of SRP was decreased, thus reducing the overall extraction yield of SRP. This reduction may be due to a lack of sufficient water to hydrate sulfate ions adequately (11).

3.1.3 Effect of the temperature on SRP yield

As shown in Figure 1C, the yield of SRP increased gradually with the increase of extraction temperature from 20–30°C; above 30°C, the yield of SRP showed a downward trend. This may be because high temperature accelerated the thermal movement of molecules in the three-phase extraction system, and thus

enhanced the hydrophilicity of polysaccharides (20). Therefore, the yield of SRP reached its highest value at the tested temperature, 30°C.

Using the single factor investigation results, an orthogonal test was used to optimize the three extraction parameters of mass fraction of ammonium sulfate, t-butanol volume ratio and extraction temperature, and three levels were set for each factor (Table 2). Without considering interaction, an L9(3³) orthogonal experiment was conducted to optimize the extraction.

As can be seen from the R-value in the Table 3, the influence of these three parameters on the yield of polysaccharides is as follows: B (t-butanol volume ratio) > C (extraction temperature) > A (ammonium sulfate mass fraction). On this basis, the optimum extraction conditions were determined as follows: mass fraction of ammonium sulfate, 20%; volume ratio of sample solution to t-butanol, 1:1.5; extraction temperature, 35°C.

3.2 Physicochemical properties

3.2.1 Physicochemical composition and monosaccharide composition

As shown in Table 4, the extraction yield of SRP was 6.85%, and the carbohydrate content of SRP was 56.18%. The protein

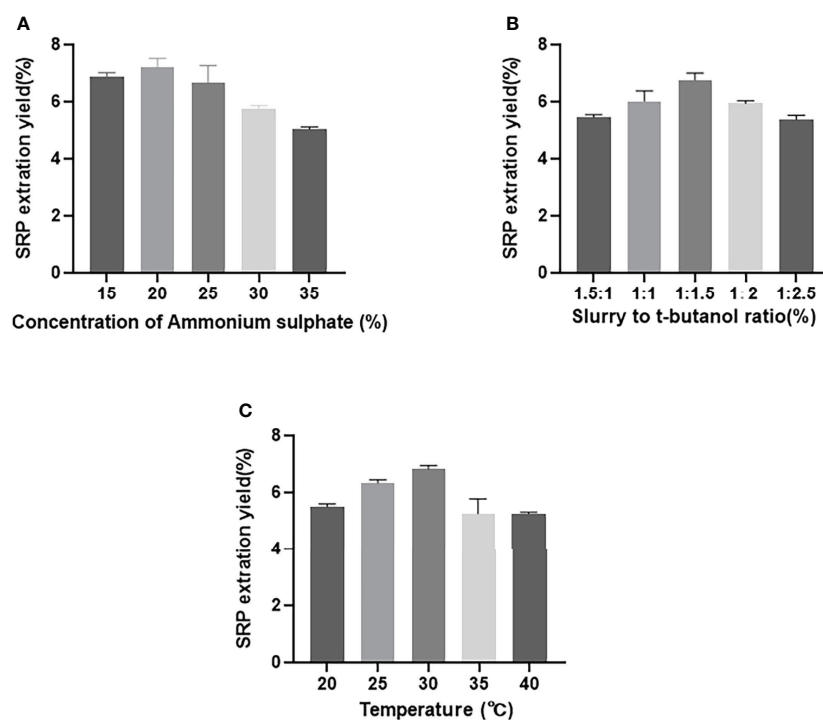


FIGURE 1
Effect of different factors on SRP yield. (A) Concentration of ammonium sulphate; (B) Slurry to t-butanol ratio; (C) Temperature.

TABLE 2 Orthogonal test factor level table.

Levels	Factors		
	Ammonium sulfate mass fraction (%)	T-butanol volume ratio	Extraction temperature (°C)
1	15	1:1	25
2	20	1:1.5	30
3	25	1:2	35

content was 6.78%, and the polyphenol content was 1.73%. The XRD pattern showed a small diffraction peak at 20°, which indicated that SRP has an amorphous structure. Its crystallinity was 18.21%. The crystal structure is directly determined by properties such as elasticity and swelling (21).

Molecular weight is an essential physicochemical parameter closely related to the biological activity of polysaccharides. The weight average molecular weight (Mw) of SRP was 27.52 kDa, and its number average molecular weight (Mn) of SRP was 26.07 kDa, which was similar to Chen (22). The polymer dispersion index Mw/Mn of SRP was 1.06, and the closer the dispersion index was to 1, the more evenly the polysaccharide was distributed.

3.2.2 Monosaccharide composition of SRP

Monosaccharide composition results (Table 5) showed that the SRP sample was composed of fucose, rhamnose, arabinose, galactose, glucose, xylose, fructose and glucuronic acid in a molar ratio of 4.19: 3.46: 3.26: 26.80: 35.79: 7.92: 8.65: 9.92. Galactose and glucose were the most abundant. The results showed that SRP was heteropolysaccharide. Liu et al. (2) identified mannose, galactose and glucose as the main monosaccharide components in SRP. Similarly, Diego Morales et al. found that the monosaccharide components of *Lentinula edodes* polysaccharides are mainly glucose, galactose and

mannose (23). Different sources of raw materials and preparation conditions may be responsible for the differences.

3.2.3 SEM analysis

The morphology of SRP was characterized by SEM. SRP had a rough surface, irregular flake and massive distribution, and pores on the surface after magnification (Figure 2). These microstructure characteristics may be caused by the destruction of cell wall structure and the decomposition of polysaccharide aggregates during the three-phase extraction processes. The surface topographic characteristics and microstructure change of SRP may be related to its physicochemical properties and antioxidant activity (24). SRP obtained by the three-phase extraction method is due to the joint action of ammonium sulfate and tert-butanol, which is affected by various forces and forms an obvious flake structure.

3.3 Antioxidant activity analysis *in vitro* of SRP

3.3.1 DPPH radical scavenging ability of SRP

The antioxidant potential of polysaccharides may be easily guaranteed by measuring their capacity to scavenge DPPH free radicals. In general, the eliminated ability of polysaccharides to

TABLE 3 Results and analysis of orthogonal experiment of SRP.

No	A	B	C	Yield (%)
1	1	1	1	5.72
2	1	2	2	6.56
3	1	3	3	5.63
4	2	1	2	6.13
5	2	2	3	7.12
6	2	3	1	5.81
7	3	1	3	6.5
8	3	2	1	6.06
9	3	3	2	6.27
K1	17.91	18.35	17.59	
K2	19.06	19.74	18.96	
K3	18.83	17.71	19.25	
R	1.15	2.03	1.66	

TABLE 4 Physicochemical composition and molecular weight.

Sample	SRP
Yield (%)	6.85 ± 0.13
Carbohydrate (%)	56.78 ± 1.34
Protein (%)	6.78 ± 0.15
Polyphenol (%)	1.73 ± 0.0050
Degree of crystallinity (%)	18.21 ± 0.34
Molecular weight (kDa)	
Weight-average molecular weight (Mw)	27.52
Number-average molecular weight (Mn)	26.07
Polymer dispersity index (PDI)	1.06

DPPH free radicals relies on the hydrogen supply ability of the antioxidant (25). Figure 3A displayed SRP's capacity to scavenge DPPH free radicals. The scavenging activities of SRP reached 88.60 percent when the SRP reached 2 mg/mL. The result indicated that SRP had the ability to clear DPPH, which was similar to Wang et al. (26).

3.3.2 Hydroxyl radical scavenging ability of SRP

Excessive levels of hydroxyl radical, one of the most powerful free radicals in the body, may disrupt the delicate equilibrium of the body. Upon contact with nearby biomolecules, hydroxyl radicals may cause extensive damage, and in extreme cases, even cell death (27). Figure 3B displayed SRP's ability to quench hydroxyl radicals. Generally, SRP had potential scavenging activity on hydroxyl radical. SRP's scavenging activity rose to 94.46 percent at 6 mg/mL. When the SRP concentration was 10 mg/mL, its scavenging efficiency was 98.06%. SRP was shown to have a clear capacity to scavenge hydroxyl radicals, as shown by the findings. SRP had the potential to remove hydroxyl radical because it has a better scavenging power on hydroxyl radical.

3.3.3 ABTS⁺ radical scavenging ability of SRP

The antioxidant potential of polysaccharides may be easily neutralized using the ABTS⁺ free radical technique (28). ABTS⁺ free radical scavenging experiments are based on electron transfer from antioxidants to ABTS⁺ free radicals. SRP's

capacity to scavenge ABTS⁺ radicals were shown in Figure 3C. As a positive control, the scavenging power of Vc remained stable between 88.13% and 99.83% in the range of experimental concentrations. At 2 mg/mL, SRP showed an 89.44 percent increase in scavenging activities. These results showed that SRP had the ability to scavenge ABTS⁺ radical.

3.3.4 Reducing power of SRP

In Figure 3D, the lowering power of SRP compared to the positive control, Vc. The concentration of SRP has a positive correlation with the reducing power. SRP had an absorbance of 0.66 at 700 nm at a dosage of 10 mg/mL. These findings demonstrated that SRP has some degree of astringent activity.

3.4 Measurement of immunomodulatory activities of SRP

3.4.1 Cell viability

The results of testing the viability of cells treated with SRP were shown in Figure 4A. By comparing with the blank group, different concentrations of SRP had different effects on RAW264.7 macrophages activity. When SRP ≤ 200 µg/mL, SRP can significantly promote cell growth ($p < 0.05$) indicating that SRP had no toxicity to cells. Concentrations greater than or equal to 400 µg/mL inhibited cell proliferation, indicating some toxicity.

Therefore, based on these results, a concentration between 25-200 µg/mL could be used for experimental treatment of cells, specifically for evaluating the immune regulatory effect of SRP on RAW264.7 macrophages.

3.4.2 Effect of SRP on phagocytosis of RAW264.7 macrophages

The effect of SRP on phagocytosis was detected by macrophage uptake of neutral red (29). The results were shown in Figure 4B. When the concentration of SRP was between 25-200 µg/mL, all samples significantly promoted the uptake of neutral red by RAW264.7 macrophages compared with the blank control group ($p < 0.05$). The results showed that SRP significantly promoted the uptake of neutral red by macrophages, thus further regulating immune activity.

3.4.3 Effect of SRP on RAW264.7 macrophages migration

The most direct method to detect cell migration is the scratch test (30). As shown in Figure 5, RAW264.7 macrophages were treated with LPS (1 µg/mL) and different concentrations of SRP (25-200 µg/mL), and the percent of cell scratch healing on the macrophages was observed. The results showed that SRP significantly improved cell scratch healing at all tested concentrations between 25-200 µg/mL compared with the

TABLE 5 Monosaccharide composition of SRP.

Monosaccharides	Molar ratio (%)
Fucose	4.19
Arabinose	3.46
Rhamnose	3.26
Galactose	26.8
Glucose	35.79
Xylose	7.92
Fructose	8.65
Glucuronic acid	9.92

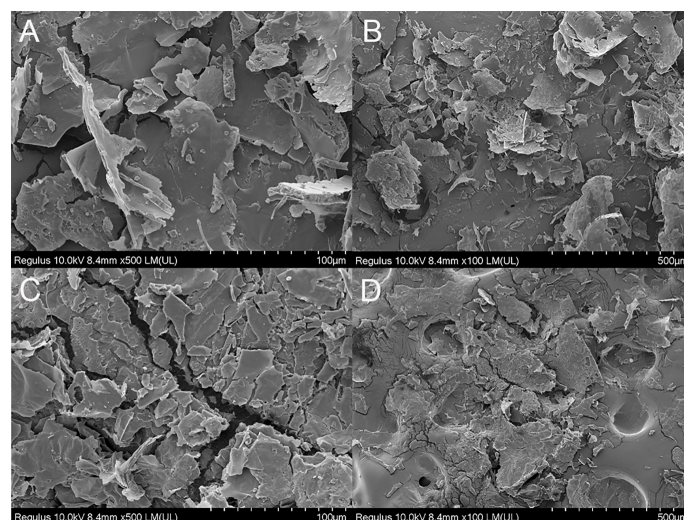


FIGURE 2
SEM images (magnification 100x and 500x). (A, C) (100 μm); (B, D) (500 μm).

blank group ($p < 0.05$), and the scratch healing rate of the RAW264.7 macrophages at 25–50 $\mu\text{g/mL}$ SRP was higher than that at 100–200 $\mu\text{g/mL}$.

3.4.4 RT-PCR test results

Cytokines are produced by activated immune cells and are considered to be major immune mediators (31). The transcription

levels of the three cytokine genes IL-1 β , IL-6 and TNF- α were detected by RT-PCR. Figure 6 showed that transcription levels of all three were significantly increased within the limits of SRP (25–50 $\mu\text{g/mL}$) or LPS (1 $\mu\text{g/mL}$) groups compared with the blank group ($p < 0.05$). The result was similar to the results reported by Liu on the immunomodulatory activity of *Sinonovacula constricta* polysaccharide (32).

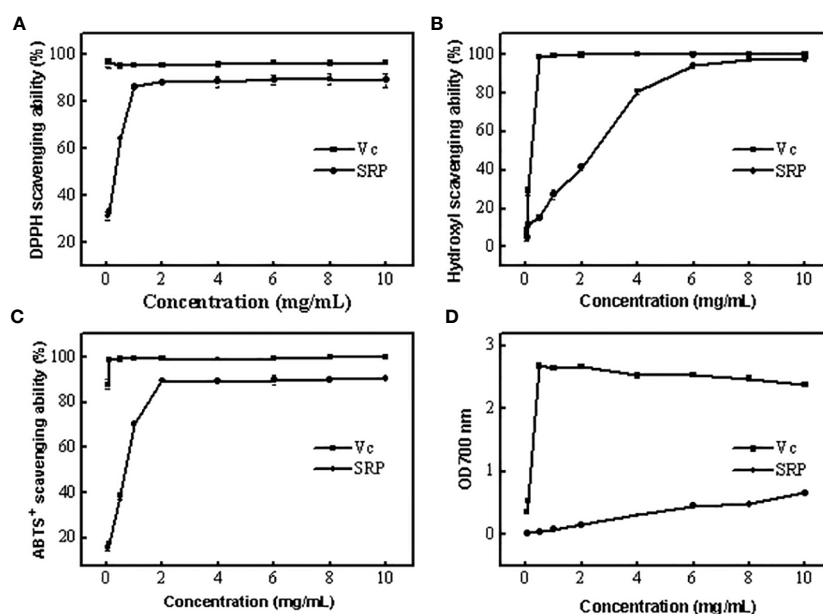


FIGURE 3
Antioxidant activity of SRP (A–D) DPPH, Hydroxyl, ABTS⁺ radical scavenging ability and reducing power.

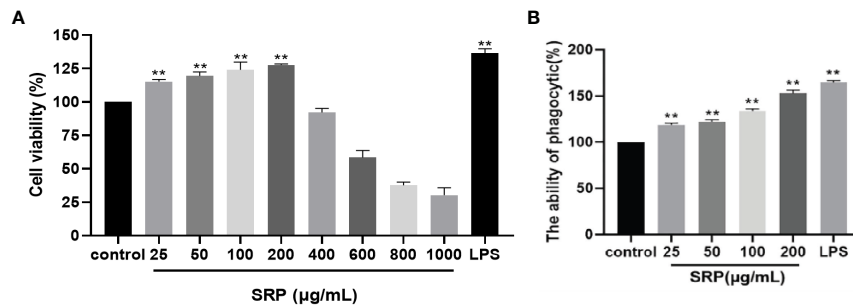


FIGURE 4

Cell viability and phagocytic capacity of the SRP. (A) Cell viability; (B) Phagocytic capacity. Significant differences with the control group: * $p < 0.05$ and ** $p < 0.01$.

3.4.5 Protein expression of TLR4/NF- κ B pathway

NF- κ B plays a crucial role in immune regulation and inflammatory responses (33). TLR4 is a significant member of the Toll-like receptor family, and breakthroughs have been made in research on TLR4. A variety of signaling pathways have been confirmed to be related to mediating immune responses (34). To determine whether the immune activity of SRP is mediated by the TLR4/NF- κ B signaling pathway, we investigated western blot analysis was performed to analyze the effect of SRP on the expression levels of key proteins in the TLR4/ NF- κ B signaling pathway in RAW 264.7 cells.

Figure 7 showed the influence of SRP on the expression levels of the key proteins TLR4, MyD88 and NF- κ B in the TLR4/ NF- κ B signaling pathway (β -actin as internal reference). Compared with the positive control group, SRP groups showed decreased the protein expression levels. Compared

with the blank group, SRP (25-50 μ g/mL) and LPS groups showed significantly increased expression of TLR4, MyD88 and NF- κ B protein ($p < 0.05$). We speculated that SRP activates RAW264.7 macrophages by up-regulating the expression of key proteins in the TLR4/NF- κ B pathway.

3.4.6 Expression of autophagy proteins

Autophagy is a cellular mechanism of self-degradation, transformation and energy production. Autophagy is closely related to inflammation. The activation of pattern recognition Toll-like receptor can induce autophagy, and autophagy can regulate the inflammatory response. Defective autophagy can induce inflammation (35). LC3 is a hallmark protein of autophagy. p62 is a substrate for autophagy degradation; it plays an important role in the recognition and encapsulation of degraded substrates. Beclin 1 over expression promotes autophagy in mammalian cells, and the expression increases

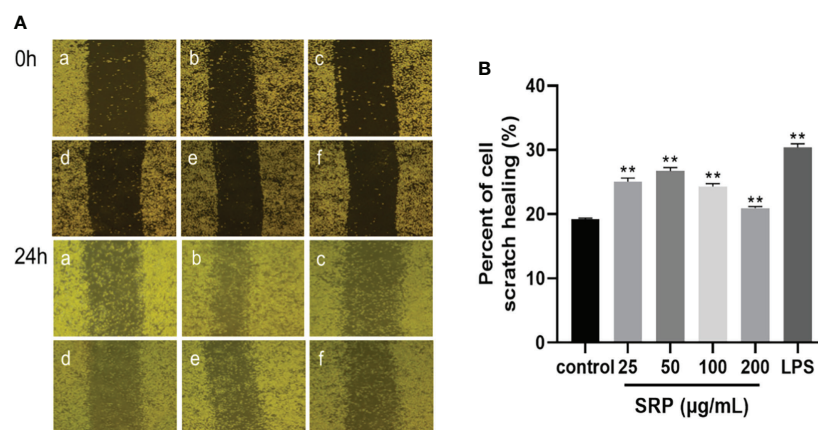


FIGURE 5

Results of the macrophages RAW264.7 scratch experiment. (A) Image of the cell scratch: a-f indicates the control, LPS, SRP (25, 50, 100, 200 μ g/mL) groups; (B) Percent of cell scratch healing. Significant differences with the control group: * $p < 0.05$ and ** $p < 0.01$.

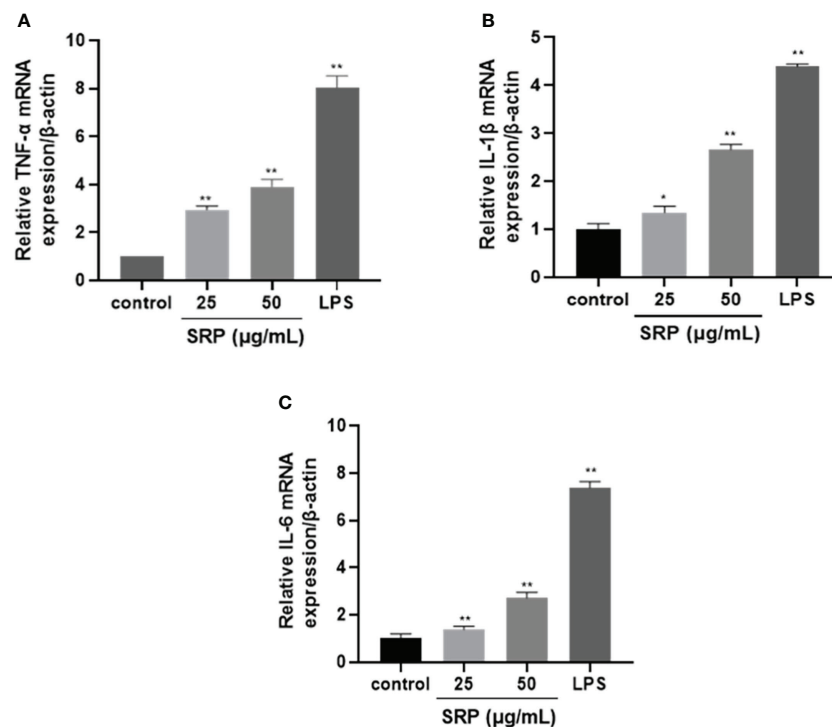


FIGURE 6
Effects of SRP on the expression of cytokine genes in RAW264.7 macrophages. (A–C) Expression of TNF- α , IL-1 β and IL-6 mRNA. Significant differences with the control group: * $p < 0.05$ and ** $p < 0.01$.

with the enhancement of autophagy. LC3, Beclin 1 and p62 are all used as indicators of autophagy (36).

Autophagic protein expression results were shown in Figure 8. The expression of autophagic protein in the positive control group was higher than in the blank group. Compared with the positive control group, the protein expression levels of LC3 and Beclin 1 increased and the protein expression levels of p62 decreased in SRP with different mass concentrations. Compared with the blank group, the protein expression levels of LC3, Beclin 1 and p62 in different mass concentrations of SRP were significantly increased ($p < 0.05$), which indicated that SRP can promote autophagy in cells.

4 Discussion

Recently, many studies have been carried out on the extraction of polysaccharides from *S. rugosoannulata*, which due to its better biological. The main extraction methods are solvent extraction, ultrasonic extraction, alkali-assisted extraction (2), etc. However, these extraction methods are complex, typically requiring a long processing time.

As a new protein separation and purification technology, three-phase extraction is a safe, effective, and environmentally friendly green technology, including salting out, isoelectric point

precipitation and solvent precipitation (37). However, most researchers mainly focus on the protein phase (38). It is rarely reported that polysaccharides are isolated and purified from edible fungi by three-phase extraction. Ours may be the first attempt to isolate SRP by three-phase extraction. Three-phase extraction is relatively simple, safe, and environmentally friendly compared to conventional extraction methods. Furthermore, the method preserves the biological activity of the polysaccharides better than the existing method.

In this study, single factor and multiple factor orthogonal tests were used to obtain the optimal extraction conditions for extracting polysaccharides. These conditions were: mass fraction of ammonium sulfate, 20%; volume ratio of sample solution to t-butanol, 1:1.5; and extraction temperature, 35°C. Under these conditions, the yield of SRP was $6.85\% \pm 0.13\%$, which was higher than that of the traditional method of water extraction and alcohol precipitation (39).

The physiological functions of polysaccharides are closely related to structure. Some scholars have studied the structure and function of polysaccharides of *S. rugosoannulata*. Chen et al. (22) obtained a polysaccharide by hot water extraction, and proved this structure was mainly composed of five monosaccharides, predominately xylose, galactose and glucose, with a relative molecular weight of about 22 kDa. Liu et al. (2)

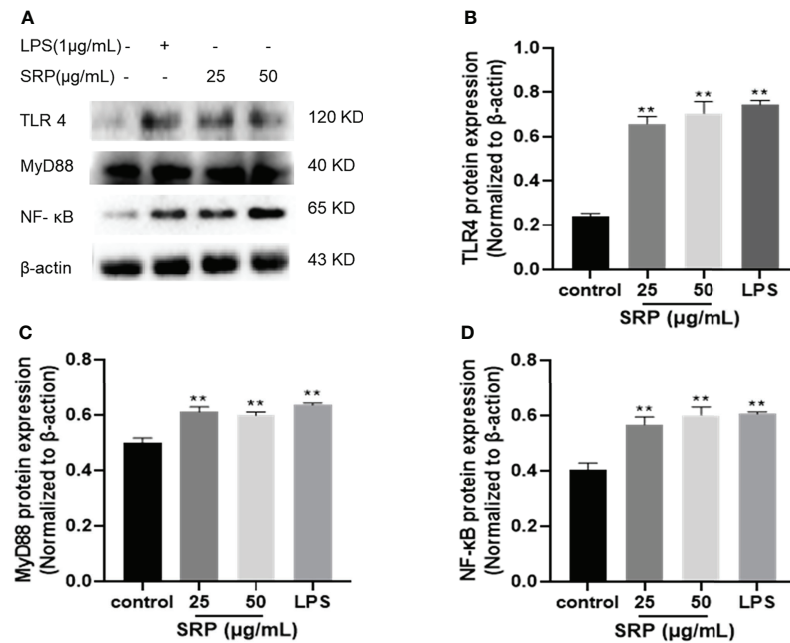


FIGURE 7

Effect of SRP on the protein expression levels of the TLR4/NF-κB pathway. (A) Western blot analysis of protein bands; (B) TLR4; (C) MyD88; (D) NF-κB protein expression. Significant differences with the control group: * $p < 0.05$ and ** $p < 0.01$.

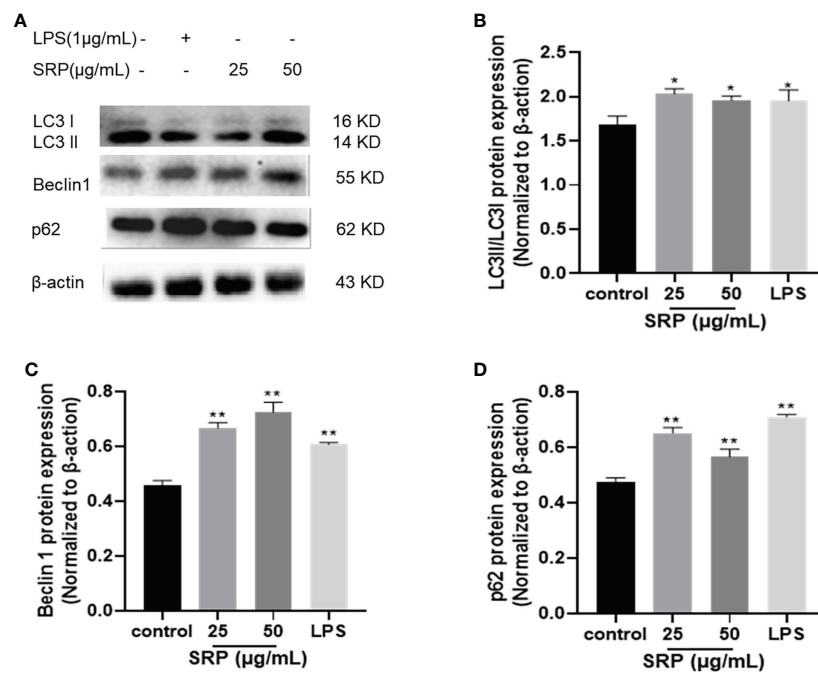


FIGURE 8

Expression of autophagic proteins. (A) Western blot analysis of protein bands; (B-D) LC3, Beclin1 and p62 protein expression. Significant differences with the control group: * $p < 0.05$ and ** $p < 0.01$.

isolated two components, SRP-1 and SRP-2 from the fruiting body of *S. rugosoannulata*. Both components contained glucose and galactose, but SRP-2 also contained ribose and uronic acid. We speculate that these differences in monosaccharide compositions of *S. rugosoannulata* were due to differences in the source material.

In our study, the polysaccharide from *S. rugosoannulata* was extracted by three-phase extraction. According to our analysis, the polysaccharide was heteropolysaccharide composed of 8 monosaccharides, and the molecular weight was 27.52 kDa, which was larger than that polysaccharides obtained by hot water extraction (22). The molecular mass of SRP was bigger, the monosaccharide composition was richer, and its physiological activity was stronger. At the same time, this method also had a positive effect on the structure modification, which can interrupt the long molecular chain of polysaccharides and the change of molecular aggregation state, so that the structure of polysaccharides can be changed. Finally, three-phase extraction affects the biological activity and chemical and physical properties, such as improving the antioxidant activity of the polysaccharides (40).

Polysaccharides can improve the immune activity of cells *in vitro*. MOP-3, a novel polysaccharide extracted from *Moringa oleifera* leaves, can enhance the ability of macrophages to secrete reactive oxygen species (ROS), nitric oxide (NO), interleukin-6 (IL-6) and tumor necrosis factor α (TNF- α), indicating that the polysaccharide can activate macrophages to produce cytokines, thus achieving the purpose of fighting pathogens (41). In this experiment, compared with blank control group, the SRP-treated group showed increased proliferation, phagocytosis and cell migration of 25-200 $\mu\text{g/mL}$.

Numerous studies have shown that polysaccharides can activate intracellular signaling pathways through TLR4 receptor-mediated macrophages, promote the release of related cytokines, and play immunomodulatory roles. For example, mushroom polysaccharides can activate peritoneal macrophages through the TLR4/NF- κB pathway, and significantly enhance the secretion of cytokines (42). Our study results showed that SRP significantly enhanced the protein expression of TLR4, MyD88 and NF- κB in the range of 25-50 $\mu\text{g/mL}$, and activated the TLR4-mediated MyD88 dependent pathway, which confirmed that TLR4/NF- κB signaling pathway is one of the important pathways through which polysaccharides exert immunomodulatory effects.

Autophagy is a highly conserved metabolic pathway in organisms. It can selectively degrade intracellular harmful components and play an important role in regulating immunity (35). At present, no articles related to SRP and autophagy have been found. So, this study confirmed that SRP can up-regulate autophagy related proteins LC3 and Beclin1, and down-regulate the expression of p62 protein to induce increased autophagy. This indicates that the mechanism of SRP's effect on inflammation is related to autophagy

induction. Moreover, the expression levels of related proteins and autophagy proteins in the TLR4/NF- κB signaling pathway were significantly increased in the macrophage SRP groups treated with 25-50 $\mu\text{g/mL}$, suggesting that SRP can activate the TLR4/NF- κB signaling pathway and autophagy.

5 Conclusion

In this study, a polysaccharide was extracted from the mushroom *Stropharia rugosoannulata*, using a new method, three-phase extraction. Extraction parameters were optimized as follows; mass fraction of ammonium sulfate, 20%; volume ratio of sample solution to t-butanol, 1:1.5; and the extraction temperature, 35°C. With these parameters, the yield of polysaccharides was $6.85\% \pm 0.13\%$. SRP had the molecular weight of 27.52 kDa. SEM showed that SRP surface was rough and flakey. XRD analysis showed that it had both crystalline and amorphous structures. The results of antioxidation experiments showed that SRP has antioxidant activity. The results of CCK-8 method showed that the polysaccharide concentration in the range of 25-200 $\mu\text{g/mL}$ promoted cell proliferation and had no cytotoxicity. This means that SRP is safe for clinical applications. RT-PCR results confirmed that SRP can significantly promote the release of cytokines such as IL-6 and TNF- α from peritoneal macrophages in the range of 25-100 $\mu\text{g/mL}$, and the purpose of immune enhancement by enhancing the activity of cytokines. Western blot results showed that SRP induced macrophages RAW264.7 to activate the TLR4/NF- κB signaling pathway of autophagy.

In conclusion, *S. rugosoannulata* has antioxidant and immunomodulatory activities. It appears to be safe. Thus, *S. rugosoannulata* has a broad prospect for further development as a new immunomodulator and antioxidant.

Data availability statement

The datasets presented in this study can be found in online repositories. The names of the repository/repositories and accession number(s) can be found in the article/Supplementary Material.

Author contributions

XL, ZZ: Research concept, Methodology, Data extraction, Analysis, Draft writing. XM: Resource searching, Verification, Formal analysis, Supervision, Manuscript reviewing and editing. LW, HZ, YJ: Resources, Methodology, Project administration, Supervision, Manuscript reviewing and editing. YW: Funding sponsorship. BM, JL: Resource searching, Manuscript reviewing and editing. All authors contributed to the article and approved the submitted version.

Funding

The present work was funded by the science and technology correspondent of Henan Province (2022, No.1963), the National Natural Science Foundation of China (Grant Nos.31602098 and 32072906), the Scientific and technological project of Henan province (Grant No. 192102110188 and 192102110184), the Special Fund for Henan Agriculture Research System (Grant No. HARS-22-16-Z1), the Science and Technology Project of Henan province (Grant No. 222102110063).

Acknowledgments

We would especially like to thank all those involved in the study.

Conflict of interest

Author JL was employed by Yucheng Jinlong Mushroom Co., LTD. Author YW was employed by GeneGenieDx Corporation.

References

- Jing W, Suzuki T, Choi JH, Yasuda N, Kawagishi H. An unusual sterol from the mushroom *Stropharia rugosoannulata*. *Tetrahedron Lett* (2013) 54(36):4900–2. doi: 10.1016/j.tetlet.2013.06.142
- Liu Y, Hu CF, Feng X, Cheng L, Huang W. Isolation, characterization and antioxidant of polysaccharides from *Stropharia rugosoannulata*. *Int J Biol Macromol* (2019) 155(19):883–889. doi: 10.1016/j.ijbiomac.2019.11.045
- He X, Fang J, Guo Q, Wang M, Huang L. Advances in antiviral polysaccharides derived from edible and medicinal plants and mushrooms. *Carbohydr Polym* (2019) 229:115548. doi: 10.1016/j.carbpol.2019.115548
- Zhang S, Li Y, Li Z, Liu W, Zhang H, Ohizumi Y, et al. Structure, anti-tumor activity, and potential anti-tumor mechanism of a fungus polysaccharide from *Fomes officinalis*. *Carbohydr Polym* (2022) 295:119794. doi: 10.1016/j.carbpol.2022.119794
- Ma X, Guo D, Peterson EC, Dun Y, Li DY. Structural characterization and anti-aging activity of a novel extracellular polysaccharide from fungus *Phellinus* sp. in a mammalian system. *Food Funct* (2016) 7(8):3468–79. doi: 10.1039/C6FO00422A
- Guo Q, Liang SM, Xiao ZC, Ge CR. Research progress on extraction technology and biological activity of polysaccharides from edible fungi: A review. *Food Rev Int* (2022) 3:1–32. doi: 10.1080/87559129.2022.2039182
- Hui HP, Gao WJ. Physicochemical features and antioxidant activity of polysaccharides from herba *Patriniae* by gradient ethanol precipitation. *Arabian J Chem* (2022) 15(5):103770. doi: 10.1016/j.arabjc.2022.103770
- Coimbra C, Lopes CE, Calazans G. Three-phase partitioning of hydrolyzed levan bioresource technology. *Bioresour Technol* (2010) 101(12):4725–8. doi: 10.1016/j.biortech.2010.01.091
- Yan JK, Wang YY, Qiu WY, Shao N. Three-phase partitioning for efficient extraction and separation of polysaccharides from *Corbicula fluminea*. *Carbohydr Polym* (2017) 163:10–9. doi: 10.1016/j.carbpol.2017.01.021
- Tan ZJ, Wang CY, Yi YJ, Wang HY, Zhou WL. Three phase partitioning for simultaneous purification of aloe polysaccharide and protein using a single-step extraction. *Process Biochem* (2015) 50(3):482–6. doi: 10.1016/j.procbio.2015.01.004
- Wang L, Liu HM, Qin GY. Structure characterization and antioxidant activity of polysaccharides from Chinese quince seed meal. *Food Chem* (2017) 234:314. doi: 10.1016/j.foodchem.2017.05.002
- Wang L, Zhao ZW, Zhao HQ, Liu M, Lin C, Li LZ, et al. Pectin polysaccharide from *Flos magnoliae* (Xin yi, *Magnolia biondii* pamp. flower buds): Hot-compressed water extraction, purification and partial structural characterization. *Food Hydrocolloids* (2022) 122:107061. doi: 10.1016/j.foodhyd.2021.107061
- Yang WJ, Pei F, Shi Y, Zhao LY, Fang Y, Hu QH. Purification, characterization and anti-proliferation activity of polysaccharides from *Flammulina velutipes*. *Carbohydr Polym* (2012) 88(2):474–80. doi: 10.1016/j.carbpol.2011.12.018
- Qiu JQ, Zhang H, Wang ZY. Ultrasonic degradation of polysaccharides from *Auricularia auricula* and the antioxidant activity of their degradation products. *LWT* (2019) 113:108266. doi: 10.1016/j.lwt.2019.108266
- Gao CJ, Wang YH, Wang CY, Wang ZY. Antioxidant and immunological activity *in vitro* of polysaccharides from *Gomphidius rutilus* mycelium. *Carbohydr Polym* (2013) 92(2):2187–92. doi: 10.1016/j.carbpol.2012.12.011
- Zhang ZQ, Li D, Ma X, Li XH, Guo ZH, Liu YL, et al. Carboxylated nanodiamond-mediated NH₂-PLGA nanoparticle-encapsulated fig polysaccharides for strongly enhanced immune responses *in vitro* and *in vivo*. *Int J Biol Macromol* (2020) 165:1331–45. doi: 10.1016/j.ijbiomac.2020.10.010
- Zubair M, Ekholm A, Nybom H, Renvert S, Widen C, Rumpunen K. Effects of *Plantago major* l. leaf extracts on oral epithelial cells in a scratch assay. *J Ethnopharmacol* (2012) 141(3):825–30. doi: 10.1016/j.jep.2012.03.016
- Wang H, Geng HY, Chen J, Wang X, Li D, Wang T, et al. Three phase partitioning for simultaneous extraction of oil, protein and polysaccharide from rice bran. *Innovative Food Sci Emerg Technol* (2020) 65:102447. doi: 10.1016/j.ifset.2020.102447
- Khataei MM, Yamini Y, Nazarpour A, Karimi M. Novel generation of deep eutectic solvent as an acceptor phase in three-phase hollow fiber liquid phase microextraction for extraction and preconcentration of steroidal hormones from biological fluids. *Talanta* (2018) 178:473–80. doi: 10.1016/j.talanta.2017.09.068
- Krisna C, Duong-Ly SB. Gabelli, chapter seven-salting out of proteins using ammonium sulfate precipitation. *Methods Enzymol* (2014) 541:85–94. doi: 10.1016/B978-0-12-420119-4.00007-0
- Ktari N, Feki A, Trabelsi I, Triki M, Maalej H, Slima SB, et al. Structure, functional and antioxidant properties in Tunisian beef sausage of a novel polysaccharide from *Trigonella foenum-graecum* seeds. *Int J Biol Macromol* (2017) 98:169–81. doi: 10.1016/j.jep.2012.03.016
- Chen JC, Weng MJ, Lai PF. Distribution of *Stropharia rugoso-annulata* polysaccharides molecular weight and component sugar. *China Agric Sci* (2011) 44(10):2109–17. doi: 10.3846/j.issn.0578-175.2011.10.016

The remaining authors declare that the research was conducted in the absence of any commercial or financial relationships that could be construed as a potential conflict of interest.

Publisher's note

All claims expressed in this article are solely those of the authors and do not necessarily represent those of their affiliated organizations, or those of the publisher, the editors and the reviewers. Any product that may be evaluated in this article, or claim that may be made by its manufacturer, is not guaranteed or endorsed by the publisher.

Supplementary material

The Supplementary Material for this article can be found online at: <https://www.frontiersin.org/articles/10.3389/fimmu.2022.994706/full#supplementary-material>

23. Morales D, Smiderle FR, Villalva M, Abreu H, Rico C, Santoyo S, et al. Testing the effect of combining innovative extraction technologies on the biological activities of obtained β -glucan-enriched fractions from *Lentinula edodes*. *J Funct Foods* (2019) 60:103446–6. doi: 10.1016/j.jff.2019.103446
24. Yang Y, Li C, Ni S, Zhang H, Dong C. Ultrastructure and development of acanthocytes, specialized cells in *Stropharia rugosoannulata*, revealed by scanning electron microscopy (SEM) and cryo-SEM. *Mycologia* (2021) 113(1):65–77. doi: 10.1080/00275514.2020.1823184
25. Li WA, Pzz A, Jws B, Yyq A, Miao LA, Yuan RA, et al. Physicochemical properties and bioactivities of original and Se-enriched polysaccharides with different molecular weights extracted from *Pleurotus ostreatus*. *Int J Biol Macromol* (2019) 141(C):150–60. doi: 10.1016/j.ijbiomac.2019.03.168
26. Wang Q, Zhao Y, Feng X, Ibrahim SA, Liu Y. Effects of drying on the structural characteristics and antioxidant activities of polysaccharides from *Stropharia rugosoannulata*. *J Food Sci Technol Mysore* (2021) 1:1–10. doi: 10.1007/s13197-021-05120-6
27. Yan JK, Ding ZC, Gao XL, Wang YY, Yang Y, Zhang HN. Comparative study of physicochemical properties and bioactivity of *Hericium erinaceus* polysaccharides at different solvent extractions. *Carbohydr Polym: Sci Technol Aspects Industrially Important Polysaccharides* (2018) 193:373–82. doi: 10.1016/j.carbpol.2018.04.019
28. Liu XG, Bian J, Li DQ, Liu CF, Xu SS, Zhang GL, et al. Structural features, antioxidant and acetylcholinesterase inhibitory activities of polysaccharides from stem of *Physalis alkekengi*. *Ind Crops Prod* (2019) 129:654–61. doi: 10.1016/j.indcrop.2018.12.047
29. Wang HL, Ma CY, Sun-Waterhouse DX, Wang JM, Waterhouse GIN, Kang WY. Immunoregulatory polysaccharides from *Apocynum venetum* L. flowers stimulate phagocytosis and cytokine expression via activating the NF- κ B/MAPK signaling pathways in RAW264. 7 cells. *Food Sci Hum Wellness* (2022) 11(4):806–14. doi: 10.1016/j.fshw.2022.03.012
30. Bobadilla AVP, Arévalo J, Sarró E, Byrne HM, Maini PK, Carraro T, et al. *In vitro* cell migration quantification method for scratch assays. *J R Soc Interface* (2019) 16(151):20180709. doi: 10.1098/rsif.2018.0709
31. Cao HY, Liu JX, Shen P, Cai JP, Han YC, Zhu KP, et al. Protective effect of naringin on DSS-induced ulcerative colitis in mice. *J Agric Food Chem* (2018) 66(50):13133–40. doi: 10.1021/acs.jafc.8b03942
32. Liu ZD, Liu ZF, Li LH, Zhang JJ, Zhao QC, Lin N, et al. Immunomodulatory effects of the polysaccharide from *Sinonovacula constricta* on RAW264.7 macrophage cells. *Food Sci Nutr* (2022) 10(4):1093–1102. doi: 10.1002/fsn3.2735
33. Ren DY, Lin DH, Alim A, Zheng Q, Yang XB. Chemical characterization of a novel polysaccharide ASKP-1 from *Artemisia sphaerocephala* krasch seed and its macrophage activation via MAPK, PI3k/Akt and NF- κ B signaling pathways in RAW264.7 cells. *Food Funct* (2017) 8(3):1299–312. doi: 10.1039/C6FO01699E
34. Chen GP, Yan F, Wei W, Wang FF, Wang ZR, Nie JH, et al. CD38 deficiency protects the retina from ischaemia/reperfusion injury partly via suppression of TLR4/MyD88/NF- κ B signalling. *Exp Eye Res* (2022) 219:109058. doi: 10.1016/j.exer.2022.109058
35. Cui B, Lin H, Yu JM, Yu JJ, Hu ZW. Autophagy and the immune response. *Autophagy: Biol Dis* (2019) 1206:595–634. doi: 10.1007/978-981-15-0602-4_27
36. Maiuri MC, Criollo A, Kroemer G. Crosstalk between apoptosis and autophagy within the beclin 1 interactome. *EMBO J* (2010) 29(3):515–6. doi: 10.1038/emboj.2009.377
37. Alves A, Sousa RA, Reis RL. A practical perspective on ulvan extracted from green algae. *J Appl Phycol* (2013) 25(2):407–24. doi: 10.1007/s10811-012-9875-4
38. Waghmare AG, Salve MK, LeBlanc JG, Arya SS. Concentration and characterization of microalgae proteins from *Chlorella pyrenoidosa*. *Biores Bioprocessing* (2016) 3(1):1–11. doi: 10.1186/s40643-016-0094-8
39. Lu QJ, Xue S, Yang DS, Wang H, Li L. Effects of three extraction methods on antioxidant properties of crude polysaccharides from *Stropharia rugoso*. *Food Sci Technol* (2021) 46(11):171–8. doi: 10.13684/j.cnki.spkj.2021.11.027
40. Ji XL, Hou CY, Shi MM, Yan YZ, Liu YQ. An insight into the research concerning *Panax ginseng* CA Meyer polysaccharides: a review. *Food Rev Int* (2020) 227:1149–65. doi: 10.1080/87559129.2020.1771363
41. Li C, Dong ZP, Zhang B, Huang Q, Liu G, Fu X. Structural characterization and immune enhancement activity of a novel polysaccharide from *Moringa oleifera* leaves. *Carbohydr Polym* (2020) 234:115897. doi: 10.1016/j.carbpol.2020.115897
42. Ghosh S, Khatua S, Dasgupta A, Acharya K. Crude polysaccharide from the milky mushroom, *Calocybe indica*, modulates innate immunity of macrophage cells by triggering MyD88-dependent TLR4/NF- κ B pathway. *J Pharm Pharmacol* (2021) 73(1):70–81. doi: 10.1093/jpp/rgaa020



OPEN ACCESS

EDITED BY

Guiyan Yang,
University of California, Davis, United States

REVIEWED BY

Haroon Kalam,
Broad Institute, United States
Said Elshafae,
Benha University, Egypt

*CORRESPONDENCE

Shouqun Jiang
✉ jiangshouqun@gdaas.cn
Mahmoud Alagawany
✉ dr.mahmoud.alagawany@gmail.com

SPECIALTY SECTION

This article was submitted to
Nutritional Immunology,
a section of the journal
Frontiers in Immunology

RECEIVED 17 October 2022

ACCEPTED 06 January 2023

PUBLISHED 31 January 2023

CITATION

El-Shall NA, Jiang S, Farag MR, Azzam M,
Al-Abdullatif AA, Alhotan R, Dhama K,
Hassan F-u and Alagawany M (2023)
Potential of *Spirulina platensis* as a feed
supplement for poultry to enhance growth
performance and immune modulation.
Front. Immunol. 14:1072787.
doi: 10.3389/fimmu.2023.1072787

COPYRIGHT

© 2023 El-Shall, Jiang, Farag, Azzam,
Al-Abdullatif, Alhotan, Dhama, Hassan and
Alagawany. This is an open-access article
distributed under the terms of the [Creative
Commons Attribution License \(CC BY\)](#). The
use, distribution or reproduction in other
forums is permitted, provided the original
author(s) and the copyright owner(s) are
credited and that the original publication in
this journal is cited, in accordance with
accepted academic practice. No use,
distribution or reproduction is permitted
which does not comply with these terms.

Potential of *Spirulina platensis* as a feed supplement for poultry to enhance growth performance and immune modulation

Nahed A. El-Shall¹, Shouqun Jiang^{2*}, Mayada R. Farag³,
Mahmoud Azzam^{4,5}, Abdulaziz A. Al-Abdullatif⁴,
Rashed Alhotan⁴, Kuldeep Dhama⁶, Faiz-ul Hassan⁷
and Mahmoud Alagawany^{8*}

¹Department Poultry and Fish Diseases, Faculty of Veterinary Medicine, Alexandria University, Edfina, El-Beheira, Egypt, ²Institute of Animal Science, Guangdong Academy of Agricultural Sciences, State Key Laboratory of Livestock and Poultry Breeding, Key Laboratory of Animal Nutrition and Feed Science in South China, Ministry of Agriculture and Rural Affairs, Guangdong Provincial Key Laboratory of Animal Breeding and Nutrition, Guangzhou, Guangdong, China, ³Forensic Medicine and Toxicology Department, Faculty of Veterinary Medicine, Zagazig University, Zagazig, Egypt, ⁴Department of Animal Production College of Food & Agriculture Sciences, King Saud University, Riyadh, Saudi Arabia, ⁵Poultry Production Department, Agriculture Faculty, Mansoura University, Mansoura, Egypt, ⁶Division of Pathology, Indian Council of Agricultural Research-Indian Veterinary Research Institute, Bareilly, Uttar Pradesh, India, ⁷Institute of animal and Dairy Sciences, University of Agriculture, Faisalabad, Pakistan, ⁸Poultry Department, Agriculture Faculty, Zagazig University, Zagazig, Egypt

Increase in drug resistance as well as ineffective immunization efforts against various pathogens (viruses, bacteria and fungi) pose a significant threat to the poultry industry. *Spirulina* is one of the most widely used natural ingredients which is becoming popular as a nutritional supplement in humans, animals, poultry and aquaculture. It contains protein, vitamins, minerals, fatty acids, pigments, and essential amino acids. Moreover, it also has considerable quantities of unique natural antioxidants including polyphenols, carotenoids, and phycocyanin. Dietary supplementation of *Spirulina* can beneficially affect gut microbial population, serum biochemical parameters, and growth performance of chicken. Additionally, it contains polyphenolic contents having antibacterial effects. *Spirulina* extracts might inhibit bacterial motility, invasion, biofilm formation, and quorum sensing in addition to acting directly on the bacterium by weakening and making the bacterial cell walls more porous, subsequently resulting in cytoplasmic content leakage. Additionally, *Spirulina* has shown antiviral activities against certain common human or animal viruses and this capability can be considered to exhibit potential benefits against avian viruses also. Spirulan, a calcium-rich internal polysaccharide of *Spirulina*, is potentially responsible for its antiviral effect through inhibiting the entry of several viruses into the host cells, boosting the production of nitric oxide in macrophages, and stimulating the generation of cytokines. Comparatively a greater emphasis has been given to the immune modulatory effects of *Spirulina* as a feed additive in chicken which might boost disease resistance and improve survival and growth rates, particularly under stress conditions. This manuscript reviews biological activities and immune-stimulating

properties of *Spirulina* and its potential use as a dietary supplement in poultry to enhance growth, gut health and disease resistance.

KEYWORDS

Spirulina platensis, poultry, production, immunity, antimicrobials, antiviral, anticoccidial, nutrition

Introduction

Numerous diseases continue to occur in the poultry industry despite the widespread use of vaccines and medications, resulting in financial losses. For instance, avian viral infections such as avian influenza (AI), infectious bronchitis (IB), infectious bursal disease (IBD), and Newcastle disease (ND) lead to significant economic losses, particularly in broilers, due to respiratory distress, increased mortality, reduced growth, and immunological suppression (1). The same is true for coccidiosis and bacterial infections like *Salmonella*, *E. coli*, etc. Until the emergence of resistant strains, chemical antimicrobials and antiprotozoals successfully inhibited and suppressed bacteria and protozoa. So there is a persistent need to use natural substances to address this issue. Algae, for instance, is a source of vital biological useful components, making the use of natural habitats as a source of these chemicals a viable strategy for creating innovative cuisines (2, 3). One of the greatest sources for organic nutrients among edible algae is the microscopic blue-green alga *Spirulina* (Arthrospira), which is used as a nutritional supplement for both human and animal feed globally (4). *Spirulina platensis* is a filamentous commercial cyanobacterium that is utilized as dietary and feed supplement in humans, aquaculture, livestock and poultry industry. *Spirulina* can grow in both saline and fresh water, and it is semi- and mass-cultivated in several countries. Dried spirulina is a rich nutritional source, with a high protein content (260–770 g/kg) representing 70% dry weight and a large fat content (10–140 g/kg) (5–7). Additionally, it has been observed that these microalgae have a high nutrient digestibility that was superior or equivalent to that of other vegetable diets and feeds (6, 8). Therefore, *Spirulina* has the potential to partially replace the traditional protein sources, particularly soybean meal (9). Oleic acid, linoleic acid, gamma-linolenic acid, docosahexaenoic acid (DHA), sulfolipids, and glycolipids are among the many polyunsaturated fatty acids found in spirulina, in addition to Omega-3 and -6 polyunsaturated fatty acids that are abundant in spirulina (25% and 60% of the total fatty acids) (5, 10). *Spirulina* also contains pigments, such as carotenoids (4000 mg/kg), which include β -carotene and zeaxanthin (10, 11), and chlorophyll pigments (12–14). Phycobiliproteins (15), vitamins (16), and macro- and micromineral components like calcium, iron, magnesium, manganese, potassium, zinc, and selenium are also found in spirulina (10, 17). Moreover, polysaccharides, pro-vitamin A, vitamin E, vitamin K and various B vitamins (10) as well as antioxidants are also important constituents of spirulina (18).

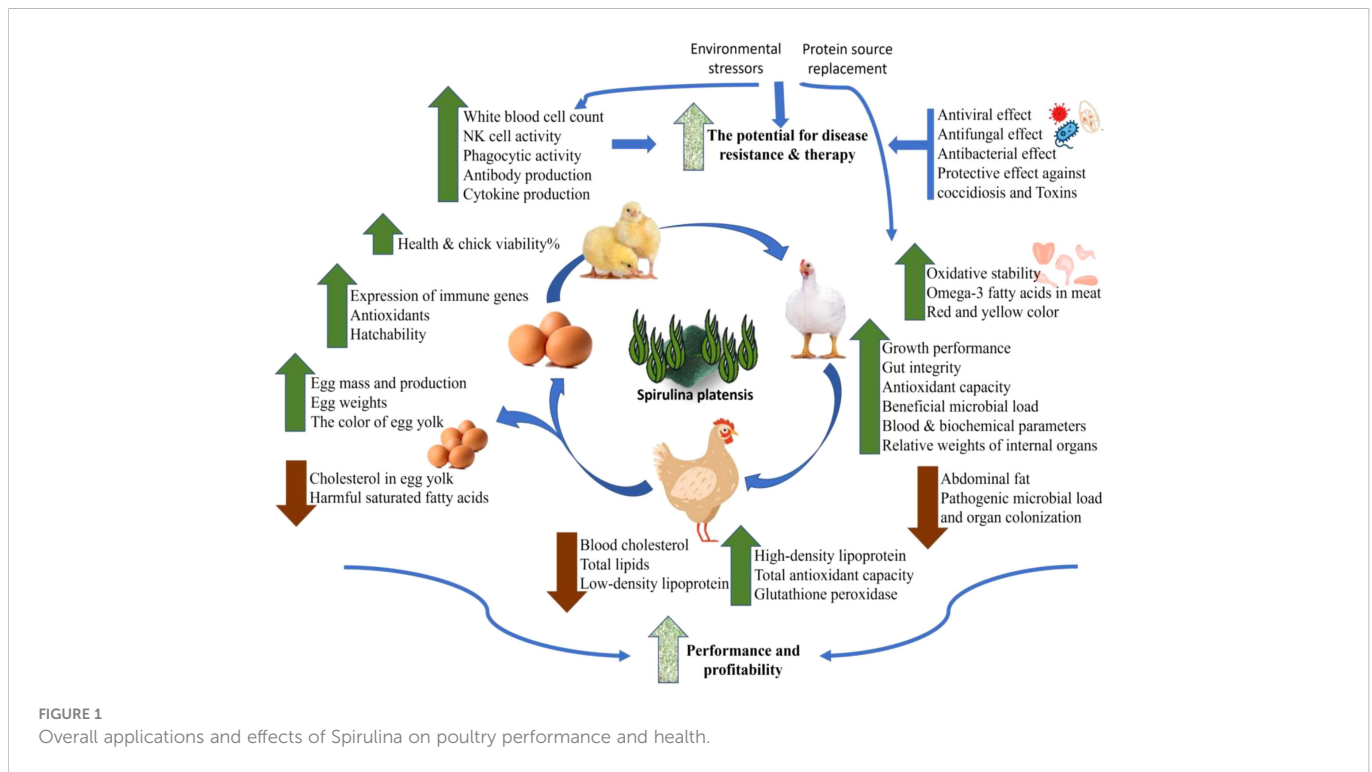
Spirulina is used as a dietary additive in a wide variety of food products due to its exceptional and impressive nutrient composition. This helps to improve the nutritional qualities of the products, as well

as their potential to improve reproductive and productive performance, general health, and the symptoms of various animal diseases like arthritis, diabetes, anaemia, hypertension, and cardiovascular disorders. *Spirulina* are strong contenders as an alternative to antibiotics in chicken feed. These substances exhibited potential medicinal properties like antimicrobial, antioxidant, anti-cancer, anti-inflammatory, immune-enhancing, and colourants (18–20) in addition to their metalloprotective, radioprotective, and hypocholesterolemic effects (4, 10). Additionally, *Spirulina* (SPA) with antiviral properties has shown to strengthen the immune system, and its rich nutritional profile promoted growth performance by improving the intestinal villi length and number of the epithelial cells particularly goblet cells (21). For a sustainable and feasible future of food security, spirulina is becoming a more affordable method of increasing poultry output (9). Here, therapeutic and immune-stimulating benefits of *Spirulina* were reviewed from another angle in case they could actually be used as nutritional supplement with antibiotic or vaccine to fight off various diseases of chicken (Figure 1).

Effects of *Spirulina platensis* on productive performance

Numerous studies have supported spirulina's ability to promote growth. From the embryonic stage until the egg is laid, spirulina can be supplemented in poultry diets. *Spirulina platensis* in ovo injection enhanced the expression of genes associated to immunity, antioxidants, and hatchability in quail chicks (22). Ibrahim et al. (23) reported that spirulina in drinking water for 4 weeks at levels of 0.5, 1 and 2 g/Liter significantly increased the average body weight gain, health, with the highest chick viability percent, best significant feed conversion ratio (FCR), feed efficiency, European Production Efficiency values, increase in the relative weights of carcass and internal organs with the significantly lowest abdominal fat. *Spirulina* supplemented (1 or 2 g/kg diet) in diets containing vegetable and animal protein in Japanese quails improved the growth performance without affecting meat quality or gut flora in quails fed with vegetable protein source but no effect was observed in animal protein based diet (24).

K-strain White Cornell Leghorns and broiler chicks grown to ages of seven and three weeks, respectively, on diets containing varied concentrations (10, 100, 1,000, and 10,000 ppm) of *Spirulina platensis* exhibited higher body weights than control birds (25). With 0.7 and 0.9 g of *Spirulina platensis* per kg of feed, Cobb broiler chickens'



growth performance, blood parameters, biochemical changes in serum, and microbial load could all be improved (26).

Dietary supplementation of Spirulina at 10g/kg of diet showed significantly higher body weight gain and, consequently, linear improvements in FCR was observed in Cobb broilers during 35 days experimental period. Additionally, dietary Spirulina levels resulted in a rise in intestine *Lactobacillus* sp. while decreasing *Escherichia coli* populations (27).

Hajati and Zaghari (28) advocate utilizing Spirulina at dosages of 5 and 3 g/kg food during the Japanese quail's growth and laying periods, respectively, using a range of varied doses. During the first 35 days of life, a diet of 5 g/kg induced a significant increase in body weight gain, breast percentage, and European production efficiency factor. When added to the diet of layers, Spirulina at a level of 3 g/kg considerably reduced the amount of cholesterol per gram of yolk while also improving the color of the egg yolks.

However, daily feed intake, FCR, the percentage of broken eggs, eggshell thickness, albumen height, Haugh unit, and egg weight were unaffected by dietary Spirulina up to 0.9%. When compared to non-supplemented birds, 0.6% algae significantly increased egg mass and production as well as egg yolk colour in laying chickens between 26 and 37 weeks of age (29).

For improved reproductive and productive performance, Mobarez et al. (30) suggested adding Spirulina to Golden Montazah layer diets. When given the basic diet with 2 or 3 g Spirulina/kg diet during the laying period from 29 to 40 weeks of age, hens and cocks had significantly improved FCR compared to the control group. Additionally, chickens fed a diet containing 3 g of Spirulina/kg had the highest levels of high-density lipoprotein (HDL), total antioxidant capacity (TAOC), glutathione peroxidase (GPx), egg quantity, egg weight, and hatchability percentage. Blood cholesterol, total lipids, and low-density lipoprotein (LDL)

were all significantly reduced with Spirulina administration at both dosages.

Microalgae in quail diets (5%, 10%, and 15%) increased egg quality and provided benefits to consumer health by functioning as an immune-stimulant and antioxidant (31). However, they had no effect on egg production. This was because it boosted amounts of monounsaturated fatty acids, which are good for consumer health, and decreased levels of harmful saturated fatty acids. Additionally, egg yolk antioxidant levels increased, which reduced lipid peroxidation. On the other hand, 32 reported a lower performance of broiler chickens supplemented with Spirulina by 15%, for 2 weeks period (21st -35th day old), compared to non-supplemented birds. They attributed this negative effect to the high digesta viscosity induced by the gelation of indigestible proteins of Spirulina. Even addition of exogenous enzymes like lysozyme or Rovabio Excel AP resulted in the same worse findings, although lysozyme succeeded in breaking Spirulina' cell wall. Pestana and hos co-authors suggested that this microalga's proteins may be more easily digested and prevented from harmfully gelling if lysozyme and an exogenous specialised peptidase were combined.

Effects of *Spirulina platensis* on the immune system

Supplementing with spirulina boosts many immune processes. Spirulina has shown a specific action on monocytes and natural killer (NK) cells, which are essential components of the innate immune system. Administration of Spirulina exhibited to enhance macrophage phagocytic response and activity of NK cells in chicken and humans (25, 33, 34). The phagocytic activity of macrophages isolated from cats was also found to be increased in response to

antigen exposure in the presence of *Spirulina* (25). A polysaccharide extract of *Spirulina platensis* has shown to increase white blood cells in a haematopoietic system damaged by irradiation (35). Oral administration of *Spirulina platensis* in healthy male volunteers increased IFN- γ production and phagocytic activity of isolated NK cells stimulated with IL-12/18. Beside this, *Spirulina* also enhanced Toll like receptor (TLR)-2 and 4 mediated production of IL-12 from peripheral blood mononuclear cells, thus indicating *Spirulina* first activates monocytes and macrophages to produce cytokines that stimulate NK cells (34). An action through TLR-2 or -4, leading to NF- κ B activation, has been suggested in studies in human monocytes (36, 37).

Spirulina's immune-modulatory action on mice through increased IL-1 antibody production was observed in 1994 for the first time (38). In this regard, Kaoud (39) found that chicken groups fed diets containing spirulina had higher relative and absolute thymus and bursa weights than the control group. Similarly, in comparison to the untreated control, the addition of *S. platensis* at levels of 0.7 and 0.9 g/kg broiler diet resulted in a considerable rise in the weights of the bursa, thymus, and spleen (26). However, broilers and K-strain chicks given *Spirulina* (0, 10, 100, 1,000, and 10,000 ppm) did not change in bursal or splenic weight, but the K-strain chicks had significant larger thymuses than the controls (25).

A considerable rise in white blood cell count and increased macrophage phagocytic activity in broilers treated with *S. platensis* algae suggested that the immune system of the animals was strengthened (40).

According to Al-Batshan et al. (33) feeding *Spirulina platensis* increases macrophage phagocytic activity in terms of the average number of sheep red blood cells (SRBC) per phagocytic macrophage (range = 2.2 to 3.6 versus 1.8 to 2.5 in the basal group) and the overall phagocytic percentage (range = 28 to 39% versus 24 to 25% in the basal group). Over the course of the three developmental ages, *Escherichia coli* lipopolysaccharides-induced nitrite levels in macrophages (increased nitric oxide synthase activity) ranged from 60 to 278 microM in the basal diet group, but they were significantly higher in all *Spirulina* dietary groups (0.5% group range = 198 to 457 microM; 1.0% group range = 161 to 359 microM; and 2.0% group range = 204 to 420 microM).

Spirulina supplementation at 10000 ppm of diet also doubled the activity of NK cells and showed a greater PHA-P-mediated lymphoproliferative response compared to controls. All *Spirulina* groups (10, 100, 1000, 10000 ppm) demonstrated greater macrophages phagocytic capacity than the 0 ppm group in K-strain and broilers (25).

When compared to 1 g *Spirulina*/kg, laying Japanese quails given 3 or 5 g *Spirulina*/kg had significantly enhanced cutaneous basophil hypersensitivity after 12 or 24 hours of phytohemagglutinin injection (28). A substantially less heterophil and more lymphocytes than the control treatment were obtained by 1, 1.5, and 2 g spirulina/kg fed to broilers for 42 days (21). It has been demonstrated to increase the potential for disease resistance in chicken by activating their mononuclear phagocytic system (41). Improvement in cellular immunity observed in response to dietary supplementation of *Spirulina* might be attributed to higher Zn concentration in spirulina like this (42, 43).

In Cornell K-strain White Leghorns and broiler chicks fed to 7 and 3 weeks of age, respectively, with meals containing varying amounts of *Spirulina platensis* (0, 10, 100, 1,000, and 10,000 ppm), anti-sheep red blood cell antibodies were not different throughout the initial reaction. However, all *Spirulina*-dietary groups with K-strain chicks exhibited greater total anti-SRBC titers during the secondary response, with the 10,000-ppm group having the highest (6.8 Log2) compared to the 0 ppm (5.5 Log2) group (25). In laying Japanese quails, different concentrations of *Spirulina* (1, 3 or 5 g/kg food) resulted in significantly greater levels of total antibody against SRBC and IgG titers (28).

Khan et al. (21) showed that the use of spirulina considerably enhanced growth performance, gut integrity, and immunity in broiler production while also providing better economics and supplementing with spirulina significantly affected the antibody titer against the ND vaccination.

In growing Japanese quail chicks, adding *Spirulina* at concentrations of 0.5, 1 and 2 g/Liter significantly raised the amount of serum antibodies against the Newcastle virus (NDV) and the plasma total protein profile (23).

Additionally, Golden Montazah laying hens and cocks supplemented with 3 g *Spirulina*/kg diet during the laying period recorded significantly higher antibody titers against NDV, Avian Influenza (AI), antibody against SRBC, and Interferon proteins (IFN- γ) concentration (30). Similarly Nia et al. (29) revealed that *Spirulina* by levels 0.3%, 0.6% or 0.9% in Lohmann Selected Leghorn (LSL) laying hens between the ages of 26 and 37 weeks had a substantial impact on the antibody titer in birds that had received the Newcastle vaccine. However, the ratio of heterophiles to lymphocytes, humoral immunity against SRBC, cell-mediated immunity response to PHA injection, and the relative weight of the bursa and spleen were not significantly affected by this dietary *Spirulina*.

Additionally, the immunosuppressive effects of diclofenac sodium, which were manifested by decreased phagocytic activity, phagocytic index, and a significant decrease in the titer of antibodies formed against NDV were significantly reversed by oral supplementation of broiler chicks with *Spirulina* at a dose of 10 gm/kg in their diet, either on therapeutic or preventive regimes (44).

Antioxidant effects and *Spirulina platensis's* impact on meat quality

Because microalgae are a significant source of C-phycoyanin, an antioxidant pigment with hypolipidemic activity, birds fed *Spirulina* showed improved antioxidant activity, which is another benefit of *Spirulina* feed (45, 46). Phycocyanin, carotene, and xanthophyll phytopigments, tocopherols, linolenic acid, and phenolic compounds are some examples of naturally occurring components in *Spirulina* that have been demonstrated to have strong antioxidant properties and potent scavenging activities against Reactive Oxygen Species like superoxide and hydrogen peroxide radicals (4).

Abdelkhalek et al. (47) reported that spirulina dramatically stimulates the activity of antioxidant enzymes preventing lipid peroxidation, DNA damage, and free radical scavenging. The total antioxidant capacity and thyroxine (T4) content were dramatically

enhanced in growing Japanese quail chicks when *Spirulina* levels of 0.5, 1 and 2 g/Liter were used. Plasma cholesterol, total lipids, ALP, ALT, and AST activity, however, had significantly lower levels (23).

Additionally, *in ovo* injections of *Arthrospira* (*Spirulina*) *platensis* at doses of 0.75–3.5 mg/egg in Japanese quails and 25–35 mg/egg in broiler breeders enhanced chick hatchability and IFN- γ expression. In quails, 2.5 or 3.5 mg *Spirulina* dramatically reduced expression of HSP70 and considerably boosted Catalase activity and GPX gene expression in hatchlings. The lowest HSP70 in chicks was induced by *in ovo* injection of 25 or 35 mg *Spirulina* in broiler breeders (22).

Moreover, spirulina inclusion in the poultry feed affects meat quality parameters like color, flavor, polyunsaturated fatty acids composition, and oxidative stability. Therefore, in terms of oxidative stability and the enhancement of omega-3 fatty acids like those of linolenic and docosahexaenoic acid by *Spirulina* feeding, 1.5% fed to Cobb 500 broiler chicks for 5 weeks could be potential functional ingredients to generate value-added broiler meat (breast and thigh meat) (48). Similarly, Abbas et al. (49) demonstrated that 3% and 4% of dietary *Spirulina* significantly increased the content of oleic acid, palmitic acid, docosahexaenoic acid, and linoleic acid in broiler carcass. Additionally, throughout the 30-day storage period, 4% *Spirulina* considerably decreased the value of peroxide. For the 60-day storage period, both *Spirulina* treatments significantly reduced the oxidation indices of total volatile nitrogen (TVN) and thiobarbituric acid (TBA), while the sensory evaluation ratings for the chest and thigh slices did not change. 50 reported an unchange of the amount of gamma-linolenic acid or omega-3 in the intramuscular fat by 75% and 50% Soy bean replacement by *Spirulina* in starter and grower feed, respectively, although the richness of *Spirulina* with polyunsaturated fatty acids. Moreover, when *Spirulina*-based meat samples were wrapped in highly oxygenated modified environment packaging, they showed higher rates of lipid oxidation than soybean meal-based meat samples (50). On another side, color of meat was improved by inclusion of spirulina at high doses in the feed that may be due to high level of carotenoids. Altmann et al. (51) found that when *Spirulina* replaces 50% of the soy protein in broiler diets, meat color could be increased to be dark reddish-yellowish flesh. Similarly, Altmann et al. (50) observed a more intensive color (higher red (a^*) and yellow (b^*)) for breast and thigh meat as well as an increased umami and chicken flavor were reported for broiler meat. 51 reported a positive effect of *Spirulina* on flavour breast filets through decreasing the score of metallic flavor (off-flavor) of breast meat, besides increasing pH value after 24 hours after death that was associated with softness and tenderness of breast filets. Feeding broiler chickens with *Spirulina* 15% for two, the breast and thighs exhibited higher values of yellowness (b^*) compared to the control, as well as total carotenoids and saturated fatty acids were increased, but levels of n-3 polyunsaturated fatty acids and α -tocopherol were reduced (32). Nevertheless, Park et al. (52) found that the quality of the breast meat of broilers fed *Spirulina* diets (0.25, 0.5, 0.75, or 1.0%) for 35 days was not substantially altered while seven-day drip loss was linearly reduced.

Anti-pathogenic effects of *Spirulina platensis*

Dietary spirulina have shown good response in several infections *in vivo* in poultry (Table 1). A wide variety of influenza viruses, including oseltamivir-resistant strains, were blocked by the cold-water *Spirulina* extract from forming viral plaques. Inhibition of influenza hemagglutination was revealed to be one of the ways by which spirulina extract acts early in the course of infection to lower viral production in cells and increase survival in influenza-infected mice (58). The ethanol extract of *Spirulina platensis* had an antiviral effect *in vitro*, decreasing the infectious units of adenovirus types 7, Coxsackievirus B4, astrovirus types 1, rotavirus Wa strain, and adenovirus types 40 by respective amounts of 53.3%, 66.7%, 76.7%, 56.7%, and 50% (59).

It was reported that a calcium-rich intracellular polysaccharide called spirulan found in *Spirulina platensis* prevents multiple viruses from replicating *in vitro* by preventing the virus' entry into the various host cells that are being utilized (60, 61), increases macrophage nitric oxide synthesis and stimulates cytokine production (62). Broiler hens infected with the H5N1 Avian Influenza virus had cardiac necrosis, although 20% of spirulina had no discernible effect on this. However, it boosted leukocytes associated with an immune function, which prevented mortality vs 30% death in the non-supplemented group (41).

Regarding Newcastle disease, most investigations such as (53, 54) found that *Spirulina* had an impact on viral challenge in birds that had received live, attenuated, and/or inactivated vaccinations. As a result, the effect of *Spirulina* supplementation was seen as an immune-stimulating effect that dramatically improved clinical protection against heterologous strains and the capacity to decrease NDV shedding. In 2019, Kumari et al. discussed an indirect benefit of spirulina on infectious bursal disease. The decreasing effect of intermediate plus vaccine (hot strain given at the age of 17 days) on serum total protein concentration was greatly reduced by spirulina supplementation at 1.0% in feed from 10 to 20 days of age.

Cyanobacteria might be considered a suitable source for the manufacturing of antimicrobial agents as purified antimicrobial compound produced by *S. platensis* were more effective against Gram positive, Gram negative, and *C. albicans*, a unicellular fungus. Organic and aqueous extracts of *S. platensis* were tested *in vitro* and demonstrated broad-spectrum antibacterial and antifungal action. 63 showed that the highest biological activity of them was against *Escherichia coli*, *Pseudomonas aeruginosa*, *Bacillus subtilis* and *Aspergillus niger*. Compared to ethanol or aqueous extracts, methanol extract exhibited superior antibacterial activity against all tested bacterial strains (Gram positive bacteria, Gram negative bacteria, and *Candida* sp.), particularly against Gram positive bacteria (*Staphylococcus aureus*, *Streptococcus pneumoniae*, *Bacillus cereus*, and *Enterococcus faecalis*). For the various strains examined, the lowest inhibitory concentration value of ethanol and methanol extract ranged between 5–100 mg/mL (64). Similarly, compared to other extracts, the methanolic extract of *Spirulina* showed a larger total phenolic content and more antibacterial activity (65, 66).

TABLE 1 Efficacy of *Spirulina platensis* (SP) supplementation in cases of various infectious diseases in poultry.

Algae/dose	Route of administration/duration	Birds	Vaccination/Age	Infectious challenge/Age/dose/route	Main results	Reference
Avian Influenza						
<i>S. platensis</i> 0%, 10%, 20%	Drinking water/7 th day to 32 nd day	Broiler chickens	No vaccine	Avian Influenza H5N1/26 days old/0.1 ml inoculum containing 10 ⁷ EID ₅₀ /nose drops	Myocardial necrosis did not differ significantly from either group. Comparing SP 10% and 20% to a control therapy without it, more leukocytes were produced. 20% SP showed no mortality, but 0% and 10% spirulina revealed 30% mortality.	(41)
New Castle disease						
<i>S. platensis</i> 0, 0.5, 1, 1.5 and 2 g/kg of ration	Feed at 7 days of age	SPF chickens	Commercial inactivated Newcastle disease (ND) vaccine at 21 days of age	NDV genotype VII/28 days post-vaccination/0.5 mL/bird containing 10 ⁶ EID ₅₀ /intramuscular (I/M)	Compared to untreated vaccinated hens, offered adequate protection against heterologous challenge virus (90%, 100%, 100%, and 100%, respectively). Compared to the untreated group (46%), treated vaccinated hens excreted fewer viruses (55%, 65%, 76%, and 87%).	(53)
0, 1% of Microalgae (<i>Scenedesmus obliquus</i> , <i>Scenedesmus quadricauda</i> , <i>Ankistrodesmus</i> , <i>Coelastrum microporum</i> , <i>Selenastrum</i> , <i>Oocystis parva</i> , <i>Dictyosphaerium pulchellum</i> , <i>Coelastrum reticulatum</i> , <i>Pediastrum gracillimum</i> , <i>Siderocells elegans</i> , <i>Eudorina elegans</i> , <i>Clamydomonas reinhardi</i> and <i>Micractinium pusillum</i> (green algae group), <i>Euglena</i> sp. (Euglenophyta), <i>Oscillatoria limnetica</i> (blue-green algae group) and <i>Nitzschia linearis</i> (diatoms group)	Feed (1 st -40 th day of age)	Broiler chickens	■live NDV La Sota strain by oculo-nasal route at 5 th day and/or ■Inactivated NDV genotype II vaccine S/C at 18 th day	vvNDV genotype VIIId/6-Log-10 EID ₅₀ given 0.5 ml/bird via I/M at 28 th day	The serological response, viral shedding after viral challenge, protection rate, and body weight increase of the chicken groups that received either a microalgae-free diet or one that included microalgae were comparable.	(54)
Infectious bursal disease						
Probiotic <i>S. platensis</i> 0, 1%	Feed (10 th -20 th day)	chickens	IBDV intermediate plus strain vaccine (hot strain)/17 days	–	The adverse effects of the IBD vaccine's hot strain on blood total protein and albumin levels could be slightly mitigated by SP supplementation.	(55)
Salmonellosis						
<i>S. platensis</i> at 0, 1, and 2 g/kg diet	Feed (7 th day–experimental end)	quail	–	<i>S. enteritidis</i> /orally/21 st day/1ml of 1.00x10 ⁷)	SP dramatically increased IL-10, antioxidant and serum biochemical markers, and growth performance. It decreased the post-challenge death rate from 23.33% in the untreated group to 10% in the groups who received both doses of treatment and had significantly lower clinical symptoms. It considerably decreased organ colonization (liver, heart, spleen, caecum). The expression of the genes for serum amyloid and the pro-inflammatory IL-6, IL1 β,	(56)

(Continued)

TABLE 1 Continued

Algae/dose	Route of administration/duration	Birds	Vaccination/Age	Infectious challenge/Age/dose/route	Main results	Reference
					and TNF- α in the cecum was considerably downregulated.	
Coccidiosis						
Microalgae-derived feed ingredients at 0.175%	Feed up to 42 days old	Ross 308 broilers	–	10X Coccivac-B52 vaccine/orally/at 14 th day of age	Birds fed algae shed 2.3 times more oocysts than birds fed the control diet. Algal inclusion had no impact on the rate of growth and did not shield birds that had been injected with <i>Eimeria</i> from the modifications that <i>Eimeria</i> caused to their splenic T cells. However, algae significantly protected jejunal villus height as early as 7 day post infection and maintained intestinal integrity during coccidiosis.	(57)

Kaushik and Chauhan (67) reported that the minimum inhibitory concentrations (MIC) of the methanol extract against *S. aureus* and *E. coli* were 128 g/ml and 256 g/ml, respectively while it had no effect was against *Klebsiella pneumoniae*. Nevertheless, *Spirulina* acetone extract shown strong biological activity against *Klebsiella pneumoniae* and modest activity against *Salmonella typhi* and *Pseudomonas aeruginosa* (68). By using an ethanol extract of *Spirulina platensis*, inhibitory zones against *Enterococcus faecalis* and *Candida albicans* were seen using the disc diffusion technique (59). The effectiveness of *Spirulina*'s antibacterial actions *in vivo* was assessed by Abd El-Dayem et al. (56) as adding 1 and 2 g of spirulina per kg of diet significantly increased growth performance, antioxidant levels, and the production of the anti-inflammatory cytokine (IL-10) while reducing organ colonization and gene expressions of IL-6, IL-1 β , and TNF- α as compared to positive and negative control groups.

According to 69, pathogens use the same adhesion and invasion mechanisms to invade the guts of both people and animals, and the antibacterial action of spirulina might be attributed to its ability to prevent pathogen motility, invasion, biofilm formation, and quorum sensing. In addition, *Spirulina*'s bioactive ingredients have shown to weaken bacterial cell walls making it more permeable, that subsequently led to leakage of cytoplasmic contents (65).

Furthermore, when broilers were given the 10X Coccivac-B52 vaccine orally while being fed microalgae-derived feed components, the intestinal integrity of the birds during coccidiosis was conserved, and the jejunal villus height was protected as early as 7 days after the challenge (57). However, the algal element changed the immune response (splenic T cells) in a way that decreased recruitment from secondary lymphoid organs (57).

Spirulina was also a powerful binder for aflatoxins in broiler breeders (70). The negative effect of 300 ppb aflatoxin on broiler chicken growth rate and lymphoid organ weights might be partially mitigated by the addition of spirulina at a level of (0.05%) although

there was no positive impact on feed consumption, the serum protein concentration, liver weights, or cholesterol levels (71). Likewise, *Spirulina* inclusion (0.02%) in feed had positive effects on growth, ready to cook yields, bursa weight, and cellular immune response in chicks fed aflatoxin (300 ppb) although there was no effect of *Spirulina* on feed intake, feed conversion efficiency, leg abnormality scores, SRBC response, and weights of the liver, giblets, spleen, and abdominal fat (72). Dietary inclusion of *Spirulina* is also recommended to protect against other toxins as shown in Table 1.

Effects of *Spirulina* on the managerial and nutritional shortages

A crucial component of broiler productivity, especially with the use of antibiotics being reduced, is immune system health. Natural antibiotic alternatives and nutritional factors like crude protein % are being studied to understand how they affect immunity. The positive benefits of *Spirulina* in reversing the management and nutrient deficits in poultry were displayed in Table 2. A promising development for reducing feed costs without compromising the health of the bird is the ability of natural feed additives to counteract the negative effects that low crude protein has on immunity in birds (74). *Spirulina* is an alternative protein-containing component that manufacturers are considering because of both its great nutritional value and its capacity to strengthen the immune system. For instance, the addition of spirulina to low protein chicken diets resulted in reduction of systemic inflammation and bacterial translocation indicating its suitability as a alternative protein source (73). Additionally, the low crude protein (LCP) diet-*Spirulina* supplemented reversed the

TABLE 2 Efficacy of *Spirulina platensis* (SP) in cases of nutritional deficiencies and managerial defects in poultry.

Algae/dose	route of administration/ duration	Birds	Nutritional or managerial defect	Main results	Reference
Low protein diet					
<i>S. platensis</i> at 0, 100 g/kg	Feed/14 th -37 th day of age	Ross 708 male broiler chickens	Low protein diet (LCP) (17%) compared to basal diet (21%)/14 th -37 th day of age	SP decreased hepatic bacterial translocation brought on by a LCP and systemic inflammation based on the percentage of basophils. Birds were given the SP had significantly reduced levels of circulating pro-inflammatory cytokines (IL-3, IL-6, IL-4, IL-18, and tumour necrosis factor), chemokines (CCL-20), and NOD-like receptor family pyrin domain containing 3 inflammasome than birds given the control diet.	(73)
<i>S. platensis</i> at 0, 100 g/kg	Feed/14 th -37 th day of age	Ross 708 male broiler chickens	LCP (17%) compared to basal diet (21%)/14 th -37 th day of age	The LCP-SP diet lessened the effects of the LCP diet, resulting in levels and ratios of monocytes that were similar to those of the control diet.	(74)
<i>S. platensis</i> at 0, 10%	Feed/15 th day-35 th day of age	Ross 708 female broiler chickens	Low protein diet (LCP) (17%)/15 th day-35 th day of age compared to basal diet (20%)/	Broilers fed SP in their diets saw considerably lower body weight gain but considerably higher feed conversion ratio compared to the other two treatments	(75)
Mycotoxins and other toxins					
<i>S. platensis</i> at 0, 0.02%	Feed/10 th day-45 th day of age	Commercial Broiler chickens	Aflatoxin (300 ppb)/10 th day-45 th day of age	SP fed to chicks who had been exposed to aflatoxin had positive benefits on their development, ready-to-cook yields, bursa weight, and cellular immune response, but SP had no impact on feed intake, feed conversion efficiency, leg abnormality scores, SRBC reaction, or the weights of the liver, gilets, spleen, or abdominal fat.	(72)
<i>S. platensis</i> at 0, 0.05%	Feed/8 th day - 42 nd day of age	Commercial Broiler chickens	Aflatoxin 0, 300 ppb B ₁ /8 th -42 nd day of age	SP slightly mitigated the adverse effects of aflatoxin on body weight gain and the weights of the thymus and spleen, but not on the weights of the liver and kidney, proteins in the serum, or cholesterol.	(71)
<i>S. platensis</i> at 0 and 0.1%	Feed for three periods of 21 days each starting from 28th week.	Broiler breeder hens	Aflatoxin 0, 300, 400 and 500 ppb for three periods, each with duration of three weeks in broiler breeders from 28 to 36 weeks of age.	SP did not change the weights of the liver or the levels of kidney, proventriculus, or gizzard lesions in groups that were either fed alone or in conjunction with various amounts of AF.	(70)
<i>S. platensis</i> at 20 g/kg	Feed for 35 days	Cobb broiler chickens	-Deltamethrin/300 mg/kg diet for 35 days	Deltamethrin levels in meat, skin, and liver were all significantly lowered by SP, falling by 63.01, 63.00, and 62.90%, respectively. When compared to the group that got Deltamethrin, Sp increased protein and significantly lowered fat, cholesterol, and triglycerides.	(76)
<i>S. platensis</i> at 30, 60 and 120 mg/L	in drinking water daily for 90 days starting from day 15	Male ducklings	Arsenic trioxide:100 mg/L drinking water daily for 90 days	The not gained body weight in ducks was better in the arsenic and SP-treated groups (4.08-11.26%) than in the arsenic-only (14.93%). The drop in Total Erythrocyte Count, Hb, and PCV was less in the arsenic plus SP-treated groups than in the arsenic treated groups.	(77)
<i>S. platensis</i> at dose (10 gm/kg of diet)	in diet for two weeks after treatment (therapeutic) or before the treatment (preventive)	Broiler chicks	Hepatotoxic effect of diclofenac sodium: (2.5 mg/kg.b.wt., i.m)/at 21 days of age old for 3 days	In the preventative and treatment groups, the death rate dropped from 64% in the control birds to 8% and 32%, respectively. Preventive treatment improved lower haematological parameters, WBCs, absolute lymphocyte, eosinophil, and monocyte counts as well as decreased AST, ALP, uric acid, and cholesterol, as well as oxidative stress better than therapeutic group. Both SP-treated groups dramatically enhanced phagocytic activity, phagocytic index, and HI antibody against NDV	(44)
Heat stress					
<i>S. platensis</i> at 0, 0.5 and 1 g/kg diet	Feed from 4 th week - 14 th week of age	Gimmizah local Egyptian strain chicks	Chronic heat stress condition (38°C ± 1; 55-65% RH)/3 days per week from 11.00 am to 15.00 pm/	Without affecting body weight gain or FCR, different <i>Spirulina</i> concentrations dramatically reduced the negative effects of heat stress on feed intake, the immune system, total lipids, LDL, WBCs, RBCs, albumin, globulin, creatinine, and liver enzymes (ALT, AST).	(78)

(Continued)

TABLE 2 Continued

Algae/dose	route of administration/duration	Birds	Nutritional or managerial defect	Main results	Reference
		(4 weeks of age)	from 4 th week – 14 th week of age		
<i>S. platensis</i> at 0, 0.5 and 1%	Feed from 17 th day to 45 th day of age	Cobb 500 Broiler chickens	Heat stress (36°C for 6 h/d) from 38 th to 44 th day of age	Spirulina supplementation increased humoral immunity response and elevated antioxidant status while decreasing concentrations of stress hormone and several serum lipid markers. However, it had no appreciable impact on performance traits.	(79)
<i>S. platensis</i> at 0, 0.1, 0.3, and 0.5%	Feed for 6 weeks	laying Japanese quails (98 days old)	Heat stress (8h of 34 ± 1°C; 60-70% RH) for 6 days	Different Spirulina concentrations had no appreciable impact on feed intake, FCR, egg weight, and hen day egg production percentage. The lowest ileal <i>E. coli</i> count, blood MDA, heterophil, and H/L ratio was obtained significantly by SP at 0.5%.	(80)
<i>S. platensis</i> at 0, 0.5, 1 or 1.5%.	Feed from 21 st day to 42 nd day of age	Cobb-500 broiler chicks	Cyclic heat stress (34 ± 1°C for 8 h per day)	SP reduced the deleterious effects of heat stress on the final average daily increase, body weight, and FCR, with the chickens given 1% Spirulina showing the highest results. SP raised Hb, hematocrit and HDL levels and markedly reduced LDL and lipid peroxidation levels compared to stressed non-supplemented group. SP 0.5 or 1% enhanced carcass dressing, breast, and leg %	(81)
<i>S. platensis</i> at 5, 10, 15 and 20 g/L	Drinking water/in the morning (06:00–12:00 PM) for 6 weeks	White broilers	The experiment was conducted using a deep litter rearing system during the hot, humid summer months (for 6 weeks)	It had neither negative nor positive effects on the performance of broilers but had a considerable impact on Hb, RBCs, and shank pigmentation. SP by 15 and 20 g/L raised blood protein concentration and reduced serum fat content and transaminases. SP by 20 g/L significantly improved humoral immunity against ND vaccination and cell-mediated immunity to phytohemagglutinin-P.	(82)
<i>S. platensis</i> at levels of 0, 5, and 10 g kg ⁻¹ individually and in combination with selenium nanoparticles (SeNPs) at 0, 0.1, and 0.2 mg.kg ⁻¹	Feed for 5 weeks	Ross-308 broiler chicks	Heat stress (34 ± 2°C for 24 h for first 14 days. Then, 34 ± 2°C for 12 h (from 9:00 to 18:00) for three consecutive days a week and then 25 ± 2°C during the remaining experimental period).	Significant improvements were made in growth performance, blood lipid profile, carcass dressing, and carcass yield percentages thanks to SP and SeNPs combinations. Both supplements induced greater levels of the IgG, IgM, and IgA and rose antibody titers to IBD, AI, and ND quantitatively compared to the control group. All groups, except SP 5g, had elevated levels of glutathione peroxidase, superoxide dismutase, and blood triiodothyronine. The greatest favourable effects were obtained by SP 5g plus SeNPs 0.2 mg kg ⁻¹ and SP 10 g plus SeNPs 0.1 mg kg ⁻¹ .	(83)

effects of the LCP diet, causing the monocyte proportions and concentrations in Ross 708 old male broilers to be similar statistically to those of the control base diet (74). However, compared to 20% crude protein without Spirulina, using a diet of 17% crude protein with 10% *S. platensis* for Ross 708 broiler females exhibited no detrimental effects on the health of broilers but substantial reduction in body weight in supplemented group led to economic losses (75).

Dietary supplementation of *S. platensis* in broiler hens has shown to alleviate the adverse effects of high ambient temperature, including impaired enzymatic antioxidant system, raised stress hormone, and altered lipid profile (84). There was a dose-related modification of productivity, physiological, and immunological parameters when chickens under heat stress were given Spirulina in drinking water or feed (78, 82). Additionally, in ovo injection of *S. platensis* improved the broiler embryo's ability to tolerate heat in the last days of incubation (22).

Limitations of Spirulina as a feed additive and future directions for its use

Spirulina as a feed additive can have implications for productivity and end product quality, depending on the system of animal production. Both swine growth performance and product quality were not negatively affected in response to dietary supplementation with spirulina which might be attributed to lower protein requirements in finishing diets. However, Spirulina negatively affected chicken and fish production performance besides altering product quality, particularly meat color, according to the consumer's opinions (85). One of major challenges regarding use of Spirulina as a feed additive at high level is that the gelation of its indigestible proteins causing birds to perform worse due to the increased digesta viscosity (32). Therefore the golden standard level of Spirulina inclusion into the feed should be

highlighted and interpreted to be applied in the field. In addition, trials to increase digestibility of *Spirulina* should be researched. Another major challenge regarding use of *Spirulina* as a feed additive is its quite higher cost compared to other protein ingredients such as soybean meal (58, 86). However, improving production efficiency and using waste streams as culture media, spirulina could replace fishmeal by becoming competitive for fish feed due to higher cost of fishmeal (86). Second major challenge with spirulina is limitation of its large scale production as presently it is produced at a smaller scale primarily for the nutritional supplement sector with few exceptions (58). Third challenge is with sustainable production of spirulina as compared to the other protein ingredients like soybean which is mainly attributed to the sensitivity of spirulina to the production system and regional climate (87). Therefore serious research and development efforts are required to improve yield of spirulina and make its production more sustainable. For example some research initiative targeted to improve sustainability of production by using biogas effluent (88) or wastewater (89) as production media. Additionally, waste heat sources (e.g. heat produced during biogas production) can be integrated as spirulina requires warm temperature (35–37°C) for cultivation (5, 90). Consequently, above mentioned challenges could be overcome by upscaling and optimizing production of spirulina. Moreover, advanced techniques can also facilitate improvement in yield and protein quality of spirulina through breeding and Finally, although spirulina has a high proportion of crude protein, improvements to protein quality could be possible through breeding and nutrition/production research (91). Therefore, future research focused on sustainable production and product processing and acceptance should investigate the trade-offs of incorporating spirulina into poultry diets.

Conclusion

Bioactive metabolites are abundant in natural products and have been used for their medicinal properties. *Spirulina* that was regarded as a blue-green filamentous algae with a spiral shape, it has been identified as a genus of photosynthetic bacteria (*Arthrospira*) more recently. It is a highly nutritious and antioxidant natural product and having the ability to improve production performance either growth, hatchability, or egg production. The cell-mediated and humoral immune response as well as antimicrobial activities of spirulina promoted disease resistance and improved survival and growth rates in chicken. However, further studies on optimum dose of *Spirulina* for different poultry species, age groups, and production

systems as well as the type of used *Spirulina* extract, organic or aqueous are required.

Author contributions

All the authors contributed significantly to this manuscript. NAE conceptualized the manuscript. NAE wrote the first draft with input from SJ, MRF, MA, AAA, RA, KD, FH, and MAL. Authors NAE, SJ, MRF, MA, AAA, RA, KD, FH, and MAL reviewed and updated the manuscript. All authors contributed to revisions and approved the final manuscript.

Funding

China Agriculture Research System of MOF and MARA (CARS-41), the Key Realm R&D Program of Guangdong Province (2020B0202090004), National Key R&D Project (2021YFD1300404), Natural Science Foundation from Guangdong Province (2022A1515012069, 2021A1515012412, 2021A1515010830), the Science and Technology Plan Project of Guangzhou (202206010168), the Science and Technology Program of Guangdong Academy of Agricultural Sciences (202106TD, R2019PY-QF008), Introduction of Talents Program from Guangdong Academy of Agricultural Sciences (R2021YJ-YB3012), Guiding Agreement of Young Scholar from Guangdong Academy of Agricultural Sciences (R2021QD-024) P. R. China.

Conflict of interest

The authors declare that the research was conducted in the absence of any commercial or financial relationships that could be construed as a potential conflict of interest.

Publisher's note

All claims expressed in this article are solely those of the authors and do not necessarily represent those of their affiliated organizations, or those of the publisher, the editors and the reviewers. Any product that may be evaluated in this article, or claim that may be made by its manufacturer, is not guaranteed or endorsed by the publisher.

References

1. El-Shall NA, Shewita RS, Abd El-Hack ME, AlKahtane A, Alarifi S, Alkahtani S, et al. Effect of essential oils on the immune response to some viral vaccines in broiler chickens, with special reference to Newcastle disease virus. *Poult Sci* (2020) 99(6):2944–54. doi: 10.1016/j.psj.2020.03.008
2. Lordan S, Paul Ross R, Stanton C. Marine bioactives as functional food ingredients: Potential to reduce the incidence of chronic diseases. *Mar Drugs* (2011) 9:1056–100. doi: 10.3390/md9061056
3. Draaisma RB, Wijffels RH, Slegers PE, Brentner LB, Roy A, Barbosa MJ. Food commodities from microalgae. *Curr Opin Biotechnol* (2013) 24:169–77. doi: 10.1016/j.copbio.2012.09.012
4. Farag MR, Mahmoud A, Mohamed Ezzat Abd E-H, Kuldeep D. Nutritional and health aspects of spirulina (*Arthrospira*) for poultry. *Anim Human. Int J Pharmacol* (2016) 12:36–51. doi: 10.3923/ijp.2016.36.51
5. Habib MAB, Parvin M, Huntington TC, Hasan MR. A review on culture, production and use of spirulina as food for humans and feeds for domestic animals and fish. In: *FAO Fisheries and Aquaculture Circular*. Rome: Food and agriculture organization of the United States Nations (2008), 1034.
6. Alvarenga RR, Rodrigues PB, Cantarelli V, Zangeronimo MG, Da Silva Junior JW, Da Silva LR, et al. Energy values and chemical composition of spirulina (*Spirulina platensis*) evaluated with broilers. *Braz J Anim. Sci* (2011) 40:992–6. doi: 10.1590/S1516-35982011000500008

7. Zahroojian N, Moravej H, Shivazad M. Effects of dietary marine algae (*Spirulina platensis*) on egg quality and production performance of laying hens. *J Agric Sci Technol* (2013) 15:1353–60.
8. Plaza M, Herrero M, Cifuentes A, Ibanez E. Innovative natural functional ingredients from microalgae. *J Agric Food Chem* (2009) 57:7159–70. doi: 10.1021/jf9101070g
9. Deepika DS, Sowmya KL, Kiran KR. Efficacy of microalgal biomass in poultry nutrition journal of poultry fisheries & wildlife sciences. *Poult Fish Wildl Sci* (2021) 9 (5):1000216.
10. Ghaeni M, Roomiani L. Review for application and medicine effects of spirulina, *Spirulina platensis* microalgae. *J Advanced Agric Technol* (2016) 3 (2). doi: 10.18178/joaat.3.2.114-117
11. Maoka T. Carotenoids in marine animals. *Mar Drugs* (2011) 9:278–93. doi: 10.3390/md9020278
12. Panyakampol J, Cheevadhanarak S, Sutheworapong S, Chaijaruwanich J, Senachak J, Siangdung W, et al. Physiological and transcriptional responses to high temperature in arthrospira (*Spirulina*) *platensis* C1. *Plant Cell Physiol* (2014) 56(3):481–96. doi: 10.1093/pcp/pcu192
13. Ciferri O, Tiboni O. The biochemistry and industrial potential of spirulina. *Ann Rev Microbiol* (1985) 39:503–26. doi: 10.1146/annurev.mi.39.100185.002443
14. Ronda RR, Lele SS. Culture conditions stimulating high ylinolenic acid accumulation by *Spirulina platensis*. *Braz J Microbiol* (2008) 39:693–7. doi: 10.1590/S1517-83822008000400018
15. Eriksen NT. Production of phycocyanin - a pigment with applications in biology, biotechnology, foods and medicine. *Appl Microbiol Biotechnol* (2008) 80:1–14. doi: 10.1007/s00253-008-1542-y
16. Becker EW. Nutrition. In: *Microalgae: Biotechnology and microbiology*. Cambridge: Cambridge University Press (1994). p. 196–249.
17. Spolaore P, Joannis-Cassan C, Duran E, Isambert A. Commercial applications of microalgae. *J Biosci Bioeng* (2006) 101:87–96. doi: 10.1263/jbb.101.87
18. Christaki E, Bonos E, Giannenas I, Florou-Paneri P. Functional properties of carotenoids originating from algae. *J Sci Food Agric* (2013) 93:5–11. doi: 10.1002/jsfa.5902
19. Freitas AC, Rodrigues D, Rocha-Santos TAP, Gomes AMP, Duarte AC. Marine biotechnology advances towards applications in new functional foods. *Biotechnol Adv* (2012) 30:1506–15. doi: 10.1016/j.biotechadv.2012.03.006
20. Batista AP, Gouveia L, Bandarra NM, Franco JM, Raymundo A. Comparison of microalgal biomass profiles as novel functional ingredient for food products. *Algal Res* (2013) 2:164–73. doi: 10.1016/j.algal.2013.01.004
21. Khan S, Mobashar M, Mahsood FK, Javaid S, Abdel-Wareth AA, Ammanullah H, et al. Spirulina inclusion levels in a broiler ration: evaluation of growth performance, gut integrity, and immunity. *Trop Anim Health Production* (2020) 52:3233–40. doi: 10.1007/s11250-020-02349-9
22. Hajati H, Zaghari M, Noori O, Negarandeh R, Cedraz de Oliveira H. Effects of in ovo injection of microalgae on hatchability, antioxidant and immunity-related genes expression, and post-hatch performance in broilers and Japanese quails. *Ital J Anim Sci* (2021) 20(1):985–94. doi: 10.1080/1828051X.2021.1910582
23. Ibrahim NS, Wakwak MM, Al-Gama MA. Productive performance and immune response in growing japanese quail supplemented with spirulina algae extract (arthrospira platensis) in drinking water. *Egypt.Poult.Sci* (2018) 38(II):409–26.
24. Yusuf MS, Hassan MA, Abdel-Daim MM, Nabtiti AS, Ahmed AM, Moawad SA, et al. Value added by *Spirulina platensis* in two different diets on growth performance, gut microbiota, and meat quality of Japanese quails. *Vet World*. (2016) 9(11):1287–93. doi: 10.14202/vetworld.2016.1287-1293
25. Qureshi MA, Garlich JD, Kidd MT. Dietary *Spirulina platensis* enhances humoral and cell-mediated immune functions in chickens. *Immunopharmacol Immunotoxicology* (1996) 18:3465–76. doi: 10.3109/08923979609052748
26. Fathi MA, Namra MMM, Ragab MS, Aly MMM. Effect of dietary supplementation of algae meal (*Spirulina platensis*) as growth promoter on performance of broiler chickens. *Egypt. Poult. Sci J* (2018) 38:375–89.
27. Alwaleed EA, El-Sheekh M, Abdel-Daim MM, Saber H. Effects of *Spirulina platensis* and amphora coffeaeformis as dietary supplements on blood biochemical parameters, intestinal microbial population, and productive performance in broiler chickens. *Environ Sci Pollut Res Int* (2021) 28(2):1801–11. doi: 10.1007/s11356-020-10597-3
28. Hajati H, Zaghari M. Effects of *Spirulina platensis* on growth performance, carcass characteristics, egg traits and immunity response of Japanese quails. *Iranian J Appl Anim Sci* (2019) 9(2):347–57.
29. Nia EA, Mehri M, Shirmohammad F. Effects of dietary *Spirulina platensis* algae powder on performance, egg quality, ovarian follicles and immune system in lohmann LSL laying hens. *Iran. J Anim. Sci* (2021) 51(4):349–59. doi: 10.22059/ijas.2021.314088.653810
30. Mobarez SM, Rizk AM, Abdel latif AM, Osama AE. Effect of supplementing diet with *Spirulina platensis* algae or turmeric on productive and reproductive performance of golden montazah layers. *Egypt. Poult. Sci J* (2018) 38:109–25.
31. Boiago MM, Dilkiln JD, Kolm MA, Barreta M, Souza CF, Baldissera MD, et al. *Spirulina platensis* in Japanese quail feeding alters fatty acid profiles and improves egg quality: Benefits to consumers. *J Food Biochem* (2019) 43(7):e12860. doi: 10.1111/jfbc.12860
32. Pestana JM, Puerta B, Santos H, Madeira MS, Alfaia CM, Lopes PA, et al. Impact of dietary incorporation of spirulina (*Arthrospira platensis*) and exogenous enzymes on broiler performance, carcass traits, and meat quality. *Poult Sci* (2020) 99(5):2519–32. doi: 10.1016/j.psj.2019.11.069
33. Al-Batshan HA, Al-Mufarrej SI, Homaidan AA, Qureshi MA. Enhancement of chicken macrophage phagocytic function and nitrite production by dietary *Spirulina platensis*. *Immunopharmacol. Immunotoxicol.* (2001) 23:281–9. doi: 10.1081/IPH-100103866
34. Hirahashi T, Matsumoto M, Hazeki K, Saeki Y, Ui M, Seya T. Activation of the human innate immune system by spirulina: augmentation of interferon production and NK cytotoxicity by oral administration of hot water extract of *Spirulina platensis*. *Int Immunopharmacol.* (2002) 2:423–34. doi: 10.1016/S1567-5769(01)00166-7
35. Zhang HQ, Lin AP, Sun Y, Deng YM. Chemo- and radio-protective effects of polysaccharide of *Spirulina platensis* on hemopoietic system of mice and dogs. *Acta Pharmacol Sin* (2001) 22:1121–4.
36. Balachandran P, Pugh ND, Ma G, Pasco DS. Toll-like receptor 2-dependent activation of monocytes by spirulina polysaccharide and its immune enhancing action in mice. *Int Immunopharmacol.* (2006) 6:1808–14. doi: 10.1016/j.intimp.2006.08.001
37. Kawanishi Y, Tominaga A, Okuyama H, Fukuoka S, Taguchi T, Kusumoto Y, et al. Regulatory effects of spirulina complex polysaccharides on growth of murine RSV-m glioma cells through toll-like receptor 4. *Microbiol Immunol* (2013) 57:63–73. doi: 10.1111/1348-0421.12001
38. Hayashi O, Hirahashi T, Katoh T, Miyajima H, Hirano T, Okuwaki Y. Class specific influence of dietary *Spirulina platensis* on antibody production in mice. *J Nutr Sci Vitaminol (Tokyo)*. (1998) 44:841–51. doi: 10.3177/jnsv.44.841
39. Kaoud HA. Effect of *Spirulina platensis* as a dietary supplement on broiler performance in comparison with prebiotics. *J Biol Sci* (2015) 1:1–6.
40. Marief Y, Samak H, Abou-Khashba H, Sayed M, Abou-Zeid A. Effect of using *Spirulina platensis* algae as a feed additives for poultry diets: 2 productive performance of broiler. *Egypt. Poult. Sci* (2014) 34:245–58.
41. Lokapinasari WL, Yulianto AB, Legowo D, Agustono. The effect of spirulina as feed additive to myocardial necrosis and leukocyte of chicken with avian influenza (H5N1) virus infection. *Proc Chem* (2016) 18:213–217. doi: 10.1016/j.proche.2016.01.033
42. Abdel-Daim MM, Abuzead SM, Halawa SM. Protective role of *Spirulina platensis* against acute deltamethrin-induced toxicity in rats. *PloS One* (2013) 8:e72991. doi: 10.1371/journal.pone.0072991
43. Abou-Gabal A, Aboul-Ela HM, Ali E, Ahemd E, Shalaby OK. Hepatoprotective, DNA damage prevention and antioxidant potential of *Spirulina platensis* on CCL4-induced hepatotoxicity in mice. *Am J Biomed. Res* (2015) 3(2):29–34. doi: 10.12691/ajbr-3-2-3
44. Mokhbatly AA, Ghazy EW, Dabdelhady DH, Walid A, Abdelwahab M. Ameliorative effect of *Spirulina platensis* against diclofenac sodium-induced hepatotoxicity in broilers: hematological, biochemical, biological, antioxidant, immunological and histopathological study. *Assiut Vet Med J* (2018) 64 No. 156:164–77.
45. Khan Z, Bhadouria P, Bisen PS. Nutritional and therapeutic potential of spirulina. *Curr Pharm Biotechnol* (2005) 6:373–9. doi: 10.2174/138920105774370607
46. Wu LC, Ho JAA, Shieh and LW. Lu MC. Antioxidant and antiproliferative activities of spirulina and chlorella water extracts. *J Agric Food Chem* (2005) 53:4207–12. doi: 10.1021/jf0479517
47. Abdelkhalek NK, Ghazy EW, Abdel-Daim MM. Pharmacodynamic interaction of *Spirulina platensis* and deltamethrin in freshwater fish Nile tilapia, oreochromis niloticus: impact on lipid peroxidation and oxidative stress. *Environ Sci Pollut Res* (2015) 22 (4):3023–31. doi: 10.1007/s11356-014-3578-0
48. Sharmin F, Sarker NR, Sarker MSK. Effect of using moringaoleifera and spirulinaplensis as feed additives on performance, meat composition and oxidative stability and fatty acid profiles in broiler chicken. *J Nutr Food Sci* (2020) 10:772. doi: 10.35248/2155-9600.20.10.772
49. Abbas MS, Bandar LK, Alkhilani FMH. (2021). Effect of using different levels of spirulina algae (*Spirulina platensis*) in the diet on concentration, types of fatty acids, oxidation indicators, and sensory characteristics of broiler carcasses. *IOP Conf Ser.: Earth Environ Sci* 910:012044. doi: 10.1088/1755-1315/910/1/012044
50. Altmann BA, Wigger R, Ciulu M, Mörlein D. The effect of insect or microalga alternative protein feeds on broiler meat quality. *J Sci Food Agric* (2020) 100:4292–302. doi: 10.1002/jsfa.10473
51. Altmann BA, Neumann C, Veltin S, Liebert F, Mörlein D. Meat quality derived from high inclusion of a micro-alga or insect meal as an alternative protein source in poultry diets: A pilot study. *Foods* (2018) 7:34. doi: 10.3390/foods7030034
52. Park JH, Lee SI, Kim IH. Effect of dietary spirulina (*Arthrospira*) *platensis* on the growth performance, antioxidant enzyme activity, nutrient digestibility, cecal microflora, excreta noxious gas emission, and breast meat quality of broiler chickens. *Poult Sci* (2018) 97(7):2451–9. doi: 10.3382/ps/pey093
53. Abotaleb MM, Mourad A, Abousenna MS, Helal AM, Nassif SA, Elsafty MM. The effect of spirulina algae on the immune response of SPF chickens to commercial inactivated Newcastle vaccine in poultry. *VacciMonitor* (2020) 29(2):51–7.
54. Abdo SM, Sameh Abdel-Moez A, Hagar Magdy A, Rehab Hamdy M, Abeer Abdallah S, Mohamed Abdel-Aziz K. Microalgae biomass application in commercial broilers nutrition and their efficacy against challenge with epidemic Newcastle disease virus in Egypt. *J World Poult. Res* (2019) 9(2):98–108. doi: 10.36380/jwpr.2019.12
55. Kumari P, Kundu P, Kajal S, Narang G. Effect of spirulina feeding on serum protein level in infectious bursal disease vaccinated chickens. *Pharma Innovation J* (2019) 8(2):543–6.

56. Abd El-Dayem GA, Saleh GK, Abd EL-Elwahab RA. Impact of dietary spirulina (arthrospira) platensis on growth performance, gene expression and antioxidant status of quail challenged with salmonella enteritidis. *Mansoura Veterinary Med J* (2021) 22:2:38–47. doi: 10.35943/mvmj.2021.66416.1040
57. Fries-Craft K, Meyer MM, Bobeck EA. Algae-based feed ingredient protects intestinal health during eimeria challenge and alters systemic immune responses with differential outcomes observed during acute feed restriction. *Poult Sci* (2021) 100 (9):101369. doi: 10.1016/j.psj.2021.101369
58. Chen YH, Chang GK, Kuo SM, Huang SY, Hu IC, Lo YL, et al. Well-tolerated spirulina extract inhibits influenza virus replication and reduces virus-induced mortality. *Sci Rep* (2016) 6:24253. doi: 10.1038/srep24253
59. El-Baz FK, El-Senousy WM, El-Sayed AB, Kamel MM. *In vitro* antiviral and antimicrobial activities of *Spirulina platensis* extract. *J Appl Pharm Sci* (2013) 3:52–6. doi: 10.7324/JAPS.2013.3.1209
60. Hayashi T, Hayashi K, Maeda M, Kojima I. Calcium spirulan, an inhibitor of enveloped virus replication, from a blue-green alga *Spirulina platensis*. *J Nat Prod* (1996) 59:83–7. doi: 10.1016/j.intimp.2005.09.009
61. Hayashi K, Hayashi T, Kojima I. A natural sulphated polysaccharide, calcium spirulan, isolated from *Spirulina platensis*: In vitro and ex vivo evaluation of anti-herpes simplex virus and anti-human immunodeficiency virus. *AIDS Res Hum Retrovir* (1996) 12:1463–71. doi: 10.1089/aid.1996.12.1463
62. Bae SY, Yim JH, Lee HK, Pyo S. Activation of murine peritoneal macrophages by sulphated exopolysaccharide from marine microalga *gyrodinium impudicum* (strain KG03): Involvement of the NF-kappa b and JNK pathway. *Int Immunopharmacol*. (2006) 6:473–484. doi: 10.1016/j.intimp.2005.09.009
63. El-Sheekh MM, Daboor SM, Swelim MA, Mohamed S. Production and characterization of antimicrobial active substance from *Spirulina platensis*. *Iran J Microbiol* (2014) 6:112–119.
64. Al-ghanayem A. Antimicrobial activity of *Spirulina platensis* extracts against certain pathogenic bacteria and fungi. *Adv Biores*. (2017) 8(6):96–101. doi: 10.15515/abr.0976-4585.8.6.96101
65. Abdel-Moneim EA-M, Mohamed TE-S, Abdelrazeq MS, Ahmed MS, Aldhumri SA, Ouda SM, et al. Antioxidant and antimicrobial activities of *Spirulina platensis* extracts and biogenic selenium nanoparticles against selected pathogenic bacteria and fungi. *Saudi J Biol Sci* (2021) 29(2):1319–562X. doi: 10.1016/j.sjbs.2021.09.046
66. Gheda SF, Ismail GA. Natural products from some soil cyanobacterial extracts with potent antimicrobial, antioxidant and cytotoxic activities. *Anais da Academia Bras Ciências* (2020) 92. doi: 10.1590/0001-3765202020190934
67. Kaushik P, Chauhan A. *In vitro* antibacterial activity of laboratory grown culture of *Spirulina platensis*. *Indian J Microbiol* (2008) 48:348–52. doi: 10.1007/s12088-008-0043-0
68. Mala R, Sarojini M, Saravanababu S, Umadevi G. Screening for antimicrobial activity of crude extracts of *Spirulina platensis*. *J Cell Tissue Res* (2009) 9:1951–5.
69. Saleh AA, Shukry M, Farrag F, Soliman MM, Abdel-Moneim A-ME. Effect of feeding wet feed or wet feed fermented by bacillus licheniformis on growth performance, histopathology and growth and lipid metabolism marker genes in broiler chickens. *Animals* (2021) 11:83. doi: 10.3390/ani11010083
70. Manafi M. Evaluation of different mycotoxin binders on broiler breeders induced with aflatoxin B1: Effects on visceral organ weight and organ lesions parameters. *Adv Environ Biol* (2011) 5(13):3795–9.
71. Raju MVLN, Rao SV, Radhika K, Chawak MM. Dietary supplementation of spirulina and its effects on broiler chicken exposed to aflatoxicosis. *Indian J Poult. Sci* (2005) 40:36–40. doi: 10.3389/fvets.2021.640968
72. Raju MVLN, Rama Rao SV, Radhika K, Chawak MM. Effects of *Spirulina platensis* or furazolidone on the performance and immune response of broiler chickens fed with aflatoxin contaminated diet. *Indian J Anim Nutr* (2004) 21(1):40–4.
73. Mullenix GJ, Greene ES, Emami NK, Tellez-Isaias G, Bottje WG, Erf GF, et al. *Spirulina platensis* inclusion reverses circulating pro-inflammatory (Chemo)cytokine profiles in broilers fed low-protein diets. *Front Vet Sci* (2021) 8:640968. doi: 10.3389/fvets.2021.640968
74. Glenn H, Mullenix GJ, Erf GF. Effects of a low crude protein diet with and without *Spirulina platensis* inclusion on white blood cell profiles in broilers. *Discovery Student J Dale Bumpers Coll Agricultural Food Life Sci* (2021) 22(1):38–44. doi: 10.1007/s11356-021-14617-8
75. Tarkington V. *Effect of dietary Spirulina platensis on stress levels and growth of female broiler chickens. animal science undergraduate honors theses* (2020). Available at: <https://scholarworks.uark.edu/anscuht/42>.
76. Ibrahim SS, Elsabagh R, Allam A, Youssef G, Fadl SE, Abdelhiee EY, et al. Bioremediation role of *Spirulina platensis* against deltamethrin-mediated toxicity and its chemical residues in chicken meat. *Environ Sci Pollut Res Int* (2021) 28(40):56188–98. doi: 10.1007/s11356-021-14617-8
77. Islam MS, Awal MA, Mostofa M, Begum F, Khair A, Myenuddin M. Effect of spirulina on toxic signs, body weight and hematological parameters in arsenic induced toxicities in ducks. *Int J Poultry Sci* (2009) 8(1):75–9. doi: 10.5713/ajas.17.0483
78. Zeweil H, Abaza IM, Zahran SM, Ahmed MH, Aboul-Ela HM, Asmaa AS. Effect of *Spirulina platensis* as dietary supplement on some biological traits for chickens under heat stress condition. *Asian J Biomed Pharm Sci* (2016) 6(56):08–12. doi: 10.1590/1806-9061-2018-0977
79. Mirzaie S, Zirak-Khattab F, Hosseini SA, Donyaei-Darian H. Effects of dietary spirulina on antioxidant status, lipid profile, immune response and performance characteristics of broiler chickens reared under high ambient temperature. *Asian-Australas J Anim Sci* (2018) 31, No. 4:556–63. doi: 10.5713/ajas.17.0483
80. Hajati H, Zaghari M, Oliveira HC. *Arthrospira (Spirulina) platensis* can be considered as a probiotic alternative to reduce heat stress in laying Japanese quails. *Braz J Poultry Sci* (2020) 22:001–8. doi: 10.1016/j.jtherbio.2021.103100
81. Moustafa ES, Alsanie WF, Gaber A, Kamel NN, Alaql AA, Abbas AO, et al. Blue-green algae (*Spirulina platensis*) alleviates the negative impact of heat stress on broiler production performance and redox status. *Animals* (2021) 11:1243. doi: 10.3390/ani11051243
82. Kolluri G, Marappan G, Yadav AS, Kumar A, Kumar MA, Tyagi JS, et al. Effects of spirulina (*Arthrospira platensis*) as a drinking water supplement during cyclical chronic heat stress on broiler chickens: Assessing algal composition, production, stress, health and immune-biochemical indices. *J Thermal Biol* (2022) 103:103100. doi: 10.1016/j.jtherbio.2021.103100
83. Abdel-Moneim AE, Shehata AM, Mohamed NG, Elbaz AM, Ibrahim NS. Synergistic effect of *Spirulina platensis* and selenium nanoparticles on growth performance, serum metabolites, immune responses, and antioxidant capacity of heat-stressed broiler chickens. *Biol Trace Elem Res* (2021). doi: 10.1007/s12011-021-02662-w
84. Mirzaie S, Zirak-Khattab F, Hosseini SA, Donyaei-Darian H. Effects of dietary spirulina on antioxidant status, lipid profile, immune response and performance characteristics of broiler chickens reared under high ambient temperature. *Asian Australas J Anim Sci* (2018) 31(4):556–63. doi: 10.5713/ajas.17.0483
85. Altmann BA, Rosenau S. *Spirulina* as animal feed: Opportunities and challenges. *Foods*. (2022) 11(7):965. doi: 10.3390/foods11070965
86. Ragaza JA, Hossain MS, Meiler KA, Velasquez SF, Kumar V. A review on spirulina: Alternative media for cultivation and nutritive value as an aquafeed. *Rev Aquac* (2020) 12:2371–95. doi: 10.1007/s00449-016-1726-2
87. Smetana S, Sandmann M, Rohn S, Pleissner D, Heinz V. Autotrophic and heterotrophic microalgae and cyanobacteria cultivation for food and feed: Life cycle assessment. *Bioresour. Technol* (2017) 245:162–70. doi: 10.1023/A:1023856702544
88. Hultberg M, Lind O, Birgersson GG, Asp HH. Use of the effluent from biogas production for cultivation of spirulina. *Bioprocess Biosyst Eng* (2017) 40:625–31. doi: 10.1016/j.resconrec.2015.05.013
89. Olguin EJ, Galicia S, Mercado G, Pérez T. Annual productivity of spirulina (*Arthrospira*) and nutrient removal in a pig wastewater recycling process under tropical conditions. *J Appl Phycol* (2003) 15:249–57. doi: 10.1016/j.anifeeds.2016.05.003
90. Taelman SE, De Meester S, Van Dijk W, da Silva V, Dewulf J. Environmental sustainability analysis of a protein-rich livestock feed ingredient in the Netherlands: Microalgae production versus soybean import. *Resour Conserv Recycl* (2015) 101:61–72. doi: 10.1016/j.biotechadv.2006.11.002
91. Stein HH, Lagos LV, Casas GA. Nutritional value of feed ingredients of plant origin fed to pigs. *anim. Feed Sci Technol* (2016) 218:33–69. doi: 10.1021/np960017o



OPEN ACCESS

EDITED BY

Guiyan Yang,
University of California, Davis,
United States

REVIEWED BY

Xu Yang,
Henan Agricultural University, China
Liyang Zhang,
Henan Agricultural University, China

*CORRESPONDENCE

Chao Su
✉ suchao503@126.com
Yonghua Qian
✉ qyh@nwfau.edu.cn

SPECIALTY SECTION

This article was submitted to
Nutritional Immunology,
a section of the journal
Frontiers in Immunology

RECEIVED 03 November 2022

ACCEPTED 21 December 2022

PUBLISHED 27 February 2023

CITATION

Cui X, Yang Y, Zhang M, Liu S, Wang H,
Jiao F, Bao L, Lin Z, Wei X, Qian W,
Shi X, Su C and Qian Y (2023)
Transcriptomics and metabolomics
analysis reveal the anti-oxidation and
immune boosting effects of mulberry
leaves in growing mutton sheep.
Front. Immunol. 13:1088850.
doi: 10.3389/fimmu.2022.1088850

COPYRIGHT

© 2023 Cui, Yang, Zhang, Liu, Wang,
Jiao, Bao, Lin, Wei, Qian, Shi, Su and
Qian. This is an open-access article
distributed under the terms of the
[Creative Commons Attribution License](#)
(CC BY). The use, distribution or
reproduction in other forums is
permitted, provided the original
author(s) and the copyright owner(s)
are credited and that the original
publication in this journal is cited, in
accordance with accepted academic
practice. No use, distribution or
reproduction is permitted which does
not comply with these terms.

Transcriptomics and metabolomics analysis reveal the anti-oxidation and immune boosting effects of mulberry leaves in growing mutton sheep

Xiaopeng Cui, Yuxin Yang, Minjuan Zhang, Shuang Liu,
Hexin Wang, Feng Jiao, Lijun Bao, Ziwei Lin, Xinlan Wei,
Wei Qian, Xiang Shi, Chao Su* and Yonghua Qian*

College of Animal Science and Technology, Northwest A&F University, Yangling, Shaanxi, China

Introduction: Currently, the anti-oxidation of active ingredients in mulberry leaves (MLs) and their forage utilization is receiving increasing attention. Here, we propose that MLs supplementation improves oxidative resistance and immunity.

Methods: We conducted a trial including three groups of growing mutton sheep, each receiving fermented mulberry leaves (FMLs) feeding, dried mulberry leaves (DMLs) feeding or normal control feeding without MLs.

Results: Transcriptomic and metabolomic analyses revealed that promoting anti-oxidation and enhancing disease resistance of MLs is attributed to improved tryptophan metabolic pathways and reduced peroxidation of polyunsaturated fatty acids (PUFAs). Furthermore, immunity was markedly increased after FMLs treatment by regulating glycolysis and mannose-6-phosphate pathways. Additionally, there was better average daily gain in the MLs treatment groups.

Conclusion: These findings provide new insights for understanding the beneficial effects of MLs in animal husbandry and provide a theoretical support for extensive application of MLs in improving nutrition and health care values.

KEYWORDS

mulberry leaves, anti-oxidation, peroxidation of polyunsaturated fatty acids, tryptophan metabolism, immunity, glycolysis

Introduction

Currently, a number of medicinal plants are widely used as functional foods and alternative medicine to prevent and treat chronic diseases (1). This is due to the numerous bioactive components with anti-oxidant capabilities, such as phenolic compounds and flavonoids (2), which may help improve immunity by coordinating the metabolism of the body. Mulberry leaves (MLs) have been used as feed for silk worms for hundreds of years and also as a traditional Chinese medicine, according to the classical medicine books. Owing to their anti-oxidative, anti-inflammatory, anti-bacterial, and anti-hyperlipidemic properties, mulberry leaves are gaining increasing attention for use in Chinese herbal medicines (3). To date, the hypoglycemic and lipid-lowering effects of extracts or active ingredients in MLs are well established, against diabetes, fatty liver, and some similar diseases related to disorders in glucose and lipid metabolism. In addition, accumulating evidence have validated the promotion of growth and rumen development, anti-oxidant properties, and improvement in milk production by MLs or their active ingredients in livestock (3–6). However, the underlying mechanism of MLs, as an unconventional feed with both nutritive and medicinal properties, on anti-oxidation and immunity in livestock remains poorly understood. In recent years, an explosion has occurred in the acquisition of biological data through the use of so-called ‘omics’ techniques. Whilst many different omics technologies are now featured in the literature, the most frequently used omics are genomics, transcriptomics, proteomics and metabolomics (7). Thus, the aim of the present study was to evaluate the roles of MLs in growth promoting and animal welfare improving aspects of mutton sheep in terms of antioxidant and immune properties and explore the mechanism by methods of transcriptomic and metabolomic. Our study provides novel insights into the role of MLs in livestock yield and the application of natural functional fodder.

Materials and methods

The experiment was conducted in accordance with the Chinese Guidelines for Animal Welfare and Experimental Protocols, and approved by the Animal Care and Use Committee of the Institute of Northwest A & F University.

Preparation and chemical indexes measurement of fermented mulberry leaves and dried mulberry leaves

MLs (species 707) are harvested in July 2021 at the Institute of Sericulture and Silk in Zhouzhi, Shaanxi Province, China. One half is sun-dried for seven days, next well-sealed in woven bags after a little rubbing and then stored in a dry, dark place for acquiring DMLs for use in feeding experiment. The other half with 65.03% moisture content after wilted by sun-shine for a half day, is a little smashed and vacuum sealed in fermentation-special bags to ferment with 5% *Lactobacillus plantarum* inoculation at room temperature (27.5–28°C) for thirty days in a dry, dark place for preparation for FMLs. Here 5% is adding 5 mL of bacterial culture suspension to 100 grams of MLs and the concentration of bacterial culture suspension is 1×10^8 CFU/mL. *Lactobacillus plantarum* (CICC 23941) purchased from the China Center of Industrial Culture Collection (www.china-cicc.org). Before feeding experiments, the pH, crude protein, crude fiber as well as gross energy of FMLs and DMLs are determined according to standard methods of AOAC. And their contents are shown in Table 1. FMLs are deemed qualified without aflatoxin B1 detected at a minimum checked value of 0.1 µg/kg by Huayan Testing Group Co., Ltd in Xi'an City, Shaanxi Province (Detection number: SP202115450).

Experimental design and feeding diets

Animal experiments are conducted on six-month-old healthy female mutton sheep (white-headed Suffolk sheep ♂ × Hu sheep ♀) weighing 30.41 kg at average without genetic modification in Gansu Qinghuan Meat Sheep Seed Production Co. Ltd (Huan County, Qingyang City, Gansu Province, China). The animals were randomly assigned to group Con feeding a normal control diet (n=18), group TR1 feeding an experimental diet with FMLs (n=18) and group TR2 feeding an experimental diet with DMLs (n=18) and then treated for an experiment of fifty days. Each group had 6 replicates with 3 sheep per replicate. Before the feeding experiment, animals undergo an acclimatization period of six days to obtain an appropriate feed intake, during which they were allowed unlimited access to their corresponding experimental diet and tap water. Experimental sheep were housed in sheepfold and given self-help feeding in three groups every day. The

TABLE 1 Chemical composition of FMLs and DMLs.

Items	DM loss/%	pH	Crude protein/%	Crude fiber/%	Gross energy/(MJ/kg)
FMLs	4.6	3.98	14.69	8.35	15.92
DMLs		6.20	15.15	9.72	14.28

FMLs, fermented mulberry leaves; DMLs, dried mulberry leaves.

ingredients and chemical composition of three experimental diets are shown in Table 2. The chemical compositions of three experimental diets are determined by Ulanqab Yima Agriculture and Animal Husbandry Technology Co., Ltd (Ulanqab City, Inner Mongolia, China).

Weighing and sample collection

Prior to the experiments, all sheep are driven to be weighed by an automatic weighing system to obtain the initial body weights. Afterwards, body weights on day 25th and 50th are weighted to calculate daily gains. On the 50th day, blood from the jugular vein was collected and placed in 5mL vacuum negative-pressure tubes with yellow cap containing separation gels for serum separation and then leave to set for one to two hours to collect rough 2.5mL serum, which is immediately stored in liquid nitrogen and taken to the lab for further analysis. At the end of the experimental period, 6 sheep per group which were representative in terms of average weight (inclusion criteria) of group were selected and slaughtered for tissue sample collection. Tissue samples (about 0.5×0.5×0.5cm³) of longissimus dorsi muscle and subcutaneous fat from the left side of the carcass

are packed into 2 mL cryopreserved tube and frozen in liquid nitrogen immediately within 20 min of slaughter for biochemical indexes and omics analysis. Weighting samples contain 18 biological repeats of each group.

Analysis of biochemical indexes

Growth hormone (GH), total antioxidant capacity (TAOC), superoxide dismutase (SOD), catalase (CAT), glutathione peroxidase (GSH-Px) and malondialdehyde (MDA) are determined using commercially available kits (HY-60021, HY-60001, HY-M0018, HY-60005, HY-60003; Beijing Huaying Biotechnology Research Institute, Beijing, China). Serum immunoglobulin A, M, G (IgA, IgM, IgG) and tumor necrosis factor (TNFα) were determined by commercially available kits (HY-N0048, HY-N0049, HY-N0050, HY-H0019; Beijing Huaying Institute of Biotechnology Research Institute, Beijing, China). Immunoglobulin (IG) is the sum of immunoglobulins IgA, IgM and IgG. Muscle tissue samples contain 5 biological repeats (group Con), 6 biological repeats (group TR2) and 5 biological repeats (group TR2), respectively. Adipose tissue samples contain 5 biological repeats (group Con), 5 biological

TABLE 2 Ingredients and chemical composition of three experimental diets.

Items	Con	TR1	TR2
Ingredients			
DMLs/%	0	0	7.11
FMLs/%	0	16.59	0
Oat hay/%	12.43	24.88	17.77
Corn silage/%	29.00	8.29	24.88
Corn/%	19.34	16.59	16.59
Wheat/%	20.72	17.77	17.77
Concentrate/%	17.68	15.17	15.17
Limestone/%	0.83	0.71	0.71
Total/%	100	100	100
Nutrients (based on dry matter)			
Dry matter/%	72.50	66.10	66.40
Crude protein/%	16.40	16.70	16.60
Metabolizable Energy/(MJ/kg)	10.46	10.63	10.30
Crude fat/%	3.00	3.40	3.00
Crude ash/%	9.58	9.24	10.59
Acid detergent fiber/%	16.80	17.50	15.30
Neutral detergent fiber/%	27.80	28.47	25.76
Lignin/%	4.30	4.40	4.80

repeats (group TR2) and 5 biological repeats (group TR2), respectively. Serum samples contain 8 biological repeats (group Con), 7 biological repeats (group TR2) and 8 biological repeats (group TR2), respectively. Technical repetition is no less than 2 for all samples. No data point from the analysis is excluded.

Widely target metabolomics analysis

Tissue samples of muscle are extracted by Metware according to standard procedures. The sample extracts were analyzed using an LC-ESI-MS/MS system (UPLC, ExionLC AD, <https://sciex.com.cn/>; MS, QTRAP[®] System, <https://sciex.com/>). LIT and triple quadrupole (QQQ) scans were acquired on a triple quadrupole-linear ion trap mass spectrometer (QTRAP), QTRAP[®] LC-MS/MS System, equipped with an ESI Turbo Ion-Spray interface, operating in positive and negative ion mode and controlled by Analyst 1.6.3 software (Sciex). Instrument tuning and mass calibration were performed with 10 and 100 $\mu\text{mol/L}$ polypropylene glycol solutions in QQQ and LIT modes, respectively. A specific set of MRM transitions were monitored for each period according to the metabolites eluted within this period. Significantly regulated metabolites between groups were determined by variable importance in projection ($\text{VIP} \geq 1$) and absolute Log_2FC (fold change) ≥ 1 . VIP values were extracted from OPLS-DA result, which also contain score plots and permutation plots, was generated using R package MetaboAnalystR. The data was log transform (\log_2) and mean centering before OPLS-DA. In order to avoid overfitting, a permutation test (200 permutations) was performed.

Transcriptomic analysis

RNA-extract and RNA-seq of muscle are conducted according to standard procedures of Majorbio with the Illumina HiSeq xten/NovaSeq 6000 sequencer (2 \times 150bp read length). The raw paired end reads were trimmed and quality controlled by SeqPrep (<https://github.com/jstjohn/SeqPrep>) and Sickle (<https://github.com/najoshi/sickle>) with default parameters. Then clean reads were separately aligned to reference genome with orientation mode using HISAT2 (<http://ccb.jhu.edu/software/hisat2/index.shtml>) software (8). The mapped reads of each sample were assembled by StringTie (<https://ccb.jhu.edu/software/stringtie/index.shtml?t=example>) in a reference-based approach (9). To identify DEGs (differential expression genes) between two different samples, the expression level of each transcript was calculated according to the transcripts per million reads (TPM) method. RSEM (<http://deweylab.biostat.wisc.edu/rsem/>) (10) was used to quantify gene abundances. Essentially, differential expression analysis was performed using the DESeq2 (11)/DEGseq

(12)/EdgeR (13) with Q value ≤ 0.05 , DEGs with $|\log_2\text{FC}| > 1$ and Q value ≤ 0.05 (DESeq2 or EdgeR)/Q value ≤ 0.001 (DEGseq) were considered to be significantly different expressed genes. The transcriptomic sequence data have been deposited in the NCBI database (Accession No. PRJNA898816).

Statistical analysis

Statistical analysis was performed by the SPSS 19.0 software (IBM-SPSS Statistics, IBM Corp., Armonk, NY, United States). Data were evaluated using a one-way ANOVA followed by Turkey's multiple range tests for physiological and biochemical indexes. Significance was declared if $p < 0.05$. Additionally, omics sequencing data are analyzed using online platforms for data analysis, including Metware cloud tools (<https://cloud.metware.cn/#/tools/tool-list>) and Majorbio cloud platform (<https://cloud.majorbio.com/>). Histograms and metabolic pathway maps are drawn respectively using Graphpad Prism 8 and Adobe Illustrator CS6.

Results

Growth performance

Throughout the trial, no significant differences were detected in daily gain (0–25d) ($\text{Con} < \text{TR2} < \text{TR1}$) and feed to gain ratio (F/G) ($\text{Con} > \text{TR2} > \text{TR1}$) ($p > 0.05$, Table 3), although group TR1 which were fed with FMLs demonstrated a little increase in daily gain (0–25d) and a slight decrease in F/G. Apparently, treatments with FMLs and DMLs (group TR2) generated an obvious increase in ADFI during the overall raising period ($p < 0.05$), which suggests MLs are a delicious feed for promotion. In addition, ADG, daily gain (25–50d) and serum growth hormone levels were significantly improved in both MLs-treatment groups ($p < 0.05$) in the study. Further, FMLs feeding resulted in a significant increase in the final body weight ($p < 0.05$).

Anti-oxidant properties

As shown in Table 4, SOD (superoxide dismutase), CAT (catalase), GSH-Px (glutathione peroxidase) and TAOC (total antioxidant activity) in serum and muscle were significantly increased in the MLs treatment group, especially in the FMLs treatment group ($p < 0.05$); SOD and GSH-Px in adipose tissue also increased significantly ($p < 0.05$), CAT and TAOC tended to increase ($\text{Con} < \text{TR2} < \text{TR1}$, $p > 0.05$). In addition, feeding MLs significantly decreased the content of MDA in serum and muscle of mutton sheep ($p < 0.05$), the content of MDA in adipose tissue was $\text{Con} > \text{TR2} > \text{TR1}$ ($p > 0.05$).

TABLE 3 Growth performance.

Items	Con	TR1	TR2	SEM	P-value
Initial BW/kg	30.36	30.36	30.50	0.589	0.994
Final BW/kg	38.03 ^b	42.05 ^a	40.86 ^{ab}	0.696	0.050
ADFI/kg	1.79 ^b	2.31 ^a	2.35 ^a	0.033	0.000
Daily gain (0-25d)/g	95.56	125.56	97.64	6.999	0.145
Daily gain (25-50d)/g	211.11 ^b	342.22 ^a	317.64 ^a	16.330	0.001
ADG (0-50d)/g	156.11 ^b	233.89 ^a	205.56 ^a	7.876	0.001
F/G	13.38	10.26	11.79	1.026	0.483
GH	4.81 ^c	5.84 ^b	7.28 ^a	0.265	0.000

BW, body weight; ADFI, average daily feed intake; ADG, average daily gain; F/G, ADFI/ADG; GH, growth hormone; SEM, standard error mean; Different letters in the same row (a–c) differed ($p < 0.05$).

To further explore how MLs cause a differences in promoting oxidation resistance, muscle widely target metabolomics was applied. A total 43 significant differential metabolites (DEMs), including 19 upregulated and 24 downregulated DEMs after FMLs treatment, were filtered according to the criteria that the metabolite contents were

within $FC \geq 2$ or $FC \leq 0.5$, and $VIP \geq 1$ (Figure 1A). On this basis, the p-value is listed ascending order and absolute value of $\log_2 FC$ is listed in descending order of 43 DEMs to further obtain the leading 20 DEMs, shown in Figure 1B. These top-ranking DEMs were mainly involved in lipid, carbohydrate, amino acid, and organic acid metabolism. As the heatmap

TABLE 4 Anti-oxidant properties of serum, muscle and adipose tissues.

Items	Con	TR1	TR2	SEM	P-value
Serum					
SOD	58.72 ^c	77.94 ^a	66.56 ^b	2.021	0.000
CAT	32.80 ^c	58.95 ^a	45.22 ^b	2.489	0.000
GSH-PX	358.13 ^c	543.05 ^a	476.41 ^b	17.737	0.000
TAOC	7.37 ^c	10.84 ^a	8.49 ^b	0.366	0.000
MDA	5.09 ^a	4.05 ^b	4.60 ^{ab}	0.150	0.013
Muscle					
SOD	5.55 ^c	9.64 ^a	7.67 ^b	0.475	0.000
CAT	2.37 ^c	4.49 ^a	3.56 ^b	0.241	0.000
GSH-PX	23.12 ^c	31.81 ^a	27.35 ^b	1.029	0.000
TAOC	3.18 ^c	5.10 ^a	4.47 ^b	0.226	0.000
MDA	4.33 ^a	3.31 ^b	3.98 ^a	0.134	0.001
Adipose					
SOD	2.18 ^c	5.23 ^a	3.58 ^b	0.371	0.000
CAT	0.72	1.68	0.98	0.201	0.126
GSH-PX	6.01 ^c	11.17 ^a	8.20 ^b	0.691	0.003
TAOC	0.98	2.05	1.26	0.254	0.212
MDA	1.32	1.17	1.00	0.185	0.809

SOD, superoxide dismutase; CAT, catalase; GSH-PX, glutathione peroxidase; TAOC, total antioxidant capacity; MDA, malonaldehyde; muscle, longissimus dorsi; adipose, subcutaneous fat. Different letters in the same row (a–c) differed ($p < 0.05$).

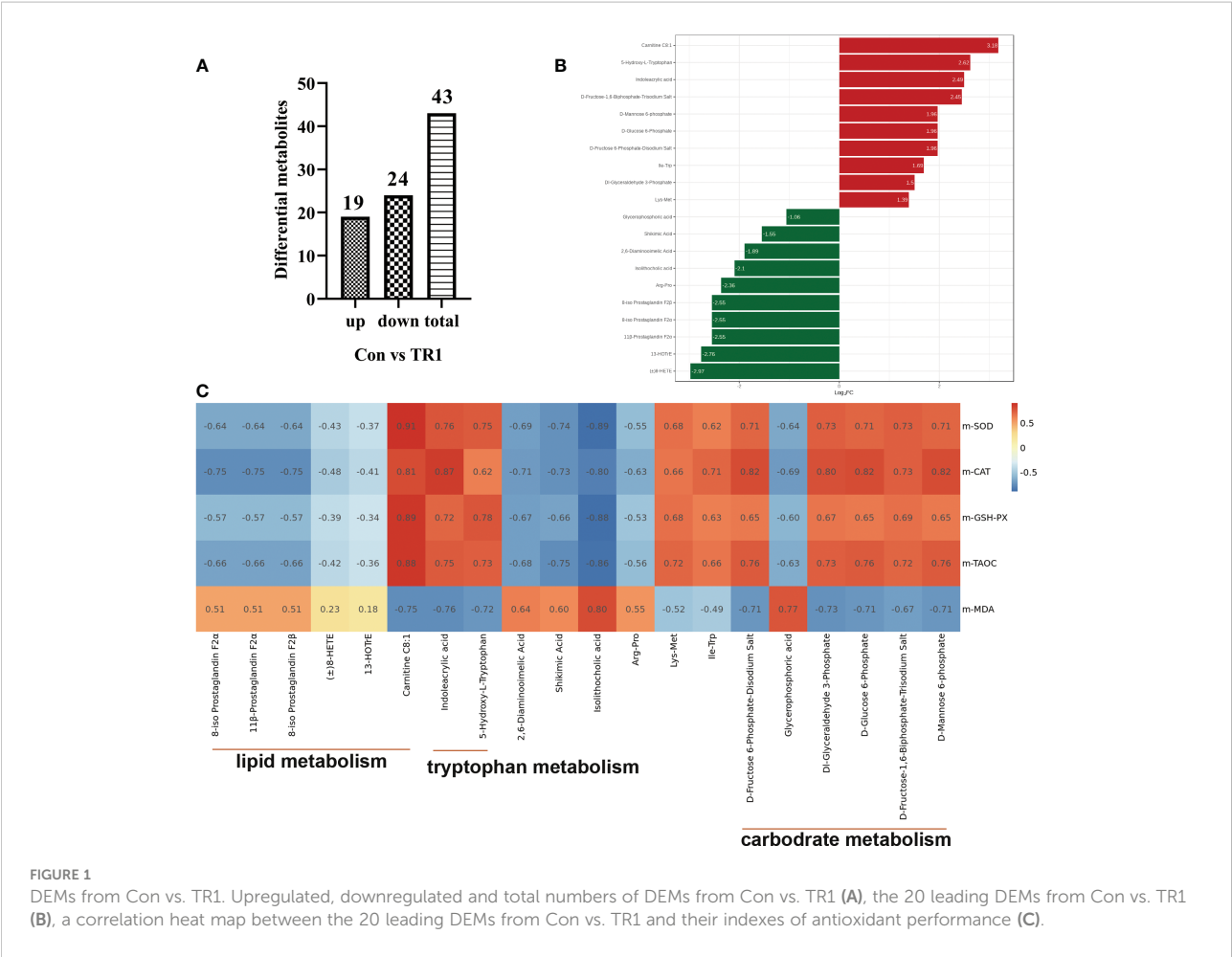


FIGURE 1 DEMs from Con vs. TR1. Upregulated, downregulated and total numbers of DEMs from Con vs. TR1 (A), the 20 leading DEMs from Con vs. TR1 (B), a correlation heat map between the 20 leading DEMs from Con vs. TR1 and their indexes of antioxidant performance (C).

shows, anti-oxidant properties were negatively correlated (dark blue) with products of lipid metabolism (8-iso Prostaglandin F2α, 11β-Prostaglandin F2α, 8-iso Prostaglandin F2β, (±)8-HETE, 13-HOTrE, Carnitine C8:1), and were positively correlated (dark red) with D-Glucose 6-Phosphate, D-Fructose 6-Phosphate-Disodium Salt, D-Fructose-1,6-Biphosphate-Trisodium Salt, and D-Mannose 6-phosphate, which are related to carbohydrate metabolism (Figure 1C). This suggests that lipid metabolism and carbohydrate metabolism in FMLs treatment regulate the anti-oxidant process. More importantly, the correlation analysis suggests that the increased expression of 5-Hydroxy-L-Tryptophan and indoleacrylic acid produced by tryptophan metabolism may play crucial roles in anti-oxidant regulation. Figure 2A exhibited the DEMs from Con vs. TR2, including 16 upregulated and 39 downregulated, 55 in total DEMs, based on the same screening criteria as FMLs treatment. Similarly, the top-ranking 20 DEMs in Figure 2B obtained in the same method, are also mainly involved in lipid metabolism (8-iso Prostaglandin F2α, 11β-Prostaglandin F2α, 8-iso Prostaglandin F2β, 13-HOTrE, Carnitine C8:1), carbohydrate metabolism (D-Mannose 6-phosphate, D-Glucose 6-Phosphate,

D-Fructose 6-Phosphate-Disodium Salt), amino acid metabolism and organic acid metabolism. However, few correlation relationships (yellow in Figure 2C) between carbohydrate metabolism and anti-oxidant properties in heatmap analysis show that DMLs supplementation might slightly, or not facilitate oxidation resistance by regulating carbohydrate metabolism.

Considering the 20 DEMs and antioxidant performance indexes between Con vs. TR1 and Con vs. TR2, It is not too difficult to discover the importance of lipid metabolism, especially the peroxidation of polyunsaturated fatty acids (PUFAs), amino acid metabolism (mainly tryptophan metabolism) for MLs treatment, and carbohydrate metabolism (mainly glycolysis and mannose 6-phosphate pathway) only for FMLs treatment in promoting oxidation resistance. The tryptophan metabolism and peroxidation of PUFAs could be promising MLs-dependent biomarkers of the anti-oxidant metabolism pathway. Indoleacrylic acid and 5-hydroxy tryptophan (5-HTP) obtained from the two routes of tryptophan metabolism (Figure 3) were significantly upregulated. Indolelactic acid, an upstream metabolite of

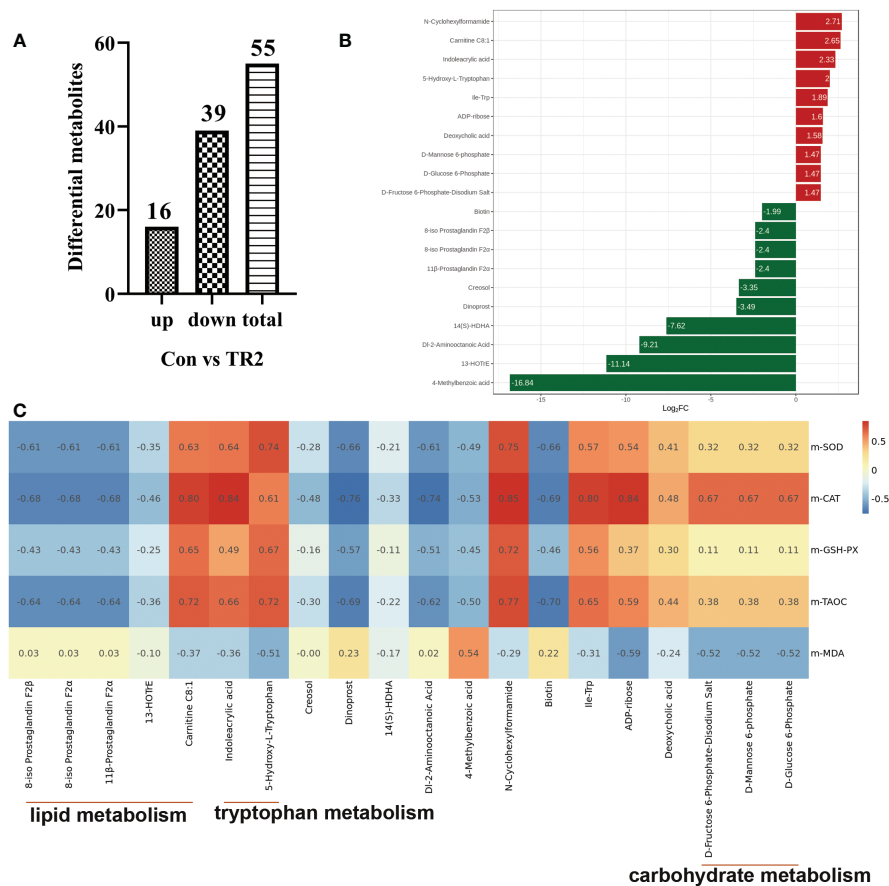


FIGURE 2
DEMs from Con vs. TR2. Upregulated, downregulated and total numbers of DEMs from Con vs. TR2 (A), the 20 leading DEMs from Con vs. TR2 (B), a correlation heat map between the 20 leading DEMs from Con vs. TR2 and their indexes of antioxidant performance (C).

indoleacrylic acid, was also significantly increased in FMLs treatment ($p=0.015$). Moreover, the markedly decreased 8-HETE, 13-HOTrE, 8-iso Prostaglandin F2 α , 11 β -Prostaglandin F2 α , and 8-iso prostaglandin F2 β levels and increased carnitine C8:1 are present after MLs treatment.

Transcriptome analysis was performed to further verify that reducing the peroxidation of PUFAs could indeed promote oxidation resistance. All filtered sequenced genes were used for weighted gene co-expression network analysis (WGCNA) analysis. Correlation analysis of different module genes and grouping factors and six DEMs related to PUFAs metabolism (8-iso Prostaglandin F2 α , 11 β -Prostaglandin F2 α , 8-iso Prostaglandin F2 β , (\pm)8-HETE, 13-HOTrE, carnitine C8:1) are shown in Figure 4A. Three module genes (underlined module in red in the Figure 4A) with almost the same correlation with the grouping factors and DEMs were integrated for further analysis. Subsequently, 14 target DEGs were obtained from the integrated genes with two criteria that their p-value must be less than 0.05, and absolute log₂FC (Con vs. TR1) value must be not less than 1. Subsequently, they were gathered with six DEMs for network

map analysis (Figure 4B). The relative expression levels of these 14 target DEGs in the three groups are shown in Figure 4C. Relative expression levels of *GCNT1*, *IFITM10*, *EXTL1*, *RILP*, *BBC3*, *RAB9A*, *MOB3B*, *SESN1*, *CDH4*, *MEIS1*, *RAB9A*, *NUDT7*, *FMO2* and *NUDT7* was decreased significantly ($p<0.05$).

Immune response

Serum immuno globulin G (IgG) and total immuno globulin (Ig) levels increased in the FMLs ($p<0.05$) remarkably and DMLs fed groups ($p>0.05$). The pro-inflammatory tumor necrosis factor- α (TNF- α) was dramatically reduced by both MLs treatments (Figure 5A) ($p<0.05$). However there is a distinctive decrease in immuno globulin M (IgM) following FMLs treatment ($p<0.05$). The decreased IgM following FMLs treatment is related to a transition in antibody class from IgM to IgG, over the course of an immune response (14) (Figure 5B).

As reported by Wu et al. (15), muscles support a strong immune response. To validate the promotion of the immune

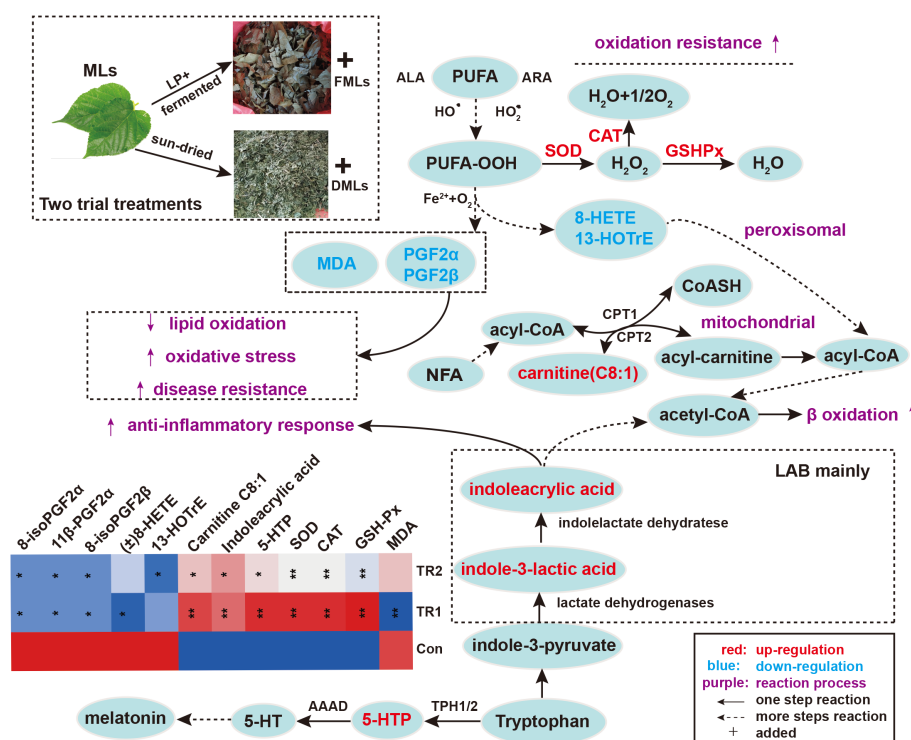


FIGURE 3

Peroxidation of PUFAs and tryptophan metabolism. Elevated metabolites are highlighted in red, reduced metabolites are shown in blue; the contents of painted green or red metabolites from top 20 DEMs and antioxidant biochemical indexes are displayed in heat map (* $p < 0.05$, ** $p < 0.01$, * and ** are TR1 or TR2 compared to Con). (MLs, mulberry leaves; FMLs, fermented mulberry leaves; DMLs, dried mulberry leaves; LP, *Lactobacillus plantarum*; LAB, lactic acid bacteria; PUFA, polyunsaturated fatty acids; ALA, α linolenic acid; ARA, arachidonic Acid; CPT1/CPT2, carnitine palmitoyltransferase 1/2; NFA, medium-chain fatty acid; 5-HTP, 5-hydroxytryptophan; 5-HT, serotonin; AAAD, aromatic amino acid decarboxylase; TPH1/2, tryptophan hydroxylase 1/2).

process of FMLs, all DEGs of FMLs treatment in muscle analyzed by transcriptomics were applied for enrichment analysis, and the top eight KEGG pathways are represented in a histogram (Figure 5C). The four leading enriched pathways (arrow's place in Figure 5C) are closely related to apoptosis and immune processes. Subsequently, a total of six annotated DEGs from the leading four pathways and immune indices were combined to analyze the relevance and a clear relationship was shown in the circular map (Figure 5D). After MLs treatment, the relative expressions of the DEGs, including *DOCK2*, *BBC3*, *MYO10*, *PIK3R3*, *PLA2G4D*, *GADD45A*, were markedly altered (Figure 5E).

Previously, we found that FMLs improves carbohydrate metabolism, and glycolysis is one of the key processes. It has been found that it can provide biosynthetic intermediates and reducing power for the growth and proliferation of immune cells. MLs treatments raise levels of glucose, the central substrate of glycolysis and FMLs supplementation significantly increases the contents of glucose-6-P, glyceraldehyde-3-P ($p < 0.05$) and almost significantly increases fructose-6-P ($p = 0.054$) (Figure 6). Additionally, there are significantly increased D-mannose in DMLs treatment ($p < 0.05$) and mannose-6-P in FMLs treatment

($p < 0.05$) (Figure 6). These two are both derived from mannose-6-P pathway.

Discussion

Numerous studies have shown the diverse growth-promoting effects of MLs (4, 16). Our study also proves this point. In addition, this study also found that FMLs are superior to FMLs in palatability and growth promotion, which is a rare feed additive, and its application prospects in animal husbandry production appear considerable.

Anti-oxidation activity

Oxidation in biological systems is mainly mediated by a series of redox enzymes. Peroxidation caused by free radical chain reactions may lead to oxidative stress (17). SOD, CAT and GSH-Px are common enzymatic antioxidants. SOD can convert free radicals ($O_2^{\cdot-}$) generated in the body's peroxidation reaction into H_2O_2 (18), and H_2O_2 can then be converted into H_2O by CAT and GSH-

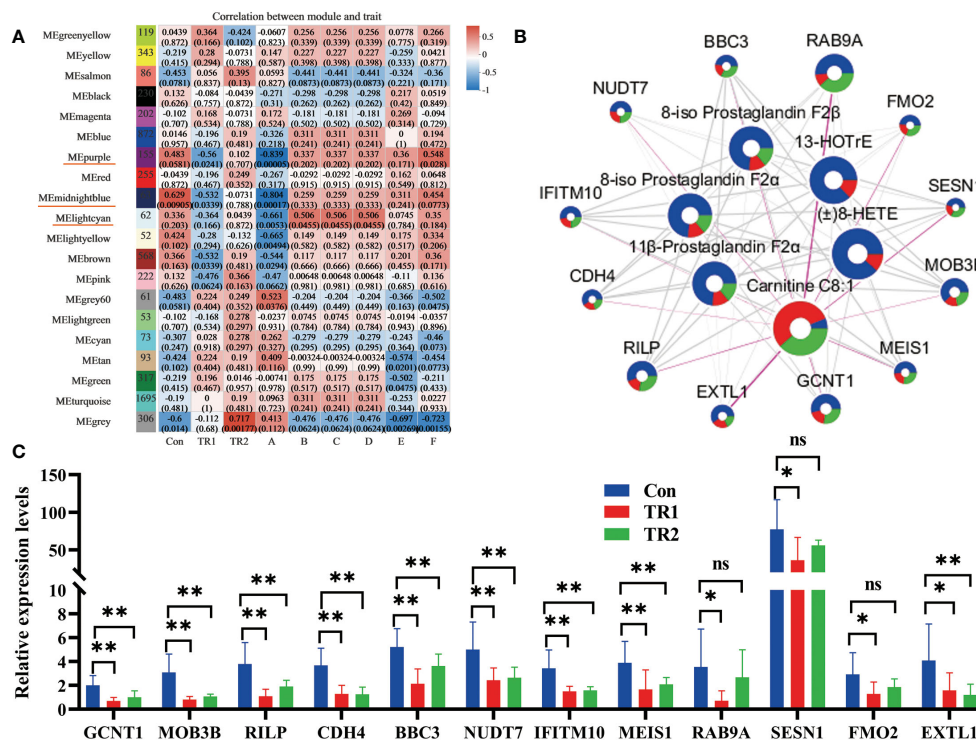


FIGURE 4

DEGs related with peroxidation of PUFAs. Module analysis of DEMs related with PUFAs metabolism and all filtered genes (Underlined modules in red represent selective modules; A, carnitine C8:1; B, 8-iso-prostaglandin F2 α ; C, 11 β -prostaglandin F2 α ; D, 8-iso-prostaglandin F2 β ; E, (\pm) 8-HETE; F, 13-HOTrE) (A), network map analysis of selective twelve DEGs and DEMs related with PUFAs metabolism (circle size represents absolute \log_2 FC (Con vs TR1) value; blue, red and green divisions in every circle are on behalf of contents of some DEGs or DEMs in Con, TR1, TR2 in turn; The thickness of the connecting wire represents the degree of connectivity) (B) and the relative expression levels of selective twelve target DEGs in three groups (*represents $p<0.05$, ** represents $p<0.01$, ns represents no differences) (C).

Px to reduce the damage resulting from free radical to the body and improve antioxidant performance. MDA is one of the representative end products under non-enzymatic lipid peroxidation, indicating the extent of lipid peroxidation (19). Meanwhile, MDA is also an important indicator of membrane damage and body aging, and one of the toxic substances produced by the increase of ROS (20). The increase of SOD, CAT, GSH-Px, TAOC and the decrease of MDA in this study all indicate that MLs can improve the antioxidant performance of the body, which is consistent with the results of previous studies (3, 21–23). The reason is that MLs are rich in bioactive ingredients. In addition, this study also found that FMLs have the strongest antioxidant properties, mainly because of their higher active ingredients than DMLs (24).

Indoleacrylic acid derived from tryptophan metabolism, has been shown to have significant anti-inflammatory effects *in vitro* and *vivo* (25) and also have beneficial effects on the intestinal epithelial barrier function (26). Indolelactic acid, an upstream metabolite of indoleacrylic acid has been shown to possess antimicrobial, anti-oxidative, anti-inflammatory activities (26, 27) and can potentially modulate immune function (28). L-5-hydroxytryptophan (5-HTP) is a monoamine neurotransmitter involved in the modulation of mood, cognition, reward, learning,

memory, sleep, and numerous other physiological processes (29), and can also suppress inflammation and arthritis by decreasing the production of pro-inflammatory mediators (30). Overall, MLs, especially FMLs, must endow anti-bacterial, anti-oxidant, anti-inflammation, and immunity-enhancing properties *via* tryptophan metabolism.

Linoleic acid (LA), arachidonic acid (ARA), eicosapentaenoic acid (EPA) and α -linolenic acid (ALA) are representative of the main PUFAs, and the major metabolic pathways of peroxidation described in mammals are both enzymatic (cyclooxygenase, COX; lipoxygenase, LOX; cytochrome P450, CYP) and non-enzymatic (31) oxidation. 8-HETE and 13-HOTrE are all oxylipins, a group of oxidized metabolites derived from PUFAs (32). Generally, the synthesis of oxylipins fluctuates with the changes of physiological or pathological states (33). 13-HOTrE is derived from ALA *via* the COX enzymatic pathway. Studies have revealed that 13-HOTrE levels are significantly increased in some diseases (34, 35), such as acute liver injury. Therefore, it is generally thought to be a proinflammatory factor. HETEs are derived from ARA through COX catalysis. Hayashi et al. (36) reported that several ARA-derived (18-HETE/20-HETE) and ALA-derived (13-

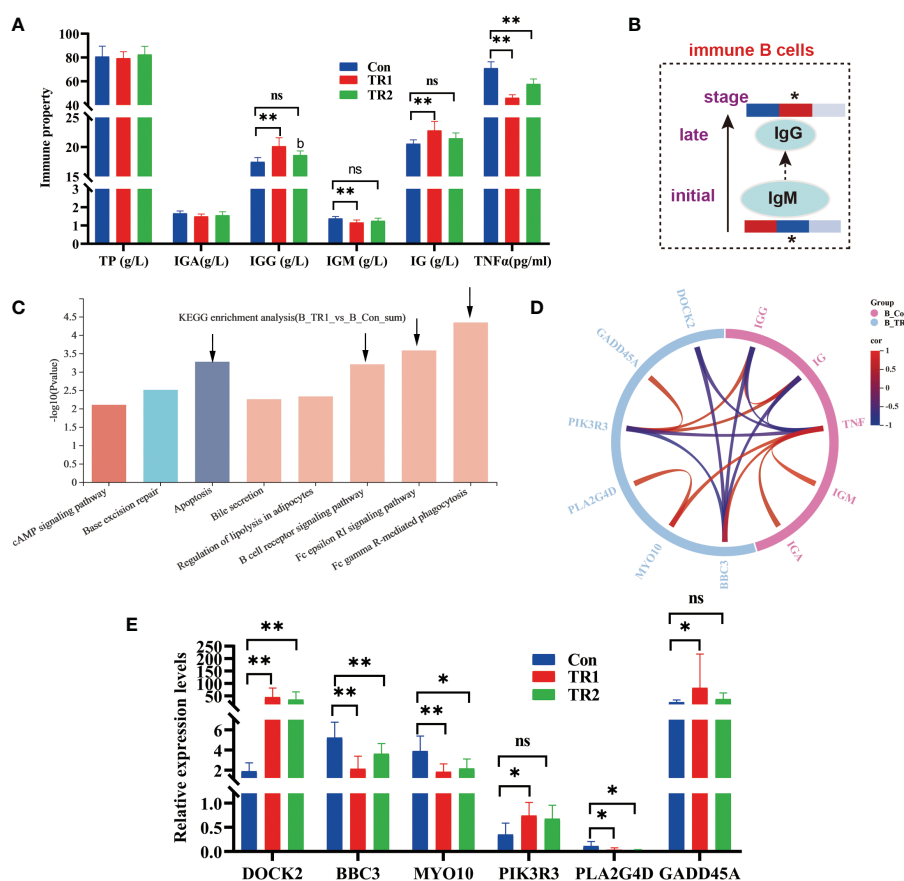


FIGURE 5

Indexes of immune properties and DEGs related to immune response. Immune indexes of serum (A) a transition from IgM to IgG in immune B cells over the course of immune response (Heat maps show the relative amounts of substances in group Con, TR1 and TR2 from left to right; * represent $p < 0.05$, indicative of the significant difference by comparing TR1 or TR2 to Con) (B), kegg enrichment analysis of all DEGs from TR1 vs. Con (C), Circular correlation analysis of six selective DEGs from top 4 kegg pathway and immune indexes of serum (D), Relative expression levels of six selective DEGs related to immune response (E) (* represents $p < 0.05$, ** represents $p < 0.01$, ns represents no differences in histograms).

HOTrE) oxylipins tend to increase in bovine mastitic milk. In this study, MLs treatments reduced the 8-HETE contents. Meanwhile Ma et al. (37) also reported that 8-HETE is relevant for the efficacy of Zuojin pill treatment in chronic nonatrophic gastritis, as the level of 8-HETE was higher before treatment than after treatment. Thus, decreased oxylipins in this study with MLs treatments probably improve the antioxidant performance and immunity of the body and will be promising markers for livestock welfare.

8-iso Prostaglandin F2α, as a final product of lipid peroxidation, is generated from ARA interacting with ROS through nonenzymatic routes and is a robust oxidative stress biomarker of some diseases (32, 38). 8-iso Prostaglandin F2β is a constitutional isomer of 8-iso Prostaglandin F2α. Oliveira et al. (39) found that 8-iso Prostaglandin F2β has much lower potency than 8-iso Prostaglandin F2α with an α-configuration. 11β-Prostaglandin F2α, as a metabolite of 8-iso Prostaglandin F2α, have been found to be associated with levels of oxidative stress in

specific diseases (40). Thus, the markedly decreased 8-iso Prostaglandin F2α, 11β-Prostaglandin F2α, and 8-iso prostaglandin F2β levels after MLs treatment indicate a decline in the peroxidation of PUFAs, which will produce beneficial effects on lowering oxidative stress and enhancing disease resistance.

Carnitine plays a key role not only in fatty acid β-oxidation, but also in immunity enhancement and disease resistance. Guo et al. (41) found that carnitine C8:1 was significantly decreased in the non-alcoholic steatohepatitis group, and this could be profoundly reversed after luteolin treatment. Studies have reported decreased serum acyl-carnitine concentrations in patients with cancer (42). It can be hypothesized that increased carnitine C8:1 levels altered by MLs supplementation might accelerate mitochondrial β-oxidation (43) thereby enhancing immunity and disease resistance.

Previous studies have shown that increased *GCNT1*, *IFITM10*, *EXTL1*, *RILP*, *BBC3*, *RAB9A*, *MOB3B*, *SESN1*,

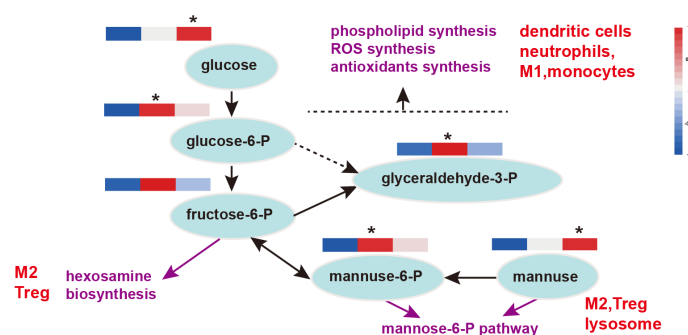


FIGURE 6

Glycolysis and the mannose-6-P pathway in immune function. Heat maps show the relative amounts of substances in group Con, TR1 and TR2 from left to right; * represent $p < 0.05$, indicative of the significant difference by comparing TR1 or TR2 to Con; M1, type 1 macrophages; M2, type 2 macrophages; Treg, regulatory T cells; P, phosphatase.

CDH4, *MEIS1*, *RAB9A*, *NUDT7*, and *FMO2* are related to immune deficiency, autophagy inhibition, disease sensitivity and oxidative stress. Therefore, after treatment of MLs, the decreased peroxidation of PUFAs (the decreasing in peroxidation products) reduced the expression of the above genes, thus improving the immune and antioxidant properties. In addition, Shumar et al. (44) and Kerr et al. (45) suggest that decreased *NUDT7* may reduce the accumulation of peroxisome through regulating the β -oxidation of peroxisome fatty acids, thus improving the antioxidant performance; Ge et al. (46) found that the decrease of *NUDT7* enhanced the immune defense response; Taniguchi et al. (47) and Liu et al. (48) reported that *NUDT7* with low expression may up-regulate heme biosynthesis and contribute to meat-redness enrichment. Therefore, the addition of MLs can not only reduce the peroxidation of PUFAs, enhancing the antioxidant capacity and immunity of the body, but also improve meat redness.

Overall, oxidation resistance is closely related to the immune response. Our study proved that MLs supplementation is effective in promoting oxidation resistance and disease resistance, which is attributed to its function in reducing peroxidation of PUFAs and increasing tryptophan metabolism. Additionally, as lipid oxidation products affect the shelf life (49), sensory characteristics (50), and nutritional composition of meat (51), the role of MLs in reducing the peroxidation of PUFAs is speculated to be linked to the improvements in meat quality.

Immune response

According to Sundling et al. (52), secreted antibodies confer immune protection by first attaching to foreign antigens through the paired variable regions of their immunoglobulin heavy and light chains. Immunity was enhanced with increased Ig, IgG and reduced TNF α in both MLs treatments. In addition, the FMLs induced maximum immunity in animals with a transition in

antibody class from IgM to IgG, over the course of an immune response (14). During which, early low-affinity IgM antibodies are progressively replaced by more-effective, high-affinity IgG antibodies (53) to achieve effective serological immunity (52).

DOCK2 regulates the migration of certain subsets of immune cells via Rac activation (54) and plays an important anti-inflammatory role in the development of various inflammatory diseases (55). *BBC3* is a transcriptional apoptotic target gene and participates in the activation of cell death processes (56). Pozo et al. (57) reported that pro-inflammatory *MYO10* mediates inflammation in cancer by regulating genomic stability. Studies have shown that *PIK3R3* is a multifunctional gene related to inflammatory diseases, livestock coat color, and cell proliferation (58–60). Shao et al. (61) clarified that *PLA2G4D*, a major pro-inflammatory factor, facilitates CD1a expression, which can be recognized by lipid-specific CD1a-reactive T cells, leading to the production of IL-22 and IL-17A. According to Ehmsen et al. (62) and Jiang et al. (63), the increased expression of *GADD45A*, a cell cycle regulator, can ameliorate liver fibrosis in rats and is a protective modifier of neurogenic skeletal muscle atrophy. Collectively, MLs supplementation improves muscle immune response and disease resistance.

Glycolysis is a critical process closely related to the immune response, as well as provides biosynthetic intermediates and reducing power for cell growth and proliferation of immune cells (64). The pentose phosphate pathway (PPP) from glucose-6-P to glyceraldehyde-3-P provides immune cells with key metabolites for immune function, such as reducing power for the synthesis of ROS and antioxidants in phagocytic cells and for phospholipid synthesis in dendritic cells. The hexosamine biosynthesis pathway, originating from fructose-6-P, provides substrates for the glycosylation of lipids and proteins that are important for Treg and M2 macrophage lineages (64). Thus FMLs treatment may enhance immunity by glycolysis, which in turn provides key metabolites for immune function.

D-mannose serves a vital function in T cell immune responses and is currently receiving increasing attention, although its normal physiological blood concentration is less than one-fiftieth of that of glucose. Zhang et al. (65) recognized that D-mannose induces regulatory T cells and suppresses immunopathology both *in vivo* and *in vitro*. Mannose-6-phosphate metabolized by D-mannose is a novel regulator of T cell immunity (66) and a promising target ligand in cancer therapy, as well as confers a better efficacy and lower toxicity in healthy tissues (67). Moreover, mannose-6-P not only plays a crucial role in lysosomal functions (such as autophagy) but also in regulating lysosome biogenesis (68). Thus, significantly increased D-mannose in DMLs treatment ($p < 0.05$) and mannose-6-P in FMLs treatment ($p < 0.05$) (Figure 6) *via* the mannose-6-P pathway enhances T cell immunity and likely regulates the lysosome biogenesis in autophagy.

Taken together, FMLs supplementation could improve the immune response *via* glycolysis and the mannose-6-P pathway and induce class switch from low-affinity IgM to high-affinity IgG antibodies.

Data availability statement

The original contributions presented in the study are publicly available. This data can be found in the NCBI repository under accession number: PRJNA898816 [<https://www.ncbi.nlm.nih.gov/search/all/?term=PRJNA898816>] and in the MetaboLights repository under accession number: MTBLS6516.

Ethics statement

The animal study was reviewed and approved by Animal Care and Use Committee of the Institute of Northwest A & F University. Written informed consent was obtained from the owners for the participation of their animals in this study.

Author contributions

XC and YY contributed to the conception and design of the study. XC performed the statistical analysis and wrote the first

draft of the manuscript. YY, MZ, FJ, LB, CS, and YQ revised the manuscript. SL, HW, ZL, XW, WQ and XS helped with the experimental sections. CS and YQ provided financial support for the manuscript. All authors contributed to manuscript revision, and read and approved the submitted version.

Funding

This study was financially supported by the Special Program in Technology and Innovation of the Shaanxi Forestry Academy (SXLK2020-0211), China Agriculture Research System of MOF (Ministry of Finance) and MARA (Ministry of Agriculture and Rural Affairs) (CARS-18), Technical System Construction of the Shaanxi Sericulture Industry (NYKJ-2022-YL(XN)29) and The special fund of key support project in Northwest A&F University extension mode (TGZX2022-13).

Acknowledgments

The authors acknowledge with the all participated in this study and we would like to thank Editage (www.editage.com) for English language editing.

Conflict of interest

The authors declare that the research was conducted in the absence of any commercial or financial relationships that could be construed as a potential conflict of interest.

Publisher's note

All claims expressed in this article are solely those of the authors and do not necessarily represent those of their affiliated organizations, or those of the publisher, the editors and the reviewers. Any product that may be evaluated in this article, or claim that may be made by its manufacturer, is not guaranteed or endorsed by the publisher.

References

1. Thaipitakwong T, Numhom S, Aramwit P. Mulberry leaves and their potential effects against cardiometabolic risks: a review of chemical compositions, biological properties and clinical efficacy. *Pharm Biol* (2018) 56 (1):109–18. doi: 10.1080/13880209.2018.1424210
2. Insang S, Kijpatanasilp I, Jafari S, Assatarakul K. Ultrasound-assisted extraction of functional compound from mulberry (*Morus alba* L.) leaf using response surface methodology and effect of microencapsulation by spray drying on quality of optimized extract. *Ultrason Sonochem* (2022) 82:1–11. doi: 10.1016/j.ultrsonch.2021.105806
3. Liu Y, Li Y, Xiao Y, Peng Y, He J, Chen C, et al. Mulberry leaf powder regulates antioxidative capacity and lipid metabolism in finishing pigs. *Anim Nutr* (2021) 7(2):421–9. doi: 10.1016/j.aninu.2020.08.005
4. Ding Y, Jiang X, Yao X, Zhang H, Song Z, He X, et al. Effects of feeding fermented mulberry leaf powder on growth performance, slaughter performance, and meat quality in chicken broilers. *Anim (Basel)* (2021) 11(11):1–15. doi: 10.3390/ani11113294
5. Li M, Hassan FU, Tang Z, Peng L, Liang X, Li L, et al. Mulberry leaf flavonoids improve milk production, antioxidant, and metabolic status of water buffaloes. *Front Vet Sci* (2020) 7:1–12. doi: 10.3389/fvets.2020.00599

6. Ouyang J, Wang M, Hou Q, Feng D, Pi Y, Zhao W. Effects of dietary mulberry leaf powder in concentrate on the rumen fermentation and ruminal epithelium in fattening hu sheep. *Anim (Basel)* (2019) 9(5):1–11. doi: 10.3390/ani9050218
7. Cavill R, Jennen D, Kleinjans J, Briede JJ. Transcriptomic and metabolomic data integration. *Brief Bioinform* (2016) 17(5):891–901. doi: 10.1093/bib/bbv090
8. Kim D, Langmead B, Salzberg SL. HISAT: a fast spliced aligner with low memory requirements. *Nat Methods* (2015) 12(4):357–60. doi: 10.1038/nmeth.3317
9. Pertea M, Pertea GM, Antonescu CM, Chang TC, Mendell JT, Salzberg SL. StringTie enables improved reconstruction of a transcriptome from RNA-seq reads. *Nat Biotechnol* (2015) 33(3):1–20. doi: 10.1038/nbt.3122
10. Li B, Dewey CN. RSEM: accurate transcript quantification from RNA-seq data with or without a reference genome. *BMC Bioinform* (2011) 12:1–16. doi: 10.1186/1471-2105-12-323
11. Love MI, Huber W, Anders S. Moderated estimation of fold change and dispersion for RNA-seq data with DESeq2. *Genome Biol* (2014) 15(12):1–21. doi: 10.1186/s13059-014-0550-8
12. Wang L, Feng Z, Wang X, Wang X, Zhang X. DESeq: an R package for identifying differentially expressed genes from RNA-seq data. *Bioinformatics* (2010) 26(1):136–8. doi: 10.1093/bioinformatics/btp612
13. Robinson MD, McCarthy DJ, Smyth GK. edgeR: a bioconductor package for differential expression analysis of digital gene expression data. *Bioinformatics* (2010) 26(1):139–40. doi: 10.1093/bioinformatics/btp616
14. Best J, Banatvala JE, Watson D. SERUM IgM AND IgG RESPONSES IN POSTNATALLY ACQUIRED RUBELLA. *Lancet* (1969) 294(7611):65–8. doi: 10.1016/S0140-6736(69)92386-1
15. Wu J, Weisshaar N, Hotz-Wagenblatt A, Madi A, Ma S, Mieg A, et al. Skeletal muscle antagonizes antiviral CD8 + T cell exhaustion. *Sci Adv* (2020) 6:1–11. doi: 10.1126/sciadv.aba3458
16. Islam MR, Siddiqui MN, A. Khatun MNAS, Rahman MZ, Selim ASM. Dietary effect of mulberry leaf (*Morus alba*) meal on growth performance and serum cholesterol level of broiler chickens. *SAARC J Agri* (2014) 12(2):79–89. doi: 10.3329/SJA.V12I2.21920
17. Huang D, Ou B, Prior RL. The chemistry behind antioxidant capacity assays. *J Agric Food Chem* (2005) 53:1841–56. doi: 10.1021/jf030723c
18. Coulombier N, Jaufrais T, Lebouvier N. Antioxidant compounds from microalgae: A review. *Mar Drugs* (2021) 19(10):1–30. doi: 10.3390/md19100549
19. Wang W, Zhang Z, Liu X, Cao X, Wang L, Ding Y, et al. An improved GC-MS method for malondialdehyde (MDA) detection: Avoiding the effects of nitrite in foods. *Foods* (2022) 11(9):1–14. doi: 10.3390/foods11091176
20. Zhang J, Yang Z, Zhang S, Xie Z, Han S, Wang L, et al. Investigation of endogenous malondialdehyde through fluorescent probe MDA-6 during oxidative stress. *Anal Chim Acta* (2020) 1116:9–15. doi: 10.1016/j.aca.2020.04.030
21. Jin Y, Tu J, Han X, Zhuo J, Liu G, Han Y, et al. Characteristics of mulberry leaf powder enriched with gamma-aminobutyric acid and its antioxidant capacity as a potential functional food ingredient. *Front Nutr* (2022) 9:1–13. doi: 10.3389/fnut.2022.900718
22. Li R, Zhu Q, Wang X, Wang H. Mulberry leaf polyphenols alleviated high-fat diet-induced obesity in mice. *Front Nutr* (2022) 9:1–9. doi: 10.3389/fnut.2022.979058
23. Shi Y, Zhong L, Fan Y, Zhang J, Zhong H, Liu X, et al. The protective effect of mulberry leaf flavonoids on high-Carbohydrate-Induced liver oxidative stress, inflammatory response and intestinal microbiota disturbance in monopterus albus. *Antioxidants (Basel)* (2022) 11(5):1–18. doi: 10.3390/antiox11050976
24. Cui X, Yang Y, Zhang M, Jiao F, Gan T, Lin Z, et al. Optimized ensiling conditions and microbial community in mulberry leaves silage with inoculants. *Front Microbiol* (2022) 13:1–14. doi: 10.3389/fmicb.2022.813363
25. Zhang B, Wan Y, Zhou X, Zhang H, Zhao H, Ma L, et al. Characteristics of serum metabolites and gut microbiota in diabetic kidney disease. *Front Pharmacol* (2022) 13:1–17. doi: 10.3389/fphar.2022.872988
26. Wlodarska M, Luo C, Kolde R, d'Hennenez E, Annand JW, Heim CE, et al. Indoleacrylic acid produced by commensal peptostreptococcus species suppresses inflammation. *Cell Host Microbe* (2017) 22(1):25–37. doi: 10.1016/j.chom.2017.06.007
27. Siedler S, Balti R, Neves AR. Bioprotective mechanisms of lactic acid bacteria against fungal spoilage of food. *Curr Opin Biotechnol* (2019) 56:138–46. doi: 10.1016/j.copbio.2018.11.015
28. Laursen MF, Sakanaka M, von Burg N, Morbe U, Andersen D, Moll JM, et al. Bifidobacterium species associated with breastfeeding produce aromatic lactic acids in the infant gut. *Nat Microbiol* (2021) 6(11):1367–82. doi: 10.1038/s41564-021-00970-4
29. Maffei ME. 5-hydroxytryptophan (5-HTP): Natural occurrence, analysis, biosynthesis, biotechnology, physiology and toxicology. *Int J Mol Sci* (2020) 22(1):1–25. doi: 10.3390/ijms22010181
30. Yang TH, Hsu PY, Meng M, Su CC. Supplement of 5-hydroxytryptophan before induction suppresses inflammation and collagen-induced arthritis. *Arthritis Res Ther* (2015) 17:1–12. doi: 10.1186/s13075-015-0884-y
31. Kuhn MJ, Mavangira V, Gandy JC, Zhang C, Jones AD, Sordillo LM. Differences in the oxylipid profiles of bovine milk and plasma at different stages of lactation. *J Agric Food Chem* (2017) 65(24):4980–8. doi: 10.1021/acs.jafc.7b01602
32. Samarra I, Masdevall C, Foguet-Romero E, Guirro M, Riu M, Herrero P, et al. Analysis of oxylipins to differentiate between organic and conventional UHT milks. *Food Chem* (2021) 343:1–14. doi: 10.1016/j.foodchem.2020.128477
33. Chavan-Gautam P, Rani A, Freeman DJ. Chapter six - distribution of fatty acids and lipids during pregnancy. *Advances in clinical chemistry* (2018) 84:209–39. doi: 10.1016/bs.acc.2017.12.006
34. Peng S, Shen Y, Wang M, Zhang J. Serum and CSF metabolites in stroke-free patients are associated with vascular risk factors and cognitive performance. *Front Aging Neurosci* (2020) 12:1–13. doi: 10.3389/fnagi.2020.00193
35. Zhan Z, Zhang T, Dai F, Wen X, Chen Y, Jiang H, et al. Effect of oridonin on oxylipins in the livers of mice with acute liver injury induced by d-galactosamine and lipopolysaccharide. *Int Immunopharmacol* (2022) 102:1–8. doi: 10.1016/j.intimp.2021.108387
36. Hayashi A, Fujii S, Nakamura T, Kobayashi K, Sakatani M, Endo M, et al. Production of lipid mediators in mastitic milk of cow. *Anim Sci J* (2019) 90(8):999–1007. doi: 10.1111/asj.13222
37. Ma X, Xie S, Wang R, Wang Z, Jing M, Li H, et al. Metabolomics profiles associated with the treatment of zuojin pill on patients with chronic nonatrophic gastritis. *Front Pharmacol* (2022) 13:1–11. doi: 10.3389/fphar.2022.898680
38. Atrosht.F. P, Kangasniemi. R, Usterman. T. Milk prostaglandins and electrical conductivity in bovine mastitis. *Veterinary Res Commun* (1987) 11:15–22. doi: 10.1007/BF00361322
39. Oliveira L, Stallwood NA, Crankshaw DJ. Effects of some isoprostanes on the human umbilical artery in vitro. *Br J Pharmacology* (2000) 129:509–14. doi: 10.1038/sj.bjp.0703083
40. O'Brien JW, Choi PM, Li J, Thai PK, Jiang G, Tschärke BJ, et al. Evaluating the stability of three oxidative stress biomarkers under sewer conditions and potential impact for use in wastewater-based epidemiology. *Water Res* (2019) 166:1–7. doi: 10.1016/j.watres.2019.115068
41. Guo W, Luo L, Meng Y, Chen W, Yu L, Zhang C, et al. Luteolin alleviates methionine-choline-deficient diet-induced non-alcoholic steatohepatitis by modulating host serum metabolome and gut microbiome. *Front Nutr* (2022) 9:1–14. doi: 10.3389/fnut.2022.936237
42. Malaguarnera M, Risino C, Gargante MP, Oreste G, Barone G, Tomasello AV, et al. Decrease of serum carnitine levels in patients with or without gastrointestinal cancer cachexia. *World J Gastroenterol* (2006) 12(28):4541–5. doi: 10.3748/wjg.v12.i28.4541
43. Ruiying C, Zeyun L, Yongliang Y, Zijia Z, Ji Z, Xin T, et al. A comprehensive analysis of metabolomics and transcriptomics in non-small cell lung cancer. *PloS One* (2020) 15(5):1–16. doi: 10.1371/journal.pone.0232272
44. Shumar SA, Kerr EW, Fagone P, Infante AM, Leonardi R. Overexpression of Nudt7 decreases bile acid levels and peroxisomal fatty acid oxidation in the liver. *J Lipid Res* (2019) 60(5):1005–19. doi: 10.1194/jlr.M092676
45. Kerr EW, Shumar SA, Leonardi R. Nudt8 is a novel CoA diphosphorylase that resides in the mitochondria. *FEBS Lett* (2019) 593(11):1133–43. doi: 10.1002/1873-3468.13392
46. Ge X, Li GJ, Wang SB, Zhu H, Zhu T, Wang X, et al. AtNUDT7, a negative regulator of basal immunity in arabidopsis, modulates two distinct defense response pathways and is involved in maintaining redox homeostasis. *Plant Physiol* (2007) 145(1):204–15. doi: 10.1104/pp.107.103374
47. Taniguchi M, Hayashi T, Nii M, Yamaguchi T, Fujishima-Kanaya N, Awata T, et al. Overexpression of NUDT7, a candidate quantitative trait locus for pork color, downregulates heme biosynthesis in L6 myoblasts. *Meat Sci* (2010) 86(3):728–32. doi: 10.1016/j.meatsci.2010.05.045
48. Liu Y, Liu X, Zheng Z, Ma T, Liu Y, Long H, et al. Genome-wide analysis of expression QTL (eQTL) and allele-specific expression (ASE) in pig muscle identifies candidate genes for meat quality traits. *Genet Sel Evol* (2020) 52(1):1–11. doi: 10.1186/s12711-020-00579-x
49. Domínguez R, Pateiro M, Gagaoua M, Barba FJ, Zhang W, Lorenzo JM. A comprehensive review on lipid oxidation in meat and meat products. *Antioxidants* (2019) 8(10):1–31. doi: 10.3390/antiox8100429
50. Chen H, Cao P, Li B, Sun D, Wang Y, Li J, et al. Effect of water content on thermal oxidation of oleic acid investigated by combination of EPR spectroscopy and SPME-GC-MS/MS. *Food Chem* (2017) 221:1434–41. doi: 10.1016/j.foodchem.2016.11.008
51. Damerau A, Ahonen E, Kortensniemi M, Pukanen A, Tarvainen M, Linderborg KM. Evaluation of the composition and oxidative status of omega-3 fatty acid supplements on the Finnish market using NMR and SPME-GC-MS in

- comparison with conventional methods. *Food Chem* (2020) 330:1–11. doi: 10.1016/j.foodchem.2020.127194
52. Sundling C, Lau AWY, Bourne K, Young C, Laurianto C, Hermes JR, et al. Positive selection of IgG(+) over IgM(+) b cells in the germinal center reaction. *Immunity* (2021) 54(5):988–1001. doi: 10.1016/j.immuni.2021.03.013
53. Mäkelä O, Rouslahti E, Seppälä IJT. Affinity of IgM and IgG antibodies. *Immunochemistry* (1970) 7(11):917–32. doi: 10.1016/0019-2791(70)90053-4
54. Chen Y, Meng F, Wang B, He L, Liu Y, Liu Z. Dock2 in the development of inflammation and cancer. *Eur J Immunol* (2018) 48(6):915–22. doi: 10.1002/eji.201747157
55. Xu X, Su Y, Wu K, Pan F, Wang A. DOCK2 contributes to endotoxemia-induced acute lung injury in mice by activating proinflammatory macrophages. *Biochem Pharmacol* (2021) 184:1–15. doi: 10.1016/j.bcp.2020.114399
56. Magalhaes-Novais S, Bermejo-Millo JC, Loureiro R, Mesquita KA, Domingues MR, Maciel E, et al. Cell quality control mechanisms maintain stemness and differentiation potential of P19 embryonic carcinoma cells. *Autophagy* (2020) 16(2):313–33. doi: 10.1080/15548627.2019.1607694
57. Pozo FM, Geng X, Tamagno I, Jackson MW, Heimsath EG, Hammer JA, et al. MYO10 drives genomic instability and inflammation in cancer. *Sci Adv* (2021) 7:1–17. doi: 10.1126/sciadv.abg6908
58. Dlamini NM, Dzomba EF, Magawana M, Ngcamu S, Muchadeyi FC. Linkage disequilibrium, haplotype block structures, effective population size and genome-wide signatures of selection of two conservation herds of the south African nguni cattle. *Anim (Basel)* (2022) 12(16):1–23. doi: 10.3390/ani12162133
59. Ibrahim S, Zhu X, Luo X, Feng Y, Wang J. PIK3R3 regulates ZO-1 expression through the NF- κ B pathway in inflammatory bowel disease. *Int Immunopharmacol* (2020) 85:1–8. doi: 10.1016/j.intimp.2020.106610
60. Polini B, Carpi S, Doccini S, Citi V, Martelli A, Feola S, et al. Tumor suppressor role of hsa-miR-193a-3p and -5p in cutaneous melanoma. *Int J Mol Sci* (2020) 21(17):1–18. doi: 10.3390/ijms21176183
61. Shao S, Chen J, Swindell WR, Tsoi LC, Xing X, Ma F, et al. Phospholipase A2 enzymes represent a shared pathogenic pathway in psoriasis and pityriasis rubra pilaris. *JCI Insight* (2021) 6(20):1–15. doi: 10.1172/jci.insight.151911
62. Ehmsen JT, Kawaguchi R, Kaval D, Johnson AE, Nachun D, Coppola G, et al. GADD45A is a protective modifier of neurogenic skeletal muscle atrophy. *JCI Insight* (2021) 6(13):1–16. doi: 10.1172/jci.insight.149381
63. Jiang Y, Xiang C, Zhong F, Zhang Y, Wang L, Zhao Y, et al. Histone H3K27 methyltransferase EZH2 and demethylase JMJD3 regulate hepatic stellate cells activation and liver fibrosis. *Theranostics* (2021) 11(1):361–78. doi: 10.7150/thno.46360
64. Andrejeva G, Rathmell JC. Similarities and distinctions of cancer and immune metabolism in inflammation and tumors. *Cell Metab* (2017) 26(1):49–70. doi: 10.1016/j.cmet.2017.06.004
65. Zhang D, Chia C, Jiao X, Jin W, Kasagi S, Wu R, et al. D-mannose induces regulatory T cells and suppresses immunopathology. *Nat Med* (2017) 23(9):1036–45. doi: 10.1038/nm.4375
66. Ara A, Ahmed KA, Xiang J. Mannose-6-phosphate receptor: a novel regulator of T cell immunity. *Cell Mol Immunol* (2018) 15(11):986–8. doi: 10.1038/s41423-018-0031-1
67. Dalle Vedove E, Costabile G, Merkel OM. Mannose and mannose-6-Phosphate receptor-targeted drug delivery systems and their application in cancer therapy. *Adv Healthc Mater* (2018) 7(14):1–37. doi: 10.1002/adhm.201701398
68. Zhang W, Yang X, Li Y, Yu L, Zhang B, Zhang J, et al. GCAF(TM251) regulates lysosome biogenesis by activating the mannose-6-phosphate pathway. *Nat Commun* (2022) 13(1):1–17. doi: 10.1038/s41467-022-33025-1

Frontiers in Immunology

Explores novel approaches and diagnoses to treat immune disorders.

The official journal of the International Union of Immunological Societies (IUIS) and the most cited in its field, leading the way for research across basic, translational and clinical immunology.

Discover the latest Research Topics

[See more →](#)

Frontiers

Avenue du Tribunal-Fédéral 34
1005 Lausanne, Switzerland
frontiersin.org

Contact us

+41 (0)21 510 17 00
frontiersin.org/about/contact

